REACTION KINETICS STUDY OF IN-SITU COMBUSTION:

INTEGRATION OF EXPERIMENTAL & ANALYTICAL APPROACHES

A Dissertation

by

NORASYIKIN BTE ISMAIL

Submitted to the Office of Graduate and Professional Studies of
Texas A&M University
in partial fulfillment of the requirements for the degree of

DOCTOR OF PHILOSOPHY

Chair of Committee,	Berna Hascakir
Committee Members,	Timothy Jacobs
	Hadi Nasrabadi
	Samuel Frans Noynaert
Intercollegiate Faculty Chair,	Timothy Jacobs

December 2019

Major Subject: Interdisciplinary Engineering

ABSTRACT

In-situ combustion (ISC) is a very promising thermal enhanced oil recovery (EOR) method to recover heavy oils and bitumen as it has a high recovery rate and is applicable to use at a varied range of reservoirs. However, as ISC involves highly exothermic reactions and complicated reaction kinetics, it is challenging to predict its performance as compared to other EOR methods. The chemical reactions associated with the ISC process are numerous and occur over different temperature ranges. The reactivity of each reaction is controlled by the chemical kinetics. The oil composition and the rock mineralogy will also affect the reaction kinetics. Thus, the ISC performance predictions are only reliable if proper reaction models are formulated.

This dissertation evaluated the ISC field performance by integrating the combustion tube and kinetic experiment results. The performance estimation of these processes is described under three distinct sections of this study. First, the role of oil composition and the effect of clay presence on ISC performance were studied through combustion tube experiments of 3 types of crude oil samples. Next, analytical modeling was done on the combustion tube results integrating with the reaction kinetic parameters. Finally, the reaction kinetics and modeling of ISC were performed to study the factors that affect ISC performance.

The result shows that crude oil combustion performance varies depending on oil compositions. Clay presence aids combustion by increasing the oxygen uptakes on asphaltenes' surface area, which results in more coke formation. Asphaltenes dispersion is encouraged by resins and aromatics fractions. Moreover, asphaltenes coagulation is

enhanced due to saturates fraction. Water presence also aids the combustion process. Heavier fractions (resins and asphaltenes) dominate the reaction pathways, thus decreasing the energy requirement and generate a large heat making the combustion effective. Water and aromatics fraction interaction at elevated temperatures favors ISC reactions.

Lastly, reservoir rocks also affect ISC performance. An increased amount of clay decreased the activation energies of the reactions and increased the heat of combustion, which was indicative of the catalytic properties of clay. However, the results might indicate that the clay-oil pair used in this study may have an optimum reaction at 9% clay content. In the presence of carbonate, calcite is generating more heat for combustion but increasing the activation energy needed for HTO region due to its interaction with aromatics. Meanwhile, the heat generation was reduced and the activation energy was increased when dolomite was the reservoir rock. This is due to dolomite interaction with resins.

The approach in this dissertation is a fresh take on determining the reaction kinetics of the ISC process by coupling the combustion tube experimental results with the kinetics experiment. This study will help reduce the complexity of the process by trying to develop a simplified approach towards a better understanding of ISC chemical reactions for different types of crude oil and reservoir.

DEDICATION

To my universe,

Ismail, Nooraisah, Noorhasyimah Munira, Noorsyahira,

Noor Athira Damia, Noor Atiqah Liyana.

ACKNOWLEDGMENTS

First and foremost, I am grateful to the Merciful Allah S.W.T for His love and blessing, as well as the strength, good health, and peace of mind granted upon the completion of this dissertation.

I am genuinely, unequivocally thankful to my advisor, Dr. Berna Hascakir, for her continuous encouragement and generous support throughout this study. Her in-depth knowledge and experiences have helped me to complete this study and in becoming a better researcher and person. I would also like to extend my deepest gratitude to the committee members, Dr. Timothy Jacobs, Dr. Hadi Nasrabadi, and Dr. Sam Noynaert for their guidance and valuable inputs towards improving my research.

Thank you to all the members of the Heavy Oil, Oil Shales, Oil Sands, and Carbonate Analysis and Recovery Methods (HOCAM) research group. They offered their help and assistance without hoping to gain anything in return. They shared their knowledge and skills generously, and there is still a lot to learn from them. To my sponsors, Universiti Malaysia Pahang and Ministry of Education Malaysia, thank you for supporting my study. Without these fantastic people and great institutions, I may not be able to complete my Ph.D. study at Texas A&M University.

To my beautiful family, friends, and BTS, thank you for your continuous support through this wonderful life journey. You are all that I have, and you are my strength and pillars. I might not be the person I am now if it were not for you.

Thank you from the bottom of my heart.

CONTRIBUTORS AND FUNDING SOURCES

Contributors

Funding Sources

NOMENCLATURE

ΔH	Enthalpy or Heat of Combustion
A	Arrhenius Constant, 1/min
API	American Petroleum Institute
ASTM	American Society for Testing and Materials
bbl/day	Barrel Crude Oil per Day
$C_{10}H_{20}O$	Decanal
$C_{10}H_{20}O$	Decanone
$C_{10}H_{22}$	Decane
$C_{10}H_{22}O$	Decanol
$CaCO_3$	Calcite
$CaMg(CO_3)_2$	Dolomite
CHN	Carbon, Hydrogen, and Nitrogen
CII	Colloidal Instability Index
cm	Centimeter
cm^3/m^3	Cubic Centimeter per Cubic Meter
cP	Centipoise
DAO	Deasphalted Oil
DSC	Differential Scanning Calorimetry
DTA	Differential Thermal Analysis
E_a	Activation Energy, BTU/lb-mole
EDS	Energy Dispersive Spectroscopy

EGA	Effluent Gas Analysis
EOR	Enhanced Oil Recovery
ft	Feet
FTIR	Fourier Transform InfraRed
H/C	Hydrogen to Carbon ratio by weight
HTO	High Temperature Oxidation
ICP	Inductively Coupled Plasma
in^3/ft^3	Cubic Inch per Cubic Feet
ISC	In-situ Combustion
kPa	Kilopascal
LTO	Low Temperature Oxidation
m	Meter
m^3/day	Cubic Meter per Day
ND	Non-detectable
psi	Pound per Square Inch
SARA	Saturates, Aromatics, Resins, and Asphaltenes
SEM	Scanning Electron Microscopy
TGA	Thermogravimetric Analysis
vol%	Volume Percent
wt%	Weight Percent
XRD	X-ray Diffraction

TABLE OF CONTENTS

LIST OF FIGURES

LIST OF TABLES

LIST OF EQUATIONS

Page

1. INTRODUCTION

Fossil fuels combustion contributed to approximately 88% of the world's energy consumption in 2016 (BP Company, 2017) (Figure 1.1). By 2017, the demand for crude oil has escalated and strained the supply of conventional oil due to its limited availability. This leads to the consideration of hydrocarbon production from unconventional resources.
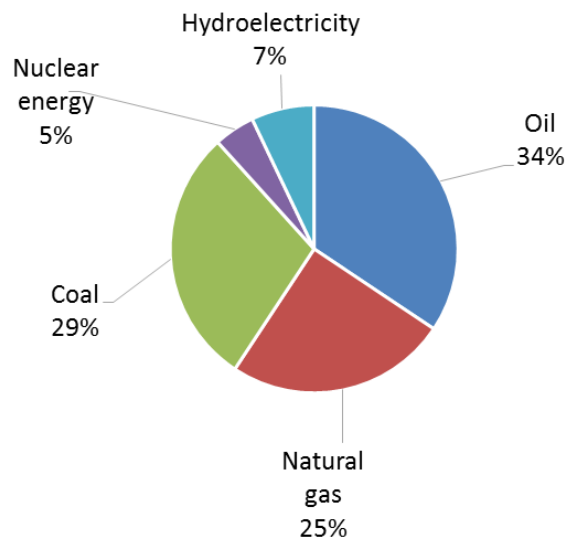
Figure 1.1─World Energy Source 2016 (BP Company, 2017)

Meyer et al. (2007) classified crude oil as conventional (light) oil (API gravity higher than 25°), medium oil (API gravity between 20° and 25°), heavy oil (API gravity between 10° and 20°, viscosity more than 100 cP), and natural bitumen (less than 10°API gravity, viscosity more than 10,000 cP). Figure 1.2 shows worldwide heavy oils and bitumen reserves. In North America, the largest heavy oil deposits are in California

1

(77.6%), Texas (14.6%), and Alberta (3.3%), with most of the bitumen resources in Alberta (69.6%), followed by Utah (12.9%) and Alaska (7.58%) (Hein 2006).

Regional Distribution of Heavy Oils

Regional Distribution of Bitumen
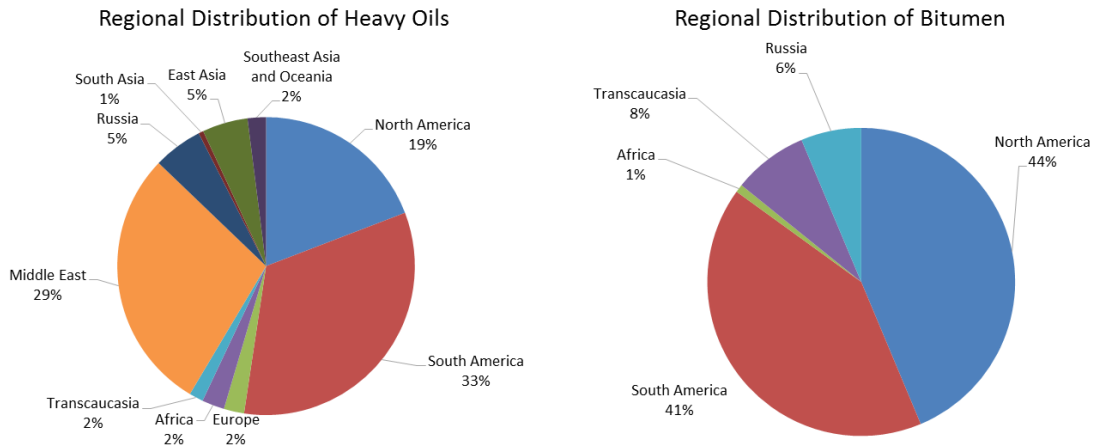
Figure 1.2—Regional Distributions of Heavy Oils and Bitumen (Meyer et al. 2007)

Efficient production of these unconventional resources requires the application of tertiary recovery techniques. This is because primary recovery involves natural flow or artificial lift to recover crude oil. So, it is not suitable for low API gravity and high viscosity oils (Prats 1982; Raicar and Procter 1984). Moreover, secondary recovery methods (waterflooding and pressure maintenance) are not effective due to high mobility ratios. These unconventional resources need to be recovered by a tertiary method, which is enhanced oil recovery (EOR) (Prats 1982; Burger et al. 1985; Radler 1996; Bai 2012). Tertiary recovery techniques are divided into thermal, chemical, gas injection, and others (microbial, microwave) (Burger et al. 1985; Meyer et al. 2007). In 2010, miscible CO_2

2

flooding recovered the most in all of the United States oil production (Koottungal 2014). Chemical and gas injection methods are the least popular methods because of the high operating cost (Burger et al. 1985; Meyer et al. 2007). As mobility is the main issue for bitumen and heavy oils, not all EOR methods will work properly for these resources.

Enhancing the mobility of crude oil is done by reducing the crude oil viscosity through the application of thermal EOR methods (Prats 1982). In 2014, thermal EOR produced almost 877,000 bbl/day, and around 77% of the productions were from North and South America (Figure 1.3) (Koottungal 2014).
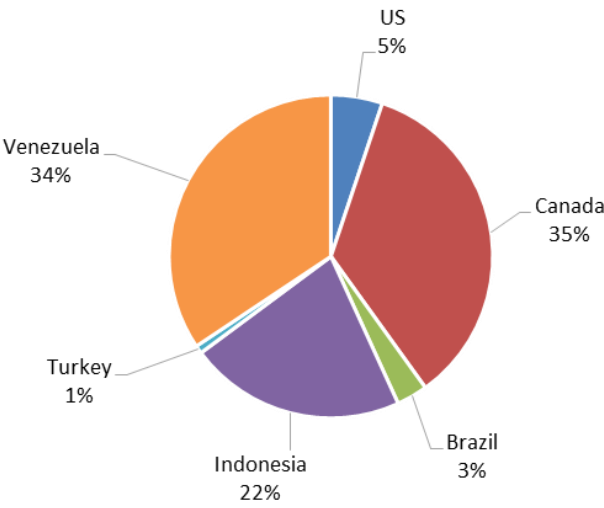
Figure 1.3—Comparison of Thermal EOR Project by Country (Koottungal 2014)

Steam injection is widely used as a thermal EOR method because water is highly accessible, and steam injection is a reliable recovery method. The heated steam transfers energy to the reservoir continuously or cyclically to reduce the viscosity of the oil (Butler 1991). There are, however, several downsides of steam injection. For one, hot water flooding proved to be less efficient due to the lower heat content of water, as compared to steam. Meanwhile, steam cannot be injected into deep reservoirs due to the pressure limitation of steam generation (Sufi 1989). As well, the steam injection method makes up environmental footprints due to steam generation. Moreover, steam generation is a cost-ineffective process; considering that if the oil prices are low, it is not economically sound (Morrow et al. 2014).

On the other hand, in-situ combustion (ISC) is one of the most promising thermal EOR methods with nearly 95% oil displacement efficiency (Sarathi 1998). ISC has a high recovery rate, which applies to a wide variety of reservoirs' condition (deeper, thinner, etc.), and upgrades the crude oil in-situ by leading the production of less viscous oil with low metal and sulfur content (Hascakir et al. 2011). In the ISC process, downhole heaters are used to initiate the combustion reactions by igniting the crude oil in place. The crude oil burning is sustained by injecting air or oxygen-rich gas into the formation. As temperature increases, oil viscosity is reduced, and the oil is driven towards the producing wells by a vigorous gas drive of the combustion gases known as the combustion front, a steam drive, and a water drive (Burger 1972; Prats 1982).

However, according to Sarathi (1998), between 1950 to 1990, there were only 42% successful ISC projects in the United States and there have been more than twenty wide-

scale ISC operations globally, having been operated for a long time as well as involving a

large number of wells in the last 60 years of the ISC application. To this point, four of the

most successful ISC projects that are still going on with the details of the operation are

examined and listed below in Table 1.1.

Table 1.1—Commercial Ongoing Worldwide Projects of ISC
(Hammershaimb et al. 1983; Marjerrison and Fassihi 1994; Turta et al. 2007;
Mitra et al. 2010)

Location	Details
Suplacu de Barcau, Romania	• Shallowest ISC operation; depth of the reservoir is between the range of 35 m to 250 m (115-820 ft) • The process displays the longest ISC front (5.3 miles) having 150 injection wells at the peak. • Oil production at approx. 1,500 m^3/day (9,435 bbl/day) • Air-oil ratio (AOR) at approx. 2,500 cm^3/m^3 (4.32 in^3/ft^3) • Operational difficulty: mud volcanoes at surfaces in areas with the lowest depth (35 m)
Balol and Santhal, India	• Highest-pressure wet ISC operation in a heavy oil reservoir containing some coal laminations • The depth of the reservoir is at approx. 1,000 m (3,280 ft); strong lateral water drive • Oil production at approx. 1,500 m^3/day (9,435 bbl/day) from 2 commercial operations • Air-Oil Ratio (AOR) at approx. 1,000 cm^3/m^3(1.73 in^3/ft^3)
Bellevue, Louisiana, USA	• Typical dry and wet ISC applied in small patterns. • Low pressure process (injection of pressure less than 1724 kPa/250 psi).
Heidelberg, Gulf of Mexico, USA	• The deepest ISC process (3,447 m/11,300 ft). • All three injectors are located up-dip.

Ongoing full-field ISC projects above are known to be successful because their reservoir fluid and rock properties entirely favored the combustion at its optimum process parameters. The optimum process parameters of ISC for these fields were determined through the coupling of the combustion tube tests with analytical models. Analytical modeling of ISC provides important ISC process parameters; such as air injection rate, coke burning reaction, etc. (Nelson and McNeil 1961). However, the combustion front movement cannot be depicted through analytical modeling. Compositional reservoir simulators are common practice to estimate any EOR front movement in four dimensions (4D).

The limited application of the full-field ISC project is due to failure in estimating the chemical reactions that occur during ISC, which would be embedded in the compositional simulators. Several chemical reactions of hydrocarbons during ISC lead to the formation of different ISC zones with different transport mechanisms (Kudryavtsev and Hascakir 2014). Hence, it is crucial to understand the mechanism of each zone at varying temperatures to better estimate ISC performance. The main oxidation reaction will be reviewed in the next section.

Chemical reactions observed during ISC are categorized into three main groups; low temperature oxidation (LTO), thermal cracking (fuel formation reactions), and high temperature oxidation (HTO) reactions (Akin et al. 2000; Cinar et al. 2011a). LTO, HTO, and thermal cracking reactions are vital for successful combustion, but it involves many intermediate chemical reactions that make ISC unpredictable (Burger et al. 1985). In the thermal cracking reaction, thermally cracked hydrocarbons will leave carbonaceous

residue behind known as coke or soot (Bagci 1998; Hascakir et al. 2013; Aleksandrov and Hascakir 2015). In ISC, the formed coke is the main fuel for combustion (Sarathi 1998; Castanier and Brigham 2003). Crude oil itself is the fuel source, and during ISC, a small portion of the crude oil (less than 5%) is converted into coke through the oxidation and cracking reaction mentioned above (Hascakir et al. 2013). Hence, the full picture of the main chemical reactions occurring during ISC is necessary to build a better understanding of their chemical reaction kinetics parameters.

Reaction kinetic experiments are used to estimate important chemical reaction parameters. Several thermal analysis experiments were introduced to study the reaction kinetics (Burger 1972; Burger et al. 1985; Kok 1993). Differential Thermal Analysis (DTA) is carried out by heating the sample together with a reference standard under identical thermal conditions in the same oven and measuring the temperature difference between the sample and reference substance during the period of heating. Differential Scanning Calorimetry (DSC) has the same principle as DTA, but the rate of heat release is recorded instead of the difference in temperature. Thermogravimetric analysis (TGA) records the weight change as the temperature increases at a constant rate. This technique is complementary to DTA or DSC, as the weight variation data is relatable to DTA or DSC peaks. Effluent Gas Analysis (EGA) technique is used based on the continuous analysis of the effluents of the reactions of a sample submitted to gas flow and programmed heating that provides a good image of the type of reaction involved (Burger et al. 1985). However, in the real field, the performance of ISC cannot be estimated by a single kinetics experiment. This is because, in one single experiment, only one heating

rate is applied but in the real combustion process, several heating rates are observed; (slow heating rate in LTO, rapid heating rates in thermal cracking, and HTO regions) (Hascakir 2015). Therefore, reaction kinetic experiments should be coupled with combustion tube tests to better estimate reaction kinetics at varying heating rates.

It should be noted that reaction kinetics tests are too complicated even for the simple hydrocarbons to estimate. For instance, reaction kinetics studies of n-decane, n-dodecane, and n-hexadecane (Douté et al. 1997; Curran et al. 2002; Ranzi et al. 2005; Ranzi 2006; Westbrook et al. 2009); methyl ethyl ketone and pentanone (Escobar et al. 2004; Serinyel et al. 2010a; Serinyel et al. 2010b); propanal, n-butanal, and isobutanal (Salooja 1965; Pepiot-Desjardins et al. 2008; Kasper et al. 2009; Akih-Kumgeh and Bergthorson 2011); n-Butanol, n-Propanol, and iso-Propanol (Barnard 1960; Barnard and Hughes 1960; Heufer et al. 2011) prove that it is challenging to estimate the reaction pathway, and consequently, the reaction kinetics for the combustion of these hydrocarbons. Thus, it will be more challenging to estimate reaction pathways for complex hydrocarbon blends like crude oil. Moreover, crude oil components and the applied heating rates used in reaction kinetic experiments alter the reaction pathways, hence, further complicate the ISC. Additionally, the contribution of reservoir rocks and formation water lead to different pathways of reactions.

Saturates, Aromatics, Resins, and Asphaltenes (SARA) fractionations are used by many researchers (Boylan and Tripp 1971; Jewell et al. 1974; Wang et al. 1994; Cho et al. 2012; Hascakir 2015; Klock and Hascakir 2015) to simplify the number of components in ISC's chemical reactions. The role of saturates in ISC is the ignitor for the combustion

(Wu and Fulton 1971; Sarathi 1998; Castanier and Brigham 2003), and asphaltenes are known to aid the fuel formation (da Silva Ramos et al. 2001; Mullins et al. 2012). Aromatics and resins contribute to the visbreaking reactions of ISC (Hascakir 2015; Ismail and Hascakir 2017), but, their formation, oxidation, and consumption are still not clear for ISC terminology.

As stated above, the chemical reactions are not only controlled by the crude oil, but also by the reservoir rock, and the mutual interaction of reservoir rock with oil at elevated temperatures (Kar et al. 2015; Kozlowski et al. 2015; Ismail et al. 2016). Carbonate is known to not favor in general combustion since they decompose at combustion temperature. This endothermic reaction requires heat and consumes the heat necessary for the cracking of hydrocarbons. This is because carbonate decomposition is an endothermic reaction which may affect ISC performance negatively (Briggs et al. 1988; Sarathi 1998; Manrique et al. 2006; Mostafavi et al. 2007; Fatemi et al. 2011).

Apart from carbonate, other reservoir rock minerals also have an impact on ISC performance. For instance, clay is known to have a catalytic impact on ISC that reduces the activation energy barrier and increases the amount of coke deposition and generated heat (Vossoughi et al. 1982b; Moore et al. 1999; Lee and Li 2007; Abuhesa and Hughes 2008; Raju et al. 2010; Shah et al. 2011; Kozlowski et al. 2015). Hence, in general, clay presence in the rock is expected to reduce the heat necessary for ignition. As well, Vossoughi and El-Shoubary (1987) observed a significant reduction of activation energy caused by the addition of kaolinite to crude oil. Fassihi et al. (1984a) observed that there is a higher amount of fuel deposition in the presence of clay. Ranjbar (1993) found that

fuel deposition and oxidation were enhanced by the catalytic impact of clay minerals. The positive contribution of clay presence in the reservoir rock to ISC performance is due to several physical and chemical changes happening in clay at a high temperature (above 600 °C). The physical and chemical changes are water loss, changes in mass and density, alteration and decomposition of clay, and deformation of clay structure, which may increase the surface area of clay and further aids combustion (Chen et al. 2016).

It is evident that the chemical reactions associated with the ISC process are numerous and occur over different temperature ranges. The reactivity of each reaction is controlled by the reaction kinetics. Both the oil composition and the rock mineralogy affect the reaction kinetics. Thus, the ISC performance predictions are only reliable if proper reaction models are formulated. It is necessary to improve our understanding of the fundamentals of the combustion process in porous media to construct these models, so the application of ISC can be more extensive and reliable.

The first part of this dissertation aims to investigate the effects of oil composition and the presence of clay on ISC performance by using combustion tube experiments. Three different heavy oils and bitumen from North and South America were used to investigate their impact. In the second part, the analytical modeling of combustion tube experiments was investigated. Finally, in the last chapter, the reaction kinetics of ISC were studied by using different kinetic models, and TGA/DSC experiments were used to obtain model parameters of crude oils and their SARA fractions.

2. THE ROLE OF OIL COMPOSITION & CLAY PRESENCE ON IN-SITU

COMBUSTION PERFORMANCE

Introduction

In-situ combustion (ISC) is a thermal enhanced oil recovery (EOR) method in which air is injected into an oil reservoir, and a combustion front sweeps the reservoir in the direction of the gas flow towards the production well (Ramey 1971). ISC is a promising method for oil recovery not only because it results in an excellent oil displacement efficiency but also it increases the produced oil quality by lowering its viscosity significantly (Martin et al. 1958; Sarathi 1998). However, there is complexity to be expected in carrying out the process. This results from the numerous chemical reactions happening at high temperatures. This intricacy can be reduced if the burning behavior of different fluid fronts formed during ISC is well-understood (Aleksandrov and Hascakir 2015).

After ignition, induced by the downhole heaters, the combustion front is sustained by a continuous air flow. The numerous distinct chemical reactions during the combustion process lead to the formation of different ISC zones from the result of heat and mass transport (Sarathi 1998; Kudryavtsev and Hascakir 2014; Aleksandrov et al. 2015). Figure 2.1 represents the different zones formed during ISC between the injection well and the producer well. The graph at the top of Figure 2.1 illustrates the temperature distribution and the diagram at the bottom of Figure 2.1 shows the location of different ISC zones.
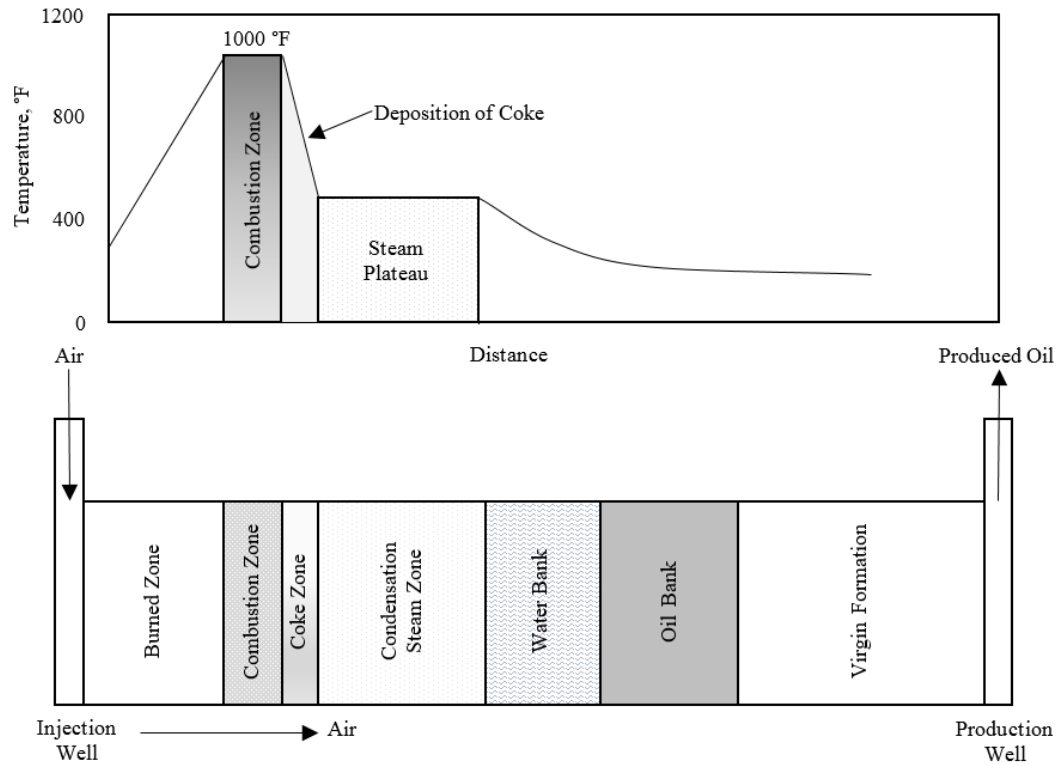
Figure 2.1—Schematic Temperature Distribution (Top) and ISC Zones Location (Bottom) Modified from Tadema (1959) and Sarathi (1998) (Figure is Not Scaled)

These zones represent the dominant fluid phase (i.e., water bank, oil bank, and steam plateau) or the chemical reactions occurring at that fluid front (i.e., combustion zone, cracking/vaporization region) (Castanier and Brigham 2003; Aleksandrov and Hascakir 2015). The first zone after the injection well is the burned zone where the combustion already happened and oil is already swept by air. Combustion front is ahead of the burned zone where reaction between oxygen and fuel takes place generating heat to produce primarily water and combustion gases (CO_2 and CO). After combustion zone is the thermal cracking zone where the crude oil is transformed into fuel or coke, a carbon-rich solid residue (Bagci 1998; Aleksandrov and Hascakir 2015). Thermal cracking

12

involves pyrolysis, and it is an endothermic reaction. The conversion of crude oil into fuel through cracking reaction will only happen if the activation energy (E_a) barrier is exceeded (Rodriguez et al. 1987). Then, the formed fuel is burned in the presence of oxygen in an exothermic reaction. The fuel burning zone is called the combustion zone. The combustion releases the chemical energy stored in the chemical bonds of the fuels called the heat of combustion (ΔH) (Moore et al. 1999). The energy (heat of combustion) generated is then consumed rapidly by the fuel formation reactions in the cracking region and this cycle continues and sustains the ISC process (Burger 1972). At high temperature, visbreaking reactions happen and reduces the crude oil viscosity significantly.

The next zone is the condensation zone (steam plateau zone) where some of the hydrocarbon vapor entering this zone condenses and dissolves in the crude (Sarathi 1998). After the steam plateau zone, a hot water bank is formed where the temperature is lower than the condensation temperature of steam in where liquid water is formed. The oil bank comes after the water bank, and it is the oil that has been displaced by the combustion gases and water drives. Finally, the virgin formation is the untouched region where combustion has not affected.

To investigate this process in the laboratory, combustion tubes are used. A well-designed combustion tube experiment can provide insightful knowledge on the combustion characteristics of crude oil in the reservoir rock. To obtain accurate field-scale ISC process parameters, combustion tube tests should meet the standards. Validated combustion tube test dimension is listed in Table 2.1 determined by different institutions or companies. In this thesis, Stanford design was used.

Table 2.1—Valid Dimensions for Combustion Tube Assembly (Leaute and Collyer 1984; Mamora et al. 1984; Bousaid 1989; Fassihi et al. 1996; Moore et al. 1997)

Facility	Length (ft-m)	Diameter (in-cm)	Wall Thickness (in-cm)
University of Calgary	6-1.83	4-10.16	0.042-0.11
*Stanford	3-0.92	3-7.62	0.016-0.04
Amoco	6-1.83	4-10.16	N/A
Texaco	5-1.52	3-7.62	0.042-0.11
Esso	4-1.22	3-7.62	0.025-0.06

* Our combustion tube experiments were based on Stanford design.

In common practice, combustion tube test results are used to obtain ISC field parameters through analytical modeling (Nelson and McNeil 1961). Because combustion tube experiment provides very important design criterion for ISC, in this chapter, the role of crude oil composition and clay on ISC were investigated through combustion tube experiments. For this purpose, combustion tube test results were evaluated in terms of combustion front speed, combustion front temperature, composition of produced gases, produced oil quality and quantity, and produced oil SARA fractions.

Experimental Procedure

Reservoir Fluid and Rock Characterization

In-situ combustion performance was studied for three oil samples from North and South America. First, the initial crude oil sample was characterized in terms of API gravity, viscosity, and SARA fractionation; results are given in Table 2.2.

Table 2.2—Properties of Initial Crude Oil Samples

Oil Sample	Gravity at 15 °C (°API)	Viscosity at 22.3 °C (cP)	Saturates (wt%)	Aromatics (wt%)	Resins (wt%)	Asphaltenes (wt%)
Oil 1	12.09	10,150	16.51	37.81	17.10	28.58
Oil 2	11.56	208,600	10.14	38.01	13.09	38.76
Oil 3	8.19	53,000	23.60	20.00	21.90	34.30

Anton Paar DMA 4100 density meter and Brookfield DV-III Ultra rheometer were used in measuring the API gravity at standard conditions and viscosity at room temperature (22.3 °C) for the initial oil samples, respectively (Prakoso et al. 2016). The weight percent of the asphaltenes fractions of the crude oil samples was attained by following ASTM D2007-11 standard (ASTM 2007). This method started with asphaltenes separation by n-pentane washing. Thus, ten grams of crude oil samples were washed through 2 µm filter paper with 500 ml n-pentane. The filtrate is called deasphalted oil (DAO) and was later separated into saturates, aromatics, and resins for further characterization. The cake that remained on the filter paper is called asphaltenes which are the n-pentane insoluble fractions of crude oil samples. The DAO was separated into saturates, aromatics, and resins by running the filtered DAO through two perforation columns (ASTM 2007). The top column was filled with only attapulgus clay to trap the resins fraction, and the bottom-most column was filled with both attapulgus clay on the top layer and silica gel on the bottom layer to trap the aromatics fraction. The run-off from the two columns was collected as the saturates fraction. Then, by washing the top column with n-pentane, aromatics were obtained. Finally, the top column was washed again with toluene and acetone mixture to extract resins fraction.

15

It can be observed from Table 2.2 that the three crude oil samples exhibit considerable variations in their physical properties. Oil 2 is the most viscous oil, with 208,600 cP viscosity and higher asphaltenes content (38.8 wt%) among all samples. At reservoir conditions, Oil 1 and Oil 3 are categorized as bitumen, and Oil 2 is in the heavy oil category (Meyer et al. 2007).

The elemental composition of all three oils was determined through a standard combustion method using a Leco CHN analyzer Carlo Erba model, and Thermo Intrepid Inductively Coupled Plasma (ICP) (Prakoso et al. 2018) (Table 2.3).

Table 2.3—Elemental composition of crude oil (Prakoso et al. 2018)

Elements	Crude Oil		
	Oil 1	Oil 2	Oil 3
C, wt.%	80.9	80.6	80.3
H, wt.%	10.8	10.5	10.3
H/C, ratio	0.133	0.130	0.128
Al, ppm	ND [†]	ND [†]	ND [†]
B, ppm	2.7	1.6	22.8
Ca, ppm	ND [†]	21.4	84.1
Cu, ppm	ND [†]	ND [†]	ND [†]
Fe, ppm	2.5	224.0	14.6
K, ppm	5.8	5.2	23.0
Mg, ppm	ND [†]	ND [†]	5.1
Mo, ppm	8.9	475.0	7.8
Na, ppm	23.3	8.5	235.0
Ni, ppm	68.1	88.4	80.3
P, ppm	2.4	2.1	2.0
Pb, ppm	ND [†]	ND [†]	ND [†]
S, ppm	44,100	52,400	68,700
Si, ppm	ND [†]	45.1	7.5
Sn, ppm	1.2	1.4	1.5
Ti, ppm	2.9	ND [†]	3.2
V, ppm	172.0	469	218.0
Zn, ppm	ND [†]	ND [†]	5.0
Metals, ppm*	**285**	**1,271**	**678**

[†]ND: Non-detectable - Signifies that the metal concentration is lower than the detection limit (0.01-0.1 μg/L)
*Metals (in ppm) is the sum of all metallic elements
The relative error range for the CHN analyzer and trace metal composition are ±1% and between ± 1.4 to 2.7%, respectively.

Carbon, hydrogen, and H/C ratio for all initial oil samples are almost similar. However, Oil 2 is high in iron (Fe), molybdenum (Mo), silicon (Si), and vanadium (V) as compared to Oil 1 and Oil 3. Meanwhile, Oil 3 is high in boron (B), calcium (Ca), potassium (K), sodium (Na), and sulfur (S) content. It should be noted that non-hydrocarbon elemental content of oils might not be in the hydrocarbon molecules but it

might be physically attached to hydrocarbon due to hydrocarbon-reservoir rock interaction. Thus, potassium (K) can be the sign of clays presence and sodium (Na) can be because of brine presence in Oil 3.

In the combustion tube experiments, besides the three crude oil samples, distilled water, clay, and sand were used to prepare reservoir rock and fluid blends. Clay and sand characterization was achieved through Scanning Electron Microscopy (SEM) – Energy Dispersive Spectroscopy (EDS) and X-ray diffraction (XRD) analysis. SEM-EDS analysis was done by using JEOL 7500 from Oxford Instruments and INCA software (Stamplecoskie et al. 2011). XRD analysis was done on Venture BRUKER-AXS CMOS IuS copper source kappa X-ray Diffractometer (Howie and Broadhurst 1958). Microscopic images were taken by SEM at 9500x magnification. SEM-EDS of the clay sample revealed that clay has oxygen (69.6 atomic wt%), silica (14.2 atomic wt%), aluminum (13.2 atomic wt%), carbon (2.4 atomic wt%), and potassium (0. 4 atomic wt%) (Kozlowski et al. 2015) (Figure 2.2 left-black bars). For sand, mostly oxygen (55.4 atomic wt%) and silica (26.2 atomic wt%) with some aluminum (0.9 atomic wt%) and carbon (6.9 atomic wt%) were detected (Figure 2.2 left-purple bars) (Kar et al. 2015). XRD analysis indicated that the clay is composed of 90 wt% kaolinite and 10 wt% illite (Unal et al. 2015) with 2.3 µm particle size (Kar et al. 2015) (Figure 2.2 right).
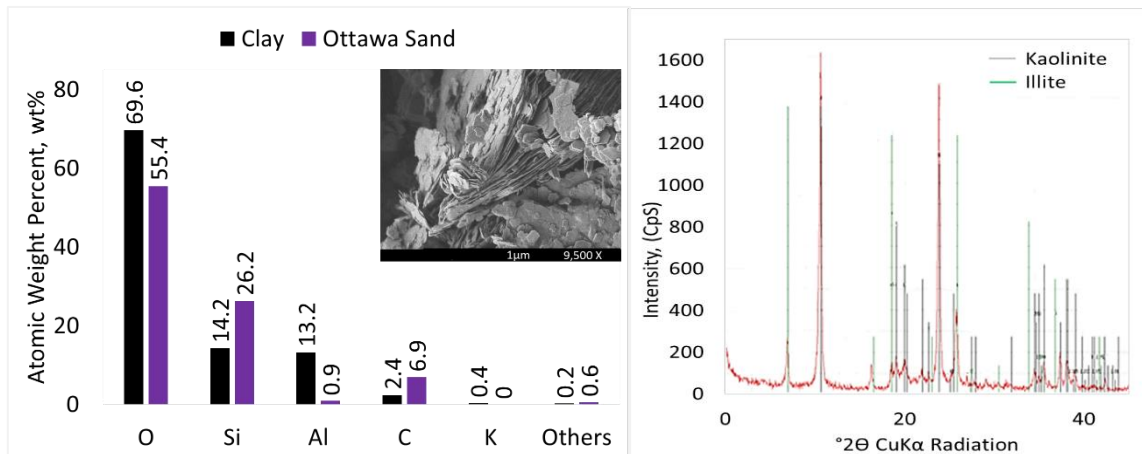
Figure 2.2—Elemental Composition of Clay and Sand Used in This Study (on the Left) & Clay Minerology (on the Right)

Combustion Tube Experiment Procedure

First, two types of pseudo-reservoir rock samples were prepared: 1) by blending 7397 g sand, 750 g oil, and 510 g water. Water and oil in this blend correspond to 60 vol% initial oil saturation and 40 vol% initial water saturation, which occupy 30 % porosity. 2) by blending 7175 g sand, 222 g clay, 750 g oil, and 510 g water. Water and oil in this blend correspond to 60 vol% initial oil saturation and 40 vol% initial water saturation which occupy 32% porosity in the reservoir rock. Then, prepared samples were packed homogenously into a 101.92 cm in length, 7.62 cm in diameter, stainless-steel combustion tube. After sealing the combustion tube, a thermowell was inserted at the center of the tube, and six J-type thermocouples were inserted in the thermowell at varying depths (5 cm, 20 cm, 24 cm, 55 cm, 60 cm, and 90 cm below from the injection point). An external band heater was placed at the top 10 cm of the combustion tube, and the combustion tube

assembly was wrapped with an insulation blanket made from fiberglass. Then, the combustion tube assembly was inserted in a calcium silicate insulation jacket that is 116.84 cm in length, 20.32 cm in diameter, and 2.54 cm wall thickness.

Afterward, the inlet of the combustion tube was connected to air and nitrogen cylinders, and the outlet of the combustion tube was connected to separators to collect and separate produced liquids and gases. The gas outlet of the separators was further connected to H_2S scrubbers and filters before gases entered the gas analyzer (Figure 2.3). Experiments were started under 0.5 L/min nitrogen injection to maintain constant 100 psig back pressure throughout the experiments. Once the heater's thermocouple has reached a temperature value around 400 °C which is defined as the necessary temperature to exceed the activation energy barrier for the fuel formation, the nitrogen injection was switched to the air injection at a constant injection rate (3.4 L/min) and the heater was turned off. For all experiments, compressed air with 79 mol% N_2 and 21 mol% O_2 was used. During the experiments, the temperature profiles were recorded every three seconds. Gases were analyzed in terms of CO, CO_2, O_2, and CH_4 at each second, and produced oil and water were collected every half an hour. At the end of the experiments, visual inspection of post mortem samples were achieved.
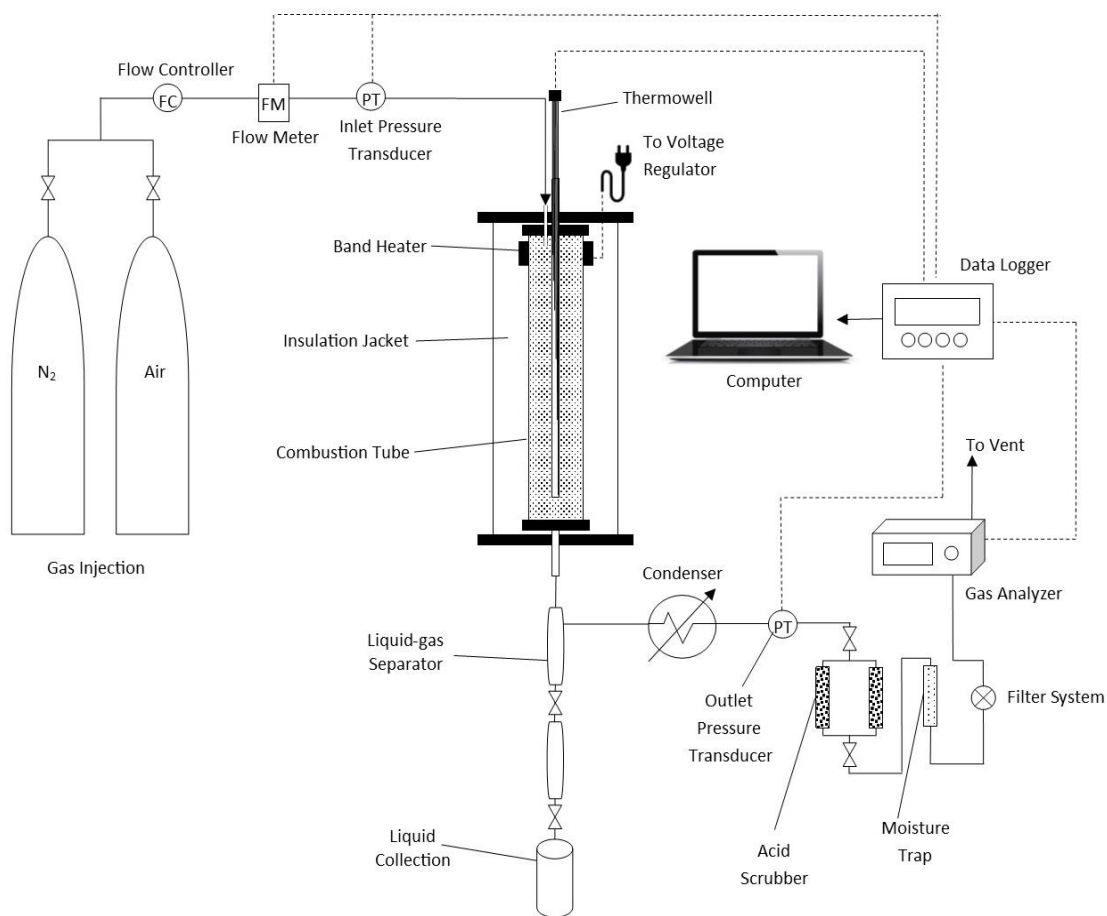
Figure 2.3－Combustion Tube Assembly Modified from Mamora et al. (1984) and Kudryavtsev and Hascakir (2014)

Six one-dimensional (1D) combustion tube experiments were conducted by following the procedure given above on three crude oils properties given in Table 2.2 and Table 2.3. Reservoir rocks were prepared with either 100 wt% 20/40 mesh size Ottawa sand (experiments E1, E2, and E3) or 97:3 wt% sand:clay mixture (experiments E1c, E2c, and E3c). Table 2.4 shows the nomenclature for the experiments.

Table 2.4—Nomenclature for Combustion Tube Experiment

Experiment	Rock Matrix
E1	Oil 1 + Ottawa Sand
E1c	Oil 1 + Ottawa Sand + Clay
E2	Oil 2 + Ottawa Sand
E2c	Oil 2 + Ottawa Sand + Clay
E3	Oil 3 + Ottawa Sand
E3c	Oil 3 + Ottawa Sand + Clay

c: Clay Presence

The produced oil samples were characterized in terms of API gravity and viscosity by using Anton Paar DMA 4100 density meter and Brookfield DV-III Ultra rheometer. The physical properties of the crude oils were then compared to their initial values (Table 2.2).

To assess the compositional changes occurring during ISC, SARA content of produced oils was analyzed through ASTM (2007) method and their molecular signature was determined by Agilent Cary 630 Fourier-Transform Infrared Spectroscopy (FTIR) spectrometer.

Visual inspection on the post mortem (spent rock) samples was carried out to identify the different zones on the spent rock samples at the end of each experiments. Different zones of spent rock samples were determined based on the variations color and textures of the spent rock. Then, each zone on the spent rock samples was analyzed with SEM-EDS by using JEOL 7500 from Oxford Instruments and INCA software (Stamplecoskie et al. 2011) to analyze the surface morphology, and elemental composition of the spent rock. Additionally, initial and produced oil asphaltenes were also subjected to SEM-EDS analysis to evaluate the effect of clay on asphaltenes morphology.

Results and Discussion

Combustion Tube Experimental Results

To investigate the effect of crude oil compositions on ISC, six combustion tube experiments were conducted with three different oils. Experimental parameters and conditions were kept constant during all runs. First, the effect of crude oil compositions is discussed, followed by the effect of clay presence. The discussion was made by assessing the combustion tube experimental results, including cumulative oil recovery, temperature profiles, and produced gas compositions. Then, the properties of the produced oils were discussed in terms of API gravity, viscosity, molecular structure, and crude oil fractions (SARA).

The results of the combustion tube experiments are summarized in Table 2.5. In this table, total experiment time, cumulative oil recovery, the maximum temperature observed during the combustion experiment, combustion front speed, and time to reach stable zone are reported. A stable zone is a zone where temperature and combustion speed are almost constant over time (Hascakir et al. 2013). Combustion tube experimental results should be evaluated for stable zone only to better estimate the real field performance of ISC.

Table 2.5—Summary of Results of Combustion Tube Experiments

Parameters	E1	E1c	E2	E2c	E3	E3c
Oil type	Oil 1	Oil 1	Oil 2	Oil 2	Oil 3	Oil 3
Clay presence	No	Yes	No	Yes	No	Yes
Total experiment time (hr)	5.87	4.78	3.08	3.73	4.70	2.98
Cumulative oil recovery (vol%)	87.74	90.26	82.08	80.10	80.51	81.99
Maximum temperature observed (°C)	462	482	554	613	537	519
Combustion front speed (ft/day)	25.37	10.95	29.81	14.08	6.4	21.75
Time to reach stable zone (hr)	1.73	2.30	1.72	1.20	1.00	0.88

With the clay addition, stable zone was reached faster for Oil 3 and slower for Oil 1 and Oil 2 (Table 2.5). Figure 2.4 reports the cumulative oil recovery and the temperature propagation at 55 cm below from the air injection location. It should be noted that temperature propagation were recorded for six fixed locations, and in Figure 2.4, the temperature profile at only one fixed location (55 cm below the injection point) was reported to compare the combustion performance of each test at stable zone. Oil 1 (E1 and E1c) had the highest cumulative oil recovery for ISC, both with and without clay (Figure 2.4 and Table 2.5). By looking at the metal content of the initial oil, iron (Fe), molybdenum (Mo), and vanadium (V) contents of Oil 2 were significantly higher than Oil 1 and Oil 3 (Table 2.3). Milliken et al. (1955) reported that clay with high iron and vanadium contents was found to produce more significant amount of coke in the catalytic-cracking process which may decrease the oil production amount. Moreover, an abundance of these elements coming from the crude oil can increase the activation energy of the crude oil component by overshadowing the catalytic effect of clay (Vossoughi et al. 1983).

A—Cumulative oil production of Oil 1	B—Temperature profile of Oil 1
C—Cumulative oil production of Oil 2	D—Temperature profile of Oil 2
E—Cumulative oil production of Oil 3	F—Temperature profile of Oil 3
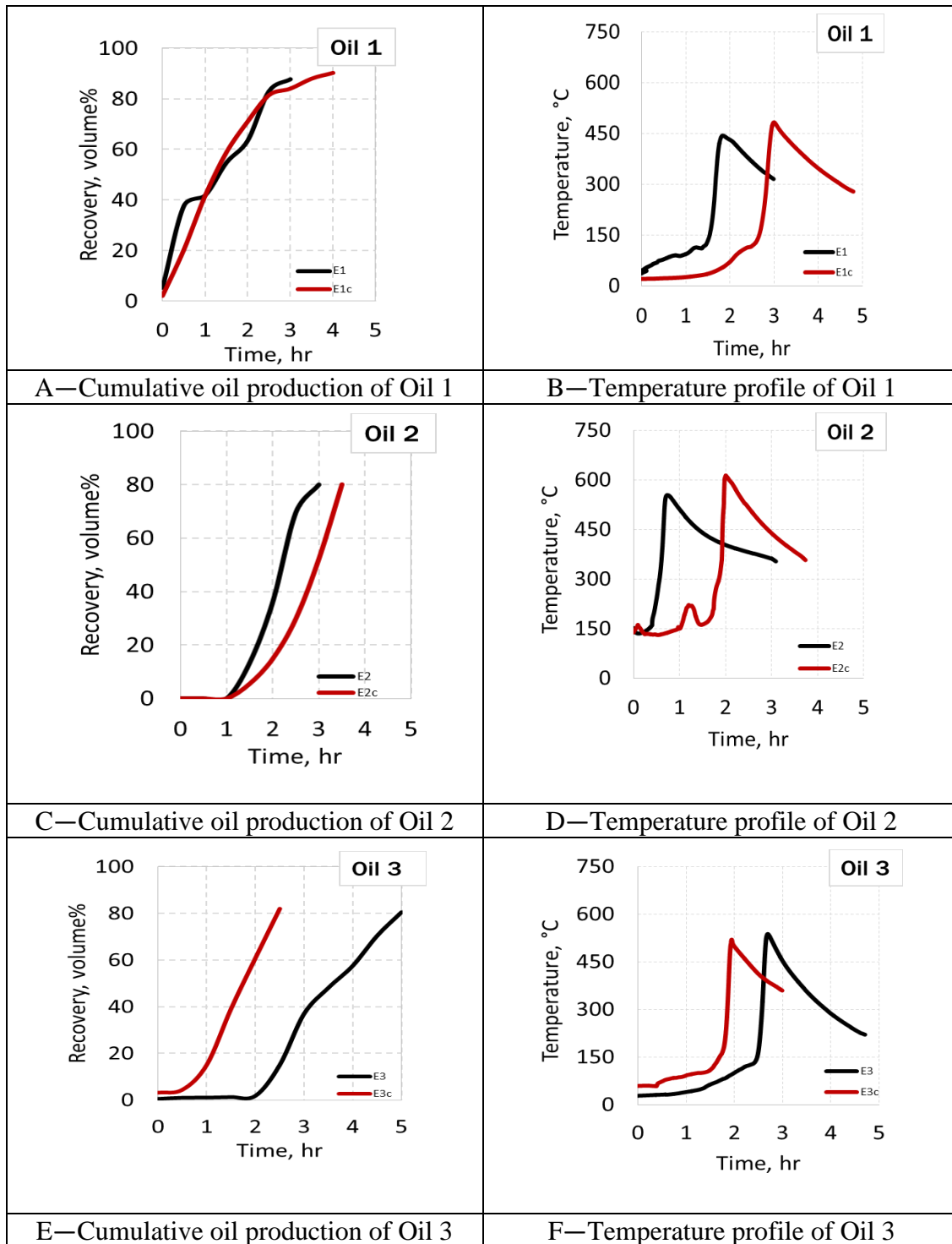
Figure 2.4—The Effect of Clay Presence on Cumulative Oil Recovery (on the Left) and the Temperature Profiles (on the Right) of ISC Experiments. (Temperature Profiles for Each Experiment Represent Fixed Position; 55 Cm below Combustion Tube Run-Stable Zone)

25

Temperature profiles (Figure 2.4 right hand side graphs) show that successful combustion front propagation was achieved for all experiments. Although the ISC process is self-sustained for all experiments, the performance of ISC differs. Oil 2 has the fastest combustion front speed without clay (E2) but the slowest, with the addition of clay (E2c) (Figure 2.4 and Table 2.5). The greatest maximum temperature was obtained for Oil 2 both for with and without clay cases (E2 and E2c), and the lowest maximum temperature was observed for Oil 1 for both with and without clay cases (E1 and E1c) (Table 2.5).

The conclusions drawn through the temperature and oil production graphs can also be supported by gas composition graphs, which reflect the success of ISC if the produced gas is stable. Successful combustion experiments are usually defined through gas composition graphs by the CO_2 concentration at around 12% and with a minimum value of O_2 (Sarathi 1998; Hascakir et al. 2013).

A—CO$_2$ Production of Oil 1

B—O$_2$ Production of Oil 1

C—CO$_2$ Production of Oil 2

D—O$_2$ Production of Oil 2

E—CO$_2$ Production of Oil 3

F—O$_2$ Production of Oil 3
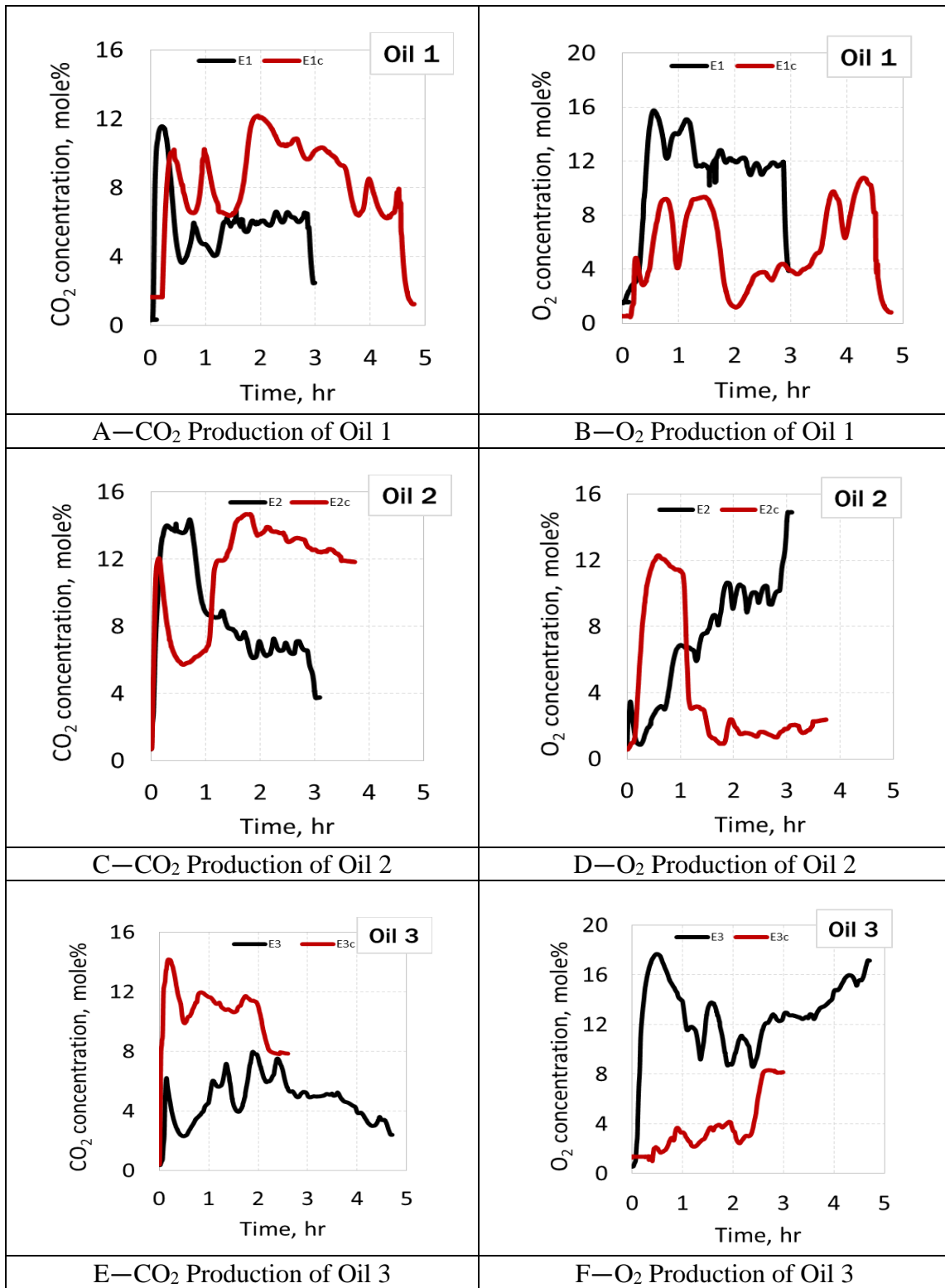
Figure 2.5—The Effect of Clay Presence on Produced CO$_2$ (on the Left) and Produced O$_2$ (on the Right) for All ISC Experiments

27

Figure 2.5 gives the CO_2 and O_2 production rates versus time graphs for all experiments. Table 2.6 provides the summary of Figure 2.5 in terms of maximum, minimum, and average CO_2 and O_2 concentrations. Maximum gas compositions are given for stable zone because when air injection starts, the fuel that is formed under nitrogen injection is consumed first, which results in instability in CO_2 concentration. At stable zone, CO_2 production reaches the maximum value and O_2 at minimum value. Hence, CO_2 and O_2 concentrations in Table 2.6 were given both at stable zone and as the average value which includes the transition period (initial stage). The beginning of the stable period indicates the end of the transition period.

Table 2.6—A Summary of the Maximum, Minimum, and Average Mole Percent of CO_2 and O_2 Produced At Stable Zone

Experiment	E1	E1c	E2	E2c	E3	E3c
Max CO_2 observed at stable zone (mol%)	6.75	10.90	7.60	14.68	7.98	12.0
Min CO_2 observed at stable zone (mol%)	5.44	9.37	6.12	11.83	3.92	9.89
Average CO_2 observed at stable zone (mol%)	6.07	10.20	6.66	13.05	5.56	11.20
Max O_2 observed at stable zone (mol%)	12.80	5.25	10.65	3.01	13.78	4.17
Min O_2 observed at stable zone (mol%)	7.38	3.17	8.86	0.92	8.59	1.02
Average O_2 observed at stable zone (mol%)	11.73	3.99	9.95	1.73	11.57	2.65

It is observed that with the addition of clay, CO_2 production is a lot higher for all types of oil (Figure 2.5 and Table 2.6) and O_2 is a lot lower which indicates more effective consumption of O_2 in the presence of clay. Based on the discussion on combustion tube experimental results, it can be concluded that clay helps to improve combustion efficiency.

28

Assessment of Produced Oil Quality

To investigate the reasons behind the performance differences in ISC, the produced

oil samples were further analyzed first, through viscosity and density measurements. The

oil density (API gravity) was measured under the standard condition (60 °F or 15 °C)

while the viscosity at room temperature (22.3 °C). Table 2.7 displays the viscosity

measurements of the initial and produced oil for all oil samples.

Table 2.7—Comparisons of All Crude Oils Before and After ISC

Experiments		Viscosity (cP) at Room Temperature (22.3 °C)	Density (°API) at Standard Condition (15 °C)
Oil 1	Initial	10,150	12.09
	E1	183.79	12.34
	E1c	18.315	11.18
Oil 2	Initial	208,600	11.56
	E2	611.44	7.08
	E2c	20.773	12.54
Oil 3	Initial	53,000	8.19
	E3	355.2	8.96
	E3c	2.6524	14.44

The table shows that ISC causes significant viscosity reduction in produced oil in

all combustion tube experiments. The visbreaking reactions that occur during ISC is the

primary reason for the produced oil to behave as such (Burger et al. 1985). More rigorous

visbreaking reactions are known to take place with the addition of clay (Kok 2006; Jia et

al. 2012). ISC alone is known to help upgrade crude oil, but the clay's catalytic

characteristic is boosting the result. It can be seen in Table 2.7 that oil viscosity was upgraded to almost 100% with the presence of clay which might be due to catalytic impact of clays and/or due to the increase in the reactive surface area. Note that it has been reported that the smaller granular size of clay can increase fuel burning efficiency by better utilizing the combustion process (Martin 1959; Kok 2006; Jia et al. 2012).

The categorization for the initial and produced oil samples was achieved based on the viscosity and API gravity variations. Figure 2.6 is simply a tool to help visualize the viscosity and density enhancement for the crude oil samples before and after ISC. Accordingly, viscosity over 10,000 cP regardless to its API gravity is called bitumen. Below 10,000 cP viscosity categorization is made based on API gravity, any oil heavier than water (10 °API gravity) is called extra heavy oil, between 10-25 °API gravity is called heavy oil, and above 25 °API gravity is light oil.

As Oil 1 is initially bitumen, after ISC, produced oil indicate heavy oil characteristics (E1). Oil 2 is heavy oil and Oil 3 is a bitumen at reservoir conditions. After ISC, Oil 2 showed extra-heavy oil characteristics at reservoir conditions (E2). Oil 3 indicated as well as extra-heavy oil (E3). After the addition of clay, all produced oil samples at reservoir temperature exhibited heavy oil characteristics (E1c, E2c, and E3c).
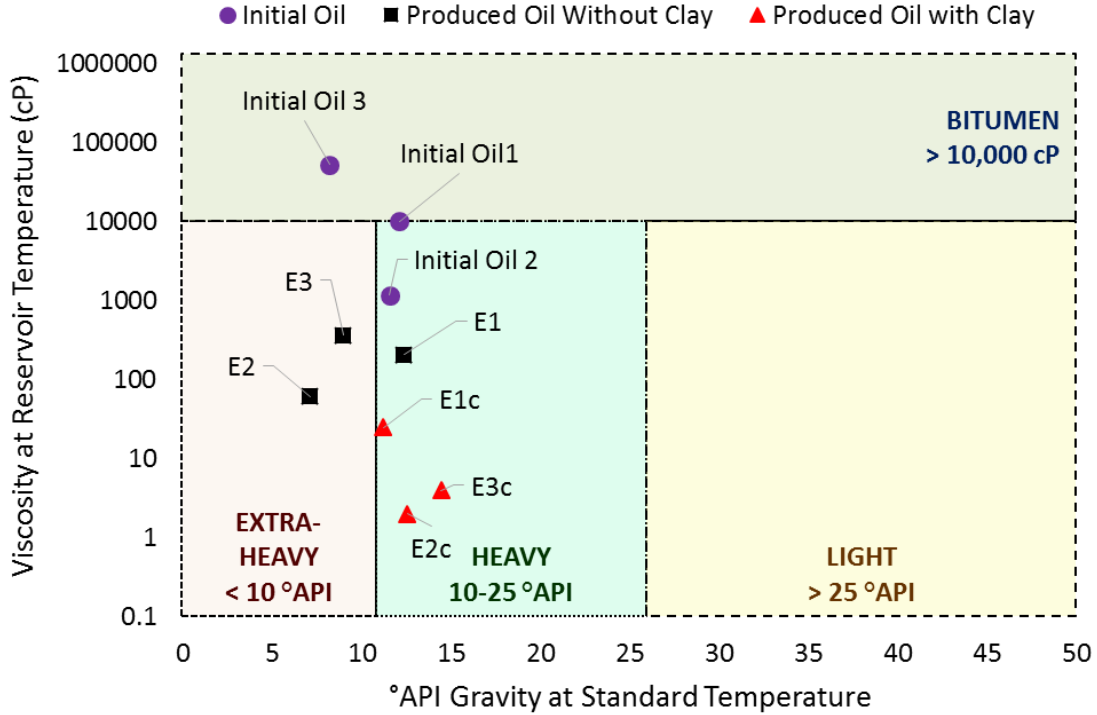
Figure 2.6—Produced Oil Quality in Terms of Viscosity at Reservoir Temperature (T_{res Oil 1}: 24 °C, T_{res Oil 2}: 70.15°C, T_{res Oil 3}: 17°C) and API Gravity at Standard Temperature (15°C)

Combustion process results in thermal cracking of hydrocarbons, hence, significant chemical changes are expected in hydrocarbon molecules. However, molecular level characterization of hydrocarbons is not practical (McCain Jr 1999). Instead, this study investigates these changes through a simplified hydrocarbon grouping by saturates, aromatics, resins, and asphaltenes (SARA) fractionation. Figure 2.7 shows the weight percent of SARA and the ratio of SARA fractions of produced oil to the initial oil. The ratios were calculated by dividing the produced oil SARA weight percent to initial oil SARA weight percent. Hence, while the values over 1 indicate an increase in the amount

31

of individual fractions in produced oil when compared to initial oil; the values below 1 designate the decreased (consumed) amount of individual fractions.

Exp	SARA Fractions (wt%)			
	Sat	Aro	Res	Asp
Initial Oil 1	16.51	37.81	17.1	28.58
E1	12.94	48.52	15.19	23.35
E1c	10.39	62.87	11.35	15.39
Initial Oil 2	10.14	38.01	13.09	38.76
E2	8.87	43.77	10.97	36.39
E2c	8.62	55.92	9.92	25.54
Initial Oil 3	23.60	20.00	21.90	34.30
E3	6.54	58.79	10.43	24.23
E3c	15.72	54.31	14.93	15.04
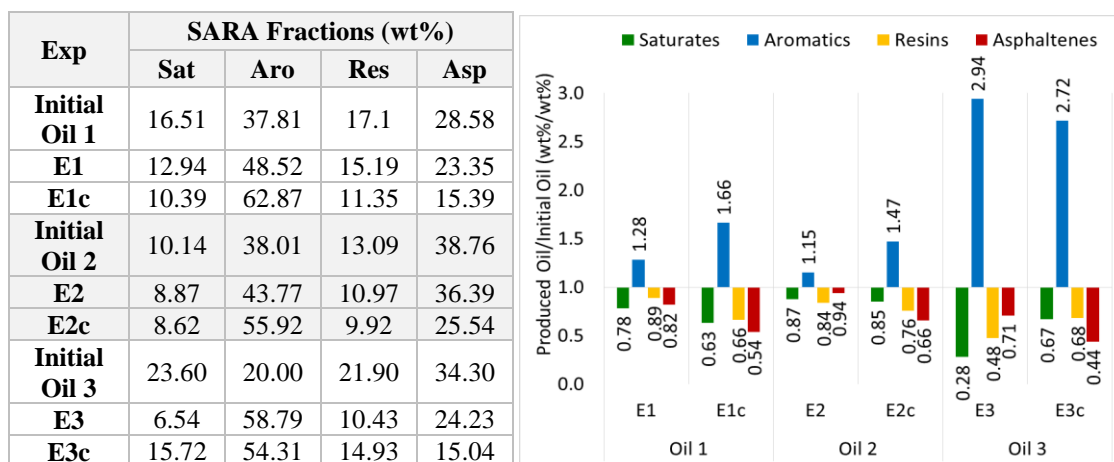
Figure 2.7—Weight Fractions of SARA (on the Left) and the Initial to Produced SARA Ratios (on the Right) Before and After the ISC Tube Test

As expected, since the saturates act as an ignitor during ISC (Wu and Fulton 1971; Sarathi 1998; Castanier and Brigham 2003), saturates fractions were consumed in all experiments regardless of oil composition or clay presence. However, when clay was added, higher ignition temperature was observed and the maximum temperature (Table 2.5) was increased at stable combustion front to a higher temperature except for Oil 3. In all experiments, the amount of the aromatics showed an increase in the produced oil which means aromatics were generated after combustion. Aromatics are good solvents (Speight 1991); hence, the increase in aromatics amount should be the main reason behind mobility enhancement (viscosity reduction) (Table 2.7 and Figure 2.6). However, the amount of

aromatics, type of aromatics, the contribution of other aromatics fractions (resins and asphaltenes), and their solvent type and power also affected the viscosity enhancement (Speight 1991). Thus, all oils were upgraded after ISC with and without clay. The amount of resins in the produced oil decreased compared to the resins content in the initial oil. Resins might have been consumed and produced as aromatics fractions that explained the increment of aromatics fractions which aided the visbreaking reactions. Asphaltenes fractions were also consumed. It might be due to conversion of asphaltenes into coke (fuel) which contributed more efficient combustion of crude oils. And the presence of clays increased the consumption of asphaltenes more which might be due to increased surface area of asphaltenes in the presence of clay (Sulzer 1955; Chu 1981). Note that asphaltenes are the heaviest fraction of crude oil (Speight 1991; Prakoso et al. 2018), thus, consumption of asphaltenes fractions is desired for upgrading the oils.

Still, no direct correlations were obtained between the viscosity, API gravity, and SARA content of produced oil samples. Asphaltenes are the heaviest component of the crude oil (da Silva Ramos et al. 2001; Mullins et al. 2012). Hence, the interaction between asphaltenes and other fractions contributes towards the viscosity enhancement as well.

As heavier components increased in the crude oil samples, viscosity also increased as expected (Figure 2.8 A&B). There is a good correlation to the viscosity increase and light fractions (saturates and aromatics) decrease (Figure 2.8 C). Resins and aromatics are asphaltenes peptizers, so they dissolved asphaltenes and reduce the viscosity (Figure 2.8 D). The summation of saturates and asphaltenes over the summation of aromatics and resins are also known as Colloidal Instability Index (CII) or asphaltenes' precipitation tendency (Pfeiffer and Saal 1940; Saal and Labout 1940; Asomaning 2003). When CII decrease, it means that asphaltenes are more stable and disperse within the crude oil and this also decrease the viscosity (Figure 2.8 E). Finally, in Figure 2.8 F, because of aromatics solvent power, it can reduce the oil viscosity and the asphaltenes content are lower.

A—Viscosity vs Asphaltenes (wt%)	B—Viscosity vs Saturates+Asphaltenes (wt%)
C— Viscosity vs Saturates+Aromatics (wt%)	D—Viscosity vs Aromatics+Resins (wt%)
E— Viscosity vs (Saturates+Asphaltenes /Aromatics+Resins) (wt%/wt%)	F— Viscosity vs Aromatics/Asphaltenes (wt%/wt%)
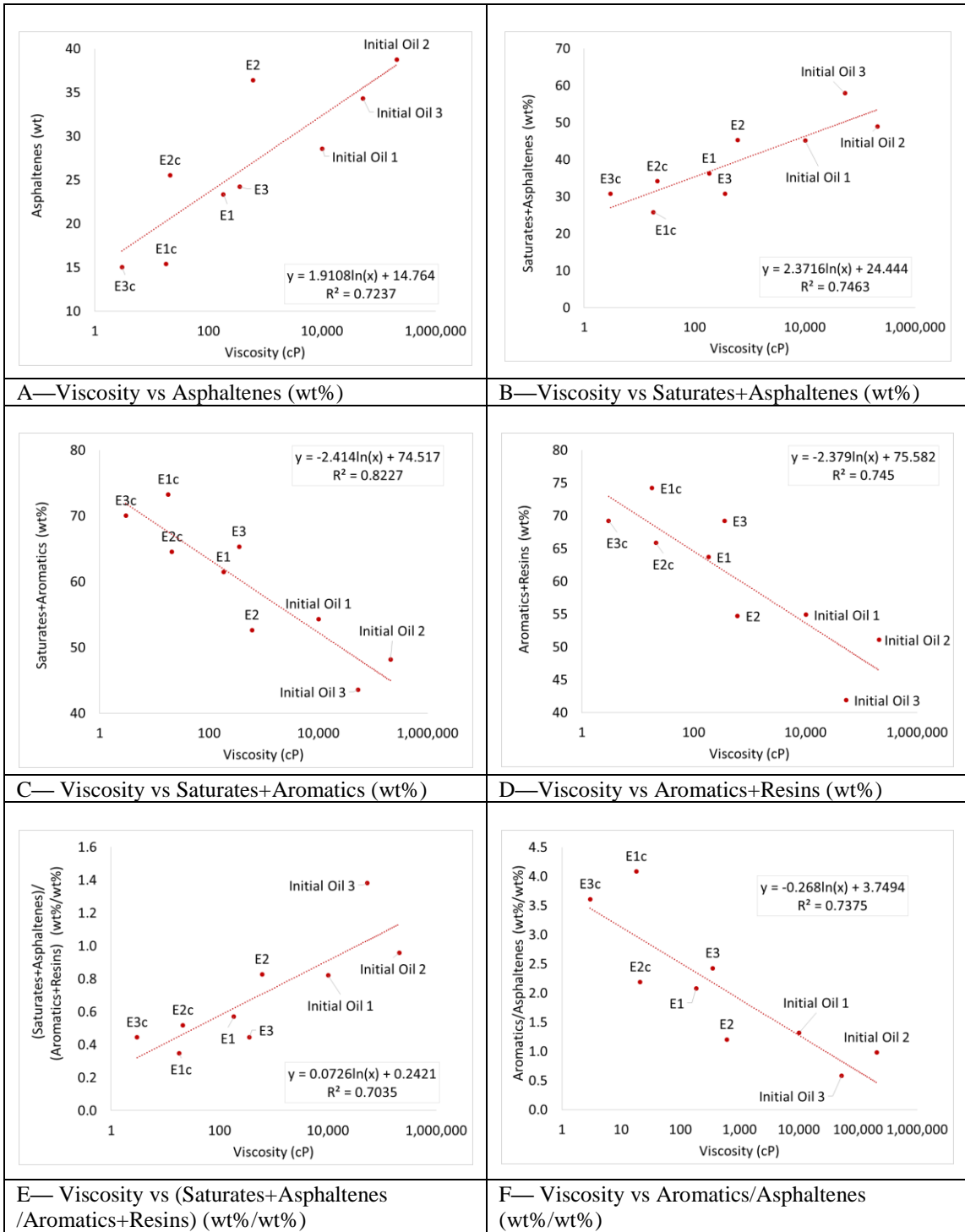
Figure 2.8—The Relation Between Produced Oil Viscosity and the SARA Content

35

Nevertheless, no significant relation was observed between the SARA content and the API gravity. This is probably because the API gravity ranges for these oils (between bitumen, extra-heavy, and heavy oils) (Figure 2.6) were close to each other's category borderline. Consequently, it is difficult to observe any changes in their API gravity; however, viscosity ranges are more extensive and easily distinguishable.

The chemical structures of functional groups in SARA fractions were further analyzed by Fourier Transform Infrared Spectroscopy (FTIR) analysis. Figure 2.9 displays the FTIR spectra for SARA fractions of all produced oil samples. It is important to note that the peaks in the 2300-1800 cm^{-1} (Figure 2.9) can be disregarded due to a noise caused by the ATR diamond crystal (Unur 2013). Table 2.8 lists the summary of absorption peaks and frequencies reported in wavenumber, for molecular bonds and functional groups that will be in the discussion.

Table 2.8—Interpretation of Infrared Absorption Frequencies based on Molecular Bonds and Functional Groups (Socrates 2004; Stuart 2004)

Molecular Motion	Wavenumber, cm^{-1}
O-H, N-H stretch	3600-3500
=CH stretch aromatics	3100-3000
C-H stretch (-CH$_2$, -CH$_3$ groups)	3000-2850
C=O stretch carbonyl	1760-1665
N-H bend / C=C stretch (aromatics)	1650-1430
-CH$_2$ and -CH$_3$ bends	1470-1300
C-O	1310-1000
S=O stretch	1060-1020
C-H bend	1000-600
CH$_2$ bend (4 or more C atoms)	720

A—FTIR for Saturates Fraction

B—FTIR for Aromatics Fraction

C— FTIR for Resins Fraction

D— FTIR for Asphaltenes Fraction
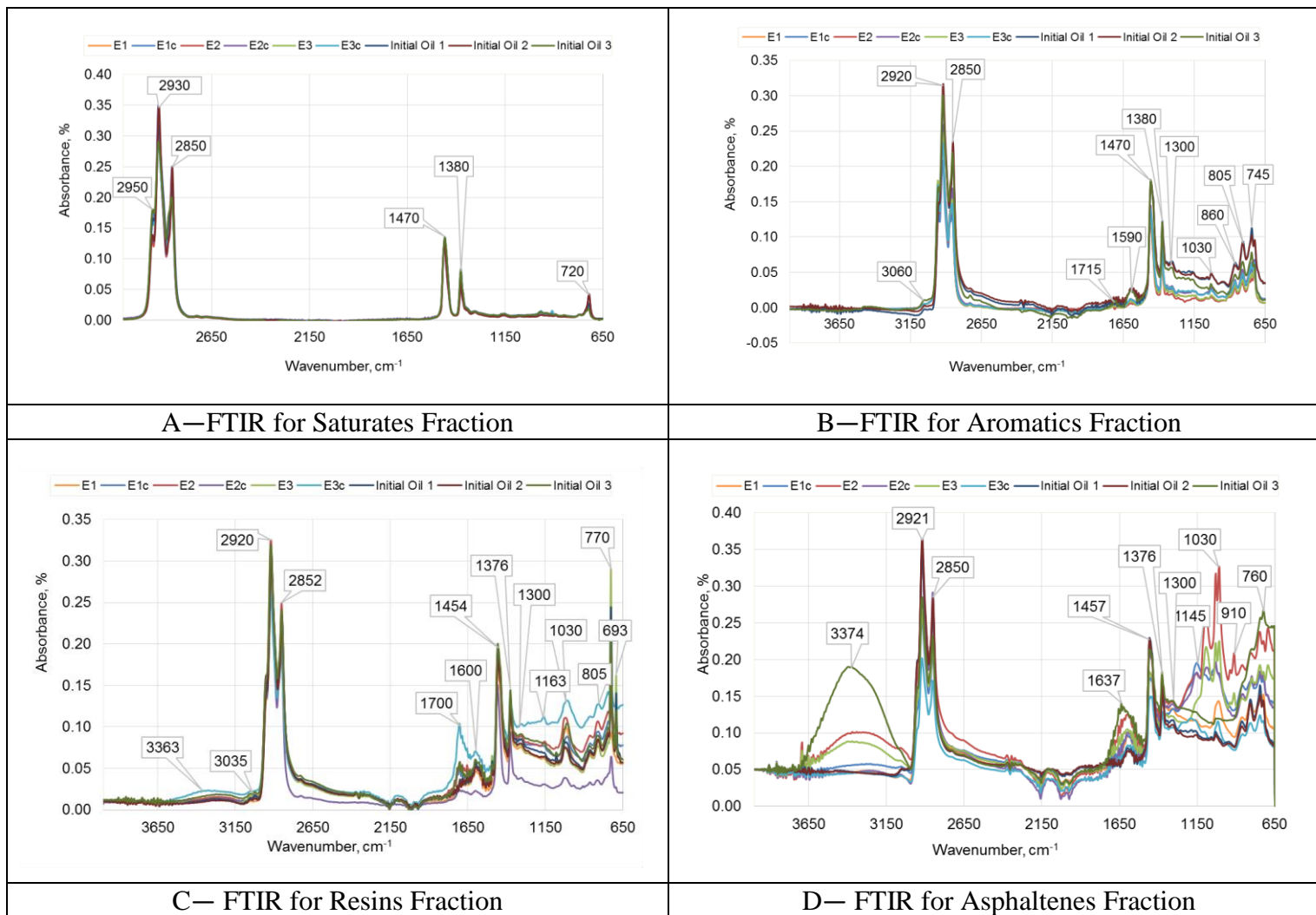
Figure 2.9—FTIR Spectra for SARA Fractions of All Produced and Initial Oil Samples

Saturates fraction (Figure 2.9 A), has both C-H stretch and C-H bends that represent the n-alkane in the fraction. From Figure 2.9 A, –CH_3 groups exhibit a significant peak around 2950 cm^{-1} while –CH_2 bonds are shown by the peak at 2850 cm^{-1} (Benkhedda et al. 1992). Significant peaks in the range of 1470 and 1380 cm^{-1} are associated with bending vibrations of methylene and methyl groups (Wilt et al. 1998). Finally, in the region where CH_2 bends are having four or more C atoms shown by the peak at 720 cm^{-1}, it represents very long aliphatic hydrocarbon chains (Musser and Kilpatrick 1998; Krump et al. 2005).
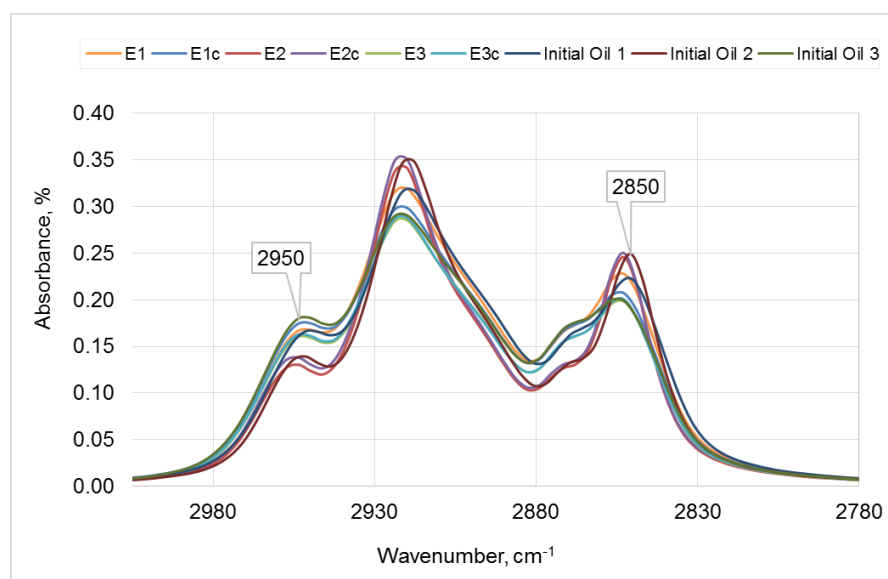
Figure 2.10—Zoom in on FTIR Spectra of Saturates Fraction from Figure 2.9 A into C-H Stretch (-CH₂, -CH₃ groups) (3000-2850 cm⁻¹)

38

When zooming into the C-H stretch peak (Figure 2.10), it is observed that Oil 2's saturates have a slightly lower CH aliphatic chains than Oil 1 and Oil 3 for both cases with and without clay. This agrees with the saturates weight percentage reported in Figure 2.7, where Oil 2 has a lower saturates weight percentage as compared to other fractions. The high absorbance of C-H stretch (3000-2850 cm^{-1}) for E1 (Oil 1) may cause saturates to ignite faster (Castanier and Brigham 2003) in E1 and E1c; which leads to faster oil recovery (Figure 2.4 on the left) as compared to other experiments.

Aromatics are the main fraction that aid the visbreaking reaction in ISC (Mamora et al. 1984; Ismail et al. 2016; Ismail et al. 2018). Hence, it is crucial to understand its role by looking at its consumption through FTIR. Aromatics fraction (Figure 2.9 B) consists of several functional groups and molecular bonds, as listed in Table 2.8. To investigate the changes in molecular bonds after ISC, we zoomed into the fingerprint region of the aromatics fraction (Figure 2.11). The fingerprint region (ranging from 1800 to 650 cm^{-1} wavenumber) usually contains a very complicated series of absorptions. These are mainly due to all manner of bending vibrations within the molecule (Rohman and Man 2010).

A—FTIR for Oil 1 Aromatics Fraction (Fingerprint region)

B—FTIR for Oil 2 Aromatics Fraction (Fingerprint region)

C—FTIR for Oil 3 Aromatics Fraction (Fingerprint region)
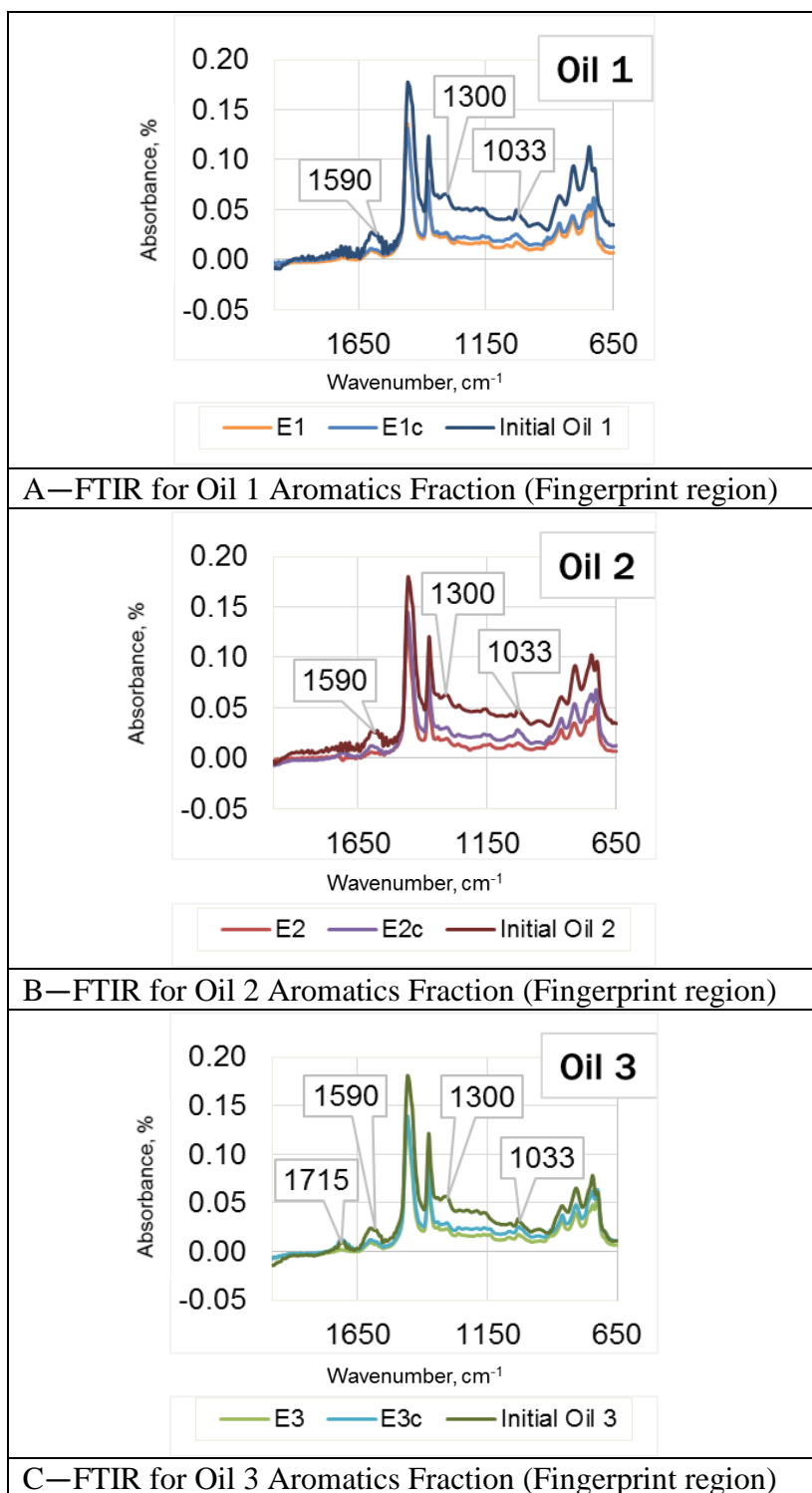
Figure 2.11—Zoom in on FTIR Spectra of Aromatics Fraction from Figure 2.9 B into Fingerprint Region (1800-650 cm⁻¹)

Based on the peaks seen in the aromatics fraction, the wavelengths indicate that the molecular bonds of C=C aromatics stretch (1650-1430 cm^{-1}), C-O aromatics (1310-1000 cm^{-1}), and S=O stretch (1060-1020 cm^{-1}) are present (Figure 2.11 and Table 2.8). However, an additional peak was seen in Oil 3 (Figure 2.11 C) that was not present in Oil 1 and Oil 2 in the range of 1760-1665 cm^{-1} (Table 2.8), suggested it was C=O carbonyl functional group. For all oil compositions (Figure 2.11), the double bond and oxygenated functional groups in aromatics reduced after combustion for both cases with and without clay. For cases with clay, the absorbance was slightly higher than the cases without clay for the fingerprint region. It should be noted that fingerprint region, generally associated to impurities such as oxygen and sulfur. It is obvious that these impurities, present in hydrocarbon molecules initially in aromatics fractions were reduce in aromatics fractions of produced oils.

Resins (Figure 2.9 C), FTIR spectra exhibit many similarities with aromatics (Figure 2.9 B). However, it can be discerned that resins display higher absorbance values in the fingerprint region as compared to aromatics. This trend suggests that resins contain more substantial amounts of heteroatoms, which is the cause for it being a heavier fraction. Thus, the fingerprint region of resins fraction is zoomed in to discuss the changes of molecular signatures after ISC (Figure 2.12).

A—FTIR for Oil 1 Resins Fraction (Fingerprint region)

B—FTIR for Oil 2 Resins Fraction (Fingerprint region)

C—FTIR for Oil 3 Resins Fraction (Fingerprint region)
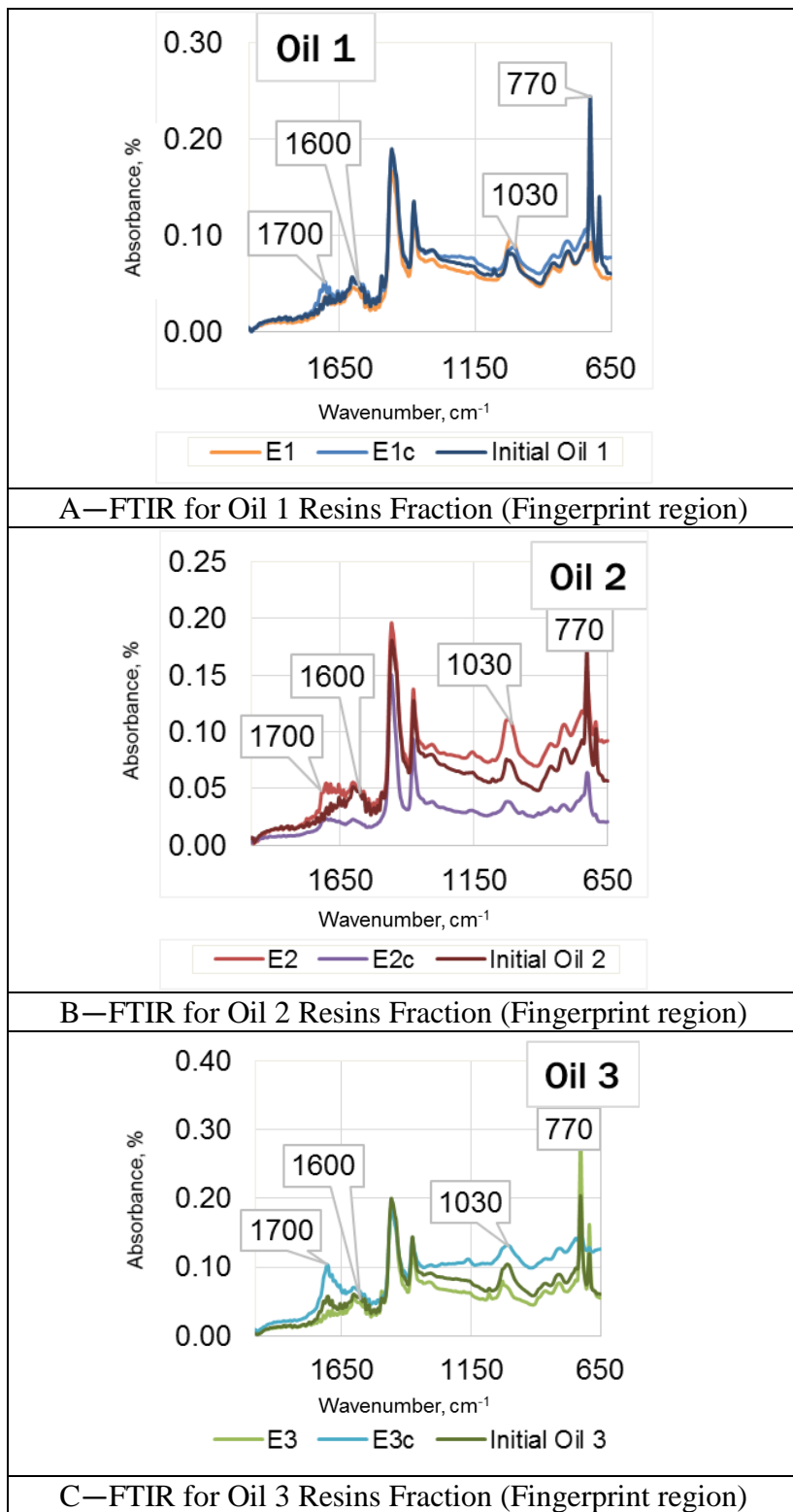
Figure 2.12—Zoom in on FTIR Spectra of Resins Fraction Figure 2.9 C into Fingerprint Region (1800-650 cm⁻¹)

42

From the fingerprint region of the resins (Figure 2.12), these peaks can be seen; C=O stretch carbonyl (1760-1665 cm^{-1}), C=C stretch aromatics (1650-1430 cm^{-1}), S=O stretch (1060-1020 cm^{-1}) and C-H bend (1000-600 cm^{-1}) (Socrates 2004; Stuart 2004). There is an insignificant change of absorbance values for Oil 1 (Figure 2.12 A) after the combustion tube experiment. However, Oil 2 (Figure 2.12 B) and Oil 3 (Figure 2.12 C) are showing interesting results. Oil 2 with clay (E2c) (Figure 2.12 B purple curve) has less oxygenated compound (1760-1665 cm^{-1}) than the initial oil (Figure 2.12 B red curve). Nevertheless, without clay (Figure 2.12 B orange curve), it was less than the initial oil (Figure 2.12 B red curve). On the other hand, Oil 3 with clay (E3c) (Figure 2.12 C blue curve) has more oxygenated compound than the initial oil (Figure 2.12 C dark green curve). Less without clay (Figure 2.12 C light green curve). These oxidation products (oxygenated functional groups: alcohols, aldehydes, ketones, and carboxylic acids) undergo oxidation reactions at a higher temperature, producing gases that indicate the completion of combustion (Verkoczy 1993; Kok and Karacan 2000). Another finding is that the C-H bend absorbance of resins (Figure 2.12) (770 cm^{-1} wavenumber) for all crude oils are relatively higher than the aromatics fraction (Figure 2.11). This might be due to contamination of resins with toluene during SARA separation.

Asphaltenes (Figure 2.9 D) have varying types of bonds in its structure; O-H stretch (3600-3500 cm^{-1}), C-H stretch (3000-2850 cm^{-1}), C=C stretch (1650-1430 cm^{-1}), C-O (1310-1000 cm^{-1}), S=O (1060-1020 cm^{-1}), and C-H bend (1000-600 cm^{-1}) (Socrates 2004; Stuart 2004) that makes it the heaviest and most complex fraction of the crude oil (da Silva Ramos et al. 2001; Mullins et al. 2012). Figure 2.13 represents the zoom in on Figure 2.9 D in the O-H region (3600-3500 cm^{-1}) and fingerprint region (1800-650 cm^{-1}).

In the O-H region (3600-3500 cm^{-1}), Oil 1 (Figure 2.13 A1), is not showing any peak which indicates that there is probably no O-H bond present in the initial and the produced oil of Oil 1. For Oil 2 (Figure 2.13 A2), there was a peak after the combustion of Oil 2 without clay (E2) (orange curve) which might be associated to formed water during ISC that is supported also by the signatures in fingerprint region. However, no peak was observed for the combustion of Oil 2 with clay (E2c) (Figure 2.13 A2 purple curve). A high peak of O-H in initial Oil 3 was seen in Figure 2.13 A3 (dark green curve). This is probably due to the emulsified water content of initial Oil 3's asphaltenes. However, the emulsified water was reduced after combustion for Oil 3 (Figure 2.13 A3 blue and light green curve). Clay addition removed the emulsified water content of crude oil attached to asphaltenes (Khvostichenko and Andersen 2008).

A1—FTIR for Oil 1 Asphaltenes Fraction (O-H region)	B1—FTIR for Oil 1 Asphaltenes Fraction (Fingerprint region)
A2—FTIR for Oil 2 Asphaltenes Fraction (O-H region)	B2—FTIR for Oil 2 Asphaltenes Fraction (Fingerprint region)
A3—FTIR for Oil 3 Asphaltenes Fraction (O-H region)	B3—FTIR for Oil 3 Asphaltenes Fraction (Fingerprint region)
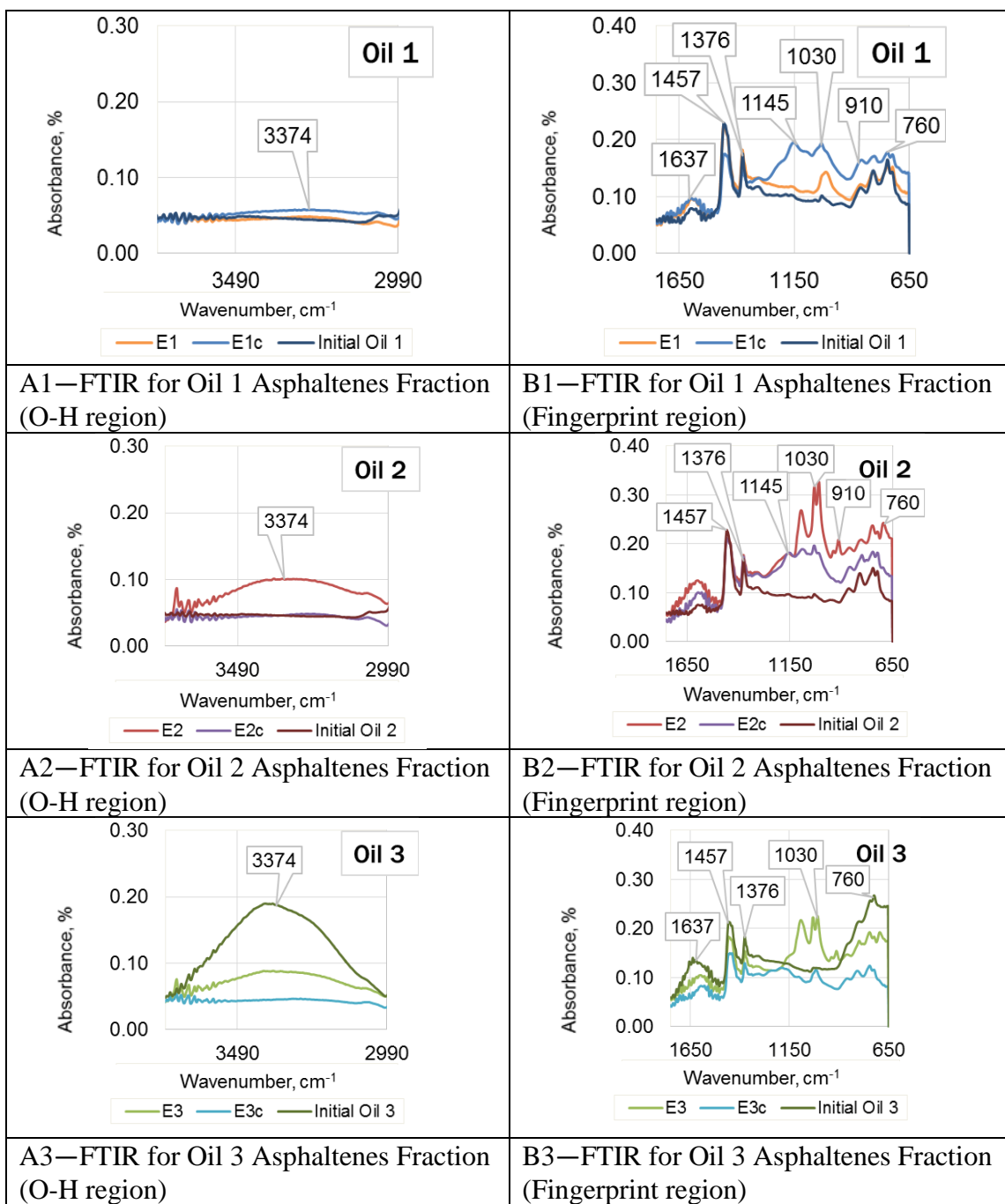
Figure 2.13—Zoom in on FTIR Spectra of Asphaltenes Fraction Figure 2.9 D into O-H region (3600-3500 cm^{-1}) (on the left) and Fingerprint Region (1800-650 cm^{-1}) (on the right)

In fingerprint region (1800-650 cm^{-1}), oxygenated functional groups, such as esters, ketones, aldehydes, carboxylic acids, and carbonyls, are found within the 1735-1650 cm^{-1} regions (Calemma et al. 1995; Kar et al. 2014). In the fingerprint region (1800 to 650 cm^{-1}) (Figure 2.13 B), combustion has increased the absorbance peak of these oxygenated groups in asphaltenes for both Oil 1 (Figure 2.13 B1) and Oil 2 (Figure 2.13 B2), except Oil 3 (Figure 2.13 B3). Clay addition in Oil 2 (E2c) (Figure 2.13 B2 purple curve) and Oil 3 (E3c) (Figure 2.13 B3 blue curve) decreased the absorbance peak in the range of 1310-1000cm^{-1} which represents the alcohol functional group (C-O) bond (Socrates 2004; Stuart 2004). On the other hand, for Oil 1, alcohol increased with the addition of clay (E1c) (Figure 2.13 B1 light curve).

Another type of heteroatoms often found in crude oils are sulfurs and can be detected in fingerprint region , especially in asphaltenes which are generally in the form of sulfoxides (1030 cm^{-1}), aliphatic sulfides, thiols (2600-2400 cm^{-1}), and thiophenes (700-600 cm^{-1}) (Green et al. 1993). Sulfoxides' signature (1030 cm^{-1}) can be seen in Figure 2.13 B especially more significant in Oil 2 and Oil 3 after combustion (E2 and E3). Generally, absorbance for S=O (1060-1020 cm^{-1}), increased for all types of crude oils (Figure 2.13 B) after combustion. Both Oil 2 (Figure 2.13 B2 purple curve) and Oil 3 (Figure 2.13 B3 blue curve) with clay are showing less absorbance peaks than the cases without clay. However, it is the other way around for Oil 1 (Figure 2.13 B1). The addition of clay (E1c) (Figure 2.13 B1 light blue curve) has increased the S=O bonds within the ranges of 1060-1020 cm^{-1}. It means cracking reaction alter the molecular structure of sulfur containing functional group.
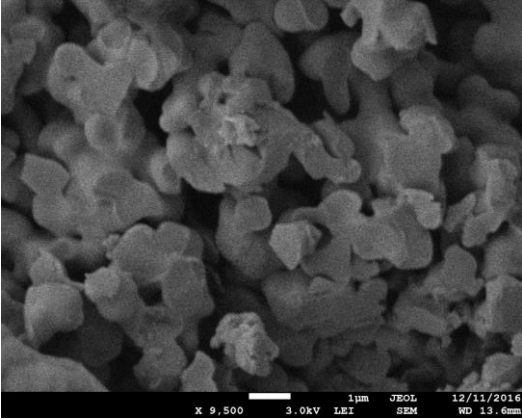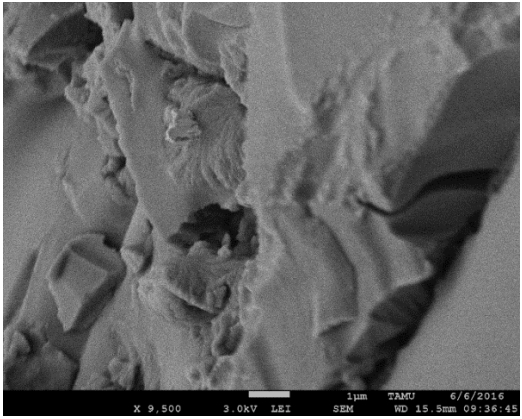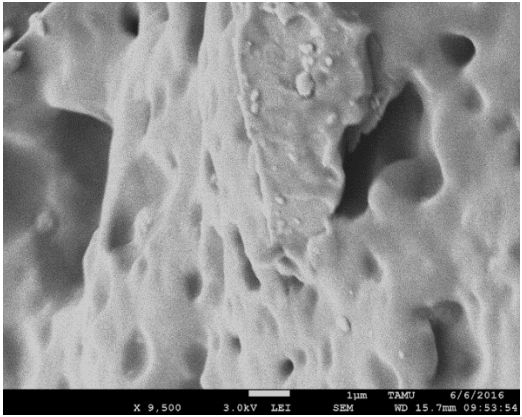
FTIR spectra provide essential information on the chemical changes of each crude oil sample after the ISC. However, it is too complicated to understand the details of these changes. Hence, SEM-EDS analyses were conducted to couple FTIR results to better analyze compositional change occurring during ISC. However, since SEM-EDS analysis can only be done on solids, these analyses were achieved only on asphaltenes. Moreover, it should be noted that SEM-EDS is a surface analysis method and can only detect elements on 1-5 µm depth of a solid sample (Klein and Hercules 1983; Lee et al. 2002). Table 2.9 shows the EDS analysis of the initial and produced asphaltenes. The SEM images of asphaltenes fractions are as shown in Figure 2.14 to Figure 2.16.

Table 2.9—EDS Analysis for the Initial and Produced Asphaltenes
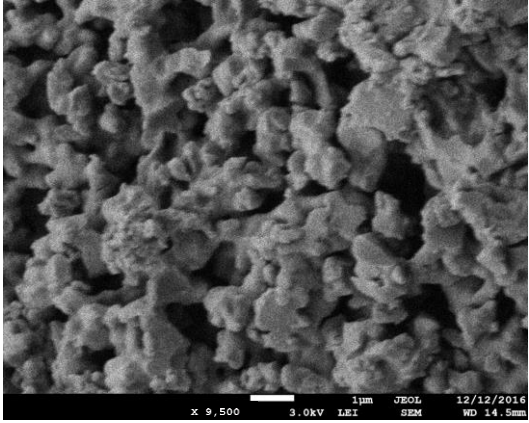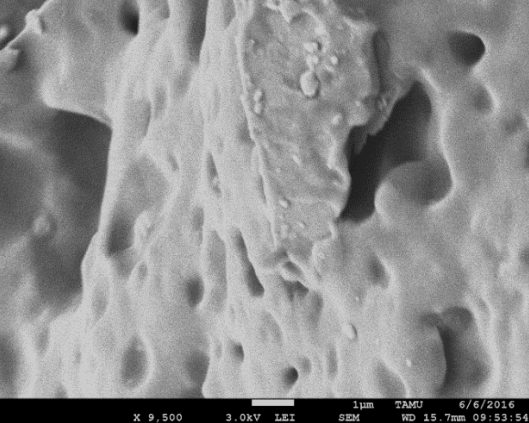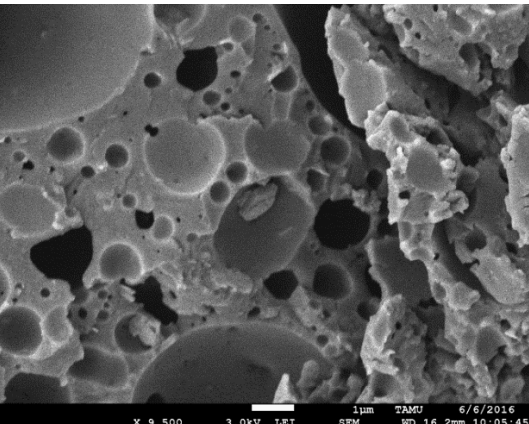
Element	Atomic Weight (%)								
	Oil 1			Oil 2			Oil 3		
	Initial	E1	E1c	Initial	E2	E2c	Initial	E3	E3c
C	90.91	97.85	89.46	91.49	97.91	93.62	92.69	94.60	92.19
O	2.50	-	7.21	3.22	-	5.23	5.44	-	6.43
S	6.59	2.15	3.33	5.00	2.09	1.15	1.09	5.40	1.38
Na	-	-	-	-	-	-	0.41	-	-
Cl	-	-	-	-	-	-	0.15	-	-
Al	-	-	-	-	-	-	0.22	-	-
Si	-	-	-	0.17	-	-	-	-	-
V	-	-	-	0.12	-	-	-	-	-

Table 2.9 illustrates that for all experiments without clay (E1, E2, and E3), carbon increases in produced oil asphaltenes as compared to the initial oil. However, for the cases with clay, carbon decreased for Oil 1 (E1c) but increased for Oil 2 (E2c) and Oil 3 (E3c). Oxygen concentration was detected on asphaltenes surfaces for the experiment conducted
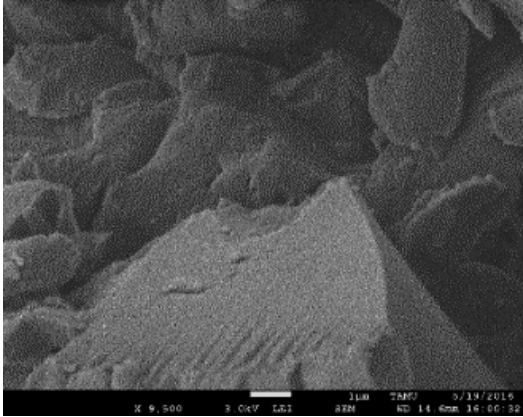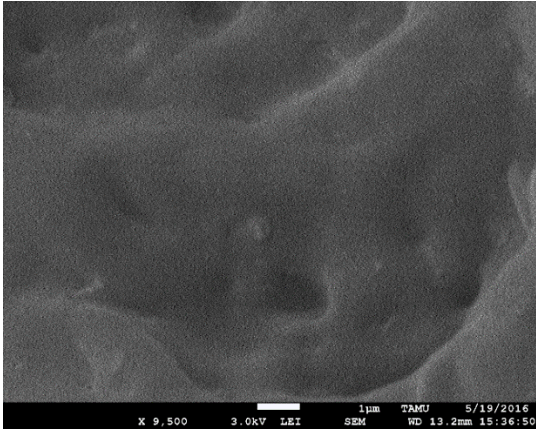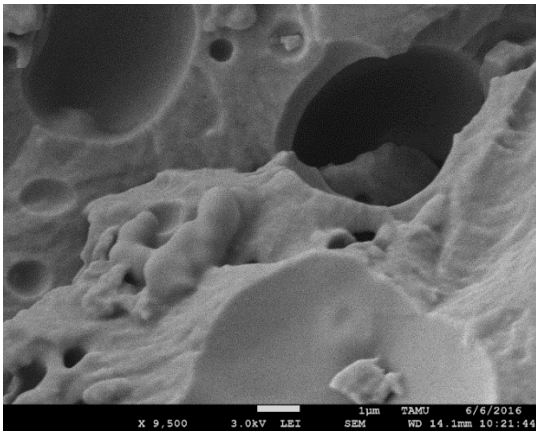
with clay. It might be due to oxygenation of asphaltenes surface which may indicate higher oxidative feature of asphaltenes in the presence of clay or it might be due to formed oxygenated hydrocarbon products which lay at the surface of asphaltenes mostly. Initial Oil 3 has Na and Cl, and the source of Na and Cl elements might be due to interaction of asphaltenes with the reservoir brines (Tang and Morrow 1999). Oil 2 has V and Si since Oil 2 has the greatest amount of V and Si (Table 2.3); which could be even observed by EDS. For Oil 1 (E1 and E1c), sulfur decreased, or surface sulfur decreased, and for Oil 3 (E3 and E3c), it increased, or surface sulfur increased. Either sulfur is deposited on the rock or has changed the chemical bond in the oil. The sulfur results obtained with EDS analyses are also supported by the FTIR spectra of asphaltenes given in Figure 2.13 B.

Asphaltenes's Type	SEM Images at 9500x Magnification
Initial Oil 1	
E1	
E1c	

Figure 2.14—SEM Images of the Initial and Produced Asphaltenes of Oil 1 at 9500x Magnification

Asphaltenes's Type	SEM Images at 9500x Magnification
Initial Oil 2	
E2	
E2c	

Figure 2.15—SEM Images of the Initial and Produced Asphaltenes of Oil 2 at 9500x Magnification

Asphaltenes's Type	SEM Images at 9500x Magnification
Initial Oil 3	
E3	
E3c	

Figure 2.16—SEM Images of the Initial and Produced Asphaltenes of Oil 3 at 9500x Magnification

Further, Scanning Electron Microscopic (SEM) images of the initial and produced asphaltenes surfaces (Figure 2.14 to Figure 2.16) are acquired. They show the smoother surfaces after ISC without presence of clay (E1, E2, E3) when compared to the initial asphaltenes surfaces. However, in the presence of clay (E1c, E2c, E3c), chiroform-like structures were observed on the produced asphaltenes surfaces, which might indicate the increase in surface area due to clay presence.

To have a complete picture on assessment of compositional differences after ISC, spent rock samples were visualized first (Figure 2.17) and then SEM-EDS analyses were conducted on the spent rock samples (Appendix 2B and Table 2.10). The spent rock samples were divided into zones based on the color and the texture differences observable with bare eyes through visual inspection (Figure 2.17).
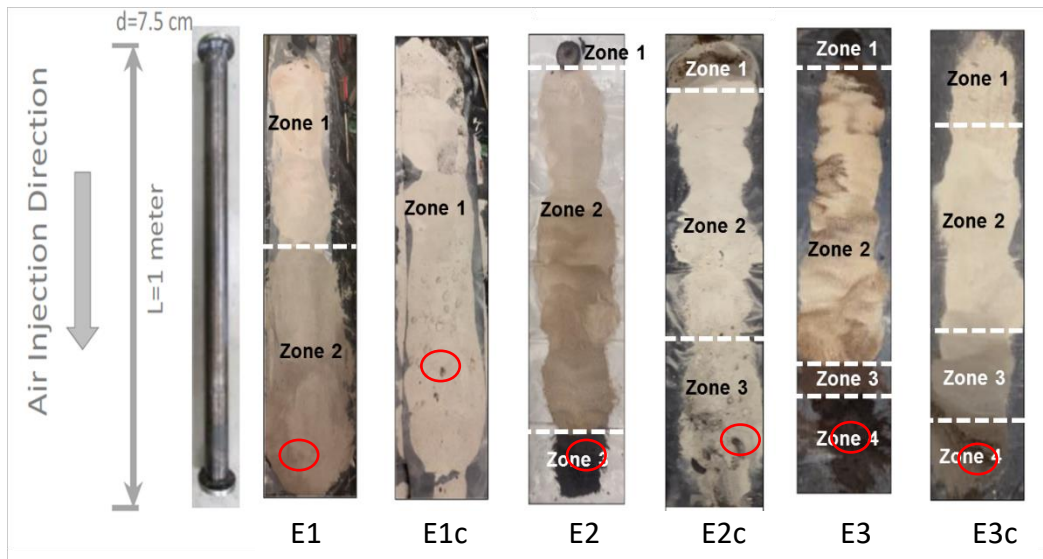
Figure 2.17—Spent Rock Zones in ISC based on Different Colors and Textures (Red Circle indicates the Spent Rock Produced Coke Collected in the Coke Zone)

Accordingly, E1 has two zones (burned zone and ash zone), E1c one zone (burned zone), E2 three zones (pyrolysis zone, burned zone, and unburned zone), E2c three zones (pyrolysis zone, burned zone, and unburned zone), E3 four zones (pyrolysis zone, burned zone, coke zone, and unburned zone), and E3c four zones (pyrolysis zone, burned zone, coke zone, and unburned zone). Then, SEM-EDS analyses were done on the samples collected from each zone. Summary of EDS results is given in Table 2.10.

Table 2.10 gives elemental composition for the initial sand and clay used to prepare reservoir rock and for spent rock samples. As the color of zones gets darker in Figure 2.17, carbon atomic weight percent increase in EDS results given in Table 2.10, Lighter zones are having higher oxygen content. Al and Si amount on spent rock samples provide important information on how much ash and coke (fuel) deposited on spent rock samples. For instance, for the sample from Zone 1 of E2, Al and Si was detected led than the Al and Si contents of initial sand and clay with high amount of carbon deposition and same observation can be done for Zone 1 from E2c, E3, and E3c. Sulfur deposition was observed when carbon deposition is high on spent rock.

Table 2.10—Spent Rock Analyses with Energy Dispersive Spectroscopy (EDS)
(Visual of each zone is given in Figure 2.17)

Exp / Elements			E1		E1c	E2			E2c			E3				E3c			
	Sand	Clay	Zone 1	Zone 2	Zone 1	Zone 1	Zone 2	Zone 3	Zone 1	Zone 2	Zone 3	Zone 1	Zone 2	Zone 3	Zone 4	Zone 1	Zone 2	Zone 3	Zone 4
C	6.9	2.4	2.43	5.05	1.56	15.82	5.4	62.04	14.31	-	4.73	59.07	18.48	51.55	61.58	28.09	7.59	3.98	7.66
O	55.4	69.6	69.27	64.49	72.10	68.93	75.48	34.61	61.59	73.1	67.50	37.37	62.38	41.83	34.61	59.42	67.71	68.5	69.04
Al	0.9	13.2	12.69	11.57	11.71	0.41	0.36	0.54	8.20	9.0	11.61	0.26	0.32	4.02	2.19	2.73	2.36	6.23	5.51
Si	26.2	14.2	15.2	18.07	14.34	14.38	18.55	2.28	14.11	17.9	14.76	2.91	18.44	2.60	1.03	9.36	22.34	20.65	17.31
S	-	-	-	-	-	0.28	0.14	0.52	0.70	-	0.33	0.39	0.37	-	0.22	0.23	-	0.12	0.11
Na	-	-	-	-	-	-	-	-	0.24	-	-	-	-	-	-	-	-	-	-
Mg	-	-	-	-	-	0.15	-	-	-	-	-	-	-	-	-	-	-	-	-
K	-	0.4	-	-	0.29	-	-	-	0.54	-	0.75	-	-	-	-	0.17	-	0.37	0.31
Fe	-	-	-	-	-	0.04	-	-	0.16	-	0.32	-	-	-	-	-	-	0.15	0.06
Ca	-	-	-	-	-	-	0.05	-	0.15	-	-	-	-	-	-	-	-	-	-
Ni	-	-	-	-	-	-	0.03	-	-	-	-	-	-	-	-	-	-	-	-
Cl	-	-	-	-	-	-	-	-	-	-	-	-	-	-	-	0.31	-	-	-

Atomic Weight (%)

54
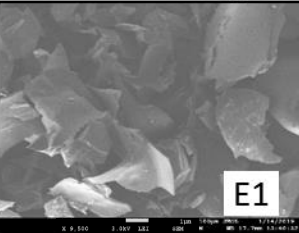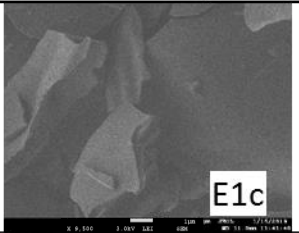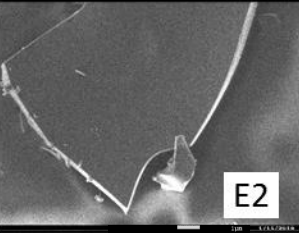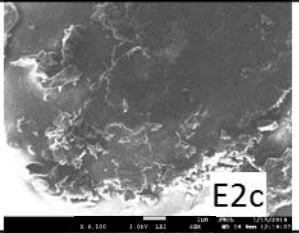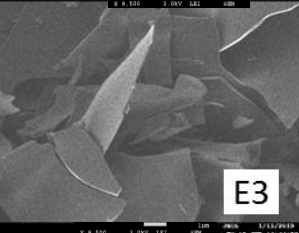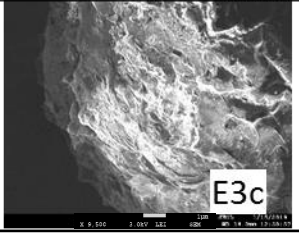
The coke (fuel) generated under oxygen environment was further analyzed with EDS. Sample locations for these tests are shown with red circles on Figure 2.17. These zones show high carbon and sulfur content. In ISC literature, coke is defined as carbon-rich residue (Bagci 1998) while our EDS results confirm this truth, they also show that coke has sulfur in its chemical composition. In some cases it may also have Vanadium. Al and Si given in Table 2.11) is due to sand and clay and not expected to be in the chemical structure of crude oil or coke.

Table 2.11—Spent Rock Coke Analyses with Energy Dispersive Spectroscopy (EDS)

Element	Atomic Weight (%)					
	Oil 1		Oil 2		Oil 3	
	E1	E1c	E2	E2c	E3	E3c
C	88.9	81.3	92.1	86.2	83.98	88.62
O	6.4	16.86	2.93	11.67	12.24	8.24
S	4.7	1.78	4.82	0.82	3.69	2.96
Al	-	0.03	0.1	0.24	0.09	0.14
Si	-	0.02	-	1.07	-	0.04
V	-	0.02	0.05	-	-	-
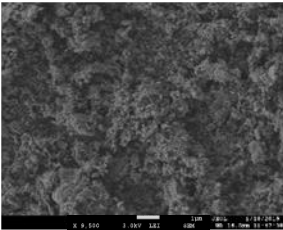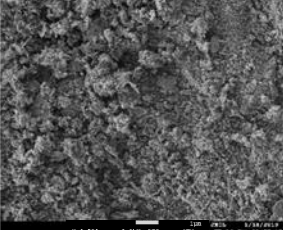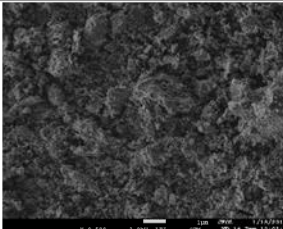
Smooth surface   Rough surface
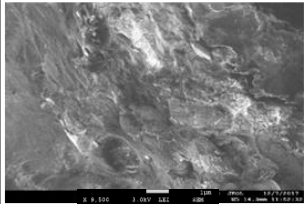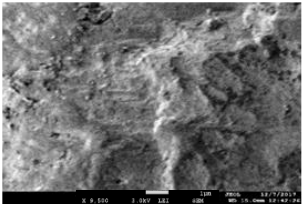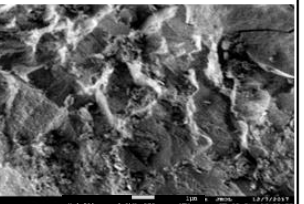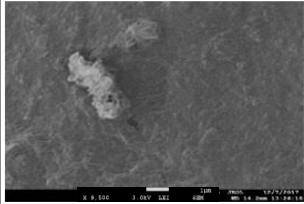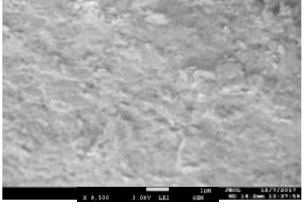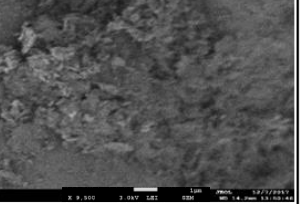
Figure 2 A1—SEM Analysis for the Spent Rock Produced Coke at 400x Magnification (Samples to be Analyzed Were Collected from the Locations Given with Red Circles in Figure 2.17)

Appendix 2B
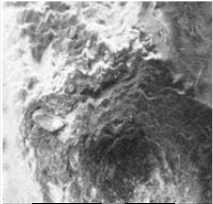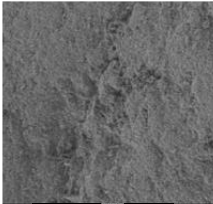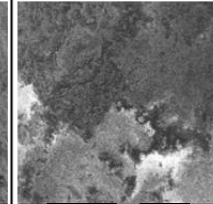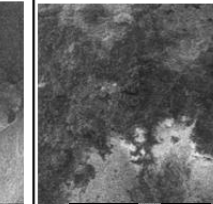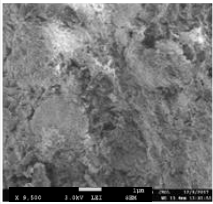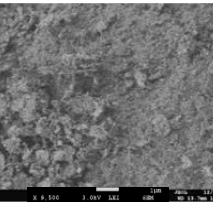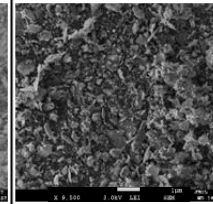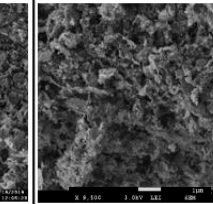
Experiment	Zone 1	Zone 2
E1		

Experiment	Zone 1
E1c	

Figure 2 B1—SEM Analysis for Oil 1 Spent Rock at 400x Magnification (Refer Figure 2.17 for Zone Visualization)

Experiment	Zone 1	Zone 2	Zone 3
E2			
E2c			

Figure 2 B2—SEM Analysis for Oil 2 Spent Rock at 400x Magnification (Refer Figure 2.17 for Zone Visualization)

Experiment	Zone 1	Zone 2	Zone 3	Zone 4
E3				
E3c				

Figure 2 B3—SEM Analysis for Oil 3 Spent Rock at 400x Magnification (Refer Figure 2.17 for Zone Visualization)

3. ESTIMATION OF IN-SITU COMBUSTION FIELD PARAMETERS THROUGH ANALYTICAL MODELING OF THE COMBUSTION TUBE TEST RESULTS AND REACTION KINETICS PARAMETER

Introduction

In-situ combustion (ISC) is a complicated process that requires to develop understanding on chemical reactions occurring in crude oil, reservoir rock, and their mutual interactions at elevated temperatures and pressures. While performance estimation of ISC, like other enhanced oil recovery (EOR) methods, necessitates full-scale analysis through compositional simulation due to the involvement of complex chemical reactions occurring in each ISC zone and due to heterogeneous nature if oil reservoir, full-field simulation of ISC by numerical means has not been accomplished yet (Burger 1972; Crookston et al. 1979; Burger et al. 1985; Sarathi 1998; Glatz 2011). Moreover, since these zones are moving along the reservoirs, field performance estimation of each moving zone with varying thickness and at varying temperatures is becoming a big challenge by using conventional reservoir simulations.

For the compositional simulation of the ISC, several studies have investigated the kinetics parameters of different oil samples (Akin et al. 2000; Kok and Karacan 2000; Kok 2002, 2006). While crude oil composition is essential to determine kinetics parameter, it should be noted that other reservoir components such as reservoir brine and rock also contributes combustion reactions and they can even change the oil combustion fate by favoring or disfavoring combustion.

Because estimation of combustion behavior by numerical means is too complicated, many researchers studied the analytical modeling of ISC. A study to model a non-steady state heat transfer problems in the radial direction was done by Vogel and Krueger (1955). The analog design was used to predict the heat transfer process in a simplified thermal oil recovery process. The simulation data was able to estimate the residual fuel requirements necessary to maintain a self-propagating isothermal front of the combustion tube experiment. Ramey (1958) did similar modeling but included conduction in the vertical direction. A more general problem has been addressed by Bailey and Larkin (1959) by taking into account the initial well heating, vertical heat losses, and frontal velocities. For all these models, the problem was only the conductive process of heat was considered.

Later, Bailey and Larkin (1960) constructed numerical modeling to estimate the fuel needed for a combustion front propagation. The model was built based on the heat flow in an underground combustion process with consideration for both the linear (combustion tube) and radial (field-scale) dimensions. This included the effects of convection in addition to the conduction of heat transfer. Chu (1963) used a two-dimensional (2D) tube by including combustion to improve the current models whereby a permeable bed was considered bounded by impermeable media. The numerical simulation also included the effects of vertical heat loss.

Thomas (1963) considered radial conduction and convection but thought of combustion as a vertical movement. The formation was assumed to be permeable to gas flow, so the convection effect was not confined to the reservoir. Penberthy et al. (1968)

performed an analytical model with the support of combustion tube experimental data to describe the steam plateau in ISC. The analytical model matched the measured experimental data, which included temperature profiles in terms of time and distance of the combustion front.

These reported studies provide essential insights into predicting ISC performance analytically. Even though some efforts are made to simulate ISC numerically, none of them can correctly estimate the field performance (Gutierrez et al. 2009). The complex chemical reactions in ISC are limiting the numerical simulation application. Thus, by using the analytical method, upscaling of the combustion tube results to a field-scale can be done (Nelson and McNeil 1961; Sarathi 1998).

Because the numerical model on ISC has not been achieved yet, there are limited field applications of ISC. So far, four successful ISC full-field applications are reported and their performance and field parameters were determined through the analytical modeling of combustion tube experimental results (Hammershaimb et al. 1983; Marjerrison and Fassihi 1994; Turta et al. 2007; Mitra et al. 2010).

In this study, analytical modeling of combustion tube tests was achieved and the results were coupled with kinetic analyses and modeling of combustion tube test. Further, simple correlations were obtained among crude oil composition, analytical modeling results of combustion tube tests, and analytical modeling of reaction kinetics experiments.

Experimental Procedure

Combustion Tube Experimental Procedure

Three oil samples were used in this study. Their characterization is given in

Table **3.1**. Anton Paar DMA 4100 density meter and Brookfield DV-III Ultra

rheometer were used to measure the API gravity at standard conditions and viscosity at

room temperature (22.3 °C) for the initial oil samples, respectively. The weight percent of

the Saturates, Aromatics, Resins, and Asphaltenes (SARA) fractions of crude oil samples

was attained by following the ASTM D2007-11 (2007) standard. It can be observed from

Table 3.1 that the three crude oil samples exhibit considerable variations in their physical

properties. Oil 2 is the most viscous oil with the greatest asphaltenes content and Oil 1 is

the lightest crude oil in term of viscosity and API gravity among the three oil samples.

Table 3.1—Properties of Crude Oils Used in this Study (Prakoso et al. 2016).

Oil Sample	Gravity at 15 °C (°API)	Viscosity at 22.3 °C (cP)	Saturates (wt%)	Aromatics (wt%)	Resins (wt%)	Asphaltenes (wt%)
Oil 1	12.09	10,150	16.51	37.81	17.10	28.58
Oil 2	11.56	208,600	10.14	38.01	13.09	38.76
Oil 3	8.19	53,000	23.60	20.00	21.90	34.30

Table 3.2—Initial Condition Comparison for All the Combustion Tube Experiments

Experiments		Oil Type	Clay Type	Clay (wt%)	Ottawa Sand (wt%)	Initial Oil Saturation (vol%)	Initial Water Saturation (vol%)
This Dissertation	E1	Oil 1	-	0	100	60	40
	E1c	Oil 1	Clay 1	3	97	60	40
	E2	Oil 2	-	0	100	60	40
	E2c	Oil 2	Clay 1	3	97	60	40
	E3	Oil 3	-	0	100	60	40
	E3c	Oil 3	Clay 1	3	97	60	40
Aleksandrov and Hascakir (2015)	E2-D	Oil 3	Clay 2	15	85	26	34
	E3-D	Oil 3	Clay 2	15	85	34	34
	E4-D	Oil 3	Clay 2	15	85	42	34
	E5-D	Oil 3	Clay 2	15	85	53	34

Ten combustion tube experiments (Table 3.2) were conducted on three different oil samples (Table 3.1). In the first six experiments in Table 3.2, the impact of crude oil composition and the impact of clay presence on ISC performance was investigated. In the last four experiments, impact of initial oil saturation was tested by testing different initial oil saturations in each experiment (Table 3.2). Two clays were used to prepare reservoir rocks in these tests; in the first six experiments, Clay 1 (90 wt% kaolinite and 10 wt% illite); in the second four combustion tube experiments, Clay 2 (100% kaolinite). The characterization analysis of the two clay samples to investigate the difference in their mineralogy was carried out with X-Ray Diffraction (XRD), the difference in their morphology was examined with Scanning Electron Microscopy (SEM), and the difference in their elemental composition was investigated with Energy Dispersive Spectroscopy (EDS) before the experiments (Figure 3.1).

63

Figure 3.1—Properties of Clays Used in this Study

Clay Type	XRD of Clays	SEM-EDS of Clays at 9500x Magnification
Clay 1		
Clay 2		
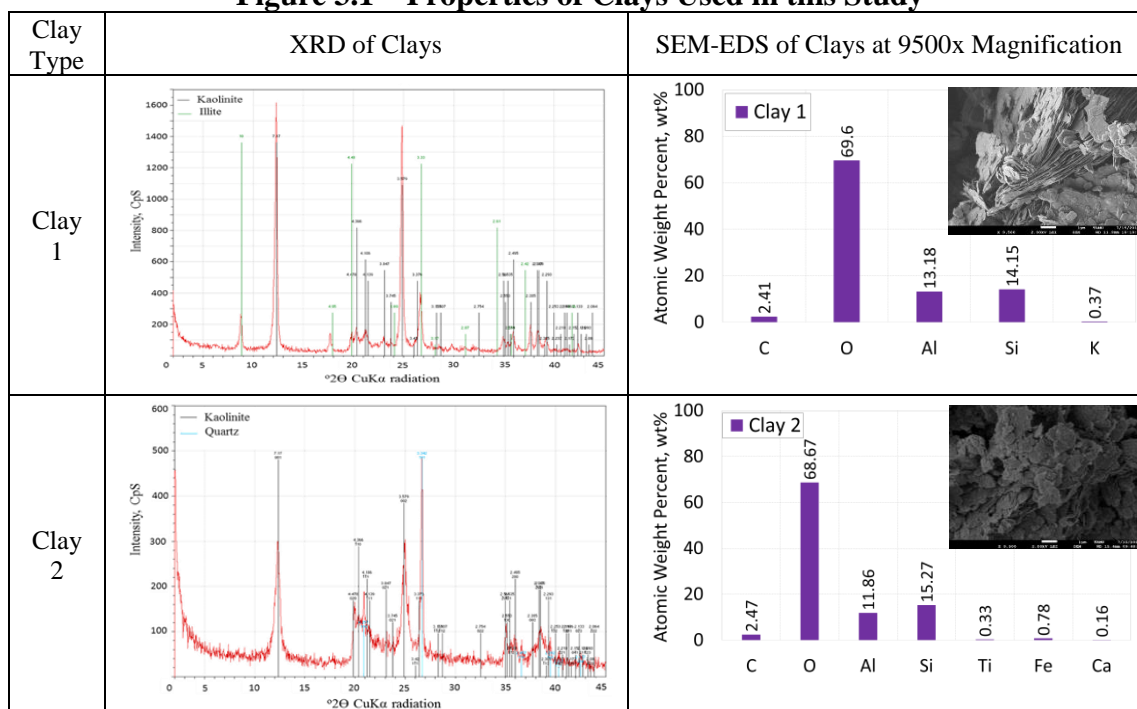
Combustion tube tests procedure were kept constant and experiments were run at 3.4 L/min of air injection rate. Ignition temperature was reached in all experiments by the help of a band heater. During ignition period (~ 2 hours), nitrogen was used to maintain anaerobic/non-oxidative environment at 100 psig back pressure. Once ignition temperature was reached, nitrogen was switched to air and heaters were turned off. The temperature profiles were recorded every three seconds during the experiments. The produced gases were analyzed in terms of CO, CO_2, O_2, and CH_4 at each second, and produced oil and water were collected every half an hour. The produced oil samples were then subjected to SARA fractionation following ASTM D2007-11 standard (ASTM 2007). This section of the dissertation concentrates on the analytical modeling of combustion tube

64

tests results rather than combustion tube test. Thus, details of experimental procedure can be found in previously published papers (Kudryavtsev and Hascakir 2014; Aleksandrov and Hascakir 2015).

Analytical Modeling Procedure for Combustion Tube Results

Analytical modeling of the combustion tube results provides an in-depth analysis of the fuel formation reactions at the stable zone. A stable zone is a zone where temperature and combustion speed are almost constant over time (Hascakir et al. 2013). Hence, ten combustion tube experimental results were modeled by integrating several analytical approaches (Nelson and McNeil 1961; Chu 1981; Kok 1993; Sarathi 1998) on three oil samples.

During combustion, produced gases were measured continuously in mole percent and this information was used as input parameters in the analytical model. It should be noted that while there are some other gases produced during combustion, such as H_2S, NO_X, SO_X, etc., their existence has been ignored in the analytical model and combustion gases have been assumed to be only O_2, CO_2, CO and N_2 (Nelson and McNeil 1961). Thus, the first step in analytical modeling was to normalize the gas concentration for O_2, CO_2, CO and N_2 composition. Then, based on these normalized data, the fuel burning reaction stoichiometry, oxygen utilization rate, air-to-fuel ratio, fuel consumed per volume of sand burned, and heat of combustion parameters were calculated. The equations used in the analytical model are listed in Appendix 3A.

Among these parameters, the heat of combustion (ΔH) is a very important parameter which provides information on if ISC will sustain or not. This quantity is obtained through the stoichiometry of the main combustion reaction (Fuel + $O_2 \rightarrow CO_2 +$ $CO + H_2O + \Delta H$). However, the necessary energy for the formation of fuel cannot be calculated by using the same analytical model and by using combustion tube results. Thus, kinetic modeling of reaction kinetics experiments were needed.

Reaction Kinetic Experiment Procedure and Analytical Modeling of Reaction Kinetic

Tests

It should be noted that during ISC, the main chemical reaction which consumes the greatest amount of energy is known as fuel formation and the main chemical reaction which produces the greatest amount of energy is coke burning reaction (combustion reaction) (Burger et al. 1985; Sarathi 1998; Kok and Acar 2005). If the activation energy (E_a) necessary to form fuel (coke) is less than the heat of combustion (ΔH) to burn fuel, the ISC reaction sustains (Belgrave et al. 1993; Sarathi 1998; Hascakir and Kovscek 2014). Therefore, for successful combustion, the activation energy (E_a) should be lower than the heat of combustion (ΔH).

To calculate the activation energy, Thermogravimetric and Differential Scanning Calorimetry (TGA/DSC) tests were conducted (ASTM 2014) using Netzsch STA 449 TGA/DSC thermal analyzer on the same initial samples from the combustion tube experiments summarized in

66

Table **3.2**. Moreover, since asphaltenes are known as the source of coke (Sarathi 1998), the role of asphaltenes on combustion kinetics was investigated separately. 20 reaction kinetics tests were conducted on crude oils, their asphaltenes and reservoir rock-fluid blends used in each combustion tube tests given in

Table **3.2**. Summary of sample composition for 20 reaction kinetics tests are given in Table 3.3. These samples underwent oxidation under continuous air injection (50 ml/min) at a constant heating rate of 20 °C/min. This heating rate was selected as it represents the heating rate during ISC in the thermal cracking and high temperature oxidation (HTO) region. Experiments were conducted from 25 °C until the sample temperatures reached 900 °C. For reference, the burning behavior of distilled water, clays, and Ottawa sand used in this study was also obtained at 20 °C/min heating rate by using TGA/DSC.

Table 3.3—Experimental Conditions for TGA/DSC

Kinetic Test Run	Sample Type	Crude Oil (wt%)	Water (wt%)	Ottawa Sand (wt%)	Clay 1 90% K 10% I (wt%)	Clay 2 100% K (wt%)	Asphaltenes (wt%)
Test 1	Oil 1-E1	8.67	5.78	85.54	-	-	-
Test 2	Oil 1-E1c	8.67	5.78	82.98	2.57	-	-
Test 3	Oil 2-E2	8.67	5.78	85.54	-	-	-
Test 4	Oil 2-E2c	8.67	5.78	82.98	2.57	-	-
Test 5	Oil 3-E3	8.67	5.78	85.54	-	-	-
Test 6	Oil 3-E3c	8.67	5.78	82.98	2.57	-	-
Test 7	Oil 3-E2-D	4.82	6.49	77.12	-	11.57	-
Test 8	Oil 3-E3-D	6.21	6.39	75.99	-	11.40	-
Test 9	Oil 3-E4-D	7.56	6.30	74.90	-	11.23	-
Test 10	Oil 3-E5-D	9.36	6.18	73.44	-	11.02	-
Test 11	Oil 1	100	-	-	-	-	-
Test 12	Oil 1's Asphaltenes	-	-	-	-	-	100
Test 13	Oil 2	100	-	-	-	-	-
Test 14	Oil 2's Asphaltenes	-	-	-	-	-	100
Test 15	Oil 3	100	-	-	-	-	-
Test 16	Oil 3's Asphaltenes	-	-	-	-	-	100
Test 17	Distilled Water	-	100	-	-	-	-
Test 18	Ottawa Sand	-	-	100	-	-	-
Test 19	Clay 1	-	-	-	100	-	-
Test 20	Clay 2	-	-	-	-	100	-

*K=Kaolinite clay, I=Illite clay

The kinetics of the combustion reaction were then investigated at low temperature oxidation (LTO) (25-300 °C) and high temperature oxidation (HTO) (300-600 °C) regions by calculating the total activation energy and heat of combustion. Activation energy were calculate based on the Arrhenius (Arrhenius 1889; Kok 1993) approximation by using the TGA/DSC graphs (Appendix 3B). Accordingly, the slope of the reaction kinetic parameters versus temperature linear graph (Figure 3 D2) gives the activation energy value (E_a) and the y intercept is giving the Arrhenius constant. DSC curve gives the heat flow (q) over time (t) during the combustion and since the heat of combustion, ΔH is the enthalpy change (heat released or absorbed during combustion reaction), ΔH is calculated by differentiating the DSC curve (dq/dt) (Kok 1993; Han et al. 2012).

Results and Discussion

Analytical Modeling of the Combustion Tube Experiment Results

First, the combustion tube test results were modeled by integrating several analytical approaches (Nelson and McNeil 1961; Chu 1981; Kok 1993; Sarathi 1998). Table 3.4 summarizes the analytical modeling results for the combustion tube experiments from this study and the four combustion tube experiments from Aleksandrov and Hascakir (2015).

It has been observed that oxygen utilization is increased in the presence of clays, hence, air to fuel ratio is decreased (compare E1 with E1c, E2 with E2c, and E3 with E3c in Table 3.4). As the oil saturation increases, oxygen utilization enhanced (compare E2-

D, E3-D, E4-D, and E5-D in Table 3.4) with an optimum oil saturation (60 vol% E4-D) at given air injection rate. This optimum oil saturation yielded the greatest oxygen utilization rate (84%) among this set of combustion tube experiments. E3, E3c, and E5-D were conducted with the same crude oil (Oil 3) and the same oil saturation (60 vol%). The only difference among these experiments was clay presence or type. While E3 did not have any clay in its reservoir rock, E3c had illite and kaolinite mixture (Clay 1) and E5-D had kaolinite (Clay 2) (detailed mineralogy of clays and reservoir rock is given in Figure 3.1). Accordingly, it can be concluded that clay presence enhance ISC performance. Based on analytical modeling result of combustion tube tests, simplified stoichiometry of coke burning reaction can be obtained for each test (Table 3.5).

Table 3.4—Analytical Modeling Results of Combustion Tube Experiments

Experiments		Oil Type	Normalized Produce Gases (vol%)				Air-to-fuel ratio (scf/lbm)	O_2 utilization rate, Y (%)	H/C ratio	Produced gas volume, V_{gas} (ft^3)	Burned Sand Volume, $V_{burned-sand}$ (ft^3)	Fuel consumed (lbm/ft^3-reservoir)
			CO_2	CO	O_2	N_2						
This Dissertation	E1	Oil 1	6.07	2.86	11.81	79.26	332	44	0.79	18.33	0.09	0.65
	E1c	Oil 1	10.22	5.01	3.89	80.88	191	82	1.28	10.79	0.12	0.27
	E2	Oil 2	6.67	3.36	9.92	80.05	290	53	1.20	6.00	0.08	1.05
	E2c	Oil 2	13.11	5.25	1.84	79.80	163	91	0.79	11.16	0.07	0.49
	E3	Oil 3	5.57	2.66	11.84	79.93	352	44	1.22	16.27	0.04	1.03
	E3c	Oil 3	11.24	6.73	3.18	78.85	165	85	0.71	9.36	0.09	0.66
Aleksandrov and Hascakir (2015)	E2-D	Oil 3	9.42	4.42	4.90	81.27	299	62	3.97	19.14	0.07	1.10
	E3-D	Oil 3	9.71	4.00	5.40	80.89	256	70	3.77	12.53	0.07	1.10
	E4-D	Oil 3	11.97	4.24	2.69	81.11	202	84	2.10	14.95	0.09	0.88
	E5-D	Oil 3	11.65	4.00	3.45	80.90	274	66	1.59	16.80	0.09	0.59

Table 3.5—Simplified Stoichiometry of Coke-Burning Reactions

Experiments		Coke Burning Reactions	ΔH (BTU/lbm)
This Study	E1	$CH_{0.78} + 1.47\,O_2 \rightarrow 0.68\,CO_2 + 0.32\,CO + 0.39\,H_2O$	14,436
	E1c	$CH_{0.80} + 1.25\,O_2 \rightarrow 0.71\,CO_2 + 0.29\,CO + 0.40\,H_2O$	15,699
	E2	$CH_{1.20} + 1.45\,O_2 \rightarrow 0.67\,CO_2 + 0.33\,CO + 0.64\,H_2O$	15,876
	E2c	$CH_{1.22} + 1.24\,O_2 \rightarrow 0.68\,CO_2 + 0.32\,CO + 0.61\,H_2O$	16,029
	E3	$CH_{1.20} + 1.43\,O_2 \rightarrow 0.67\,CO_2 + 0.33\,CO + 0.60\,H_2O$	14,695
	E3c	$CH_{0.70} + 1.16\,O_2 \rightarrow 0.63\,CO_2 + 0.37\,CO + 0.35\,H_2O$	13,563
Aleksandrov and Hascakir (2015)	E2-D	$CH_{1.46} + 1.03\,O_2 \rightarrow 0.32\,CO_2 + 0.68\,CO + 0.73\,H_2O$	19,230
	E3-D	$CH_{1.28} + 0.97\,O_2 \rightarrow 0.29\,CO_2 + 0.71\,CO + 0.64\,H_2O$	18,919
	E4-D	$CH_{1.18} + 0.93\,O_2 \rightarrow 0.26\,CO_2 + 0.74\,CO + 0.59\,H_2O$	17,727
	E5-D	$CH_{1.12} + 0.91\,O_2 \rightarrow 0.26\,CO_2 + 0.74\,CO + 0.56\,H_2O$	17,156

Table 3.5 exhibits the fuel/coke burning reactions during ISC for all ten combustion tube experiments. The mole of O_2 in Table 3.5 reflects the amount of oxygen that was consumed to burn one mole of formed fuel. Fuel-burning reactions indicate that the mole difference amount decreased when clay was added (E1c, E2c, and E3c). Moreover, this amount decreases with increasing initial oil saturation (E2-D to E5-D).

Reaction Kinetics Experiment Results and Analytical Modeling of Reaction Kinetics

Parameters

20 TGA/DSC experiments were run on the initial samples properties given in Table 3.3. The results are given in Appendix 3C. By using Model Fitting method, TGA/DSC results were converted into reaction kinetics parameter for both low and high temperature oxidation (LTO and HTO) regions. These values were calculated by converting the TGA/DSC graphs into differential thermogravimetric (DTG) and Arrhenius model fitting graphs (Appendix 3D).

Test 17 through Test 20 in Table 3.3 are control experiments to understand individual role of each reservoir components in ISC dynamics they have been conducted. Distilled water (Test 17 in Table 3.3) was lost completely at around 120 °C (Figure 3 C2 A&B). Clays' decomposition (Test 19 and 20 in Table 3.3) started at around 500 °C and ended at around 650 °C and around 10 wt% of clay was lost (Figure 3 C2 C&D). Ottawa sand (Test 18 in Table 3.3) has not been reactive and neither significant weight loss (Figure 3 C2 E) nor significant chemical reactions (Figure 3 C2 F) were observed. .

Table 3.6—Kinetic Modeling Results of Oil Samples At HTO Region under Constant Heating Rate Combustion

Experiments		Region	Activation Energy, Ea (BTU/lb-mole)	Arrhenius Constant, A (1/min)
Test 1	E1	LTO	8,983.84	3.85E+00
		HTO	44,195.30	4.18E+00
Test 2	E1c	LTO	5,038.49	3.92E-01
		HTO	14,471.81	8.69E+00
Test 3	E2	LTO	7,751.27	1.54E+00
		HTO	33,263.83	7.97E+03
Test 4	E2c	LTO	1,477.65	3.67E-02
		HTO	18,099.44	8.67E+01
Test 5	E3	LTO	20,200.25	3.36E+04
		HTO	4,965.61	1.62E+01
Test 6	E3c	LTO	3,794.80	5.01E+00
		HTO	6,536.98	7.59E+03
Test 7	E2-D	LTO	5,739.15	2.82E-02
		HTO	49,685.74	5.75E+05
Test 8	E3-D	LTO	2,800.56	6.76E-03
		HTO	34,205.12	1.02E+03
Test 9	E4-D	LTO	12,125.58	1.05E+00
		HTO	45,552.47	1.32E+05
Test 10	E5-D	LTO	6,390.56	6.46E-02
		HTO	31,457.84	4.57E+02

Chemical reactions during the in-situ combustion can occur if the necessary heat to exceed the activation energy barrier is obtained through the oxidation and combustion reactions (Burger 1972; Sarathi 1998). The heat requirements (activation energy) (Table 3.6) decreases with the presence of clay in the HTO region. This indicates the catalytic impact of clay. Only for Oil 3 (E3 and E3c), activation energy in HTO (Table 3.6) tends to increase in the presence of clay. Another observation was Oil 3 without clay (E3) has high E_a in the LTO region. However, with clay presence in Oil 3 (E3c), the E_a in the LTO

region decreases. This is due to the characteristic of Oil 3 that has emulsified water in its oil structure. Emulsified water might have interacted with clay that helps the combustion to become more effective for Oil 3 (Martin 1959).

This hypothesis was deduced by observing Figure 3 C1 that gives weight loss and heat flow graphs versus temperature for the initial oils and their asphaltenes. In Figure 3 C1 F, the endothermic peak observed at around 100 °C indicates the emulsified water content of Oil 3, and Figure 3 C1 E shows the amount of emulsified water (in weight percent) at corresponding temperatures. This chemical reaction might be the reason for a lower heat generation in the HTO zone (473-660 °C) which results in the lowest exothermic valley in DSC graphs among all crude oils.

For Oil 1, presence of clay reduced the heat generation and shifted the HTO zone to elevated temperature region (~600 °C) (Figure 3 C1 A&B). This increase is not due to asphaltenes alone, since asphaltenes generated more heat in the presence of clay at lower temperature when compare to without clay case. For Oil 2 (Figure 3 C1 C&D), similar behavior was observed in bulk crude oil and for this oil, asphaltenes might be the reason in having lower heat generation in HTO region, since asphaltenes alone in the presence of clay yielded less heat at the HTO region. Oil 3 exhibited exactly the same behavior as Oil 1.

Furthermore, the activation energy for the HTO region in Table 3.6 was compared to the heat of combustion from combustion tube experiment in Table 3.4. The heat of combustion (ΔH) in Table 3.4 was calculated based on the produced gas mole percent

74

obtained through the combustion tube experiments and represented only the combustion of coke and did not include the heat produced by LTO and HTO reactions. Hence, we only report the activation energy for the HTO region in Table 3.6 to compare the activation energy and heat of combustion needed for each combustion. Out of all the experiments, only Oil 3 (E3 and E3c) generates more heat of combustion (ΔH) than the activation energy (E_a) (Table 3.6). This indicates that the activation energy barrier achieved in Oil 3 has exceeded the required minimum for effective combustion.

In regards to the effect of initial oil saturation, there was no significant trend observed on the activation energy values of E2-D to E5-D. However, for all experiments, the activation energy was increased in HTO region. When comparing to E3c that was conducted on the same oil sample (Oil 3), but with different type of clay, Clay 1 used in E3c was resulting in a better combustion.

Integration of Analytical Modeling and Kinetic Modeling Results with Oil Composition

The results for analytical modeling parameters for ISC and the combustion kinetics parameter were then correlated to the Saturates, Aromatics, Resins, and Asphaltenes (SARA) fractions of produced oil (

Table **3.7**). It should be noted that asphaltenes (fuel source) are insoluble in saturated hydrocarbons and soluble in aromatics (Speight 1991). Thus, the behaviors of asphaltenes stability on fuel deposition mechanism were investigated on two specific bases. First, the saturates fraction of crude oil might enhance asphaltenes deposition. Secondly, the aromatics and resins fractions of crude oil might stabilize back the

75

asphaltenes (Prakoso et al. 2016). Colloidal Instability Index (CII) is defined as the asphaltenes' instability or the asphaltenes' precipitation tendency and given with the following formula (Equation 3.1) (Pfeiffer and Saal 1940; Saal and Labout 1940; Asomaning 2003). The SARA fractions was obtained by following the ASTM D2007-11 standard (ASTM 2007) and the CII were calculated.

Equation 3.1—Colloidal Instability Index (CII)

$$\text{CII} = \frac{\textbf{Flocculants}}{\textbf{Peptizers}} = \frac{\textbf{saturates [wt\%] + asphaltenes [wt\%]}}{\textbf{aromatics [wt\%] + resins [wt\%]}}$$

Table 3.7—SARA Fractions and Colloidal Instability Index (CII) of Produced Oil

Experiments		SARA Fractions (wt%)				CII
		Saturates	Aromatics	Resins	Asphaltenes	
This Dissertation	E1	12.94	48.52	15.19	23.35	0.97
	E1c	10.39	62.87	11.35	15.39	0.48
	E2	8.87	43.77	10.97	36.39	0.83
	E2c	8.62	55.92	9.92	25.54	0.52
	E3	6.54	58.79	10.43	24.23	0.44
	E3c	15.72	54.31	14.93	15.04	0.44
Aleksandrov and Hascakir (2015)	E2-D	20.00	34.00	11.00	35.10	1.22
	E3-D	19.50	33.80	14.10	32.60	1.09
	E4-D	19.60	32.50	15.50	32.40	1.08
	E5-D	18.70	42.40	13.60	25.30	0.79

It has been observed that the produced asphaltenes to aromatics ratio, aromatics fraction, and CII^{-1} correlated well with the activation energy (Figure 3.2 A, B, & C). As well, H/C ratio correlated well with heat of combustion (Figure 3.2 D). It should be worth mentioning here that in Figure 3.2, the x-axis and the y-axis values were obtained through different experiments and analytical model. The aromatics (wt%) and the asphaltenes to aromatics ratio in the y-axis of Figure 3.2 A & B were obtained through SARA fractionation on the produced oil samples. The CII^{-1} (y-axis) in Figure 3.2 C was also from SARA fractions calculated by using Equation 3.1. Meanwhile, the activation energy (Figure 3.2 A, B, & C) values (x-axis) were calculated from TGA/DSC experiment and kinetic modeling. Both axes in Figure 3.2 D are from analytical modeling of the combustion tube results. It is interesting that even though different oil compositions, clay types, and water saturation combinations were used with a different TGA/DSC experiment, there are interactions between these parameters. Note that E3, E3c, E2-D, E3-D, E4-D, and E5-D were conducted on the same bitumen. However, the clays are different; no clay (E1, E2, E3), Clay 1 (kaolinite and illite) (E1c, E2c, E3c), and Clay 2 (kaolinite) (E2-D, E3-D, E4-D, and E5-D).

| A— Produced Asphaltenes to Aromatics Ratio vs Activation Energy | B— Produced Aromatics vs Activation Energy |
| C—CII^{-1} vs Activation Energy | D—H/C Ratio vs Heat of Combustion |
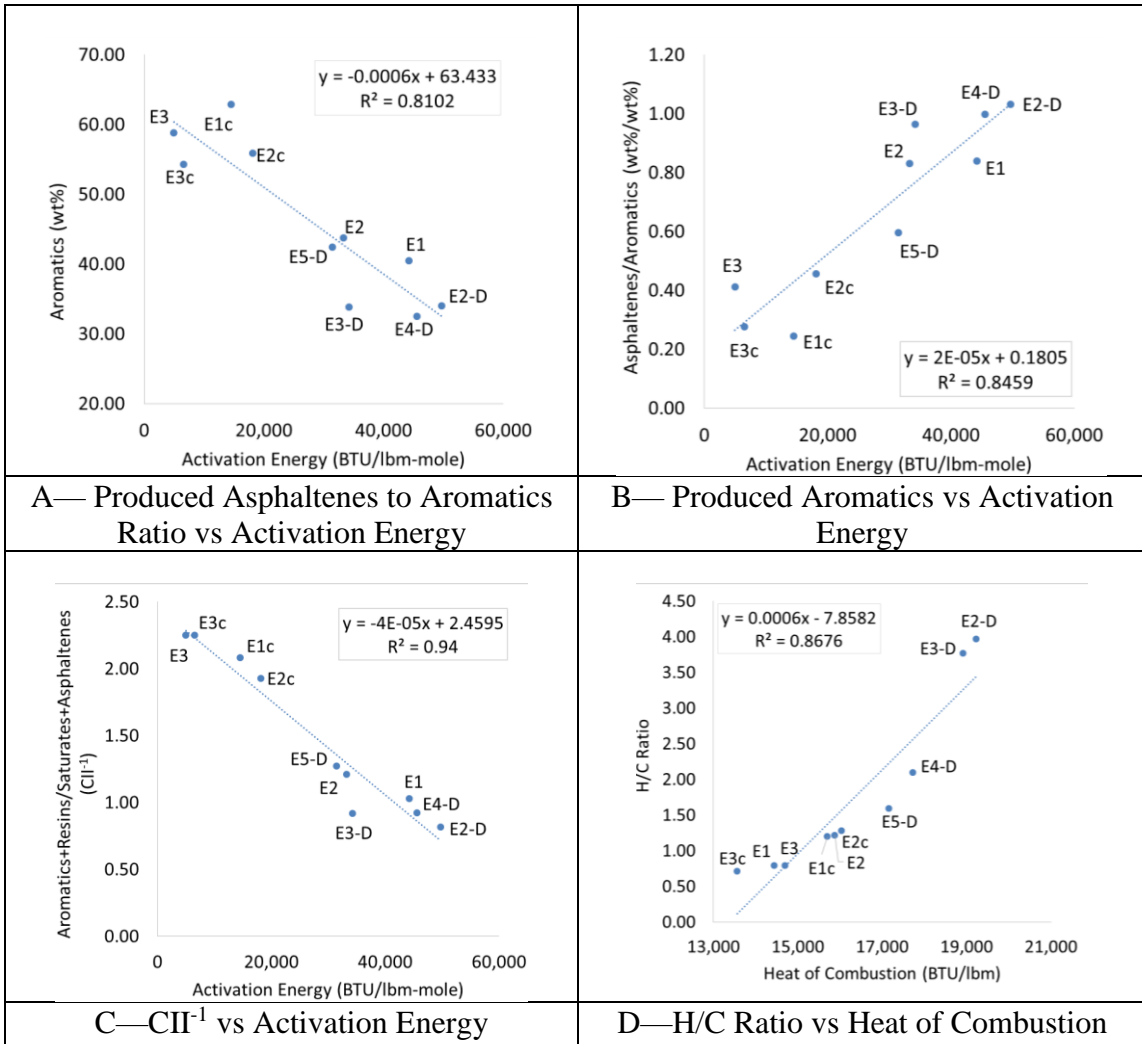
Figure 3.2—Relationship between SARA Fractions and Activation Energy and H/C Ratio and Heat of Combustion in the HTO Region

As the asphaltenes increase, activation energy increases (Figure 3.2 A). Aromatics fraction behaves like buffer (Figure 3.2 A) and increase in aromatics fraction content in oil makes the activation energy lesser (Figure 3.2 B). This should be due to dispersion of asphaltenes in oil phase. Asphaltenes dispersion is encouraged by resins and aromatics fractions and asphaltenes coagulation is enhanced due to saturates fraction. As asphaltenes dispersed more in the crude oil, the asphaltenes breaking should become more favorable (Asomaning 2003). This hypothesis is also supported by Figure 3.2 C as the asphaltenes coagulation tendency increases (in other words, CII^{-1} decreases), activation energy increases. This behavior implies that stable asphaltenes (dispersed in crude oil) require less heat to be cracked to form fuel. The formed fuel is defined with H/C ratio, as the H increases in the fuel, it becomes more saturated. Based on the analytical simulation results (Table 3.4, Table 3.5, and Table 3.6), more saturated fuel with H atom yields higher heat generation (Figure 3.2 D).

Appendix 3A

Equation 3 A1—Stoichiometry of the fuel burning reaction

$$CH_n + \frac{1}{Y}\left(\frac{2m+1}{2m+2} + \frac{n}{4}\right)O_2 + \frac{R}{Y}\left(\frac{2m+1}{2m+2} + \frac{n}{4}\right)N_2 \rightarrow$$

$$\frac{m}{m+1}CO_2 + \frac{1}{m+1}CO + \frac{1-Y}{Y}\left(\frac{2 \cdot m+1}{2 \cdot m+2} + \frac{n}{4}\right)O_2 + \frac{n}{2}H_2O + \frac{R}{Y}\left(\frac{2m+1}{2m+2} + \frac{n}{4}\right)N_2$$
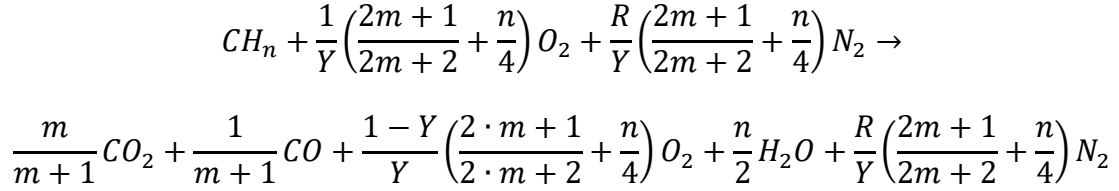
Where;

$$n = \frac{H}{C} = \frac{4\left(\frac{[N_2]}{R} - [CO_2] - \frac{[CO]}{2} - [O_2]\right)}{([CO_2] + [CO])} \qquad and \qquad m = \frac{[CO]}{[CO_2]}$$

[N_2]: Normalized value of produced nitrogen;

[CO_2]: Normalized value of produced carbon dioxide;

[CO]: Normalized value of produced carbon monoxide;

[O_2]: Normalized value of produced oxygen;

R: Ratio of injected nitrogen to injected oxygen (79 vol%/21 vol%);

Equation 3 A2—Air to fuel ratio

$$\frac{\text{Air}}{\text{Fuel}} = (1 + R) \left\{ \frac{379\frac{[N_2]}{R}}{12.011([CO_2] + [CO]) + 4.032 \left(\frac{[N_2]}{R} - [CO_2] - \frac{[CO]}{2} - [O_2]\right)} \right\}$$

Where;

R: Ratio of injected nitrogen to injected oxygen (79 vol%/21 vol%);

$[N_2]$: Normalized value of produced nitrogen;

$[CO_2]$: Normalized value of produced carbon dioxide;

$[CO]$: Normalized value of produced carbon monoxide;

$[O_2]$: Normalized value of produced oxygen;

Equation 3 A3—Oxygen utilization rate, Y (%)

$$Y = \frac{\frac{[N_2]}{R} - [O_2]}{\frac{[N_2]}{R}}$$

Where;

[N$_2$]: Normalized value of produced nitrogen;

[O$_2$]: Normalized value of produced oxygen;

R: Ratio of injected nitrogen to injected oxygen (79 vol%/21 vol%);

Equation 3 A4—Fuel consumed per volume of sand burned (lb/ft^3)

$$\text{Fuel consumed} = \left(\frac{4[N_2]}{R} - 4[O_2] + 8[CO_2] + 10[CO]\right)\left(\frac{V_{gas}}{V_{burned-sand} \times 100 \times 379.1}\right)$$

Where;

R: Ratio of injected nitrogen to injected oxygen (79 vol%/21 vol%);

[N$_2$]: Normalized value of produced nitrogen;

[CO$_2$]: Normalized value of produced carbon dioxide;

[CO]: Normalized value of produced carbon monoxide;

[O$_2$]: Normalized value of produced oxygen;

V_{gas}: Total produced gas volume at the stable zone;

$V_{burned-sand}$: Total volume of burned sand at the stable zone;

Equation 3 A5—Heat of combustion, ΔH (BTU/lbm)

$$H_c = \Delta H = \left(\frac{174000\frac{[CO_2]}{[CO]}}{\frac{[CO_2]}{[CO]} + 1} + \frac{52500}{\frac{[CO_2]}{[CO]} + 1} + \frac{123000\frac{[H]}{[C]}}{2} \right)\left(\frac{1}{12 + \frac{[H]}{[C]}} \right)$$

Where;

[H/C]: Hydrogen to carbon ratio;

[CO$_2$]: Normalized value of produced carbon dioxide;

[CO]: Normalized value of produced carbon monoxide;

[O$_2$]: Normalized value of produced oxygen;

Appendix 3B

Equation 3 B1—**Arrhenius Equation**

$$\ln \frac{dW/dt}{W} = -\frac{E}{2.303R}\left(\frac{1}{T}\right) + \log A$$

Where;

W: Mass of sample;

E: Activation Energy (J/mol);

R: Gas Constant (8.314 J/mol K);

T: Temperature (K);

A: Arrhenius Constant (1/min).

A—TGA of Oil 1 and its asphaltenes without (E1) and with (E1c) clay	B—DSC of Oil 1 and its asphaltenes without (E1) and with (E1c) clay
C—TGA of Oil 2 and its asphaltenes without (E2) and with (E2c) clay	D—DSC of Oil 2 and its asphaltenes without (E2) and with (E2c)
E—TGA of Oil 3 and its asphaltenes without (E3) and with (E3c) clay	F—DSC of Oil 3 and its asphaltenes without (E3) and with (E3c) clay
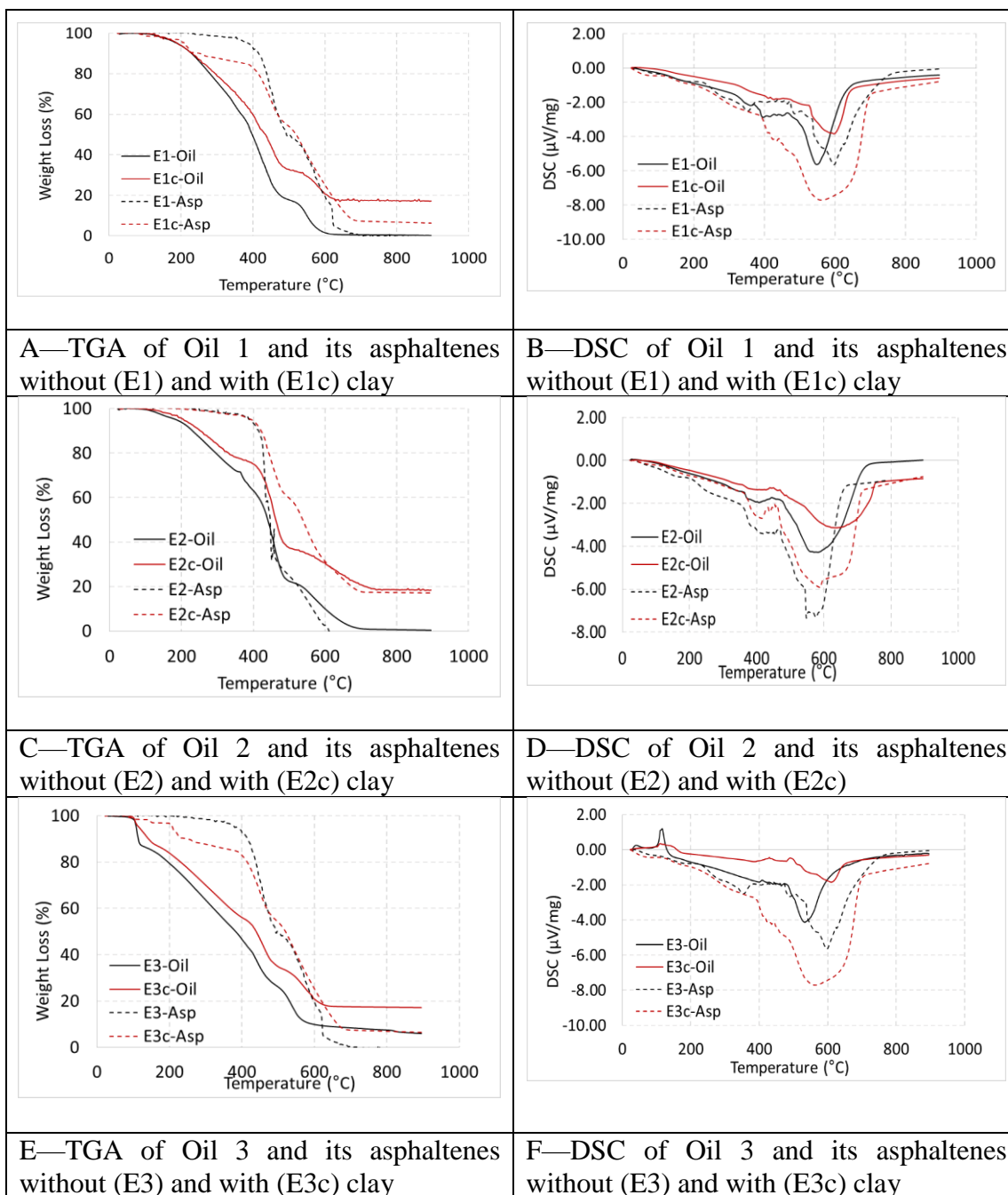
Figure 3 C1—TGA/DSC Results for the Initial Oil Samples and their Asphaltenes Conducted at High Heating Rate Observed during Combustion at HTO Region (20 °C/min)

A—Weight loss behavior of water at a heating rate of 20 °C/min during combustion under air injection	B—Heat flow behavior of water at a heating rate of 20 °C/min during combustion under air injection
C—Weight loss behavior of clays at a heating rate of 20 °C/min during combustion under air injection	D—Heat flow behavior of clays at a heating rate of 20 °C/min during combustion under air injection
E—Weight Loss behavior of Ottawa sand at a heating rate of 20 °C/min during combustion under air injection	F—Heat flow behavior of Ottawa sand at a heating rate of 20 °C/min during combustion under air injection

Figure 3 C2—Weight Loss Behavior (TGA) Graphs (on the left) and Heat Flow Behavior (DSC) Graphs (on the right) of Reservoir Rock and Fluid Components other than Oil at High Heating Rate of 20 °C/min Under Air Injection

A—TG and DTG graphs for E1	B—TG and DTG graphs for E1c
C—TG and DTG graphs for E2	D—TG and DTG graphs for E2c
E—TG and DTG graphs for E3	F— TG and DTG graphs for E3c
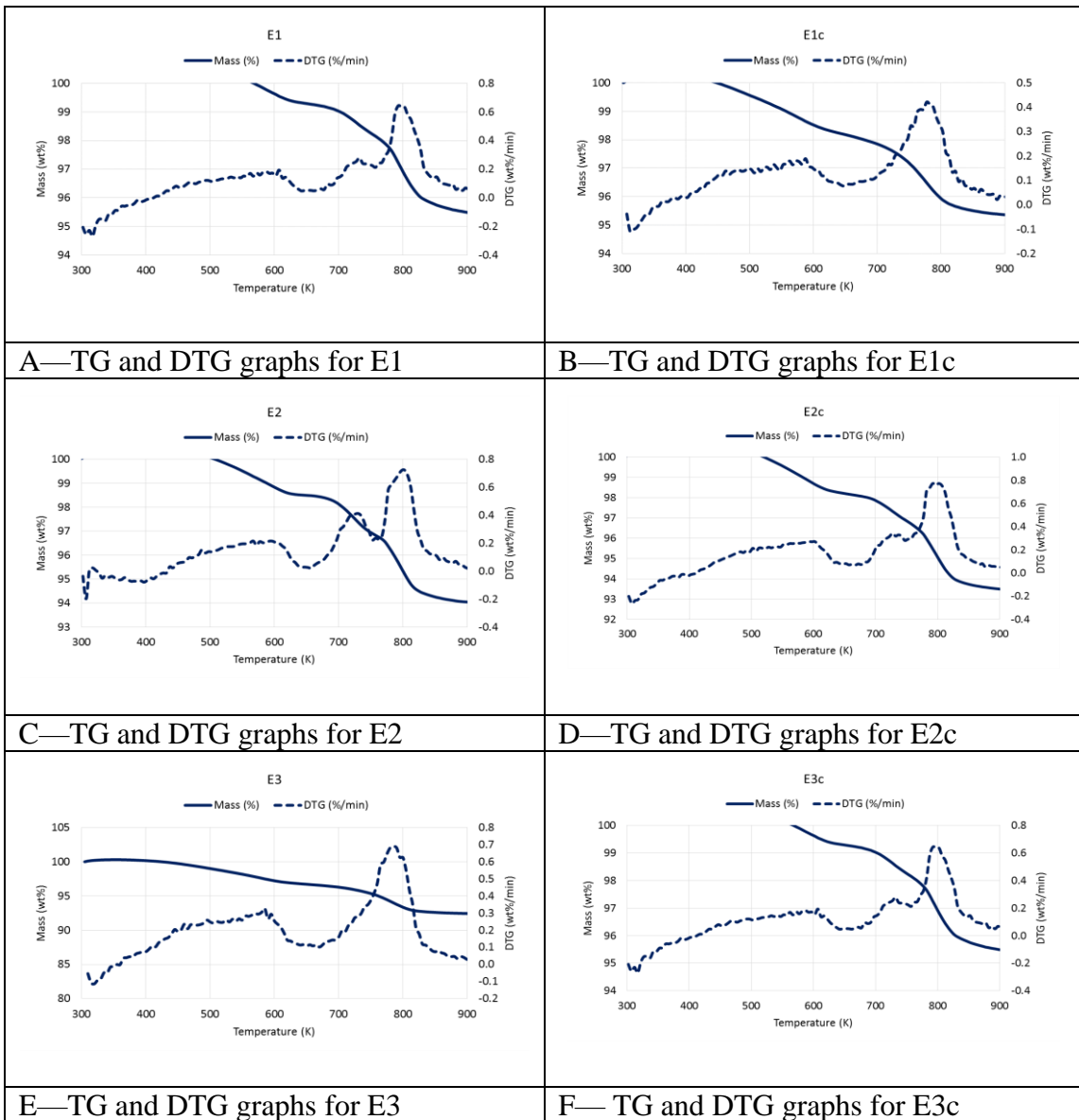
Figure 3 D1—TG/DTG Graphs for Arrhenius Model Calculation

G— TG and DTG graphs for E2-D	H— TG and DTG graphs for E3-D
I— TG and DTG graphs for E4-D	J— TG and DTG graphs for E5-D
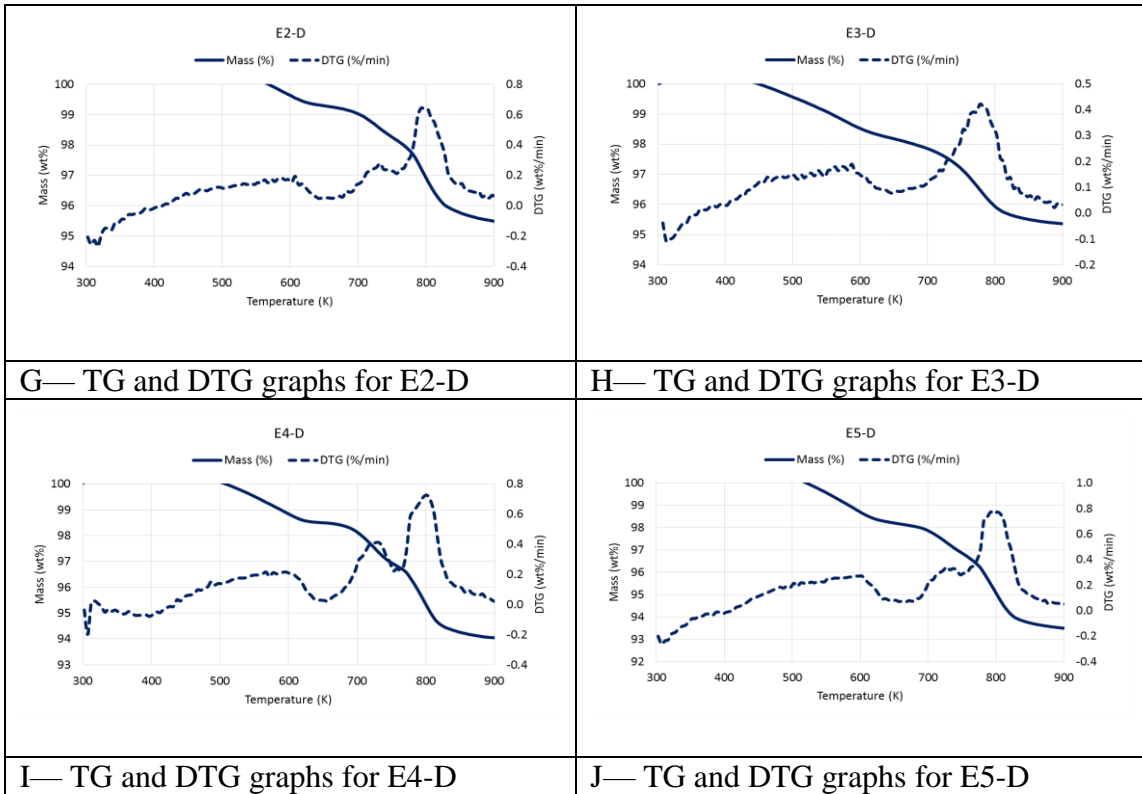
Figure 3 D1 (cont.)—TG/DTG Graphs for Arrhenius Model Calculation

A—Arrhenius Model Fitting for E1	B—Arrhenius Model Fitting for E1c
C—Arrhenius Model Fitting for E2	D—Arrhenius Model Fitting for E2c
E—Arrhenius Model Fitting for E3	F—Arrhenius Model Fitting for E3c
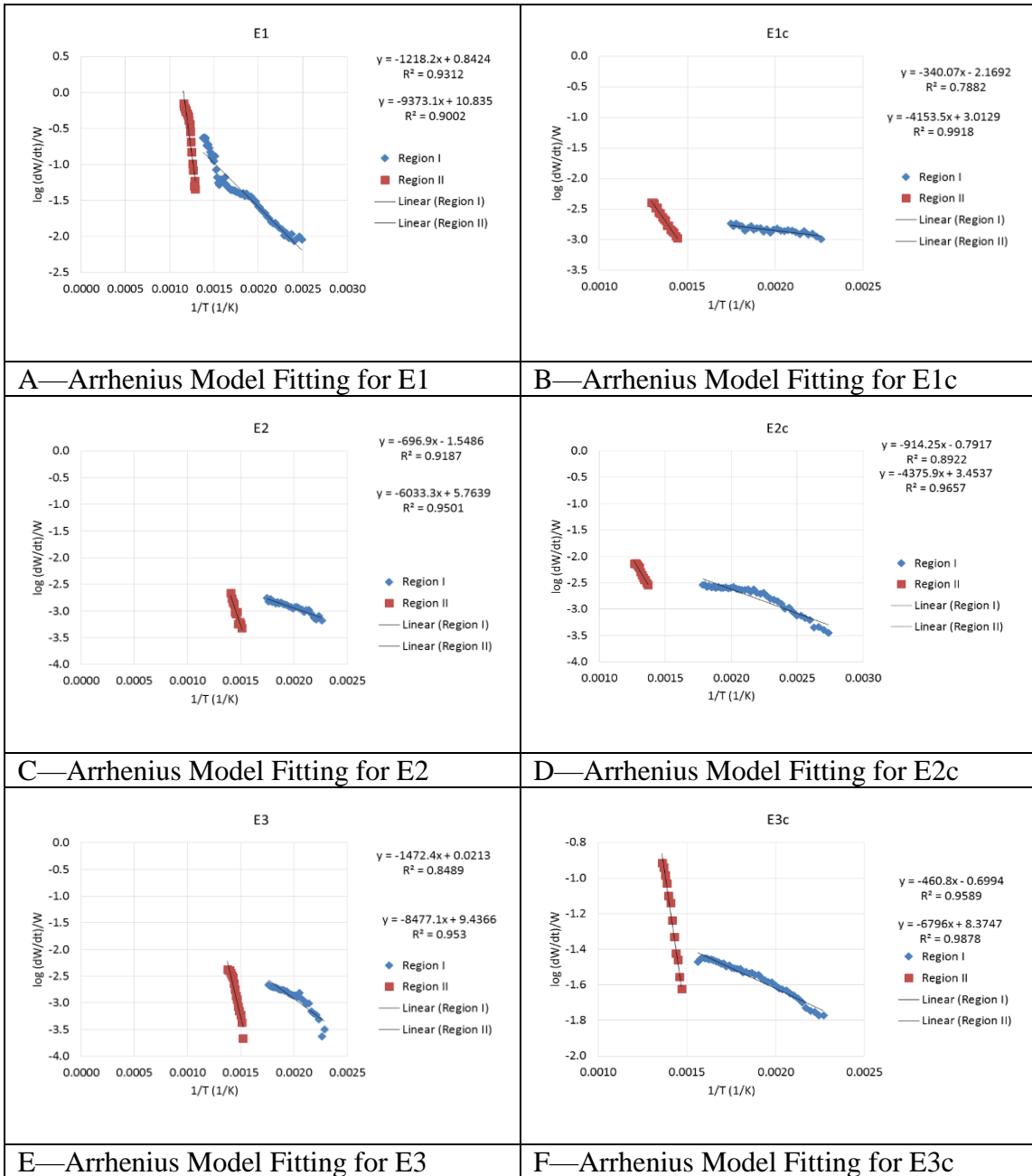
Figure 3 D2—Arrhenius Model Fitting Graphs for LTO (Region I) and HTO (Region II)

89

G—Arrhenius Model Fitting for E2-D	H—Arrhenius Model Fitting for E3-D
I—Arrhenius Model Fitting for E4-D	J—Arrhenius Model Fitting for E5-D
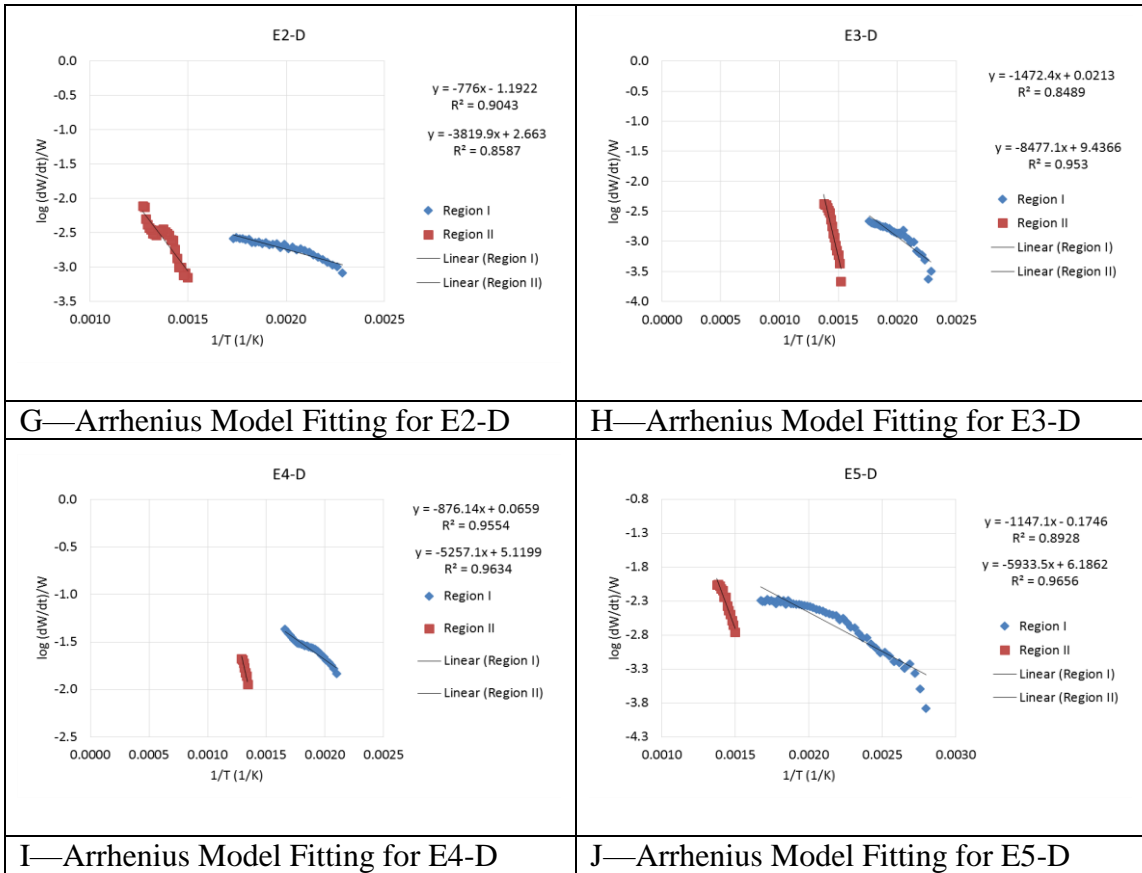
Figure 3 D2 (cont.)—Arrhenius Model Fitting Graphs for LTO (Region I) and HTO (Region II)

4.   THE ROLE OF RESERVOIR FLUIDS AND RESERVOIR ROCK

MINERALOGY ON IN-SITU COMBUSTION KINETICS

Introduction

ISC is an enhanced oil recovery (EOR) method with several potential benefits; i.e., improving oil mobility and quality, achieving high oil recovery, and the low cost of delivering thermal energy into the reservoir (Butler 1991; Sarathi 1998). However, despite its discovery for nearly a century, there are still limited successful field applications of ISC, indicating the lack of knowledge surrounding the theory (Sarathi 1998; Turta et al. 2007). This stems from the heterogeneous nature of reservoirs that restricts the performance prediction of the chemical reactions happening during ISC. The key aspects that influence ISC application in the field the most are the composition and mutual interactions of reservoir fluids and reservoir rocks. Because of the involvement of numerous chemical reactions in ISC, it is necessary to understand and determine the type of reactions that occurs during ISC as well as the reaction kinetics which deal with the rates of chemical processes during chemical interactions.

The chemical reactions during ISC in crude oil were defined with pseudo reaction models at different levels of complexity by different researchers. In general, those reactions used crude oil fractions, mainly asphaltenes and maltenes. Asphaltenes are insoluble in n-alkanes (e.g. n-C5, n-C7) but soluble in aromatic solvents (e.g. toluene, benzene) and are the heaviest component of the crude oil (da Silva Ramos et al. 2001;

Mullins et al. 2012). Maltenes (deasphalted oil) are the filtrate of asphaltenes separation and consist of saturates, aromatics, and resins. Meanwhile, coke, fuel or soot are defined as carbonaceous residue formed by thermally cracked hydrocarbons (Bagci 1998; Hascakir et al. 2013; Aleksandrov and Hascakir 2015).

Hayashitani et al. (1978) introduced the first model to simplify oil cracking reactions with at least three different components (asphaltenes, maltenes, and distillates). This model fails to explain all aspects of the combustion reactions, since each component was behaving like a single component without considering their mutual interactions by omitting one of the most important reaction which is coke formation reaction. Crookston et al. (1979) then represented the reactions for coke formation, coke burning, and direct oil burning. However, this reaction scheme was also unrealistic because it was specifying the reaction products only as carbon oxides and water while formation and oxidation of hydrocarbons which lead the formation of oil in the oil bank were neglected.

Later, Adegbesan et al. (1986) simplified the reactions for coke and asphaltenes formation when reacting with oxygen. In disagreement with the assumption of heterogeneous reactions, Adegbesan et al. (1986) claimed that low temperature oxidation (LTO) reactions occurred when oxygen dissolved in the oil phase and hence argued for the importance of the accurate description of oxygen solubility. The reactions are constructed based on the reaction of oil components with soluble oxygen in liquid form and limited to LTO region which does not represent the whole chemical reactions in ISC.

Belgrave et al. (1993) then combined the studies by Hayashitani et al. (1978) and Adegbesan et al. (1986). This model represents both individual reactions on thermal cracking and LTO of Athabasca bitumen, and also the high temperature oxidation (HTO) reactions of coke. Dechelette et al. (2006) used an adiabatic disk reactor for their kinetic study and the heating schedule was imposed by two steps. In the first step, the temperature is increased by 10 K/min up to a temperature at which the temperature starts to increase by itself. Then, a linear schedule is imposed at a rate of 1 K/min.

Kinetics of a light Australian crude oil oxidation was studied by Kisler and Shallcross (1997) via an evolved gas analysis method by mixing sand, water, and crude oil. The mixture was heated at a constant rate with an oxidizing gas. The study also investigated the pressure, sand grain size and carbon dioxide content effects on the kinetic parameters. It was found that the oxidation behavior of light crude oil was significantly different from heavy crudes. In the oxygen consumption versus temperature graph, light crudes show three peaks: LTO, middle temperature oxidation (MTO), and HTO, while heavy crudes provide only two peaks: LTO and HTO.

Multiple researchers have conducted Thermogravimetric Analysis/Differential Scanning Calorimetry (TGA/DSC) experiments on crude oil samples at an average heating rate of 10 °C/min (Vossoughi et al. 1982a; Verkoczy and Jha 1986; Kok 1993; Belgrave et al. 1997; Kok and Acar 2005). A few did their kinetic study at different heating rates up to 20 °C/min (Cinar et al. 2011a; Cinar et al. 2011b; Klock and Hascakir 2015). The

heating rate affects the combustion behavior of crude oil by giving different reaction region intervals, peak and burn-out temperatures (Cinar et al. 2011b).

Vossoughi et al. (1983) used the kinetic model from TGA/DSC experimental results to predict the fuel deposition and combustion rate in a combustion tube that results in a good agreement between the predicted and observed data. Kok (2002) studied the reaction rates for ISC for different heating rates and crude oil compositions. The results show that the oxidation of crude oil in porous media can be categorized into a low temperature oxidation (LTO) region, fuel deposition/thermal cracking region, and high temperature oxidation (HTO) region.

While these works provide important information on the combustion behavior of crude oil, it should be noted that the other reservoir components (reservoir rocks and water) may also have significant impact on combustion, hence, it cannot be ignored. Moreover, the heterogeneous nature of the reservoirs makes the chemical reactions more complicated to estimate since the study on mutual interaction between the reservoir fluids and rocks is limited (Hascakir and Kovscek 2014; Aleksandrov and Hascakir 2015; Ismail et al. 2016).

Reservoir rock may favor or disfavor combustion process, if they are reactive at combustion temperatures. For instance, clays are known as catalyst for combustion and they are also known as increasing the surface area for the fuel combustion (Vossoughi et al. 1982b; Kok 2006).Thus, it is crucial to study the effect of clay on ISC performance. A few studies have emphasized that the catalytic impact of clays towards ISC reduces the

activation energy barrier and increases the amount of coke deposition and generated heat (Vossoughi et al. 1982b; Moore et al. 1999; Lee and Li 2007; Abuhesa and Hughes 2008; Raju et al. 2010; Shah et al. 2011; Kozlowski et al. 2015). An increase in the reactive surface area due to the smaller granular size of clays can increase the fuel burning efficiency. Ranjbar (1993) observed this enhancement on the fuel deposition during pyrolysis with the addition of clay minerals in the rock matrix.

A Thermogravimetric Analysis/Differential Scanning Calorimetry (TGA/DSC) study on the effect of clay (kaolinite) burning behavior conducted by Vossoughi et al. (1983) on an oil sample from Iola Field, Kansas shows a significant reduction in the activation energy. Bousaid and Ramey Jr (1968) also reported a decrease in activation energy and an increase in fuel deposition. Combustion tube experiments were conducted on four different oil samples (viscosity of these oils ranged from 0.0001 to 0.015 cP and oil gravity ranged from 10 to 18° API) mixed with fire-clay (mainly kaolinite) (Fassihi et al. 1984a, 1984b). A similar trend was observed (higher fuel deposition with clay presence) and the authors claimed that it is due to clay adsorption characteristics.

Kok (2006) investigated the effect of clay on crude oil combustion by using Thermogravimetric-Differential Thermal Analysis (TG-DTA) experiments. The crude oil samples used during the experiments were from Turkish oil fields: Garzan (37 cP) and Raman (2260 cP). Kaolinite clay (5 and 10 wt%) was mixed with crude oils to see the effect of clay on combustion. It was proven that activation energies and Arrhenius constants decrease as the clay content increases. The reason for these positive effects on

combustion behavior is due to the clay catalytic effect and the increased surface area of clay.

Besides the positive catalytic effect, clay is also known to have a negative effect when it interacts with reservoir fluids. Some, like kaolinite which is known as pore-filling clay, smectite as pore-lining clay and illite pore-bridging (Neasham 1977; Crocker et al. 1983). Pore-filling, pore-lining, and pore-bridging reduce the effectiveness of ISC performance by clogging the pore throats and decreasing the reservoir permeability and consequently oil mobility.

Not only clays, but also other reservoir rocks/minerals may have impact on ISC performance. For instance, ISC in carbonate reservoirs is also possible, but the reactivity of these reservoir rocks can negatively influence the ISC performance. The main chemicals found in carbonate reservoirs are calcite ($CaCO_3$) and dolomite ($CaMg(CO_3)_2$), which are both highly reactive minerals at elevated temperature (~500 °C) and/or interact with acids and heat (Burger 1972; Wang et al. 1993). As in-situ combustion results in cracking of heavy-high molecular weight hydrocarbons, it generates H_2S which makes the end product sour, consequently, acidic. Thus, it is also important to investigate the role of carbonates on ISC performance before field implementation (Sarathi 1998; Fatemi et al. 2011; Hascakir and Kovscek 2014).

The unpredictable and complex combustion behaviors of crude oil in carbonate formations were reported before through combustion tube experiments on five crude oils and their respective carbonate rocks (Fatemi et al. 2011). The experiments were first run

96

with the crude oils and their reservoir rocks. Then, some different oil-rock combinations were tested with a similar type of combustion experiments. Although these crude oils and rocks are located close geographically, the combustion performances varied greatly. Hence, they concluded that all combustion experiments should be conducted with reservoirs' own rock and fluid samples (Hascakir and Kovscek 2014).

Moreover, not only the reservoir rock and oil have significant contributions on ISC performance determination but also reservoir water. The effect of reservoir water on in-situ combustion performance has not been documented very well before (Verkoczy and Jha 1986; Ambalae et al. 2006; Hascakir et al. 2013; Hascakir and Kovscek 2014). During combustion, the presence of water is known to lead aquathermolysis (hydrous pyrolysis) reactions (Belgrave et al. 1994, 1997). Aquathermolysis results in the decomposition of asphaltic components, thus, decreases the concentration of the least-desired fractions and increases oil mobility (Johnson Jr and Romanowski Jr 1987; Brons and Siskin 1994).

This chapter will discuss the role of crude oil fractions, the role of aquathermolysis reactions, and the reactivity of reservoir rocks on combustion kinetics.

Experimental Procedure

The crude oils samples properties given in Table 4.1 were used in this study. Anton Paar DMA 4100 density meter and Brookfield DV-III Ultra rheometer were used in measuring the API gravity at standard conditions (15 °C) and viscosity at room temperature (22.3 °C) for the initial oil samples, respectively (Prakoso et al. 2016).

Saturates, aromatics, resins, and asphaltenes (SARA) fractionations of the crude oil samples were conducted by following ASTM D2007-11 standard (ASTM 2007). Asphaltenes were separated by using n-pentane and the filtrate, deasphalted oil (DAO) was later separated into saturates, aromatics, and resins through column separation. Carbon and hydrogen weight percentage in oil and in their asphaltenes were determined by using LECO Carlo Erba CHN analyzer and the metal content was determined by Thermo Intrepid Inductively Coupled Plasma (ICP) analyzer (Prakoso et al. 2018).

Table 4.1—Characterization of Initial Crude Oil Samples and Elemental Composition of Deasphalted Oil (DAO) and Asphaltenes (ASP) (Prakoso et al. 2015)

Parameter	Oil A			Oil B		
	Initial Oil	ASP	DAO	Initial Oil	ASP	DAO
Gravity at 15 °C, °API	8.19	-	-	7.97	-	-
Viscosity at 22.3 °C, cP	53,000	-	-	251,000	-	-
Saturates, wt%	23.6	-	-	12.7	-	-
Aromatics, wt%	20.2	-	-	42.1	-	-
Resins, wt%	21.9	-	-	22.9	-	-
Asphaltenes,wt%	34.3	-	-	22.3	-	-
C	83.5	18.20	65.30	80.3	22.77	57.53
H	10.6	1.78	8.82	10.3	2.73	7.57
Other*	5.83	2.27	3.56	9.27	8.77	0.50
S	0.036	0.016	0.020	0.068	0.035	0.033
Metals†	0.0361	0.0003	0.0358	0.0685	0.0011	0.0674

*Other elements are mainly oxygen and also contain non-metal and non-sulfur elements
†Metals are alkaline metals, alkaline earth metals, semimetals, and transition metals

Three sets of reaction kinetics experiments were conducted on these two oil samples by Thermogravimetric Analysis/Differential Scanning Calorimetry (TGA/DSC) under 50 ml/min air injection (20 ml/min nitrogen was used as the purge gas) (ASTM 2014). For all experiments, TGA/DSC tests were started at 25 °C and ended at 900 °C. Varying heating rates were tested (5 °C/min and 20 °C/min) to also investigate the impact of heating rate on combustion kinetics.

In the first set (Table 4.2), the role of crude oil components was studied on Oil A. TGA/DSC tests were conducted on Initial Oil A, its individual saturates, aromatics, resins, and asphaltenes (SARA) fractions, and the pseudo blends of SARA fractions. It is known that the heating rate greatly influences the type of reactions and product distribution (Verkoczy and Jha 1986). The experiments were conducted at 5 °C/min constant heating rate which was representing slow increase heating rate region that controls low temperature oxidation (LTO) products for ISC (Adegbesan et al. 1986; Pu et al. 2017).

Table 4.2—Nomenclature for the First Set of Reaction Kinetics Experiments to Investigate the Role of Crude Oil Composition on Combustion at 5 °C/min Heating Rate

Kinetic Test Run	Samples	Amount (wt%)
Test 1	Oil A	100
Test 2	Saturates (S) of Oil A	100
Test 3	Aromatics (A) of Oil A	100
Test 4	Resins (R) of Oil A	100
Test 5	Asphaltenes (Asp) of Oil A	100
Test 6	S : Asp of Oil A	40.96 : 59.04
Test 7	A : Asp of Oil A	36.83 : 63.17
Test 8	R : Asp of Oil A	38.67 : 61.03
Test 9	S : A of Oil A	54.33 : 45.67
Test 10	S : R of Oil A	52.08 : 47.92
Test 11	A : R of Oil A	47.73 : 52.27
Test 12	S : A : Asp of Oil A	30.47 : 25.61 : 43.92
Test 13	S : R : Asp of Oil A	29.75 : 27.38 : 42.88
Test 14	A : R : Asp of Oil A	26.25 : 28.74 : 45.01
Test 15	S : A : R of Oil A	36.23 : 30.44 : 33.33
Test 16	S : A : R : Asp of Oil A	23.8 : 20 : 21.9 : 34.3

*Ratios for Test 6-16 were based on initial oil sample given in Table 4.1

Arrhenius (Arrhenius 1889; Kok 1993), Coats-Redfern (Coats and Redfern 1964), Horowitz-Metzger (Horowitz and Metzger 1963), and Ingraham-Marrier (Ingraham and Marrier 1964) models were used to determine the average activation energy (Appendix 4A). All of these methods are derived based on Arrhenius kinetic theory to find the activation energy (E_a) as a function of reaction conversion (α) and temperature (T) in a linear correlation from Thermogravimetric Analysis (TGA) data. By deriving TGA graphs over time (Arrhenius 1889; Kok 2002), differential thermogravimetric (DTG) graphs were obtained and the linear correlations of the model fitting equation (Appendix 4B) were calculated. Model fitting methods are generally preferred to calculate kinetic energy parameters since they can be determined by using only one heating rate (β).

In this study, as model assumption, first order reaction was used to calculate kinetics parameters (Arrhenius 1889; Kok 1993). The total enthalpy (H) of a system cannot be measured directly, but, only a change or difference in energy can be measured (ΔH) (Van Wylen et al. 1994). Thus, the heat of combustion (ΔH) was also calculated by integrating the area under the Differential Scanning Calorimetry (DSC) curves (Kok 1993; Cinar et al. 2011a).

It has been reported previously that combustion could not be sustained for Oil A if there is no initial water in the medium (Kudryavtsev and Hascakir 2014). Thus, the second set of reaction kinetics experiments were conducted to investigate the impact of water on ISC performance. The behavior of both oil samples properties given in Table 4.1 was investigated. 40 reaction kinetics experiments were performed at two heating rates (5 and 20 °C/min). Nomenclature for kinetics test is summarized in Table 4.3.

Table 4.3—Nomenclature for the Second Set of Reaction Kinetics Experiments to Investigate the Role of Water for Combustion

Kinetic Test Run	Samples	Amount (wt%)	Heating Rate (°C/min)
Test 1	Oil A	100	5
Test 2	Oil A	100	20
Test 3	Oil A : Water	66 : 34	5
Test 4	Oil A : Water	66 : 34	20
Test 5	Saturates (S) of Oil A	100	5
Test 6	Saturates (S) of Oil A	100	20
Test 7	Saturates (S) of Oil A : Water	66 : 34	5
Test 8	Saturates (S) of Oil A : Water	66 : 34	20
Test 9	Aromatics (A) of Oil A	100	5
Test 10	Aromatics (A) of Oil A	100	20
Test 11	Aromatics (A) of Oil A : Water	66 : 34	5
Test 12	Aromatics (A) of Oil A : Water	66 : 34	20
Test 13	Resins (R) of Oil A	100	5
Test 14	Resins (R) of Oil A	100	20
Test 15	Resins (R) of Oil A : Water	66 : 34	5
Test 16	Resins (R) of Oil A : Water	66 : 34	20
Test 17	Asphaltenes (Asp) of Oil A	100	5
Test 18	Asphaltenes (Asp) of Oil A	100	20
Test 19	Asphaltenes (Asp) of Oil A : Water	66 : 34	5
Test 20	Asphaltenes (Asp) of Oil A : Water	66 : 34	20
Test 21	Oil B	100	5
Test 22	Oil B	100	20
Test 23	Oil B : Water	66 : 34	5
Test 24	Oil B : Water	66 : 34	20
Test 25	Saturates (S) of Oil B	100	5
Test 26	Saturates (S) of Oil B	100	20
Test 27	Saturates (S) of Oil B : Water	66 : 34	5
Test 28	Saturates (S) of Oil B : Water	66 : 34	20
Test 29	Aromatics (A) of Oil B	100	5
Test 30	Aromatics (A) of Oil B	100	20
Test 31	Aromatics (A) of Oil B : Water	66 : 34	5
Test 32	Aromatics (A) of Oil B : Water	66 : 34	20
Test 33	Resins (R) of Oil B	100	5
Test 34	Resins (R) of Oil B	100	20
Test 35	Resins (R) of Oil B : Water	66 : 34	5
Test 36	Resins (R) of Oil B : Water	66 : 34	20
Test 37	Asphaltenes (Asp) of Oil B	100	5
Test 38	Asphaltenes (Asp) of Oil B	100	20
Test 39	Asphaltenes (Asp) of Oil B : Water	66 : 34	5
Test 40	Asphaltenes (Asp) of Oil B : Water	66 : 34	20

In the second set, the impact of water, crude oil composition, heating rate, and crude oil fractions on crude oil combustion were investigated. Two heating rates were used for each case; 5 °C/min and 20 °C/min. It should be noted that in the natural behavior of combustion process, several different heating rates are observed. However, two main heating rates region can be distinguished; low and high heating rates. Low heating rates are observed till the reaction zone temperature reaches steam temperature, then, heating rates increased suddenly and jumped to combustion temperature by utilizing high heating rates. To replicate the behavior observed during ISC, in the second set reaction kinetics experiments, two heating rates were used (Sarathi 1998; Kudryavtsev and Hascakir 2014; Aleksandrov and Hascakir 2015).

A previous study on the effect of initial oil and water saturations towards the dynamics of ISC (Kudryavtsev and Hascakir 2014; Aleksandrov and Hascakir 2015) determined that 34 volume percent oil and water saturations were the optimal saturation value for the best ISC performance of Oil A at given experimental conditions. The same oil and water saturations (34 volume percent) were used to study the impact of water presence on Oil B as well.

Subsequently, similar reaction kinetics analyses given in second set were conducted on hydrocarbons with known molecular formulas (Table 4.4). Four different hydrocarbon groups (alkanes, aldehydes, alcohols, and ketones) were selected which represent the simplified low temperature oxidation (LTO) products, to investigate how the reaction kinetics tests of these four groups resemble the reaction kinetics of SARA

103

fractions from Oil A and Oil B. This way, the functional groups present in SARA fractions that cause differences in burning behavior of bulk crude oil can be identified.

This set of reaction kinetics experiments named as control experiments were conducted on n-decane ($C_{10}H_{22}$), n-decanal ($C_{10}H_{20}O$), n-decanol ($C_{10}H_{22}O$), and decanone ($C_{10}H_{20}O$). All these chemicals have 10 carbons and they all have a saturated hydrocarbon chains. However, decane is a normal alkane, decanal is an aldehyde, decanol is an alcohol, and decanone is a ketone. Apart from decane, the other chemicals were selected due to their oxygen content that represents the LTO products observed in ISC (Burger et al. 1985). 16 reaction kinetics experiments were conducted on these samples in the presence and absence of water at 5 and 20 °C/min heating rates.

Table 4.4—Nomenclature for the Control Experiments to Investigate the Role of Simple LTO Products on Crude Oil Combustion in the Presence of Water at Low and High Heating Rates

Kinetic Test Run	Samples	Amount (wt%)	Heating Rate (°C/min)
Test 41	Decane	100	5
Test 42	Decane	100	20
Test 43	Decane : Water	66 : 34	5
Test 44	Decane : Water	66 : 34	20
Test 45	Decanal	100	5
Test 46	Decanal	100	20
Test 47	Decanal : Water	66 : 34	5
Test 48	Decanal : Water	66 : 34	20
Test 49	Decanol	100	5
Test 50	Decanol	100	20
Test 51	Decanol : Water	66 : 34	5
Test 52	Decanol : Water	66 : 34	20
Test 53	Decanone	100	5
Test 54	Decanone	100	20
Test 55	Decanone : Water	66 : 34	5
Test 56	Decanone : Water	66 : 34	20

Lastly, the third set evaluated the impact of reservoir rock mineralogy (clay and carbonate) and amount of clay on Oil A (Table 4.5). Clay (90 wt% kaolinite and 10 wt% illite) was blended with non-reactive Ottawa sand (Svrcek and Mehrotra 1989) to prepare the reservoir rock samples for the tests conducted with clay. The impact of carbonates on ISC performance was investigated by using 100 wt% carbonates; calcite ($CaCO_3$) and dolomite ($CaMg(CO_3)_2$). Pure calcium carbonate powder (100% calcite) was acquired from Sigma-Aldrich with particle size of 9.4 ± 0.9 µm (Sigma-Aldrich, 2019). Dolomite was obtained from a local company (Kocurek Industries) and X-ray fluorescence (XRF) test confirmed that dolomite contains 94 wt% calcium, magnesium, carbon, and oxygen. Because the XRF results show that the calcium to magnesium molar ratio is nearly 1.20, the dolomite that we used in this study may also contain calcite since calcium to magnesium molar ratio in pure dolomite should be 1.0.

Both Oil A and its SARA fractions were subjected to TGA/DSC analyses in the presence and absence of carbonate minerals. The pore space in clay-sand blends and carbonates were filled with 60 vol% oil or SARA fractions. To simplify the study, TGA/DSC was conducted only at one constant heating rate (15 °C/min) which represents high heating rates observed after reaching LTO region (Vossoughi et al. 1982a; Vossoughi et al. 1983; Kok 2002; Pu et al. 2017). Activation energy was then calculated by using the Arrhenius (Arrhenius 1889; Kok 1993) model (Appendix 4A).

Table 4.5—Nomenclature for the Third Set of Reaction Kinetics Experiments to Investigate the Role of Reservoir Rock Mineralogy on Combustion at 15 °C/min Heating Rate

Kinetic Test Run	Sample Type	Hydrocarbon (wt%)	Ottawa Sand (wt%)	Clay (wt%)	Calcite (wt%)	Dolomite (wt%)
Test 1	Oil A	100	-	-	-	-
Test 2	Clay	-	-	100	-	-
Test 3	Ottawa Sand	-	100	-	-	-
Test 4	Clay + Sand	-	97	3	-	-
Test 5	Calcite	-	-	-	100	-
Test 6	Dolomite	-	-	-	-	100
Test 7	Oil A + Sand + 3% Clay	9.21	88.07	2.72	-	-
Test 8	Oil A + Sand + 6% Clay	9.21	85.34	5.45	-	-
Test 9	Oil A + Sand + 9% Clay	9.21	82.62	8.17	-	-
Test 10	Oil A + Sand + 12% Clay	9.21	79.90	10.89	-	-
Test 11	Oil A + Calcite	22	-	-	78	-
Test 12	Oil A + Dolomite	22	-	-	-	78
Test 13	Oil A Saturates	100	-	-	-	-
Test 14	Oil A Saturates + Calcite	22	-	-	78	-
Test 15	Oil A Saturates + Dolomite	22	-	-	-	78
Test 16	Oil A Aromatics	100	-	-	-	-
Test 17	Oil A Aromatics + Calcite	22	-	-	78	-
Test 18	Oil A Aromatics + Dolomite	22	-	-	-	78
Test 19	Oil A Resins	100	-	-	-	-
Test 20	Oil A Resins + Calcite	22	-	-	78	-
Test 21	Oil A Resins + Dolomite	22	-	-	-	78
Test 22	Oil A Asphaltenes	100	-	-	-	-
Test 23	Oil A Asphaltenes + Calcite	22	-	-	78	-
Test 24	Oil A Asphaltenes + Dolomite	22	-	-	-	78

Results and Discussion

The detailed reaction kinetic analyses were conducted on Oil A. The role of crude oil components has been investigated on individual SARA fractions and their pseudo blends (Table 4.2). Four reaction kinetics models were tested: Arrhenius, Coats-Redfern, Horowitz-Metzger, and Ingraham-Marrier methods. The equations for the four kinetics models were summarized in Appendix 4A.

106

Table 4.6—Determination of ISC Performance by Heat Generation and Heat Consumption

[Heat Generation — Heat Consumption] at Low Heating Rate	Values	[Heat Generation — Heat Consumption] at High Heating Rate	ISC Performance
Positive	Similar	Positive	Successful
Negative	Similar	Negative	Unsuccessful
Positive	Larger	Negative	Successful
Negative	Larger	Positive	Unsuccessful
Positive	Smaller	Negative	Unsuccessful
Negative	Smaller	Positive	Unsuccessful

Table 4.6 helps visualize how heat generation and heat consumption determine the success of ISC. To summarize Table 4.6, the heat generation at low heating rate zone should be high enough so that after consumption, it will be sufficient to sustain the combustion reaction in high heating rate zone. If the heat generation is not enough, ISC will not sustain and will be unsuccessful.

Thermogravimetric (TG) results are given in Appendix 4B for the first set of reaction kinetics experiments (Table 4.2). The TG results were then derived to obtain DTG graphs and are represented in Figure 4 B1 in Appendix 4B. These data were then used to construct model fitting graphs (Figure 4 B2 to Figure 4 B17). Accordingly, activation energy, E_a which is the slope of the curve and Arrhenius constant, A which is the y-intercept were calculated and they have been reported in Table 4.7 for the first set of reaction kinetics experiments. The heat of combustion, ΔH was also reported in Table 4.7, calculated from the area under the curves of DSC graphs.

In the TG/DTG curves of crude oil combustion (Figure 4 B1 A), three distinct reaction regions were observed. The first region was the water evaporation zone, where the water content within the crude oils evaporated in an endothermic reaction. It should be noted that in the first set of experiment, since no water was added, the water evaporated from samples is emulsified water. The second region was the low temperature oxidation (LTO) region, where mass was lost due to distillation and oxidation reactions. Lastly, the third region was the high temperature oxidation (HTO) region, where visbreaking and thermal cracking reactions of crude oil took place. However, for the rest of the experiments in Figure 4 B1, there were only two regions observed: LTO and HTO. Thus, in Table 4.7, crude oil (Test 1) results were reported for three regions: water evaporation, LTO, and HTO, while the rest of the test results are given for LTO and HTO regions. After E_a was calculated from the model parameters given in Appendix 4A, the mean values (E_{mean}) for all four reaction kinetics models are reported in Table 4.7.

Table 4.7—Reaction Kinetics Parameter of Oil A and Its SARA Fractions Obtained through TGA/DSC Experiments and Calculated by Using 4 Different Reaction Kinetics Models (Refer to Table 4.2 for Nomenclature)

Test Run	Samples	Temperature Ranges (°C)	Arrhenius E_a (BTU/lb-mol)	Arrhenius A (1/min)	Coats-Redfern E_a (BTU/lb-mol)	Coats-Redfern A (1/min)	n	Horowitz-Metzger E_a (BTU/lb-mol)	Ingraham-Marrier E_a (BTU/lb-mol)	E_{Mean} (BTU/lb-mol)	Heat of Combustion, ΔH (BTU/lb-mol)
Test 1	Crude Oil	Water: 27-157	32,873	9.55E+08	33,224	1.48E+21	1.0	43,162	37,570	36,707	1,656
		LTO: 157-407	6,057	0.33	4,554	7.94E-07	1.5	5,544	3,459	4,904	-14,448
		HTO: 407-627	119,699	1.45E+18	118,799	2.57E+00	1.0	134,698	162,399	133,899	-29,386
Test 2	Saturates (S)	LTO: 27-395	23,121	5.80E+03	28,757	511.09	0.9	29,461	20,830	25,542	-28,238
		HTO: 395-627	43,968	2.35E+05	42,734	3.50E-04	0.8	44,581	46,616	44,475	-25,318
Test 3	Aromatics (A)	LTO: 27-408	15,240	1.09E+02	19,463	4.29E-07	1.2	12,279	14,273	15,314	-31,132
		HTO: 408-627	72,935	2.58E+10	71,980	7.20E-08	1.0	78,822	78,584	75,580	-29,184
Test 4	Resins (R)	LTO: 27-497	16,147	50.65	17,758	23.07	1.2	16,155	12,785	15,711	-35,819
		HTO: 497-627	100,635	4.63E+14	137,054	2.12E-08	1.7	152,742	154,035	136,117	-82,732
Test 5	Asphaltenes (Asp)	LTO: 27-500	42,090	1.76E+06	47,267	2.41E-07	1.9	42,126	42,037	43,380	-12,539
		HTO: 500-627	74,985	4.04E+10	78,224	2.84E+09	1.3	70,696	77,316	75,305	-50,095
Test 6	S : Asp	LTO: 27-329	17,102	314.34	13,353	6.51E-08	1.0	16,092	13,899	15,112	-27,258
		HTO: 329-627	61,635	9.43E+09	68,146	1.73E+06	1.0	69,205	74,638	68,406	-98,642
Test 7	A : Asp	LTO: 27-364	10,747	1.11E+00	11,155	3.93E-10	1.0	12,810	18,758	13,368	-27,688
		HTO: 364-627	98,848	5.73E+14	98,522	256.86	1.3	94,636	91,143	95,787	-80,922
Test 8	R : Asp	LTO: 27-369	20,670	349.22	23,314	9.55E-11	1.0	20,348	23,076	21,852	-41,117
		HTO: 369-627	71,251	2.13E+10	67,802	1.96E-03	1.0	59,537	72,845	67,859	-83,497
Test 9	S : A	LTO: 27-383	19,457	1.21E+03	26,444	8.03E+04	1.0	19,753	17,213	20,717	-36,903
		HTO: 383-627	85,581	7.36E+12	83,975	1.34E-06	1.0	87,158	87,501	86,054	-44,957
Test 10	S : R	LTO: 27-393	14,413	57.53	15,811	6.33E-08	1.2	15,569	14,433	15,057	-30,483
		HTO: 393-627	112,378	1.81E+16	128,631	1.92E-10	1.7	125,239	126,609	123,214	-34,882
Test 11	A : R	LTO: 27-404	19,887	3.97E+03	21,981	1.44E-08	1.0	21,234	19,387	20,622	-90,240
		HTO: 404-627	98,651	3.80E+14	95,078	1.10E-05	1.0	95,293	93,755	95,694	-105,290
Test 12	S : A : Asp	LTO: 27-349	17,754	1.35E+02	14,442	1.53E-03	1.2	20,146	16,674	17,254	-34,748
		HTO: 349-627	132,892	1.70E+20	125,497	4.98E+03	1.7	146,371	151,281	139,010	-91,285
Test 13	S : R : Asp	LTO: 27-339	19,550	509.10	16,692	439.14	1.2	18,644	18,279	18,291	-23,009
		HTO: 339-627	101,870	3.10E+15	107,387	1.01E-02	1.0	104,618	108,271	105,537	-37,182
Test 14	A : R : Asp	LTO: 27-369	19,098	1.09E+02	20,138	1.6	1.0	22,843	26,020	22,025	-49,600
		HTO: 369-627	82,937	1.17E+12	88,424	1.61E+07	1.3	80,915	86,571	84,712	-138,989
Test 15	S : A : R	LTO: 27-373	19,252	1.02E+03	23,187	3.17E-06	1.0	22,403	23,799	22,160	-39,547
		HTO: 373-627	41,445	6.44E+04	41,158	2.71E-04	1.0	42,576	45,458	42,659	-55,952
Test 16	S : A : R : Asp	LTO: 27-379	17,507	115.08	20,401	5.85E-05	1.0	23,717	21,712	20,834	-26,694
		HTO: 379-627	98,807	3.70E+14	104,525	9.33E+03	1.5	95,343	103,840	100,629	-77,232

* Temperature (K) = Temperature (°C) + 273.15

The four models (Model Fitting) used to calculate reaction kinetics parameters for this set of experiments are Arrhenius, Coats-Redfern, Horowitz-Metzger, and Ingraham-Marrier methods. In general, similar activation energy values were obtained for different kinetic methods. The activation energy variation of samples for different models can be explained with the different equation parameters that the models were based on. This plays a vital role in determining the slope of the graphs in the path of calculating the reaction kinetics parameter and the temperature ranges for LTO and HTO regions.

Another model that can be used to calculate the reaction kinetics parameter is the Model Free (Ozawa-Flynn-Wall, Kissinger-Akahira-Sunose, Friedman, Augis & Bennett) methods (Friedman 1964; Ozawa 1965, 1970). This model allows kinetic properties to be determined without any reaction model assumption and can be used to represent the conversion rate of reactions (Kok and Acar 2005). However, the experiments for the same samples need to be conducted in at least three different heating rates where the extent of decomposition is higher for a slower heating rate compared to sudden increase in heat (Arrhenius 1889; Akin et al. 2000). For further studies, additional experiments can be done at different heating rates to thoroughly study the kinetic process which cannot be directly obtained from Model Fitting methods given in Table 4.7.

For combustion to sustain, activation energy (E_a) has to be lower than heat of combustion (ΔH) (Sarathi 1998; Kok 2002). Overall, from the results reported in Table 4.7, most of the experiments were showing a good result (activation energy values are lower than the heat generated). However, crude oil results (Test 1 in Table 4.7) show that the summation of activation energies (energy consumption) at water evaporation, LTO

region, and HTO region is way higher than the summation of enthalpy (heat generation). This indicates that Oil A alone does not favor ISC. The components responsible from this result was investigated with Test 2 through Test 16 (Table 4.7).

Saturates fractions consumes more heat in LTO and HTO regions than they generate heat. Thus, they might be responsible from the failure of ISC (Test 2 through Test 5 in Table 4.7). However, for two-components pseudo blends (Test 6 through Test 11 in Table 4.7), saturates-asphaltenes, resins-asphaltenes, aromatics-resins mutual interaction favors ISC. Aromatics and asphaltenes mutual interaction does not have significant impact on ISC. Saturates-aromatics and saturates-resins interaction disfavor ISC. In the three-pseudo fractions experiments (Test 12 through Test 15 in Table 4.7), saturates-aromatics-asphaltenes and saturates-resins-asphaltenes disfavor combustion. Aromatics-resins-asphaltenes favor combustion and saturates-aromatics-resins barely favor combustion.

This discussion above proves that saturates fraction of crude oil mainly responsible from the failure of ISC for Oil A. Saturates ignition properties alone is not sufficient to start combustion reactions. However, aromatics-resins-asphaltenes mutual interactions (Test 14 in Table 4.7) shows that ISC can be successful if at the ignition, saturates fraction can be used more effectively.

When SARA fractions were separated and remixed (Test 16 in Table 4.7), the mixture resulted in lower but similar activation energy for both LTO and HTO regions. The higher activation energy at the water evaporation zone for the original bitumen (Test 1 in Table 4.7) was mainly due to the water content in the crude oil, causing the increase

in activation energy compared to the activation energy of the SARA pseudo-mixture. Note that during SARA separation, water is lost. Thus, emulsified water presence can be very critical for the combustion kinetics of some oils and ignoring its presence may generate misleading results.

In the second set, the impact of water presence on ISC performance was further studied (Table 4.3). TGA/DSC experiments were conducted on Oil A and Oil B at two different fixed heating rates: low heating rates (5 °C/min) and high heating rates (20 °C/min) to mimic the behavior observed in LTO and HTO regions of ISC. The reaction kinetics study (TGA/DSC) summary given in Figure 4 C1, Figure 4 C2 , and Figure 4 C3 shows that both oil samples exhibit different combustion behaviors in the presence and absence of water phase in the system. The reaction kinetics of both crude oils and its individual fractions were studied in this work to develop an understanding of the role of each SARA fraction during ISC through a simplified approach.

Table 4.8—Kinetics Parameter for Oil A, Oil B, their SARA Fractions at Low (5 °C/min) and High (20 °C/min) Heating Rates (Refer to Table 4.3 for Nomenclature)

Kinetic Test Run	Samples	Heating Rate (°C/min)	E_a (BTU/lb-mol)	Heat of Combustion, ΔH (BTU/lb-mol)
Test 1	Oil A	5	32,873	-35,824
Test 2	Oil A	20	37,856	-14,034
Test 3	Oil A : Water	5	36,341	-55,597
Test 4	Oil A : Water	20	18,088	-48,014
Test 5	Saturates (S) of Oil A	5	23,620	-18,903
Test 6	Saturates (S) of Oil A	20	23,612	-24,583
Test 7	Saturates (S) of Oil A : Water	5	14,618	-47,552
Test 8	Saturates (S) of Oil A : Water	20	80,560	-31,771
Test 9	Aromatics (A) of Oil A	5	15,240	-25,369
Test 10	Aromatics (A) of Oil A	20	68,045	-37,924
Test 11	Aromatics (A) of Oil A : Water	5	10,582	-45,235
Test 12	Aromatics (A) of Oil A : Water	20	33,439	-46,611
Test 13	Resins (R) of Oil A	5	32,233	-25,495
Test 14	Resins (R) of Oil A	20	74,998	-22,123
Test 15	Resins (R) of Oil A : Water	5	11,190	-40,911
Test 16	Resins (R) of Oil A : Water	20	29,967	-65,401
Test 17	Asphaltenes (Asp) of Oil A	5	30,918	-50,052
Test 18	Asphaltenes (Asp) of Oil A	20	39,152	-34,989
Test 19	Asphaltenes (Asp) of Oil A : Water	5	49,437	-10,132
Test 20	Asphaltenes (Asp) of Oil A : Water	20	25,514	-54,996
Test 21	Oil B	5	5,349	-62,259
Test 22	Oil B	20	26,707	-16,162
Test 23	Oil B : Water	5	17,434	-27,253
Test 24	Oil B : Water	20	7,171	-35,736
Test 25	Saturates (S) of Oil B	5	20,396	-18,728
Test 26	Saturates (S) of Oil B	20	15,980	19,412
Test 27	Saturates (S) of Oil B : Water	5	11,648	-47,438
Test 28	Saturates (S) of Oil B : Water	20	17,093	-22,034
Test 29	Aromatics (A) of Oil B	5	18,220	-79,010
Test 30	Aromatics (A) of Oil B	20	11,031	-63,337
Test 31	Aromatics (A) of Oil B : Water	5	19,142	-37,946
Test 32	Aromatics (A) of Oil B : Water	20	17,226	-78,238
Test 33	Resins (R) of Oil B	5	18,673	-57,331
Test 34	Resins (R) of Oil B	20	36,200	-37,504
Test 35	Resins (R) of Oil B : Water	5	23,768	-10,241
Test 36	Resins (R) of Oil B : Water	20	38,729	-35,073
Test 37	Asphaltenes (Asp) of Oil B	5	54,139	-73,949
Test 38	Asphaltenes (Asp) of Oil B	20	31,176	-23,665
Test 39	Asphaltenes (Asp) of Oil B : Water	5	53,721	-60,415
Test 40	Asphaltenes (Asp) of Oil B : Water	20	3,527	-36,920

Table 4.9—Kinetics Parameter for Known Hydrocarbons at Low (5 °C/min) and High (20 °C/min) Heating Rates (Refer to Table 4.4 for Nomenclature)

Kinetic Test Run	Samples	Heating Rate (°C/min)	E_a (BTU/lb-mol)	Heat of Combustion, ΔH (BTU/lb-mol)
Test 41	Decane	5	27,988	-15,146
Test 42	Decane	20	38,438	-30,556
Test 43	Decane : Water	5	20,738	-14,640
Test 44	Decane : Water	20	25,856	-20,241
Test 45	Decanal	5	29,692	-30,734
Test 46	Decanal	20	22,515	-33,836
Test 47	Decanal : Water	5	42,754	-32,748
Test 48	Decanal : Water	20	17,682	-22,004
Test 49	Decanol	5	31,595	-22,735
Test 50	Decanol	20	40,493	-35,653
Test 51	Decanol : Water	5	13,336	-21,690
Test 52	Decanol : Water	20	14,646	-29,975
Test 53	Decanone	5	26,046	-22,686
Test 54	Decanone	20	21,388	-24,224
Test 55	Decanone : Water	5	13,710	-21,193
Test 56	Decanone : Water	20	39,779	-25,094

Water presence in Oil A enhances ignition characteristics of saturates (Test 7 in Table 4.8) by lowering the activation energy for saturates and increasing the heat generation, and enhances burning behavior of aromatics (Test 11 in Table 4.8) at low heating rates region. Water presence significantly reduces the activation energy necessary to crack resins (Test 15 and Test 16 in Table 4.8) both in low and high heating rates region. Due to lighter fractions, combustion of Oil B can still sustain without water. Water for sure aids combustion for Oil B as well and gives better results. The lighter components ignition and asphaltenes cracking become better in the presence of water for Oil B.

The control experiments in Table 4.9 were considered only for low heating rates (5 °C/min) since they are LTO products which will only be observed at low heating rates.

Decane (Test 41 and Test 43 in Table 4.9) in burning behavior did not improve significantly but its activation energy decreased. Decanal (Test 47 in Table 4.9) combustion behavior became worse in the presence of water. Meanwhile, decanol (Test 51 in Table 4.9) and decanone (Test 55 in Table 4.9) combustion behavior became better in the presence of water. Thus, in Oil A, it should have alcohol and ketone structures for the combustion to be successful in the presence of water.

The chemical reactions in ISC are not only controlled by the reservoir fluids (oil components and water), but also by reservoir rock components, and the mutual interactions of reservoir rocks with oil at elevated temperature (Kar et al. 2015; Kozlowski et al. 2015; Ismail et al. 2016). Thus, the third set of reaction kinetics experiments evaluated the impact of reservoir rocks mineralogy (clay and carbonate) on Oil A. The role of clay amount on ISC kinetics will be discussed first. Clay is known to increase the surface area and is a highly reactive reservoir rock (Vossoughi et al. 1983). Figure 4 D1 A & B show the TGA/DSC curves for Oil A-clay-sand mixture and in the presence of 3 wt%, 6 wt%, 9 wt%, and 12 wt% of clay (Tests 7-10 in Table 4.5). Figure 4 D1 C & D provide the TGA/DSC curves for initial Oil A, Ottawa sand, clay, and clay-sand mixture (Tests 1-4 in Table 4.5) as reference. Table 4.10 reports the kinetic modeling results for all experiments listed in Table 4.5.

Table 4.10— Kinetics Parameter for Oil A, Its SARA, and Rock Matrix Combustion at 15 °C/min Heating Rate (Refer to Table 4.5 for Nomenclature)

Test Run	Samples	Temperature Ranges (°C)	Activation Energy, Ea (BTU/lb-mole)	Heat of Combustion, ΔH (BTU/lb-mol)
Test 1	Oil A	Water: 25-157	32,873	1,656
		LTO: 158-407	6,057	-14,448
		HTO: 408-650	119,699	-29,386
Test 2	Clay	Decomp:465-900	36,639	-221,621
Test 3	Ottawa Sand	Non-reactive	Non-reactive	Non-reactive
Test 4	Clay + Sand	Decompose: 424-659	26,487	-54,059
Test 5	Calcite	Decompose: 729-900	101,096	-40,374
Test 6	Dolomite	Decompose: 591-900	91,337	-7,801
Test 7	Oil A + Sand + 3% Clay	LTO: 25-395	5,689	-6,012
		HTO: 395-650	27,418	-36,710
Test 8	Oil A + Sand + 6% Clay	LTO: 25-395	3,876	-17,578
		HTO: 395-650	26,207	-42,579
Test 9	Oil A + Sand + 9% Clay	LTO: 25-395	2,937	-32,558
		HTO: 395-650	25,486	-71,361
Test 10	Oil A + Sand + 12% Clay	LTO: 25-395	4,1670	-23,980
		HTO: 395-650	34,311	-39,959
Test 11	Oil A + Calcite	Water: 25-154	50,140	-654
		LTO: 155-364	13,288	-20,128
		HTO: 365-584	116,282	-46,199
		Decompose: 585-892	105,543	-5,083
Test 12	Oil A + Dolomite	Water: 25-215	42,389	1,758
		LTO: 216-325	10,685	-3,913
		HTO: 326-472	22,407	-4,398
		Decompose: 473-892	44,736	-6,681
Test 13	Oil A Saturates	LTO: 25-395	23,121	-28,238
		HTO: 395-650	43,968	-25,318
Test 14	Oil A Saturates + Calcite	LTO: 25-534	22,613	-25,976
		HTO: 534-892	104,456	-31,672
Test 15	Oil A Saturates + Dolomite	LTO: 25-470	25,448	-23,659
		HTO: 471-892	67,571	-24,160
Test 16	Oil A Aromatics	LTO: 25-408	15,240	-31,132
		HTO: 408-650	72,935	-29,184
Test 17	Oil A Aromatics + Calcite	LTO: 25-418	24,632	-160,390
		HTO: 418-892	130,941	-178,635
Test 18	Oil A Aromatics + Dolomite	LTO: 25-490	22,841	-13,487
		HTO: 491-892	84,329	-21,047
Test 19	Oil A Resins	LTO: 25-497	16,147	-35,819
		HTO: 497-650	100,635	-82,732
Test 20	Oil A Resins + Calcite	LTO: 25-630	18,520	-27,385
		HTO: 630-892	113,103	-35,886
Test 21	Oil A Resins + Dolomite	LTO: 25-511	10,222	-7,189
		HTO: 512-892	64,223	-17,093
Test 22	Oil A Asphaltenes	LTO: 25-500	42,090	-12,539
		HTO: 500-650	74,985	-50,095
Test 23	Oil A Asphaltenes + Calcite	LTO: 25-630	18,919	-47,296
		HTO: 630-892	66,638	-70,305
Test 24	Oil A Asphaltenes + Dolomite	LTO: 25-510	7,880	-5,944
		HTO: 510-892	76,065	-33,251

Presence of clay in Oil A reservoir decreases the activation energy slightly in the LTO region and significantly in the HTO region. However, heat of combustion decreases

in the LTO region but increases in the HTO region. As the clay content increases, these changes seem more significant until reaching 12% clay. For 12 % clay, the reverse relations were observed. The catalytic effect of clay might be surpassed by an element from the crude oil component which overshadowed it (Vossoughi et al. 1983). The results might indicate that this clay-oil pair may have an optimum reaction at 9% clay content which yields the greatest heat generation. Below and above this value, the heat generation might reduce.

In regards to the discussion of the parameters of in-situ combustion in carbonate reservoirs, it is established that the reservoirs' reactivity stimulates a higher-risk ISC process. Oil burning reaction with and without the presence of calcite and dolomite were investigated in this study. Figure 4 D4 provides the TGA/DSC curves for Ottawa sand, dolomite, and calcite (Tests 3, 5, 6 in Table 4.5) as reference. TGA/DSC graphs for Oil A and its SARA combustion (Tests 11-24 in Table 4.5) for the presence of carbonate are reported in Figure 4 D5.

Initial bitumen combustion using TGA/DSC with a constant heating rate under air injection results in three distinct regions: water evaporation zone (25-157 °C), low temperature oxidation (LTO) zone (158-407 °C) and high temperature oxidation (HTO) zone (408-650 °C) (Figure 4 D5 A&B). However, combustion of bitumen in presence of carbonate rocks produced four different regions: water evaporation zone, low temperature oxidation (LTO) zone, high temperature oxidation (HTO) zone, and carbonate decomposition zone (Figure 4 D5 A&B). The temperature ranges for these zones are different for calcite and dolomite since they have different decomposition temperatures

and are reported in Table 4.10. Dolomite started to decompose earlier at ~500 °C while calcite started to decompose at ~650 °C. These values were also reported by Burger et al. (1985) for thermal decomposition of carbonates under air injection.

Table 4.10 reports the kinetic modeling results for all experiments. The model fitting results in Table 4.10 show that E_a of the crude oil combustion (Tests 1, 11, and 12) varied considerably when carbonate was present. Experiments with calcite have the highest heat generation (heat of combustion, ΔH) for crude oil and all individual SARA fractions at the HTO region except for resins (Figure 4 D5 and Table 4.10). DSC graphs (Figure 4 D5 B) and heat of combustion (Table 4.10) show that dolomite was reducing the heat generation of Oil A due to a high E_a (76,065 BTU/lb-mole) needed to overcome the energy barrier for asphaltenes (Test 24).

Aromatics fraction seems to favor reactions with calcite (Test 17 in Table 4.10) only and not dolomite (Test 18 in Table 4.10) (Figure 4 D5 F). Since aromatics ring is also present in the resins and asphaltenes fractions (Wang et al. 1994), it reduces the heat generation for dolomite. Resins have the highest sensitivity to carbonate (Table 4.10 Test 19, 20, and 21) hence lessen the heat generation of resins a lot (Figure 4 D5 H). The activation energy of resins at the HTO region was decreased by 36% from 100,635 BTU/lb-mole (Test 19 in Table 4.10) to 64,223 BTU/lb-mole (Test 21 in Table 4.10) when dolomite was added. Overall, calcite generates more heat for combustion but increases the activation energy needed for the HTO region. It could be concluded that the presence of carbonate in ISC can be useful, but the heat generation can be decreased by resins fraction for this particular oil (Oil A).

Appendix 4A

Equation 4 A1—Arrhenius Equation

$$\ln \frac{dW/dt}{W} = - \frac{E}{2.303R}\left(\frac{1}{T}\right) + \log A$$

Where;

W: Mass of sample;

E: Activation Energy (J/mol);

R: Gas Constant (8.314 J/mol K);

T: Temperature (K);

A: Arrhenius Constant (1/min);

Equation 4 A2—Coats-Redfern Equation

$$\ln \frac{1-(1-\alpha)^{1-n}}{T^2(1-n)} = -\frac{E}{R}\left(\frac{1}{T}\right) + \ln\left(\frac{AR}{\beta E}\left(1 - \frac{2RT}{E}\right)\right) \quad \text{for } n \neq 1$$

$$\ln \frac{-\ln(1-\alpha)}{T^2} = -\frac{E}{R}\left(\frac{1}{T}\right) + \ln\left(\frac{AR}{\beta E}\left(1 - \frac{2RT}{E}\right)\right) \quad \text{for } n = 1$$

Where;

α: Conversion Degree

β: Heating Rates (K/min);

A: Arrhenius Constant (1/min);

E: Activation Energy (J/mol);

R: Gas Constant (8.314 J/mol K);

T: Temperature (K);

Equation 4 A3—Horowitz-Metzger Equation

$$\ln\left[-\ln(1-\alpha)\right] = \frac{E}{RT_P{}^2}(\theta)$$

Where;

α: Conversion Degree

E: Activation Energy (J/mol);

R: Gas Constant (8.314 J/mol K);

T_P: Peak Temperature (K);

θ: T-T_p

Equation 4 A4—Ingraham-Marrier Equation

$$\log\frac{dW}{dT} + \log T + \log\beta = -\frac{E}{2.303R}\left(\frac{1}{T}\right) + \log A$$

Where;

β: Heating Rates (K/min);

A: Arrhenius Constant (1/min);

E: Activation Energy (J/mol);

R: Gas Constant (8.314 J/mol K);

W: Mass of sample;

T: Temperature (K);

A—TG and DTG graphs for Crude Oil (Test 1)	B—TG and DTG graphs for Saturates (Test 2)
C—TG and DTG graphs for Aromatics (Test 3)	D—TG and DTG graphs for Resins (Test 4)
E—TG and DTG graphs for Asphaltenes (Test 5)	F—TG and DTG graphs for Saturates-Asphaltenes (Test 6)
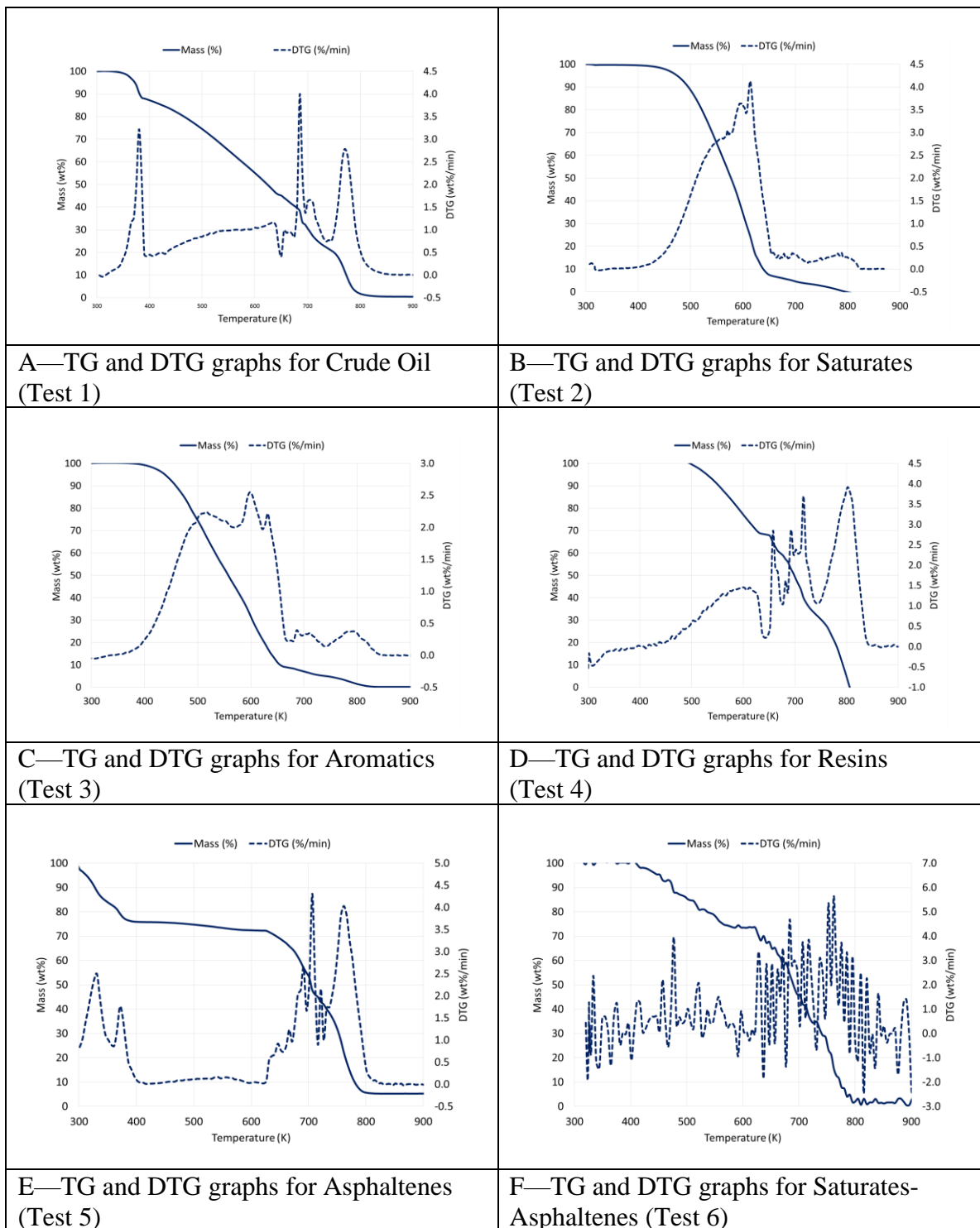
Figure 4 B1—TG/DTG Graphs for Kinetics Modeling Calculation of Oil A and Its Pseudo Fractions Combustion (Refer Table 4.2 for Experiment Name Coding)

G—TG and DTG graphs for Aromatics-Asphaltenes (Test 7)	H—TG and DTG graphs for Resins-Asphaltenes (Test 8)
I—TG and DTG graphs for Saturates-Aromatics (Test 9)	J—TG and DTG graphs for Saturates-Resins (Test 10)
K—TG and DTG graphs for Aromatics-Resins (Test 11)	L—TG and DTG graphs for Saturates-Aromatics-Asphaltenes (Test 12)

Figure 4 B1 (cont.)—TG/DTG Graphs for Kinetics Modeling Calculation of Oil A and Its Pseudo Fractions Combustion (Refer Table 4.2 for Experiment Name Coding)

M—TG and DTG graphs for Saturates-Resins-Asphaltenes (Test 13)	N—TG and DTG graphs for Aromatics-Resins-Asphaltenes (Test 14)

O—TG and DTG graphs for Saturates-Aromatics-Resins (Test 15)	P—TG and DTG graphs for Saturates-Aromatics-Resins-Asphaltenes (Test 16)
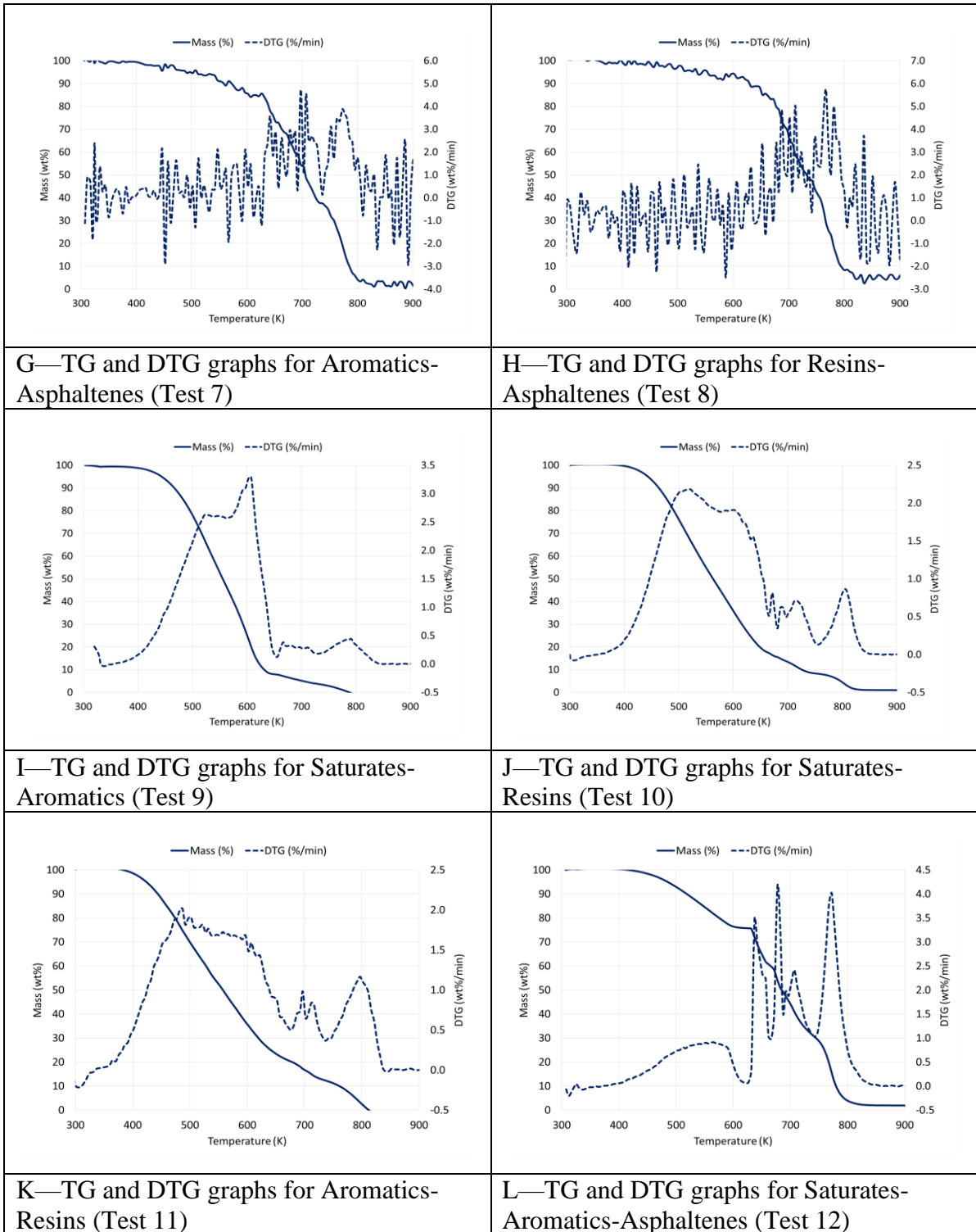
Figure 4 B1 (cont.)—TG/DTG Graphs for Kinetics Modeling Calculation of Oil A and Its Pseudo Fractions Combustion (Refer Table 4.2 for Experiment Name Coding)
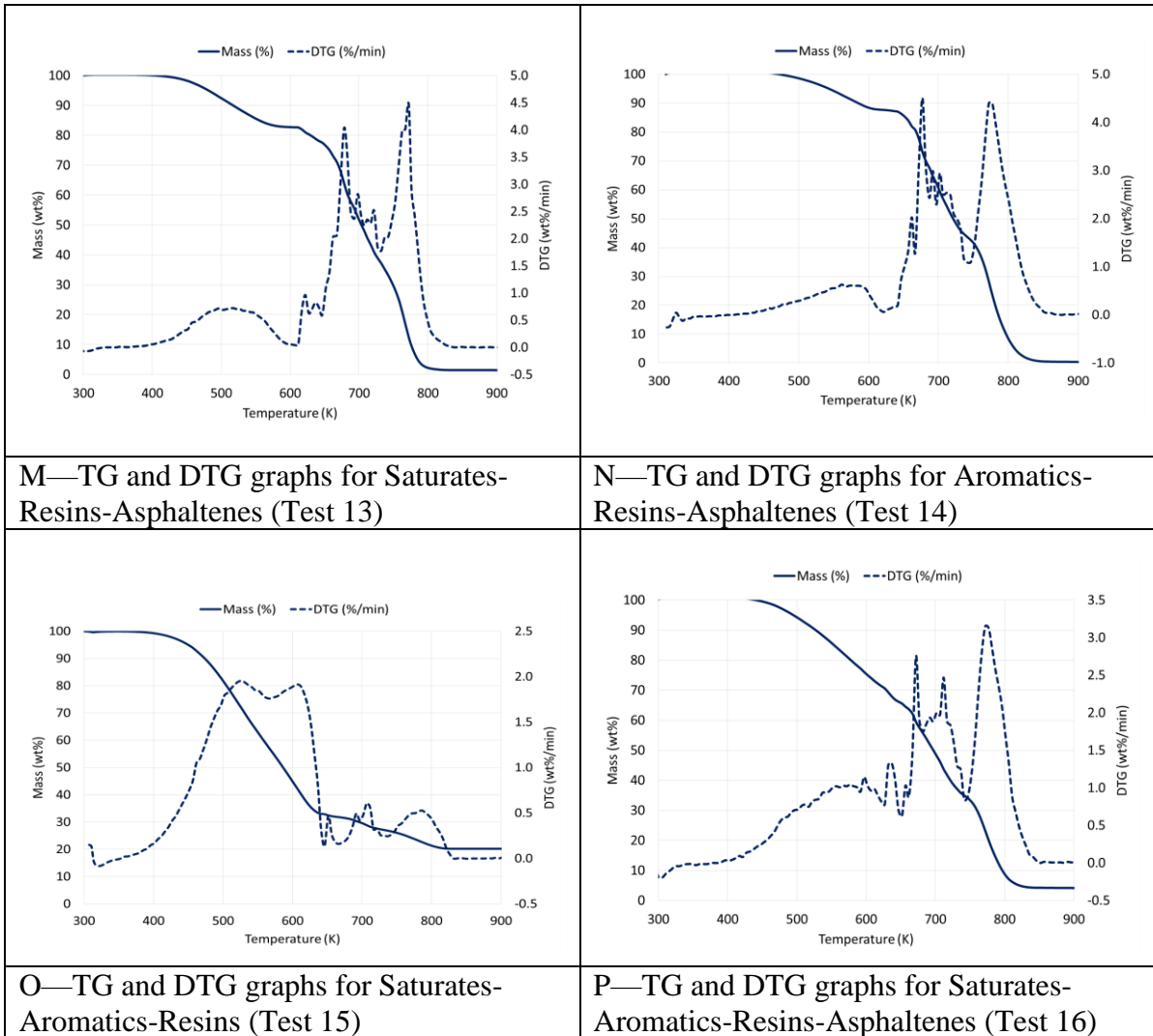
| A—Arrhenius Model Fitting | B—Coats-Redfern Model Fitting |
| C—Horowitz-Metzger Model Fitting | D—Ingraham-Marrier Fitting |
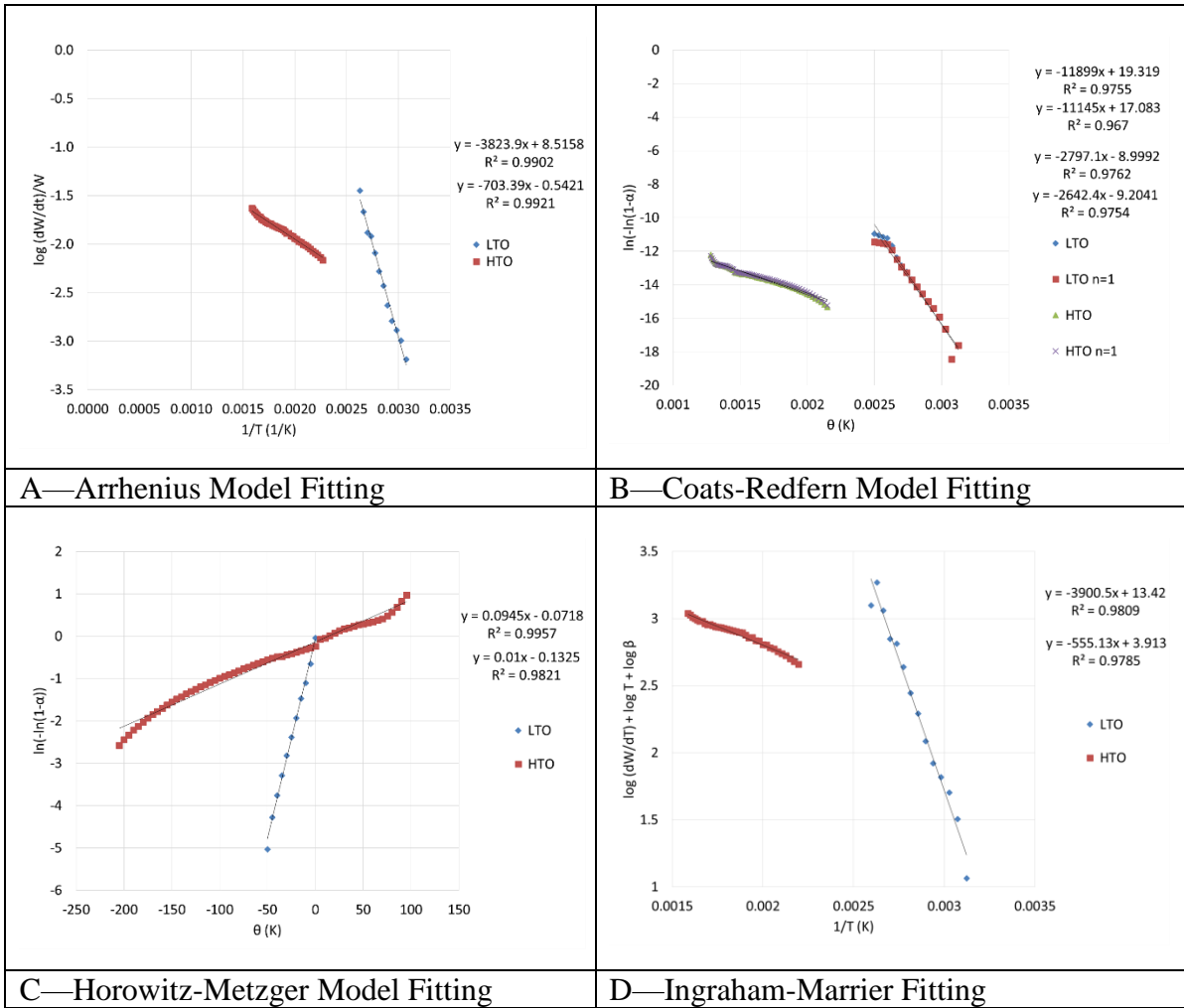
Figure 4 B2—Kinetic Modeling Fitting Graphs for Oil A Bitumen (Test 1)

| A—Arrhenius Model Fitting | B—Coats-Redfern Model Fitting |
| C—Horowitz-Metzger Model Fitting | D—Ingraham-Marrier Fitting |
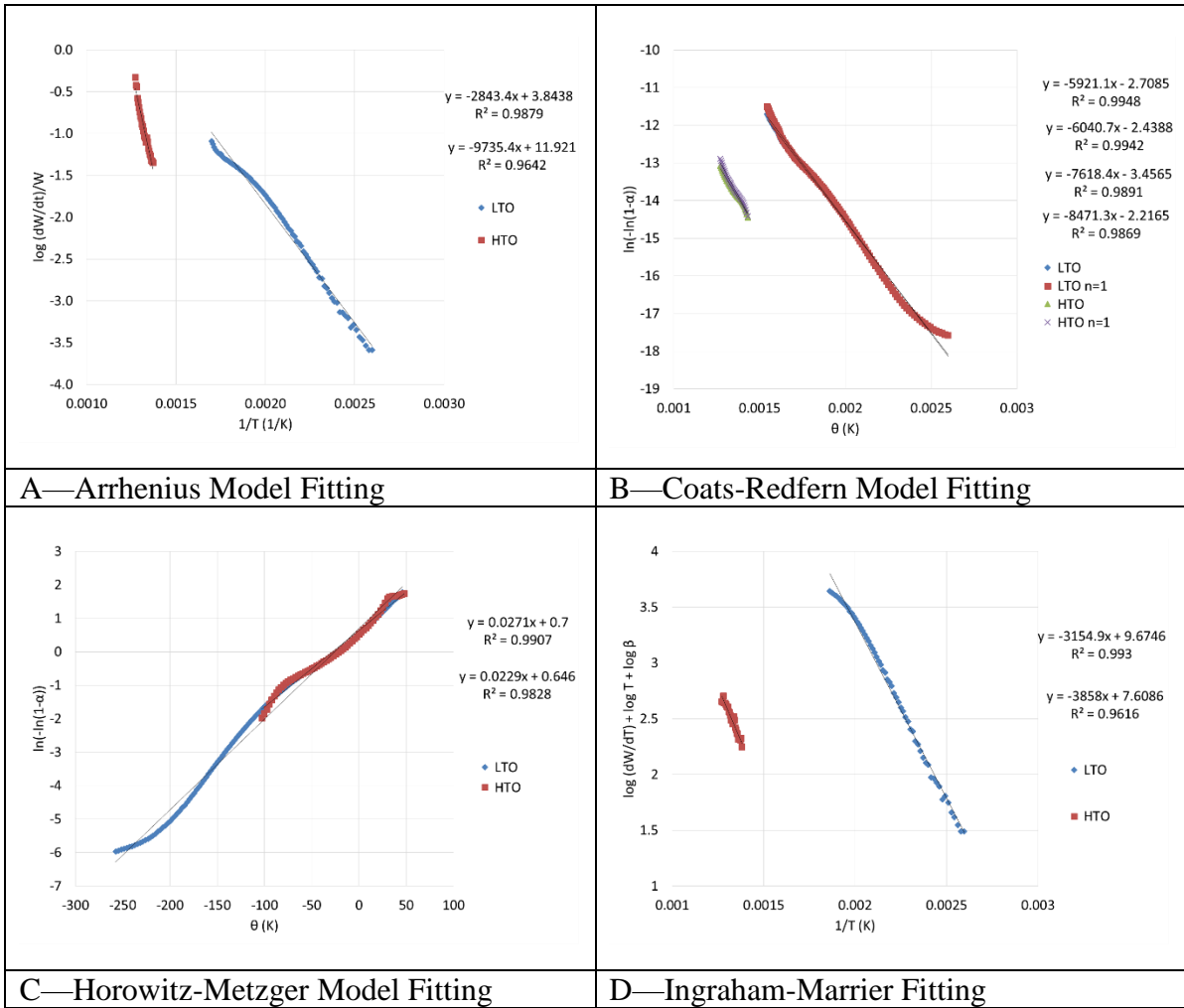
Figure 4 B3—Kinetic Modeling Fitting Graphs for Oil A Saturates (Test 2)
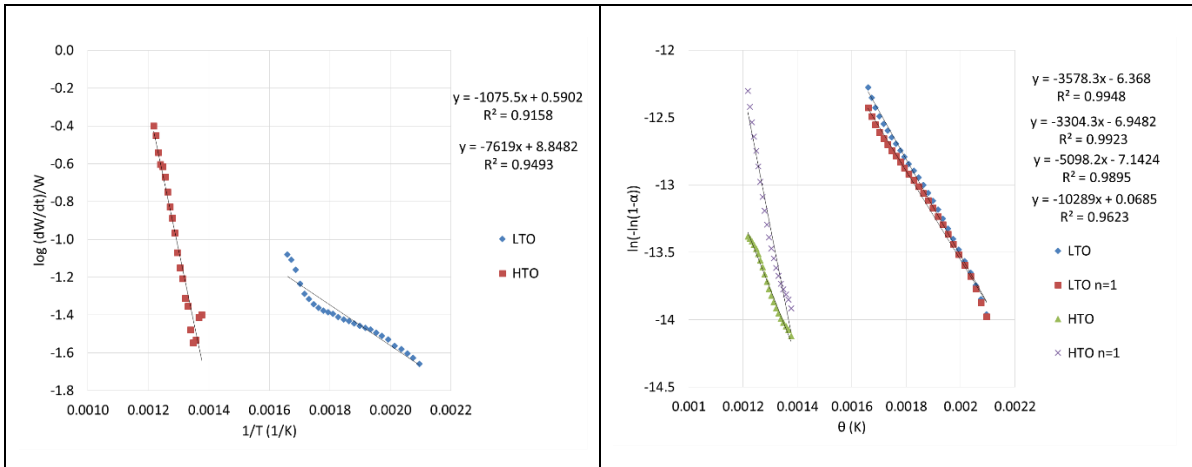
125
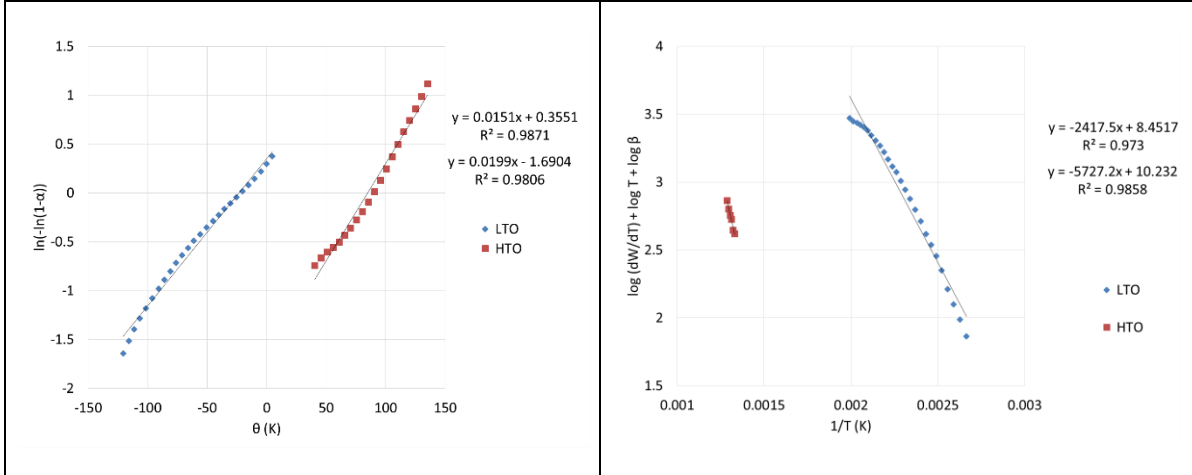
| A—Arrhenius Model Fitting | B—Coats-Redfern Model Fitting |
| C—Horowitz-Metzger Model Fitting | D—Ingraham-Marrier Fitting |

Figure 4 B4—Kinetic Modeling Fitting Graphs for Oil A Aromatics (Test 3)
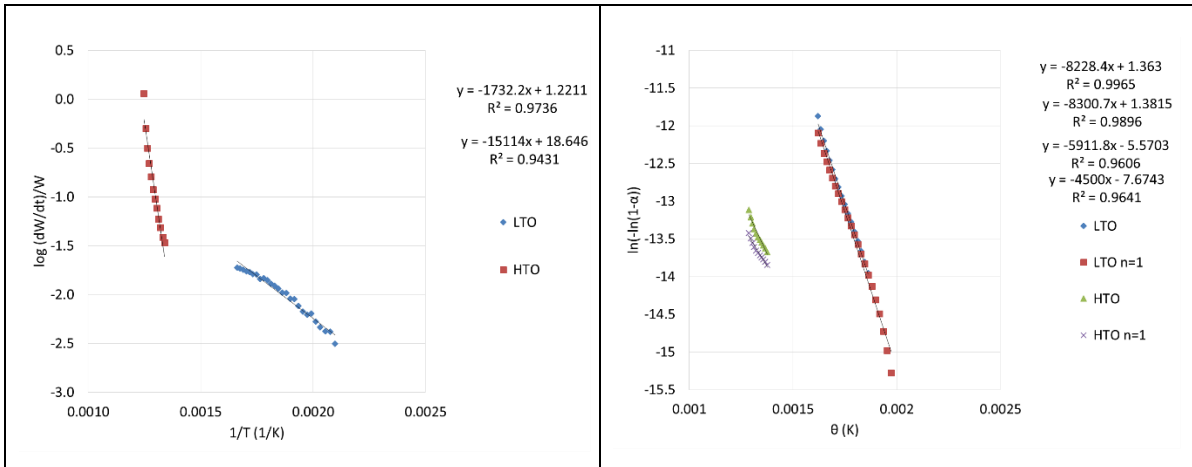
126
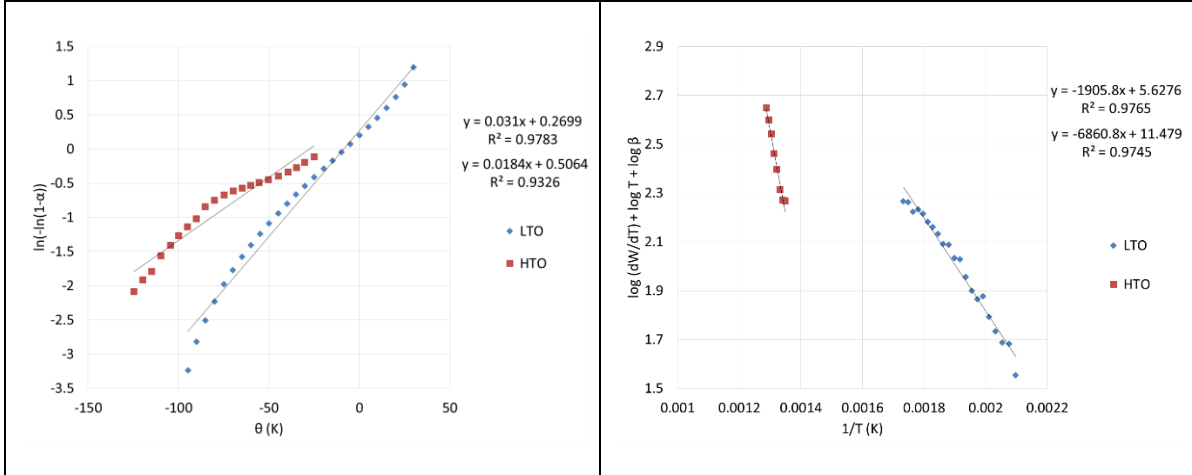
| A—Arrhenius Model Fitting | B—Coats-Redfern Model Fitting |
| C—Horowitz-Metzger Model Fitting | D—Ingraham-Marrier Fitting |

Figure 4 B5—Kinetic Modeling Fitting Graphs for Oil A Resins (Test 4)

| A—Arrhenius Model Fitting | B—Coats-Redfern Model Fitting |
| C—Horowitz-Metzger Model Fitting | D—Ingraham-Marrier Fitting |
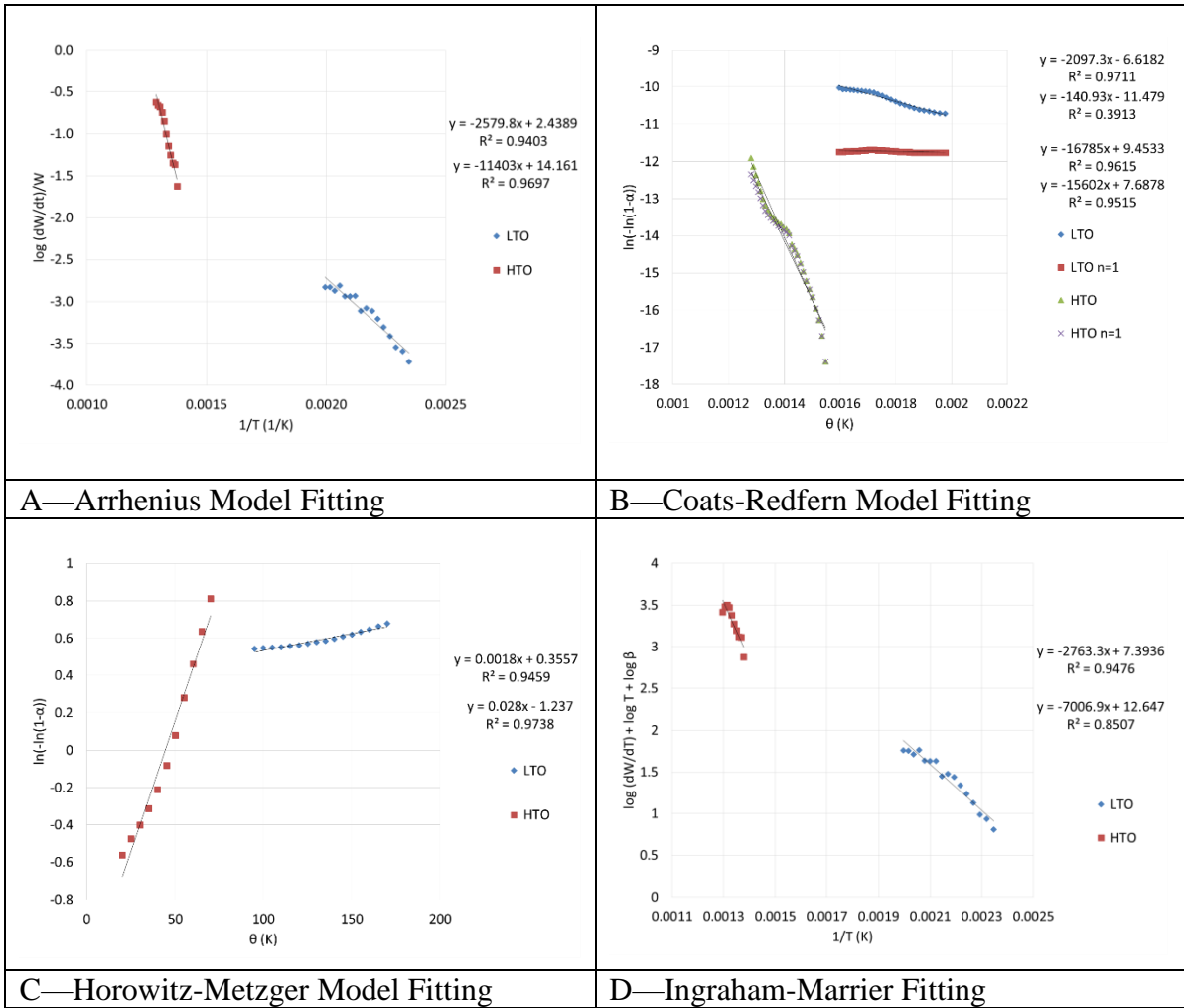
Figure 4 B6—Kinetic Modeling Fitting Graphs for Oil A Asphaltenes (Test 5)
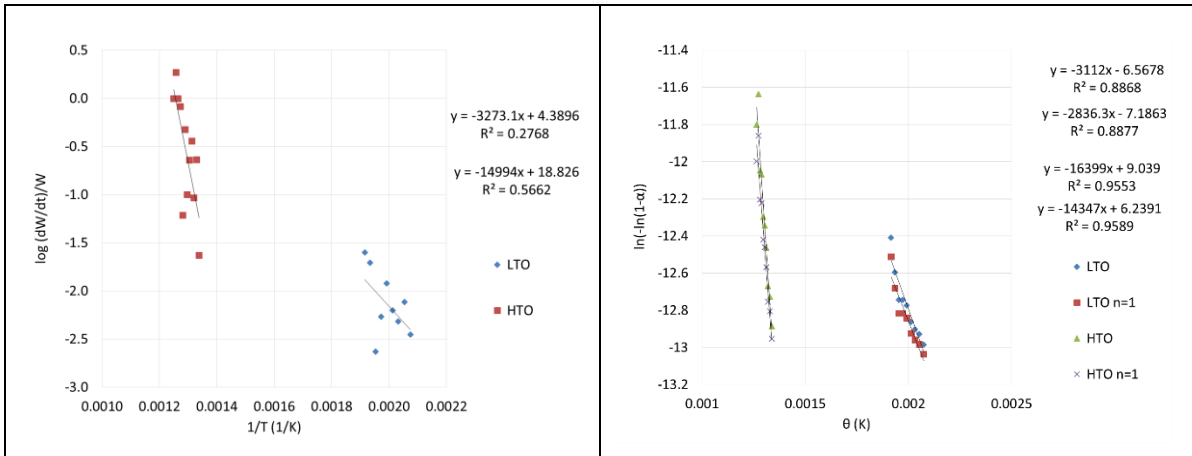
A—Arrhenius Model Fitting | B—Coats-Redfern Model Fitting
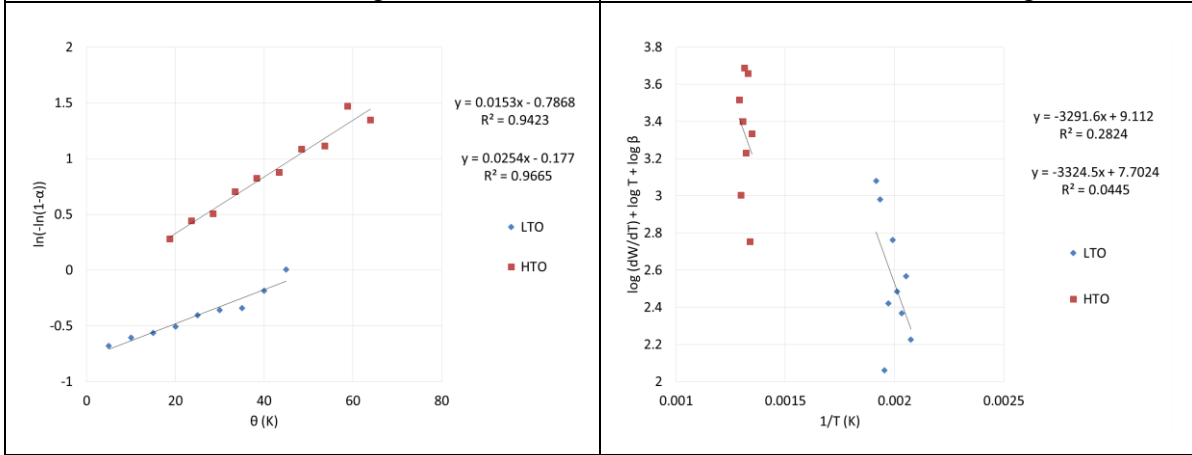
C—Horowitz-Metzger Model Fitting | D—Ingraham-Marrier Fitting

Figure 4 B7—Kinetic Modeling Fitting Graphs for Oil A Saturates-Asphaltenes (Test 6)

A—Arrhenius Model Fitting

B—Coats-Redfern Model Fitting

C—Horowitz-Metzger Model Fitting

D—Ingraham-Marrier Fitting
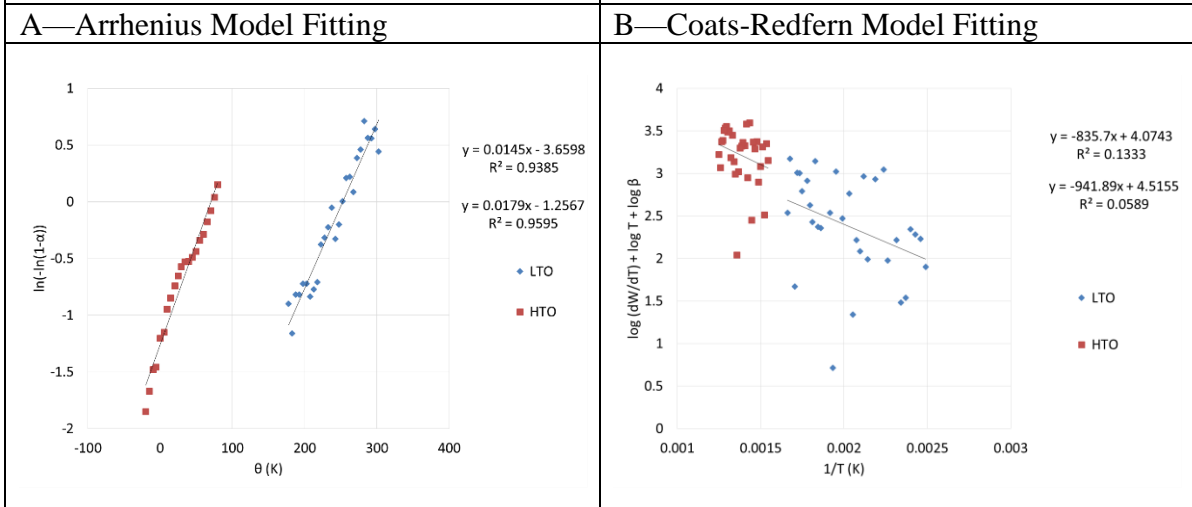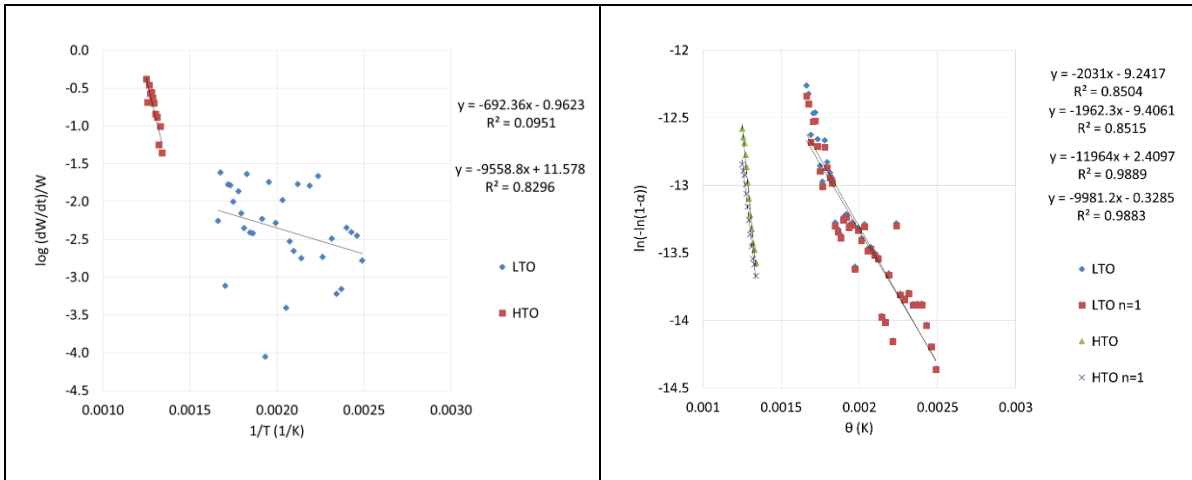
Figure 4 B8—Kinetic Modeling Fitting Graphs for Oil A Aromatics-Asphaltenes (Test 7)
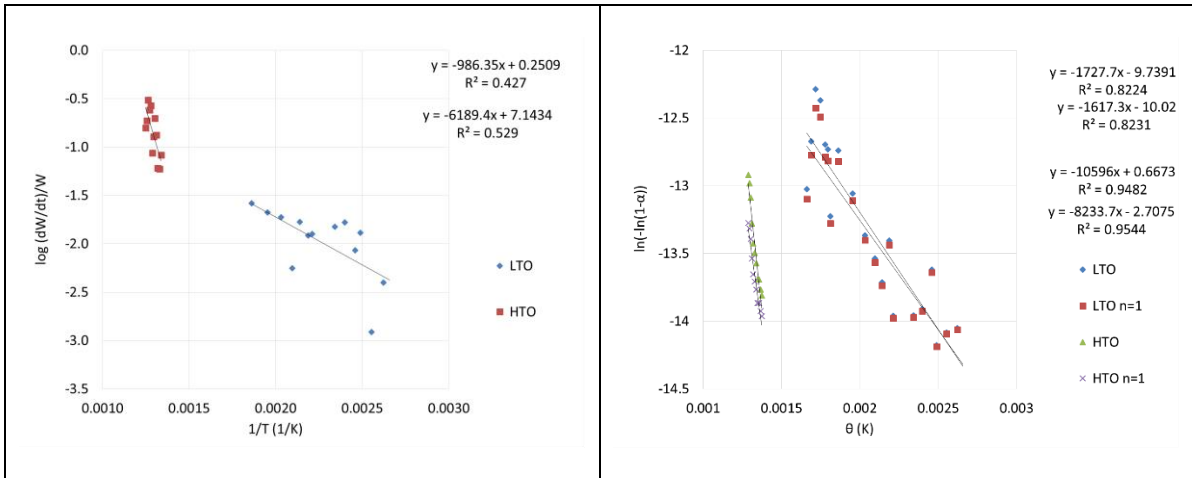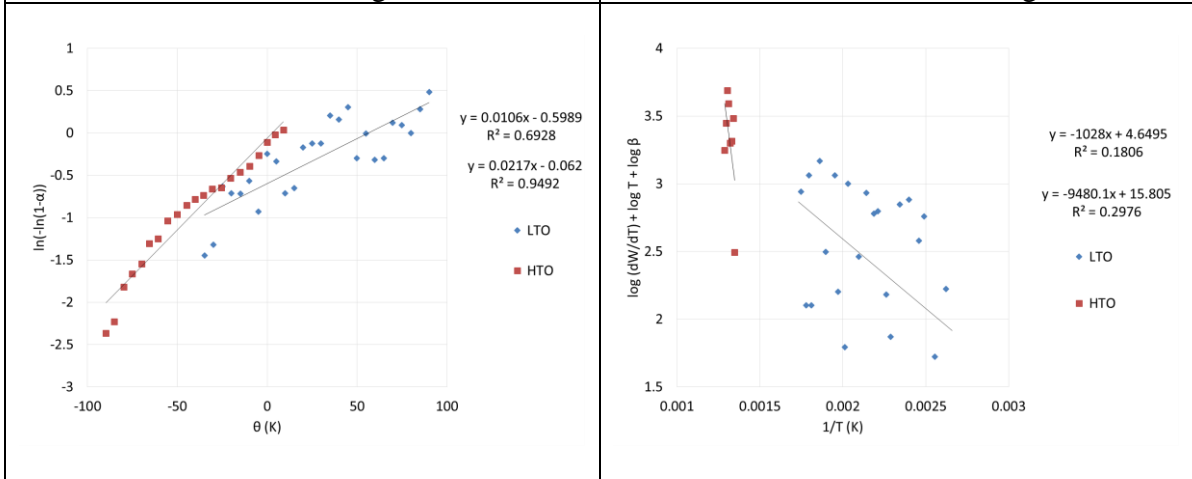
| A—Arrhenius Model Fitting | B—Coats-Redfern Model Fitting |
| C—Horowitz-Metzger Model Fitting | D—Ingraham-Marrier Fitting |

Figure 4 B9—Kinetic Modeling Fitting Graphs for Oil A Resins-Asphaltenes (Test 8)

A—Arrhenius Model Fitting

B—Coats-Redfern Model Fitting

C—Horowitz-Metzger Model Fitting

D—Ingraham-Marrier Fitting
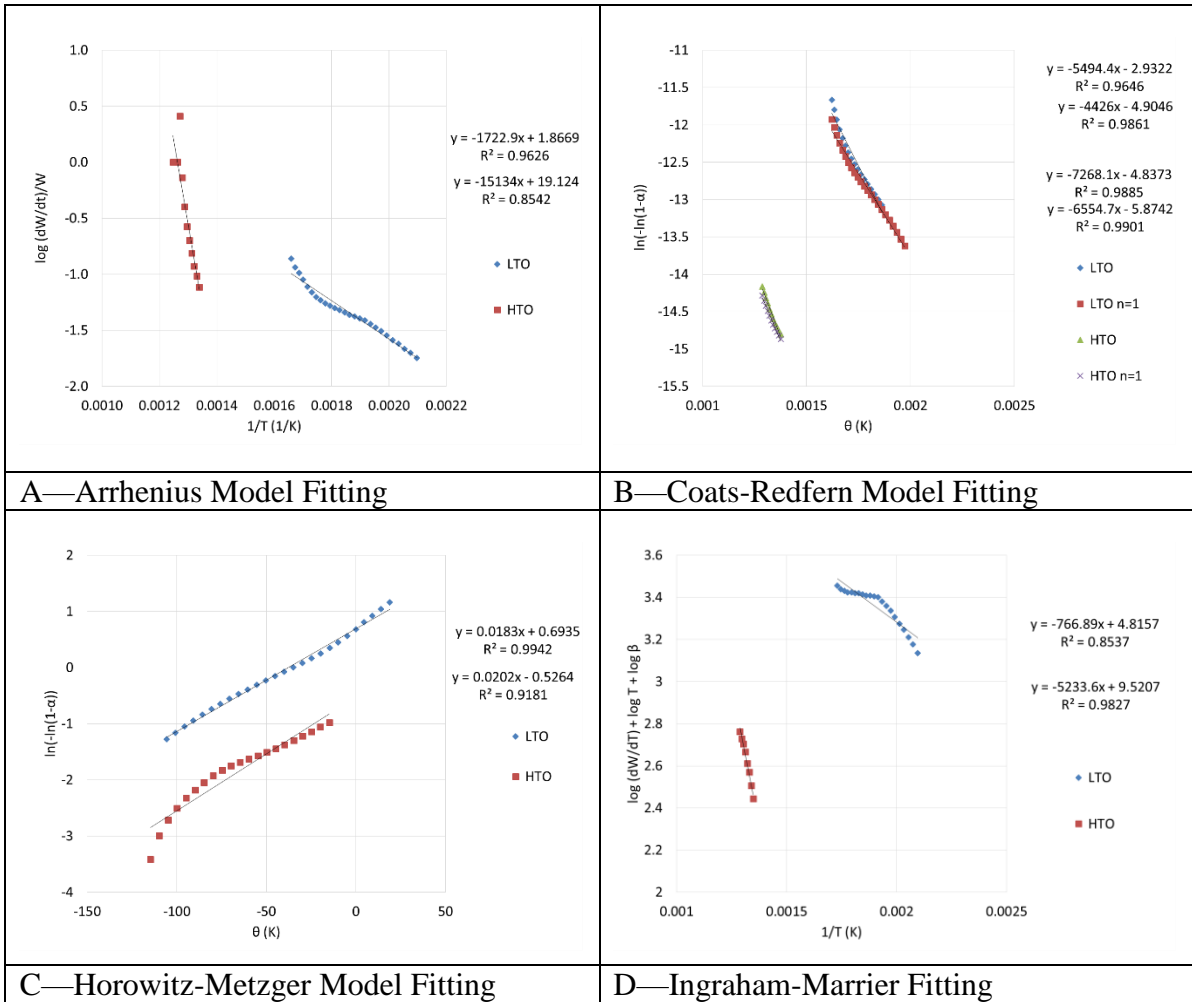
Figure 4 B10—Kinetic Modeling Fitting Graphs for Oil A Saturates-Aromatics (Test 9)

A—Arrhenius Model Fitting

y = -802.8x + 0.0347
R² = 0.974

y = -11514x + 13.535
R² = 0.8914

B—Coats-Redfern Model Fitting

y = -3568.7x - 6.3296
R² = 0.9944

y = -3134.8x - 7.1987
R² = 0.9981

y = -3477.3x - 9.7167
R² = 0.905

y = -2889.1x - 10.634
R² = 0.8879

C—Horowitz-Metzger Model Fitting

y = 0.0137x - 0.6898
R² = 0.9963

y = 0.011x - 2.4697
R² = 0.9487

D—Ingraham-Marrier Fitting

y = -197.68x + 3.6027
R² = 0.4498

y = -11652x + 17.592
R² = 0.9977
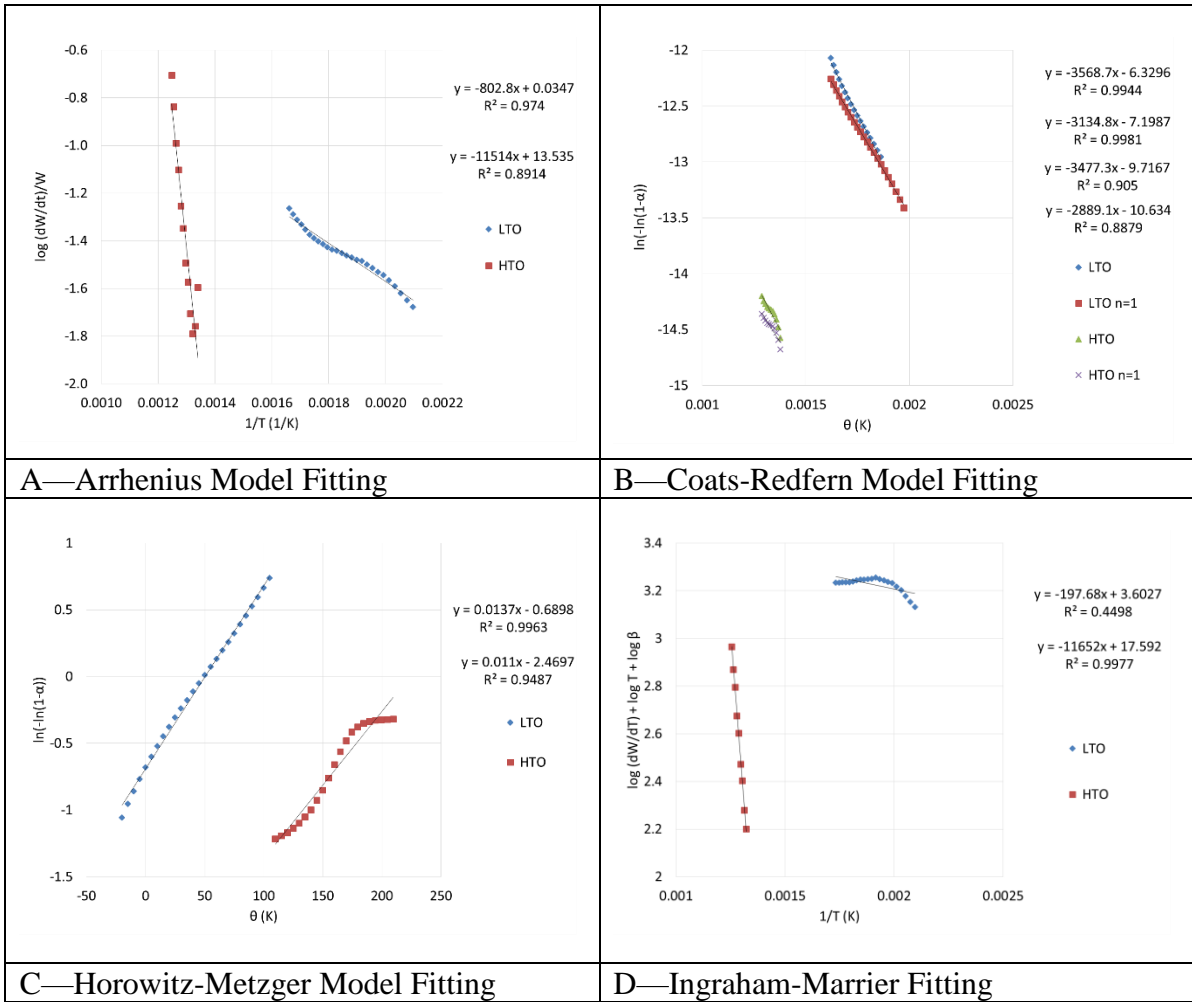
Figure 4 B11—Kinetic Modeling Fitting Graphs for Oil A Saturates-Resins (Test 10)

133

| A—Arrhenius Model Fitting | B—Coats-Redfern Model Fitting |
| C—Horowitz-Metzger Model Fitting | D—Ingraham-Marrier Fitting |
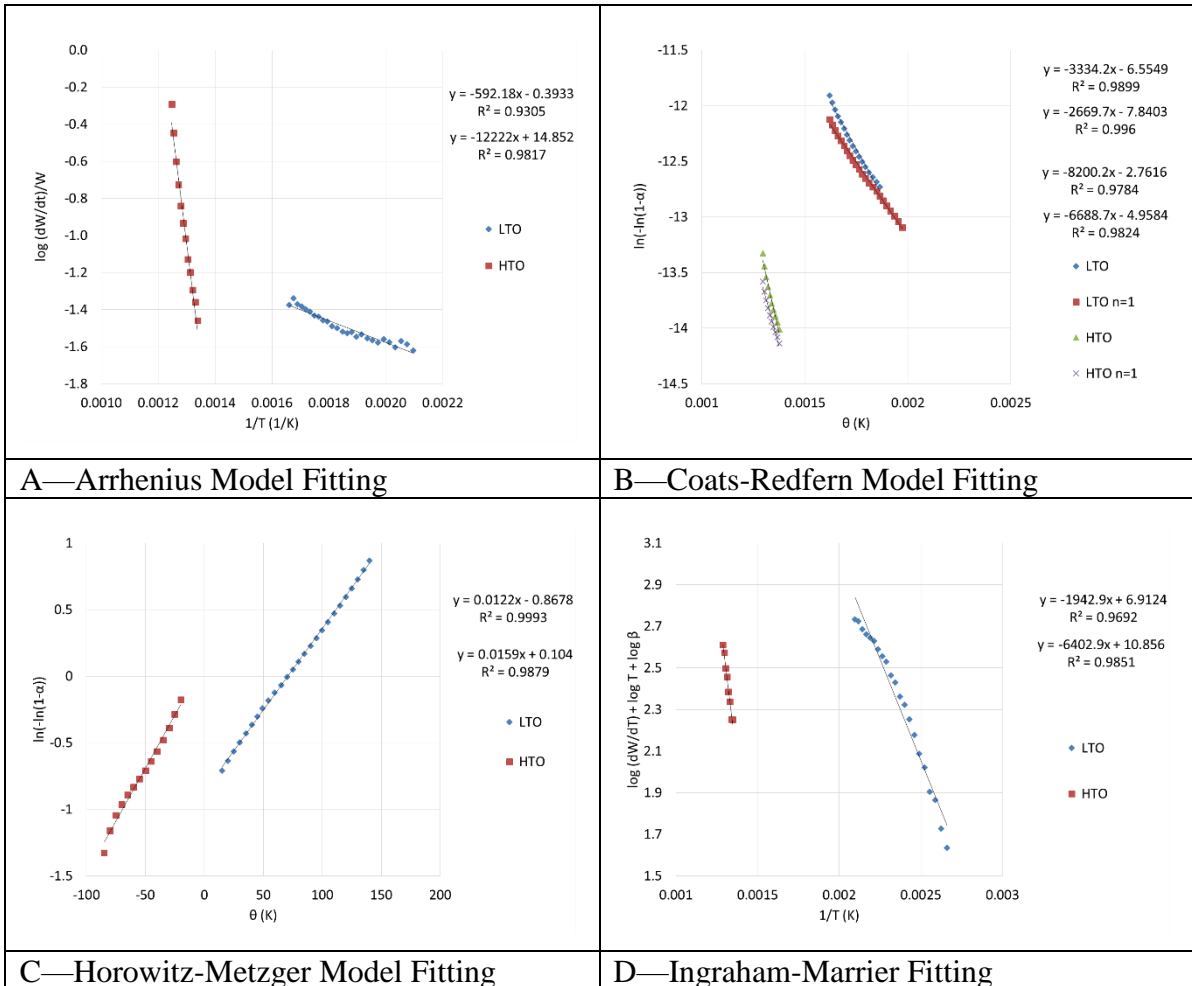
Figure 4 B12—Kinetic Modeling Fitting Graphs for Oil A Aromatics-Resins (Test 11)

A—Arrhenius Model Fitting

y = -18662x + 23.551
R² = 0.9891
y = -806.1x - 0.506
R² = 0.9592

B—Coats-Redfern Model Fitting

y = -5397.2x - 2.8141
R² = 0.9994
y = -4695.2x - 4.297
R² = 0.9971

y = -21030x + 15.009
R² = 0.9286
y = -12811x + 3.6974
R² = 0.9438

C—Horowitz-Metzger Model Fitting

y = 0.016x - 0.0844
R² = 0.9744

y = 0.0167x + 0.437
R² = 0.9712

D—Ingraham-Marrier Fitting

y = -742.88x + 4.0461
R² = 0.9257

y = -11192x + 17.966
R² = 0.9267
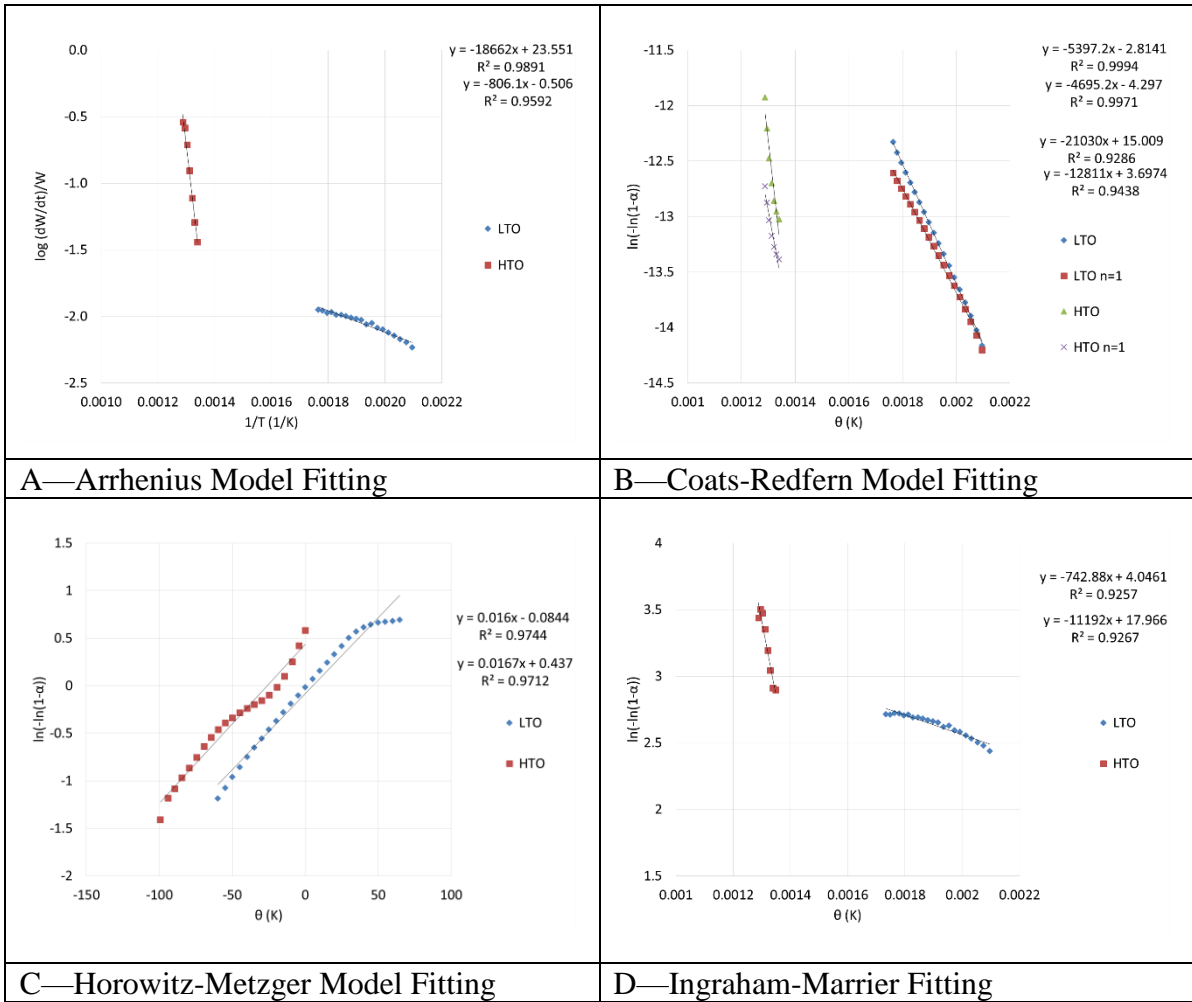
Figure 4 B13—Kinetic Modeling Fitting Graphs for Oil A Saturates-Aromatics-Asphaltenes (Test 12)

A—Arrhenius Model Fitting

B—Coats-Redfern Model Fitting

C—Horowitz-Metzger Model Fitting

D—Ingraham-Marrier Fitting
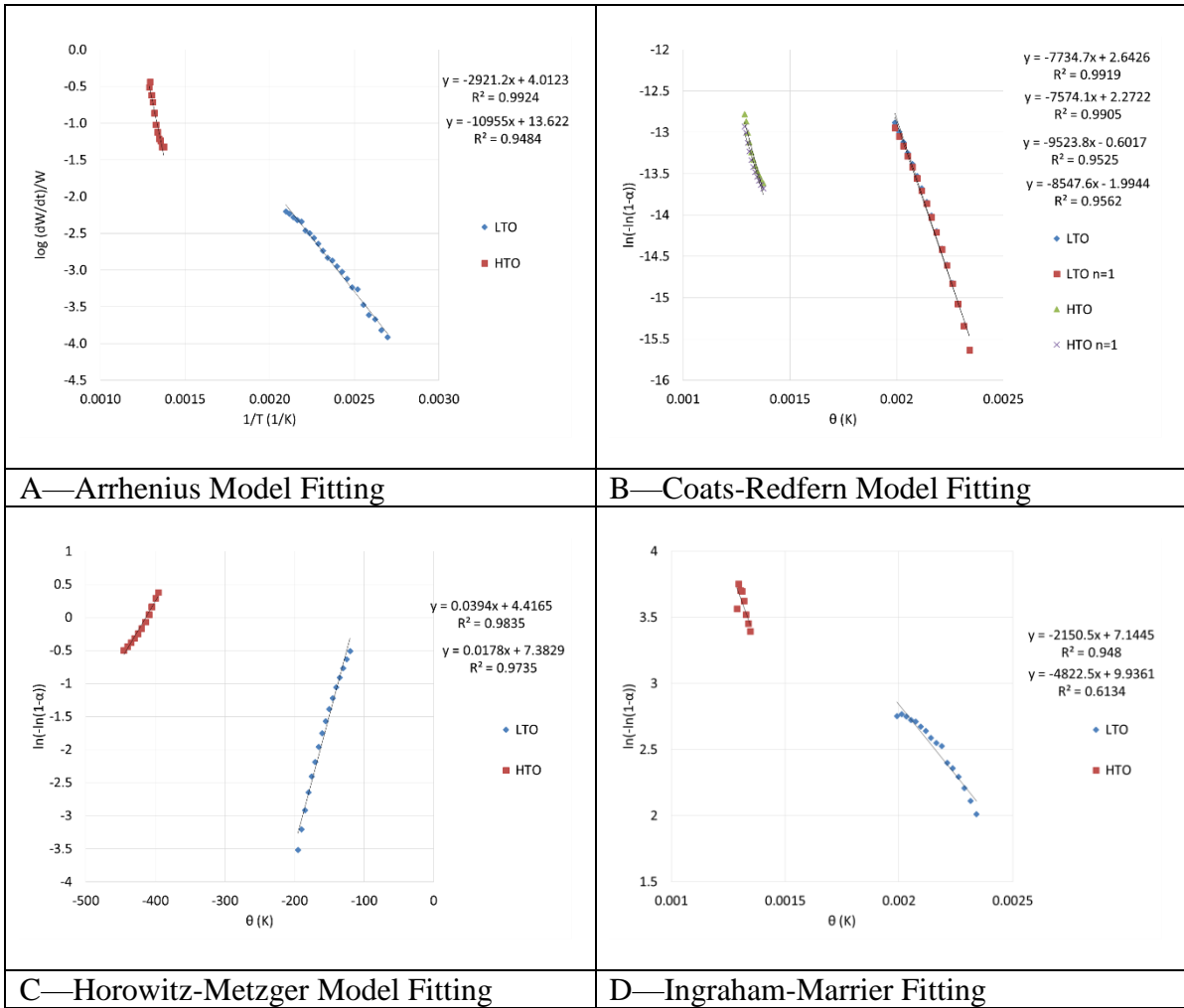
Figure 4 B14—Kinetic Modeling Fitting Graphs for Oil A Saturates-Resins-Asphaltenes (Test 13)

A—Arrhenius Model Fitting

B—Coats-Redfern Model Fitting

C—Horowitz-Metzger Model Fitting

D—Ingraham-Marrier Fitting
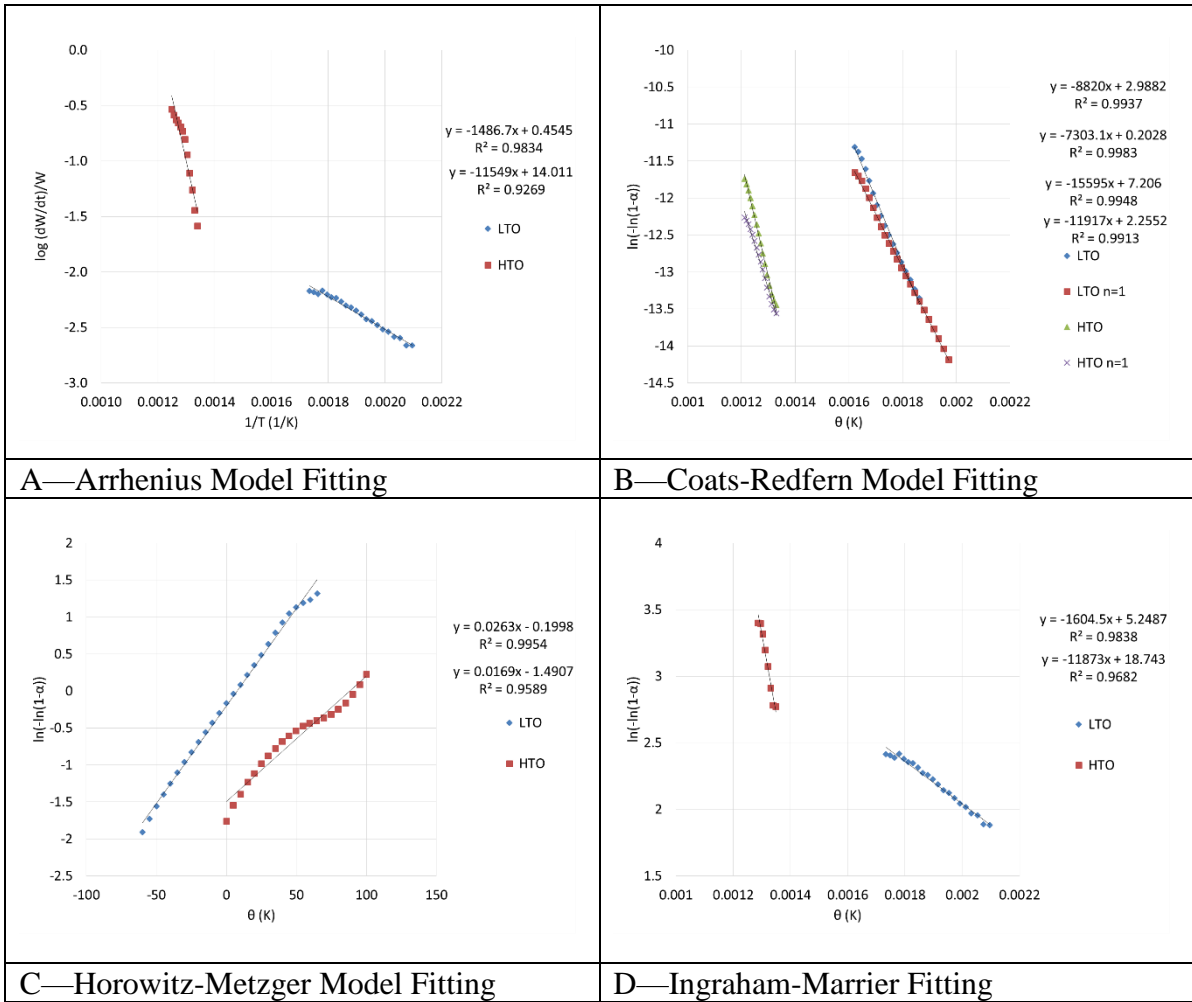
Figure 4 B15—Kinetic Modeling Fitting Graphs for Aromatics-Resins-Asphaltenes (Test 14)

A—Arrhenius Model Fitting

B—Coats-Redfern Model Fitting

C—Horowitz-Metzger Model Fitting

D—Ingraham-Marrier Fitting
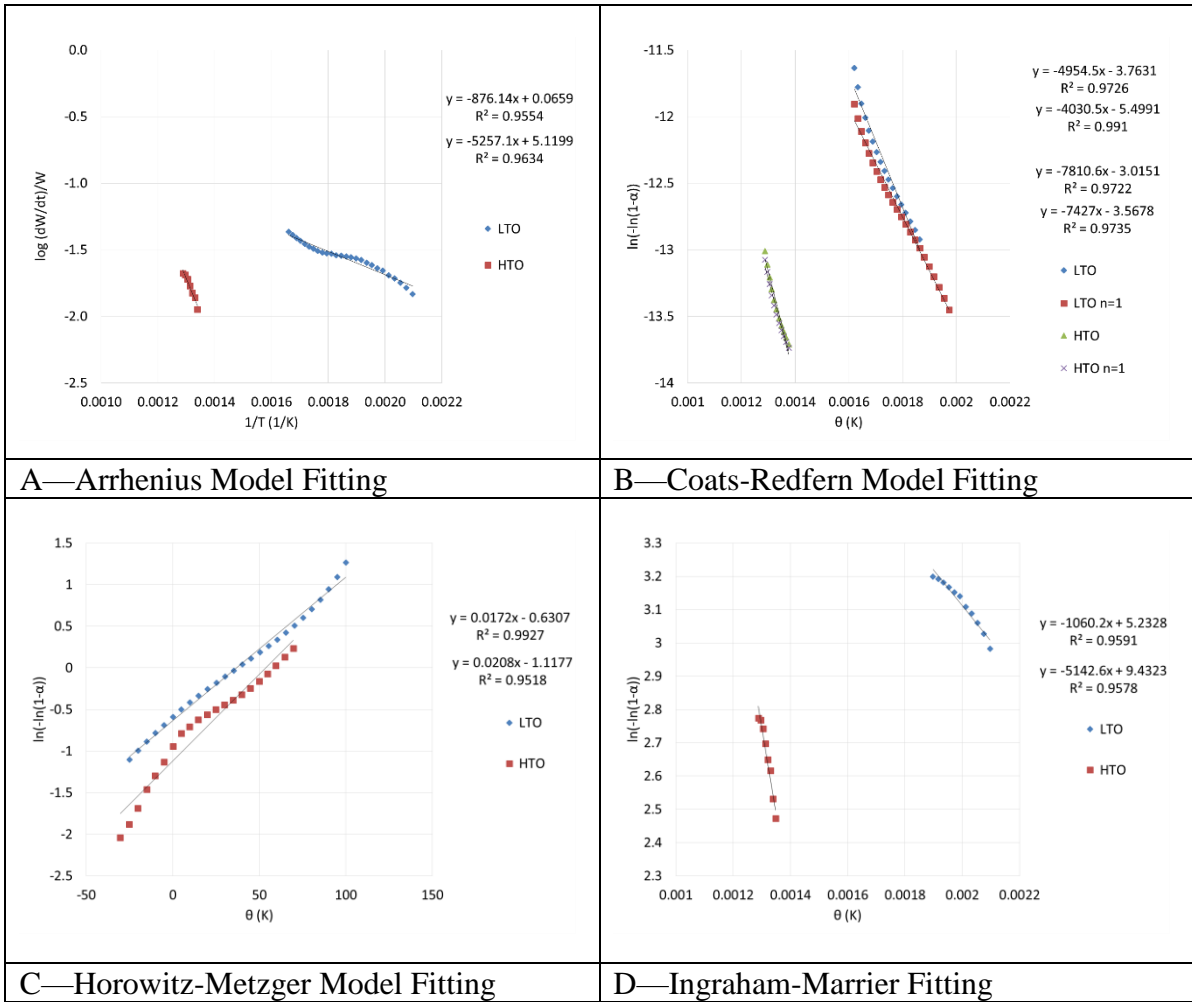
Figure 4 B16—Kinetic Modeling Fitting Graphs for Oil A Saturates-Aromatics-Resins (Test 15)

| A—Arrhenius Model Fitting | B—Coats-Redfern Model Fitting |
| C—Horowitz-Metzger Model Fitting | D—Ingraham-Marrier Fitting |
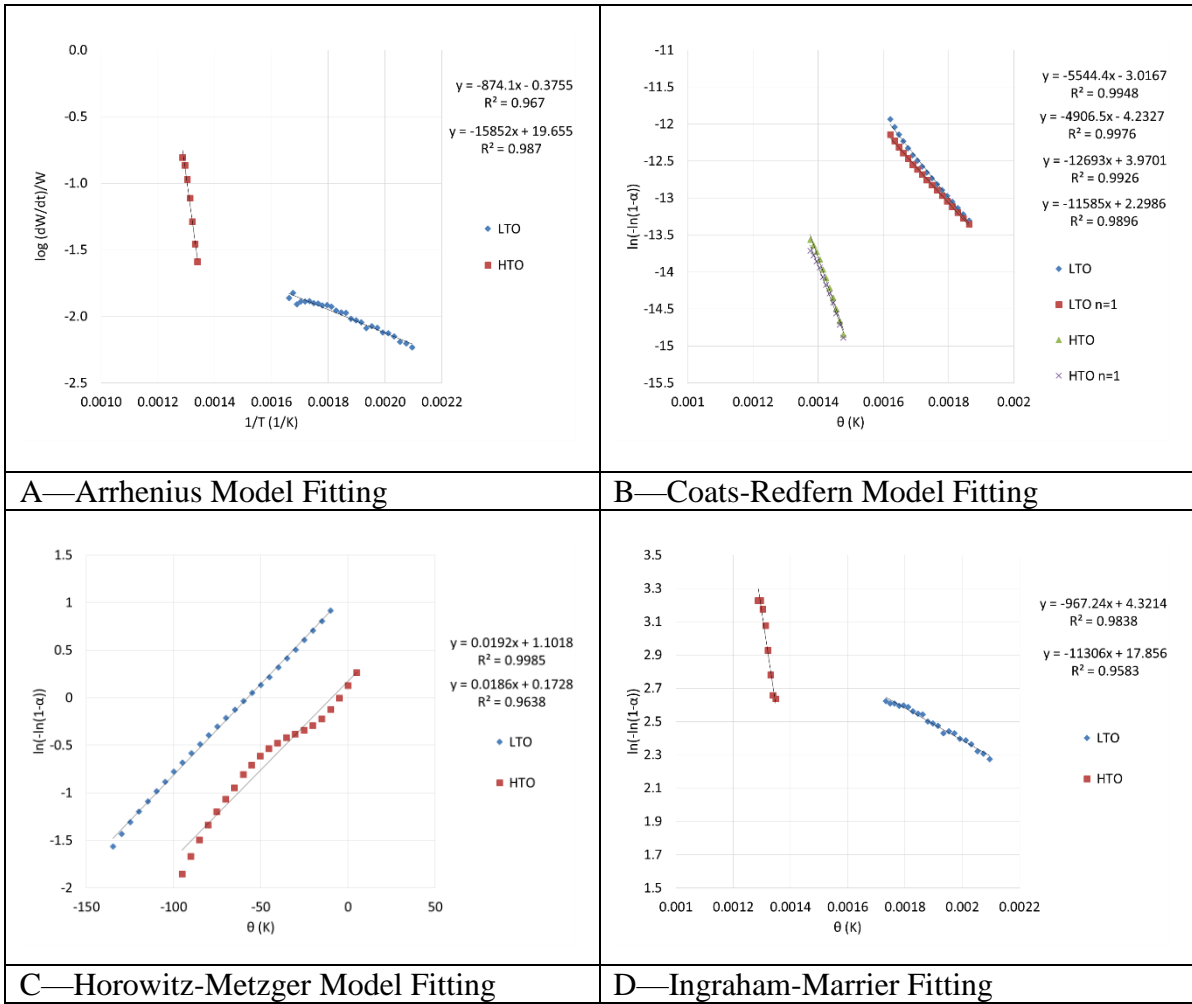
Figure 4 B17—Kinetic Modeling Fitting Graphs for Oil A Saturates-Aromatics-Resins-Asphaltenes (Test 16)

139

Appendix 4C

A—TGA of Oil A and Oil B with and without water at low heating rate (5 °C/min)	B—TGA of Oil A and Oil B with and without water at high heating rate (20 °C/min)
C—DSC of Oil A and Oil B with and without water at low heating rate (5 °C/min)	D—DSC of Oil A and Oil B with and without water at high heating rate (20 °C/min)
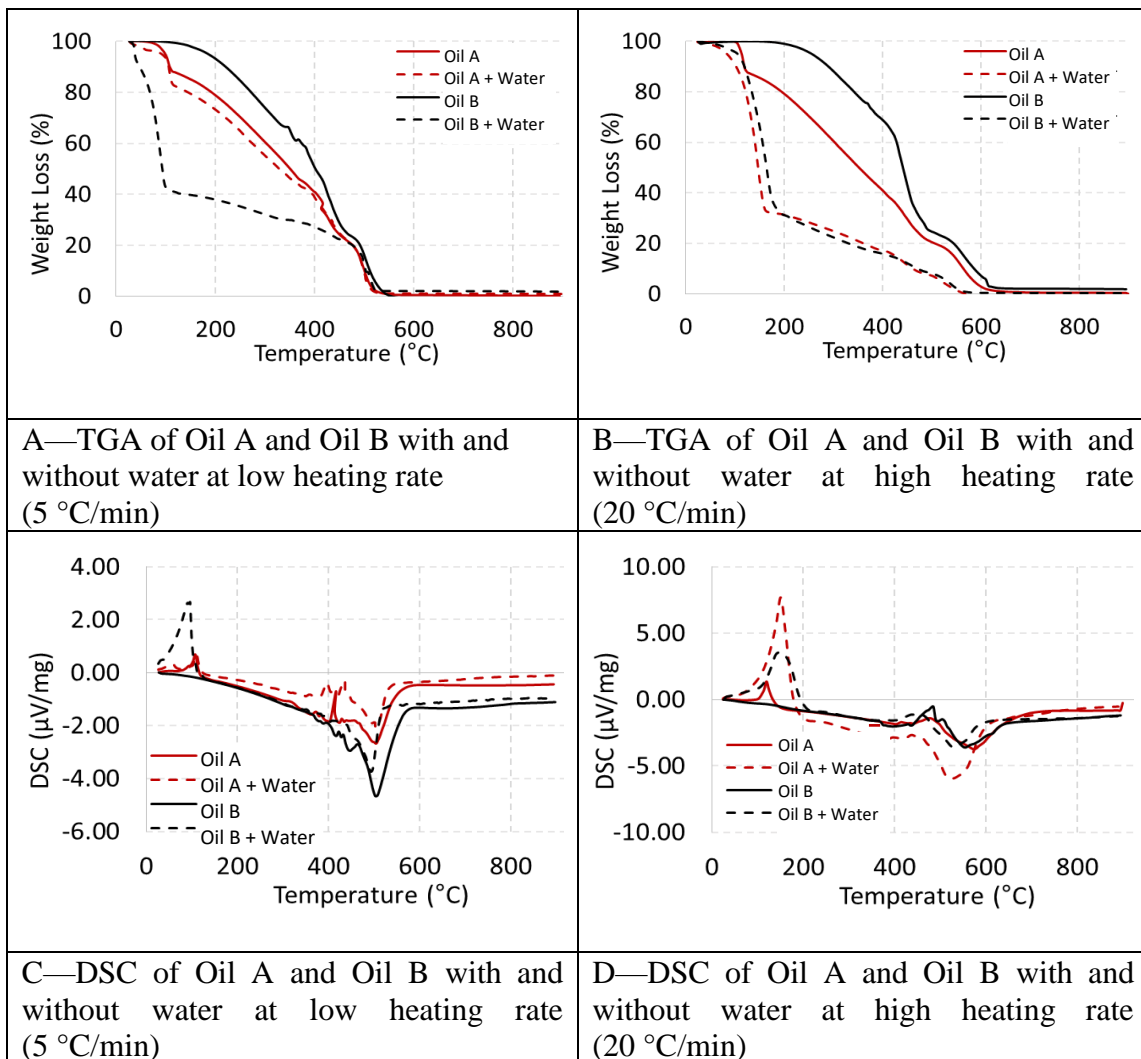
Figure 4 C1—Combustion Behavior of Crude Oil Samples at Low (5°C/Min) and High (20°C/Min) Heating Rates Under Air Injection

A—Weight loss behavior of saturates fraction at low heating rate (5 °C/min)

B—Weight loss behavior of saturates fraction at high heating rate (20 °C/min)

C—Weight loss behavior of aromatics fraction at low heating rate (5 °C/min)

D—Weight loss behavior of aromatics fraction at high heating rate (20 °C/min)

E—Weight loss behavior of resins fraction at low heating rate (5 °C/min)

F—Weight loss behavior of resins fraction at high heating rate (20 °C/min)

Figure 4 C2—Weight Loss Behavior of Crude Oil Fractions With and Without Water Addition at Low (5 °C/Min) and High (20 °C/Min) Heating Rates Under Air Injection

141

Weight loss behavior of asphaltenes fraction at low heating rate (5 °C/min)	Weight loss behavior of asphaltenes fraction at high heating rate (20 °C/min)
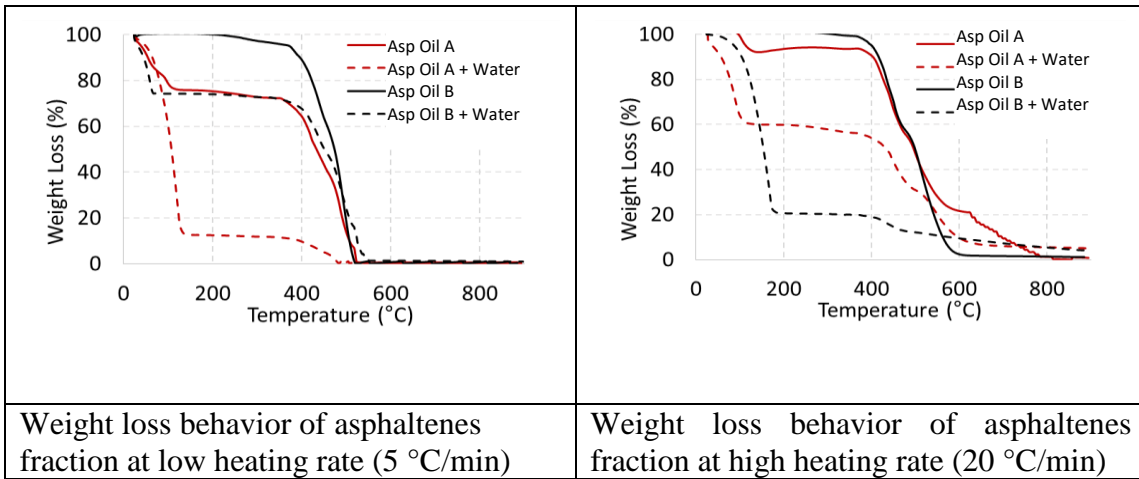
Figure 4 C2 (cont.)—Weight Loss Behavior of Crude Oil Fractions With and Without Water Addition at Low (5 °C/Min) and High (20 °C/Min) Heating Rates Under Air Injection

142

A— Heat flow behavior of saturates fraction at low heating rate (5 °C/min)	B—Heat flow behavior of saturates fraction at high heating rate (20 °C/min)
C—Heat flow behavior of aromatics fraction at low heating rate (5 °C/min)	D—Heat flow behavior of aromatics fraction at high heating rate (20 °C/min)
E—Heat flow behavior of resins fraction at low heating rate (5 °C/min)	F—Heat flow behavior of resins fraction at high heating rate (20 °C/min)
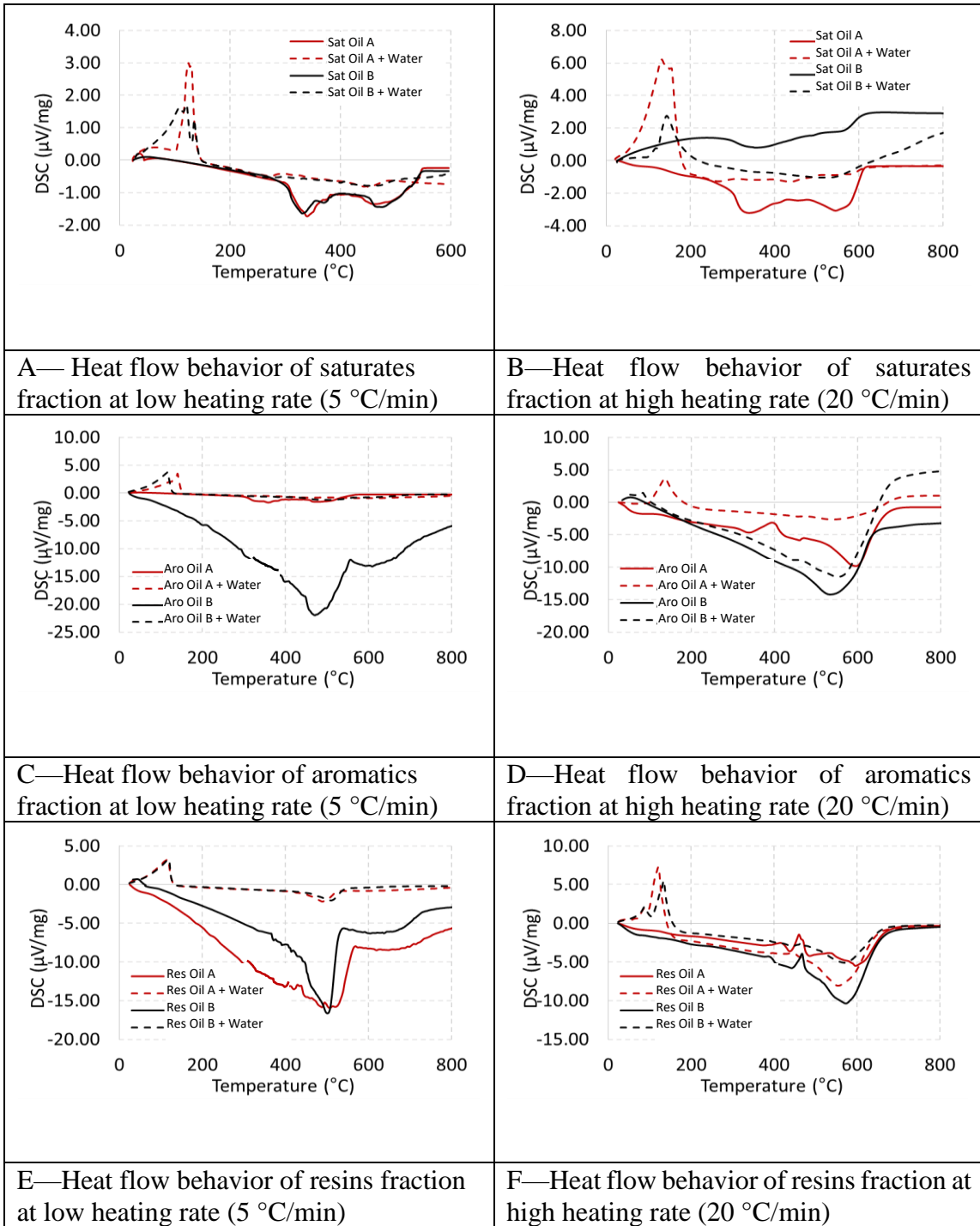
Figure 4 C3—Heat Flow Behavior of Crude Oil Fractions With and Without Water Addition at Low (5 °C/Min) and High (20 °C/Min) Heating Rates Under Air Injection

143

| G—Heat flow behavior of asphaltenes fraction at low heating rate (5 °C/min) | H—Heat flow behavior of asphaltenes fraction at high heating rate (20 °C/min) |
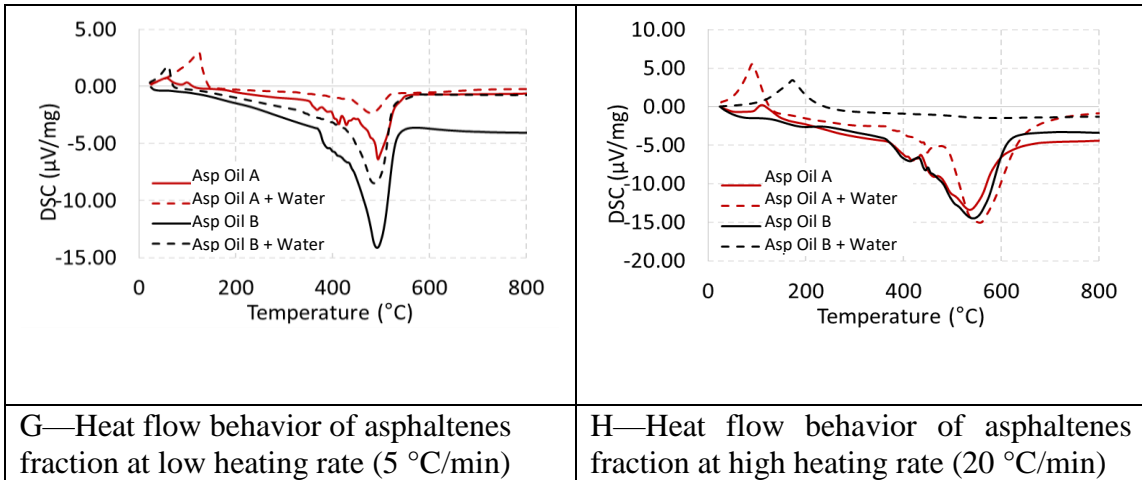
Figure 4 C3 (cont.)—Heat Flow Behavior of Crude Oil Fractions With and Without Water Addition at Low (5 °C/Min) and High (20 °C/Min) Heating Rates Under Air Injection

| A—Weight loss behavior of water at low heating rate of 5 °C/min during combustion under air injection | B—Heat flow behavior of water at low heating rate of 5 °C/min during combustion under air injection |
| C—Weight loss behavior of water at high heating rate of 20 °C/min during combustion under air injection | D—Heat flow behavior of water at high heating rate of 20 °C/min during combustion under air injection |
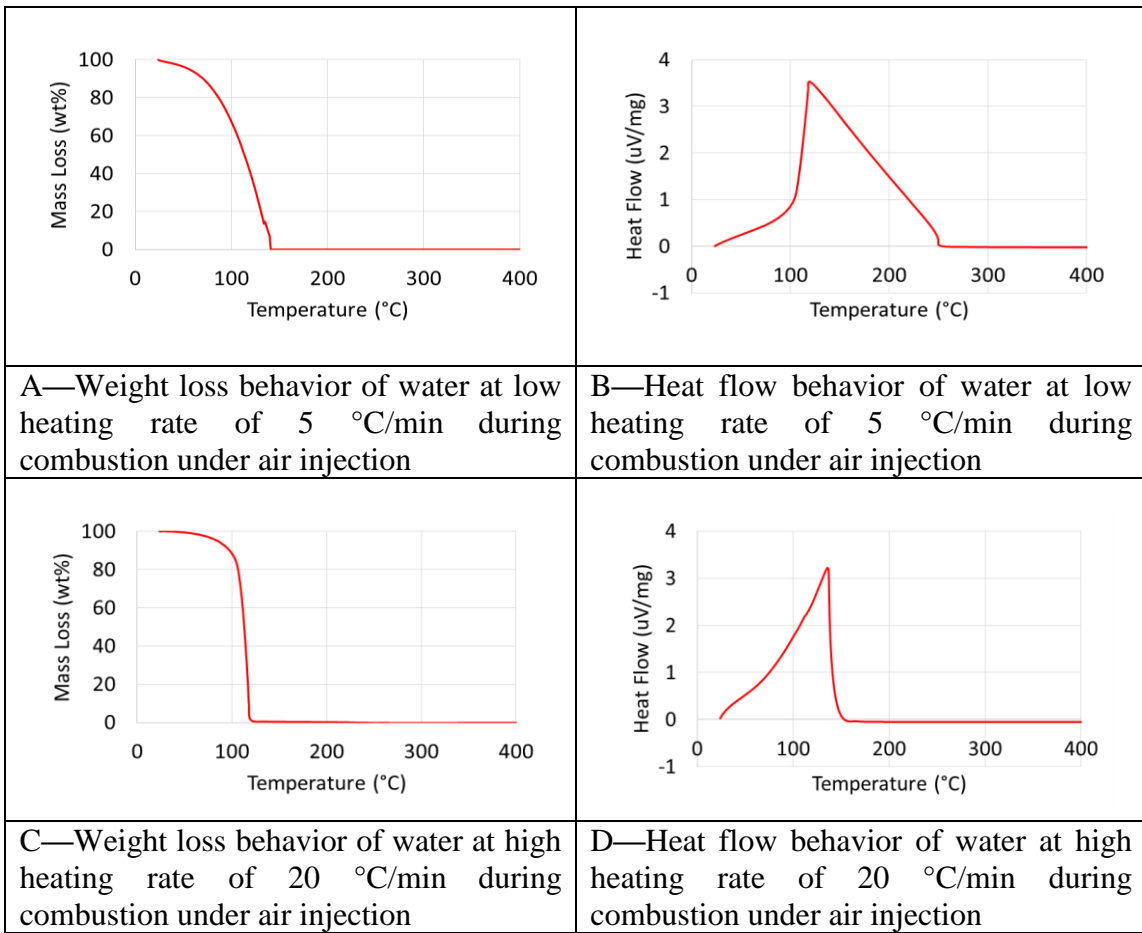
Figure 4 C4—Weight Loss and Heat Flow Behavior of Water at Low (5 °C/Min) and High (20 °C/Min) Heating Rates Under Air Injection

144

A—TG and DTG graphs for Crude Oil without water (Test 1)	B—TG and DTG graphs for Crude Oil with water (Test 3)
C—TG and DTG graphs for Saturates without water (Test 5)	D—TG and DTG graphs for Saturates with water (Test 7)
E—TG and DTG graphs for Aromatics without water (Test 9)	F—TG and DTG graphs for Aromatics with water (Test 11)
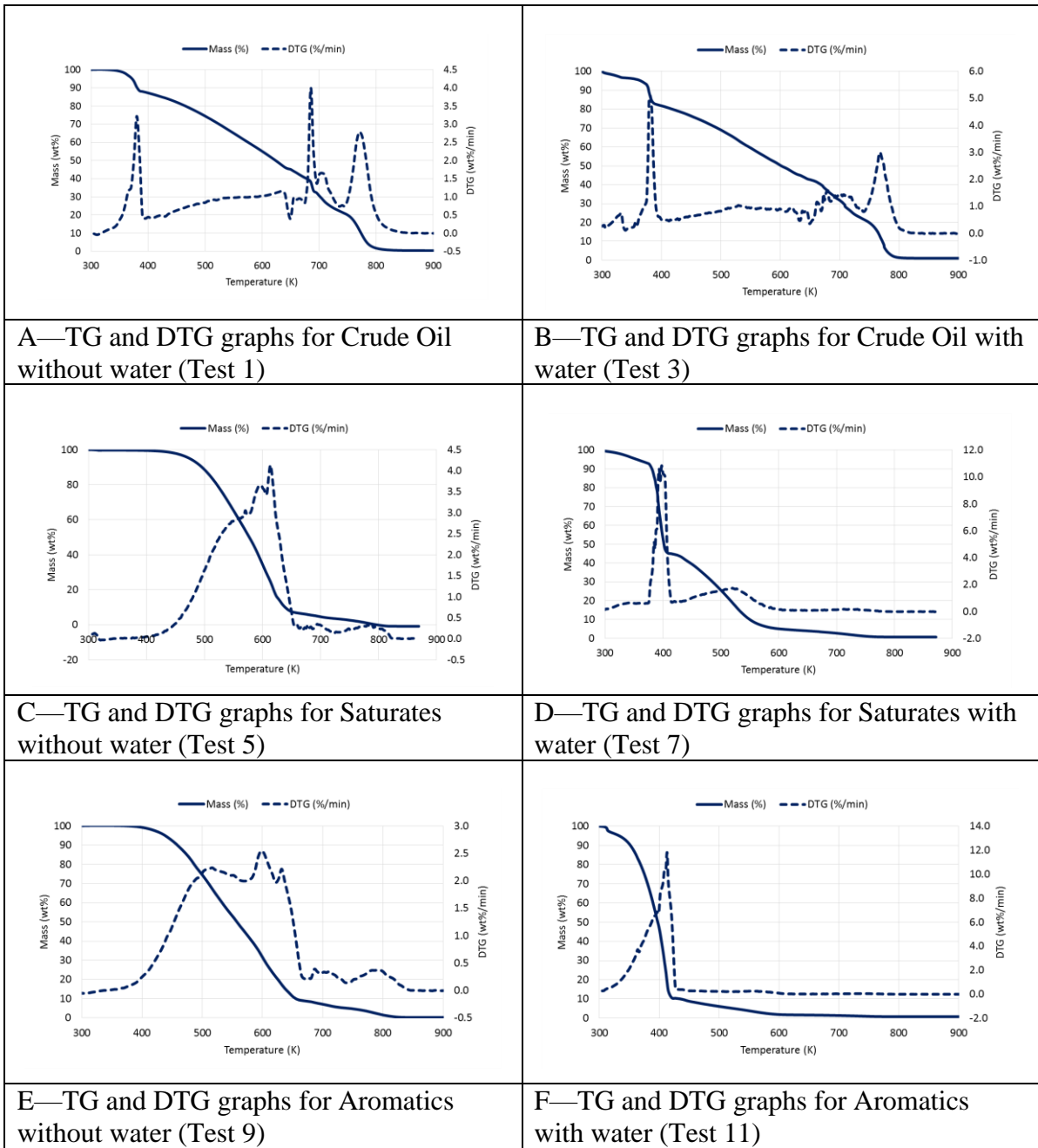
Figure 4 C5—TG/DTG Graphs for Arrhenius Model Calculation of Oil A Combustion at Low Heating Rate (Refer Table 4.3 for Experiment Name Coding)

G—TG and DTG graphs for Resins without water (Test 13)	H—TG and DTG graphs for Resins with water (Test 15)
I—TG and DTG graphs for Asphaltenes without water (Test 17)	J—TG and DTG graphs for Asphaltenes with water (Test 19)
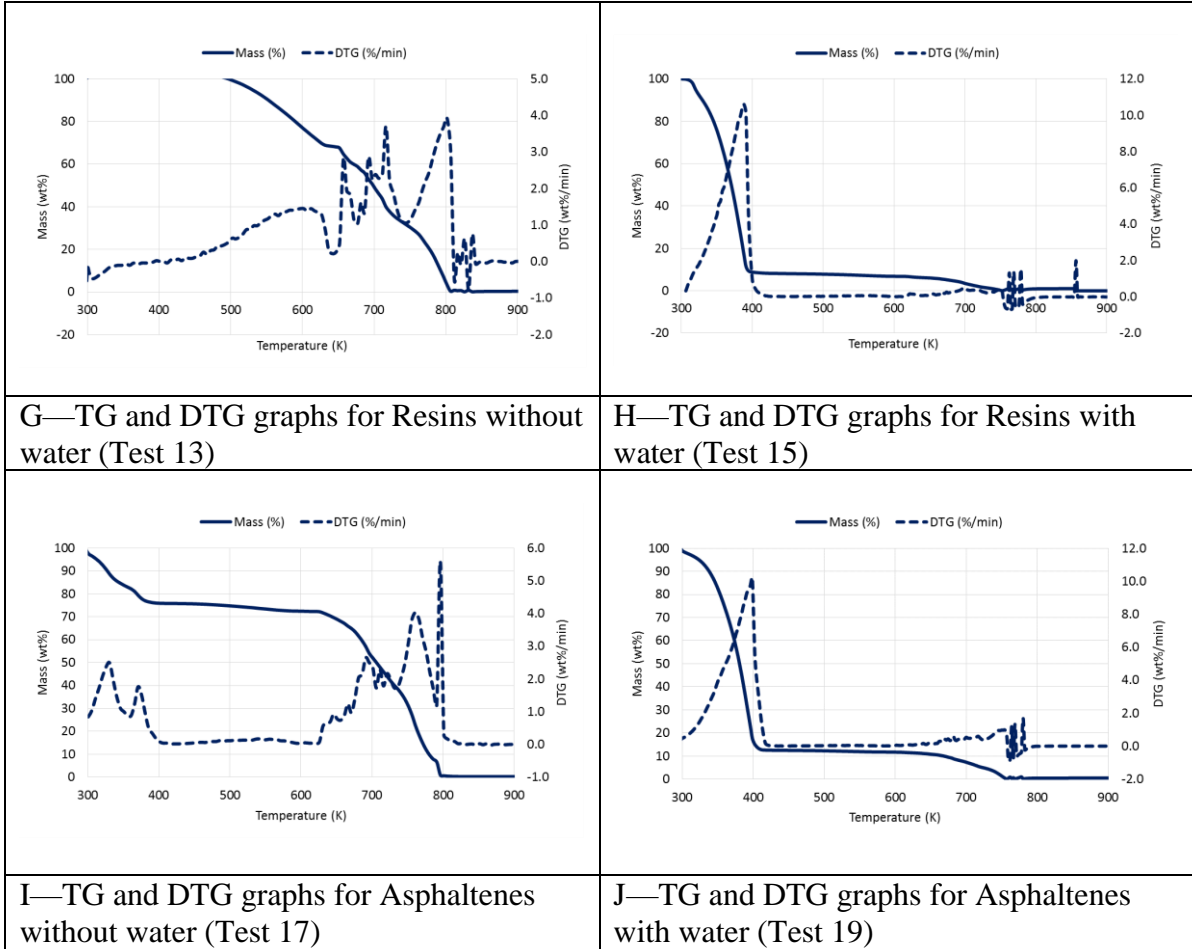
Figure 4 C5 (cont.)—TG/DTG Graphs for Arrhenius Model Calculation of Oil A Combustion at Low Heating Rate (Refer Table 4.3 for Experiment Name Coding)

A— Arrhenius Model Fitting for Crude Oil without water (Test 1)	B— Arrhenius Model Fitting for Crude Oil with water (Test 3)
C— Arrhenius Model Fitting for Saturates without water (Test 5)	D—Arrhenius Model Fitting for Saturates with water (Test 7)
E—Arrhenius Model Fitting for Aromatics without water (Test 9)	F—Arrhenius Model Fitting for Aromatics with water (Test 11)
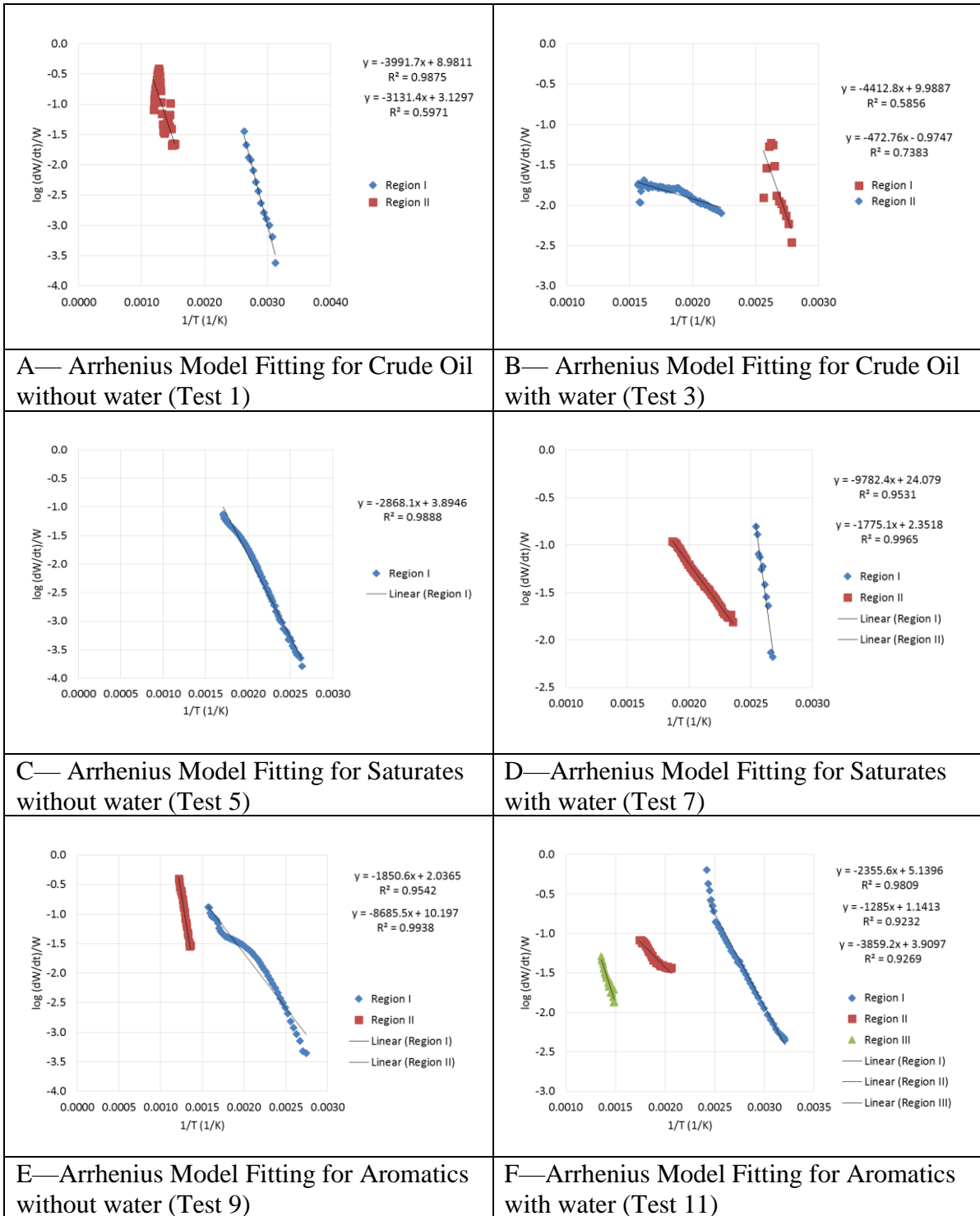
Figure 4 C6—Arrhenius Model Fitting Graphs for Oil A Combustion at Low Heating Rate (Refer Table 4.3 for Experiment Name Coding)

147

| G—Arrhenius Model Fitting for Resins without water (Test 13) | H—Arrhenius Model Fitting for Resins with water (Test 15) |
| I—Arrhenius Model Fitting for Asphaltenes without water (Test 17) | J—Arrhenius Model Fitting for Asphaltenes with water (Test 19) |

Figure 4 C6 (cont.)—Arrhenius Model Fitting Graphs for Oil A Combustion at Low Heating Rate (Refer Table 4.3 for Experiment Name Coding)

148

A—TG and DTG graphs for Crude Oil without water (Test 2)	B—TG and DTG graphs for Crude Oil with water (Test 4)
C—TG and DTG graphs for Saturates without water (Test 6)	D—TG and DTG graphs for Saturates with water (Test 8)
E—TG and DTG graphs for Aromatics without water (Test 10)	F—TG and DTG graphs for Aromatics with water (Test 12)
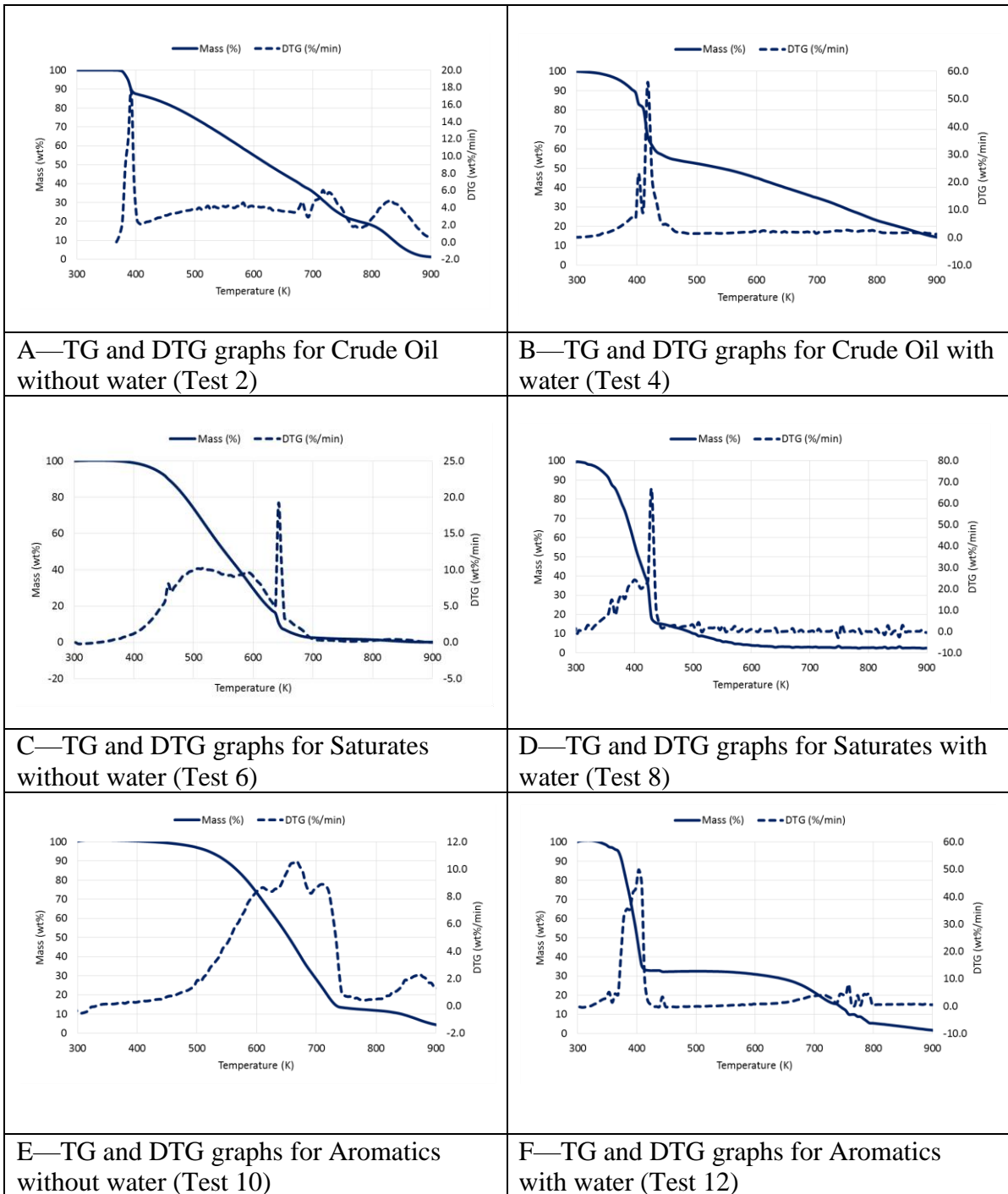
Figure 4 C7—TG/DTG graphs for Arrhenius Model Calculation of Oil A Combustion at High Heating Rate (Refer Table 4.3 for Experiment Name Coding)

149

G—TG and DTG graphs for Resins without water (Test 14)	H—TG and DTG graphs for Resins with water (Test 16)
I—TG and DTG graphs for Asphaltenes without water (Test 18)	J—TG and DTG graphs for Asphaltenes with water (Test 20)

Figure 4 C7 (cont.)—TG/DTG graphs for Arrhenius Model Calculation of Oil A Combustion at High Heating Rate (Refer Table 4.3 for Experiment Name Coding)

A—Arrhenius Model Fitting for Crude Oil without water (Test 2)	B—Arrhenius Model Fitting for Crude Oil with water (Test 4)
C—Arrhenius Model Fitting for Saturates without water (Test 6)	D—Arrhenius Model Fitting for Saturates with water (Test 8)
E—Arrhenius Model Fitting for Aromatics without water (Test 10)	F—Arrhenius Model Fitting for Aromatics with water (Test 12)

Figure 4 C8—Arrhenius Model Fitting Graphs for Oil A Combustion at High Heating Rate (Refer Table 4.3 for Experiment Name Coding)

151

G—Arrhenius Model Fitting Resins without water (Test 14)	H—Arrhenius Model Fitting for Resins with water (Test 16)
I—Arrhenius Model Fitting for Asphaltenes without water (Test 18)	J—Arrhenius Model Fitting for Asphaltenes with water (Test 20)
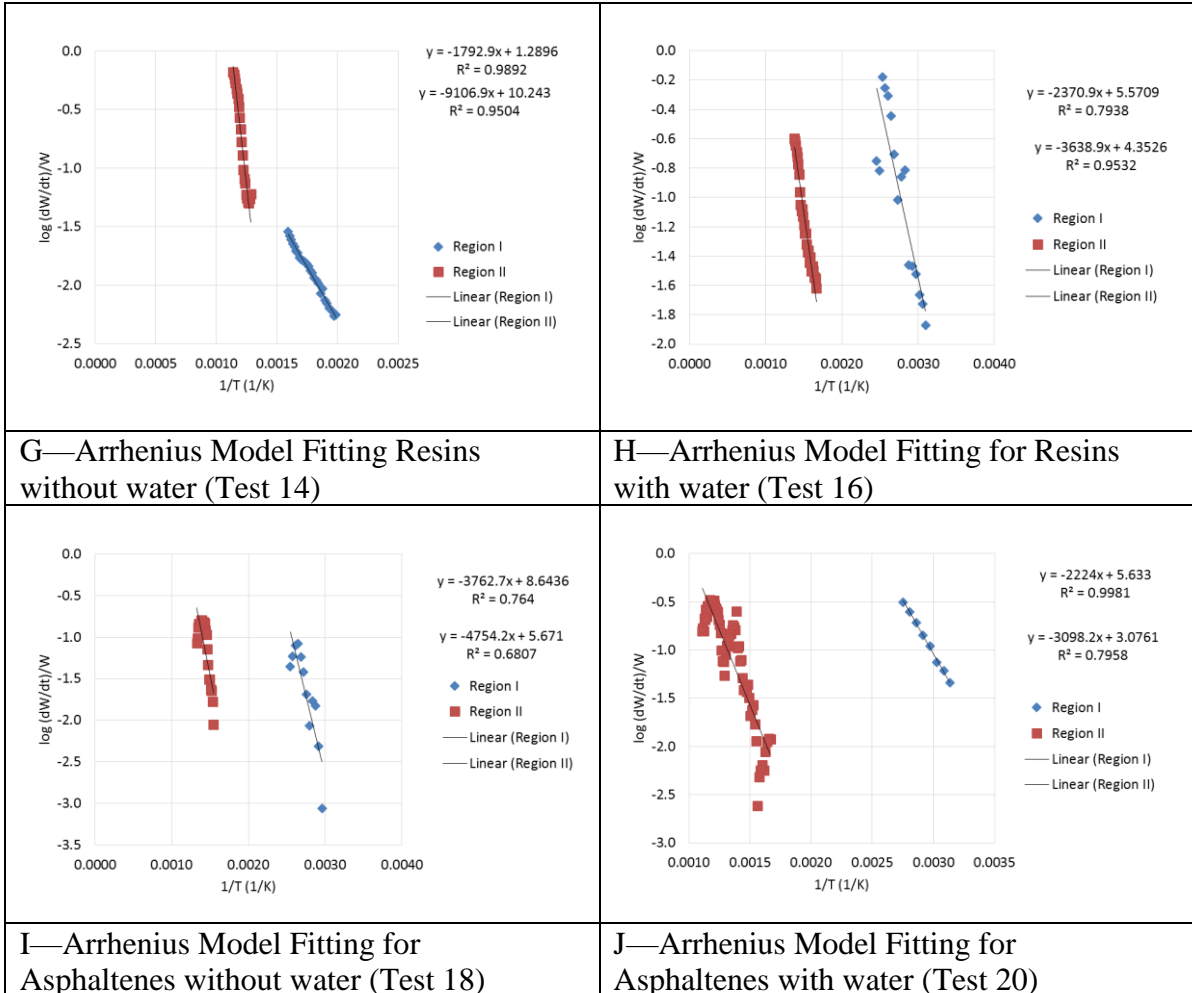
Figure 4 C8 (cont.)—Arrhenius Model Fitting Graphs for Oil A Combustion at High Heating Rate (Refer Table 4.3 for Experiment Name Coding)

A—TG and DTG graphs for Crude Oil without water (Test 21)	B—TG and DTG graphs for Crude Oil with water (Test 23)
C—TG and DTG graphs for Saturates without water (Test 25)	D—TG and DTG graphs for Saturates with water (Test 27)
E—TG and DTG graphs for Aromatics without water (Test 29)	F—TG and DTG graphs for Aromatics with water (Test 31)

Figure 4 C9—TG/DTG graphs for Arrhenius Model Calculation of Oil B Combustion at Low Heating Rate (Refer Table 4.3 for Experiment Name Coding)

153

G—TG and DTG graphs for Resins without water (Test 33)	H—TG and DTG graphs for Resins with water (Test 35)
I—TG and DTG graphs for Asphaltenes without water (Test 37)	J—TG and DTG graphs for Asphaltenes with water (Test 39)

Figure 4 C9 (cont.)—TG/DTG graphs for Arrhenius Model Calculation of Oil B Combustion at Low Heating Rate (Refer Table 4.3 for Experiment Name Coding)

A— Arrhenius Model Fitting for Crude Oil without water (Test 21)	B— Arrhenius Model Fitting for Crude Oil with water (Test 23)
C—Arrhenius Model Fitting for Saturates without water (Test 25)	D—Arrhenius Model Fitting for Saturates with water (Test 27)
E—Arrhenius Model Fitting for Aromatics without water (Test 29)	F—Arrhenius Model Fitting for Aromatics with water (Test 31)
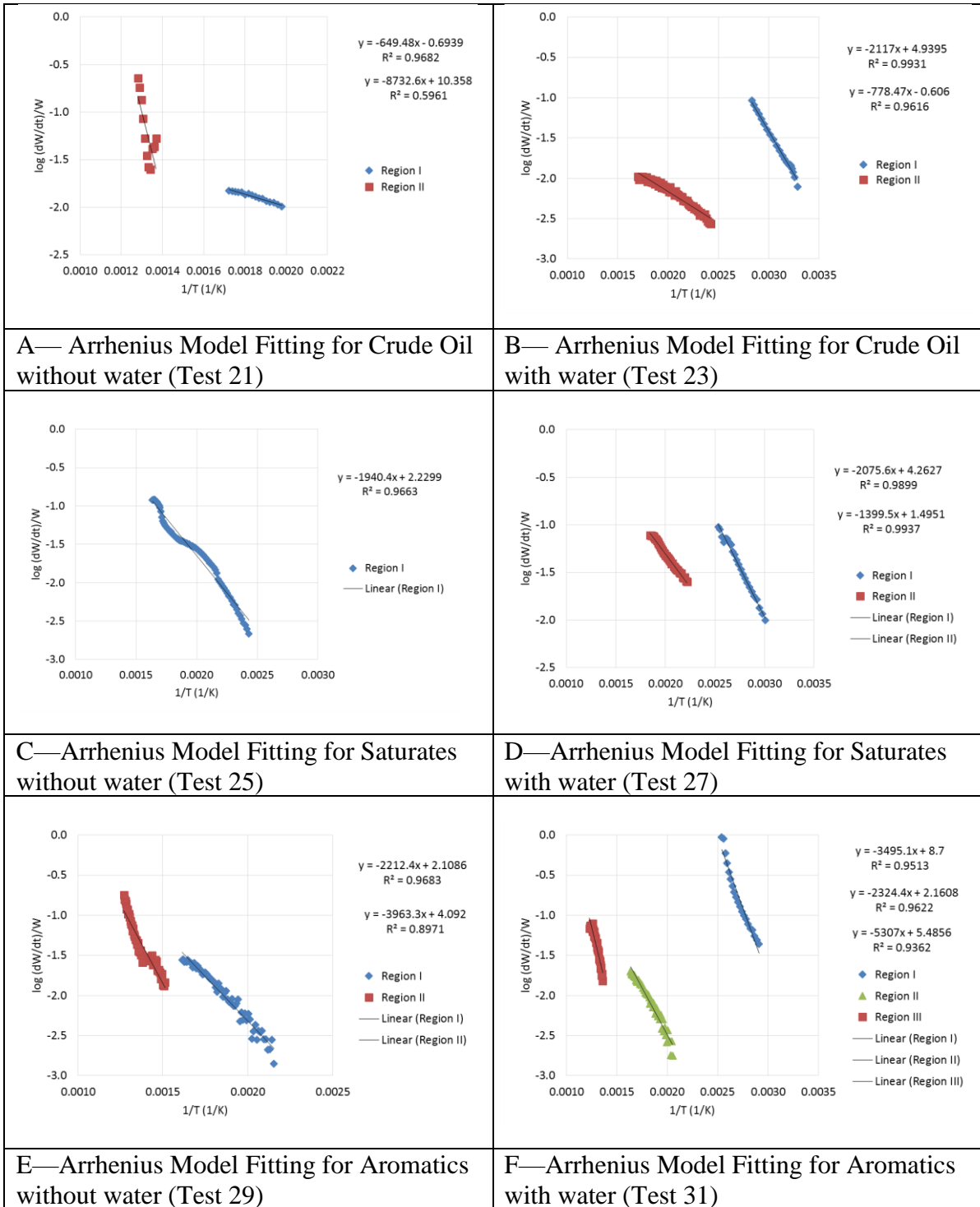
Figure 4 C10—Arrhenius Model Fitting Graphs for Oil B Combustion at Low Heating Rate (Refer Table 4.3 for Experiment Name Coding)

155

G—Arrhenius Model Fitting for Resins without water (Test 33)	H—Arrhenius Model Fitting for Resins with water (Test 35)
I—Arrhenius Model Fitting for Asphaltenes without water (Test 37)	J—Arrhenius Model Fitting for Asphaltenes with water (Test 39)

Figure 4 C10 (cont.)—Arrhenius Model Fitting Graphs for Oil B Combustion at Low Heating Rate (Refer Table 4.3 for Experiment Name Coding)

A—TG and DTG graphs for Crude Oil without water (Test 22)	B—TG and DTG graphs for Crude Oil with water (Test 24)
C—TG and DTG graphs for Saturates without water (Test 26)	D—TG and DTG graphs for Saturates with water (Test 28)
E—TG and DTG graphs for Aromatics without water (Test 30)	F—TG and DTG graphs for Aromatics with water (Test 32)

Figure 4 C11—TG/DTG Graphs for Arrhenius Model Calculation of Oil B Combustion at High Heating Rate (Refer Table 4.3 for Experiment Name Coding)

G—TG and DTG graphs for Resins without water (Test 34)	H—TG and DTG graphs for Resins with water (Test 36)
I—TG and DTG graphs for Asphaltenes without water (Test 38)	J—TG and DTG graphs for Asphaltenes with water (Test 40)

Figure 4 C11 (cont.)—TG/DTG Graphs for Arrhenius Model Calculation of Oil B Combustion at High Heating Rate (Refer Table 4.3 for Experiment Name Coding)

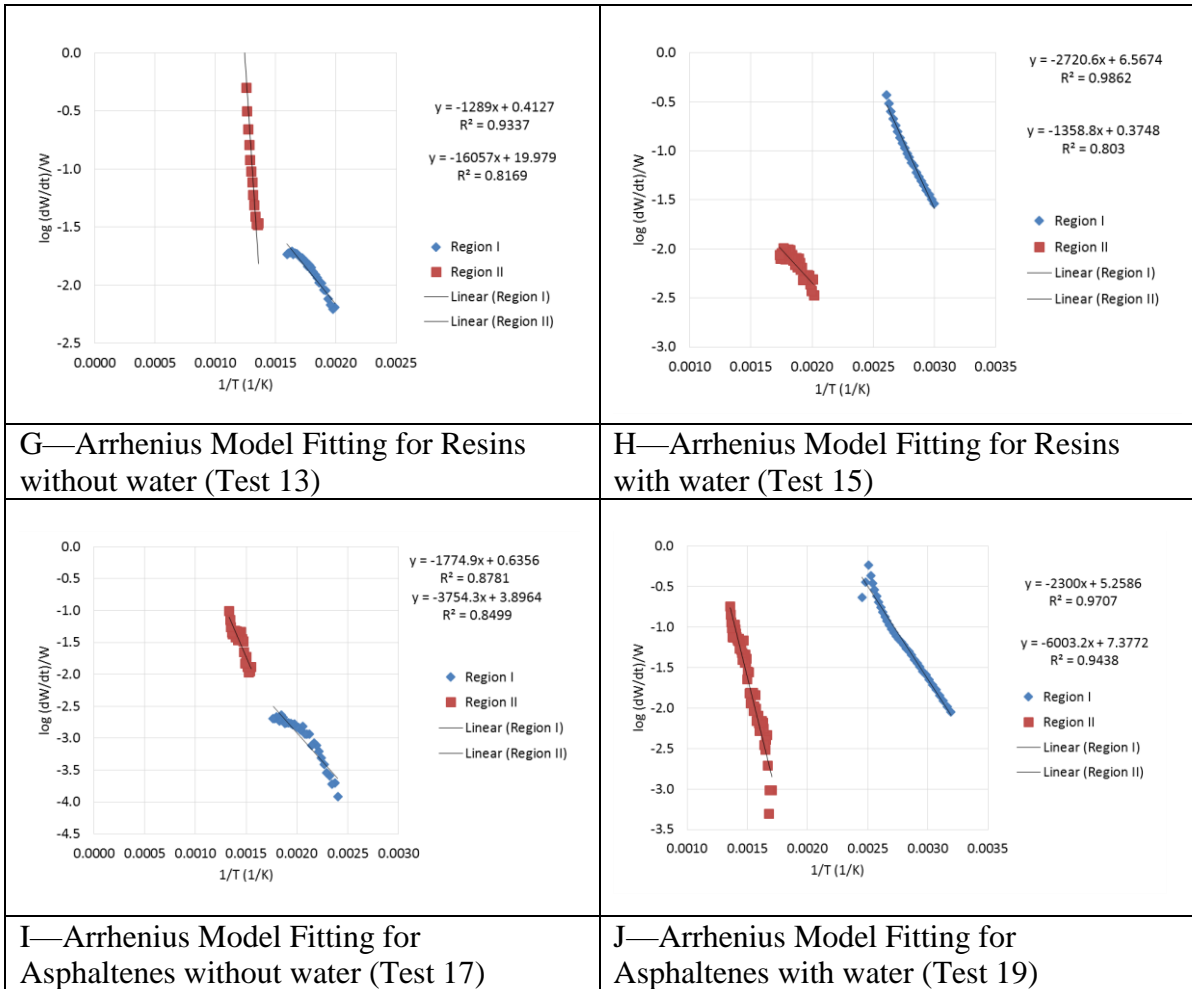|	
A—Arrhenius Model Fitting for Crude Oil without water (Test 22)	B—Arrhenius Model Fitting for Crude Oil with water (Test 24)
C—Arrhenius Model Fitting for Saturates without water (Test 26)	D—Arrhenius Model Fitting for Saturates with water (Test 28)
E—Arrhenius Model Fitting for Aromatics without water (Test 30)	F—Arrhenius Model Fitting for Aromatics with water (Test 32)

Figure 4 C12—Arrhenius Model Fitting Graphs for Oil B Combustion at High Heating Rate (Refer Table 4.3 for Experiment Name Coding)

159

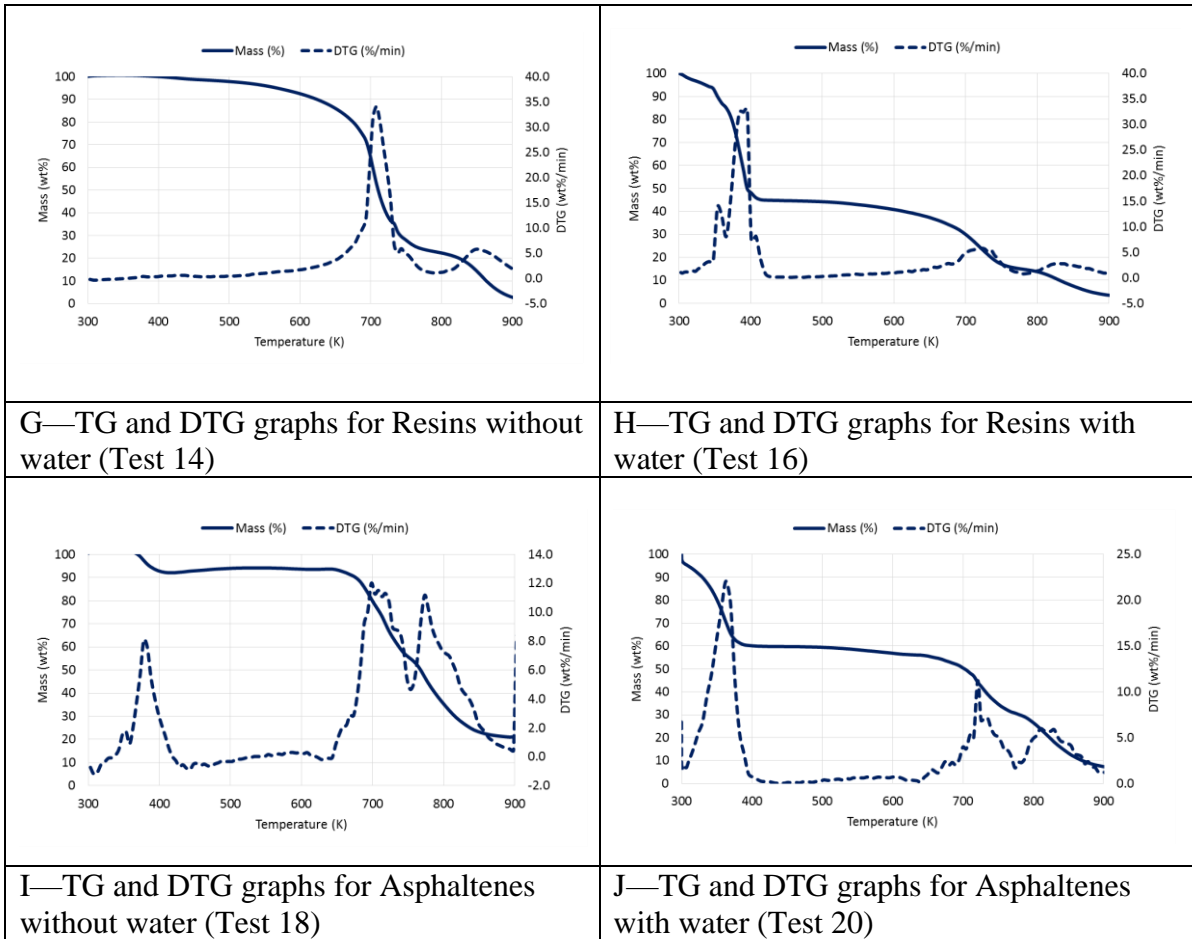|	
G—Arrhenius Model Fitting for Resins without water (Test 34)	H—Arrhenius Model Fitting for Resins with water (Test 36)
I—Arrhenius Model Fitting for Asphaltenes without water (Test 38)	J—Arrhenius Model Fitting for Asphaltenes with water (Test 40)

Figure 4 C12 (cont.)—Arrhenius Model Fitting Graphs for Oil B Combustion at High Heating Rate (Refer Table 4.3 for Experiment Name Coding)
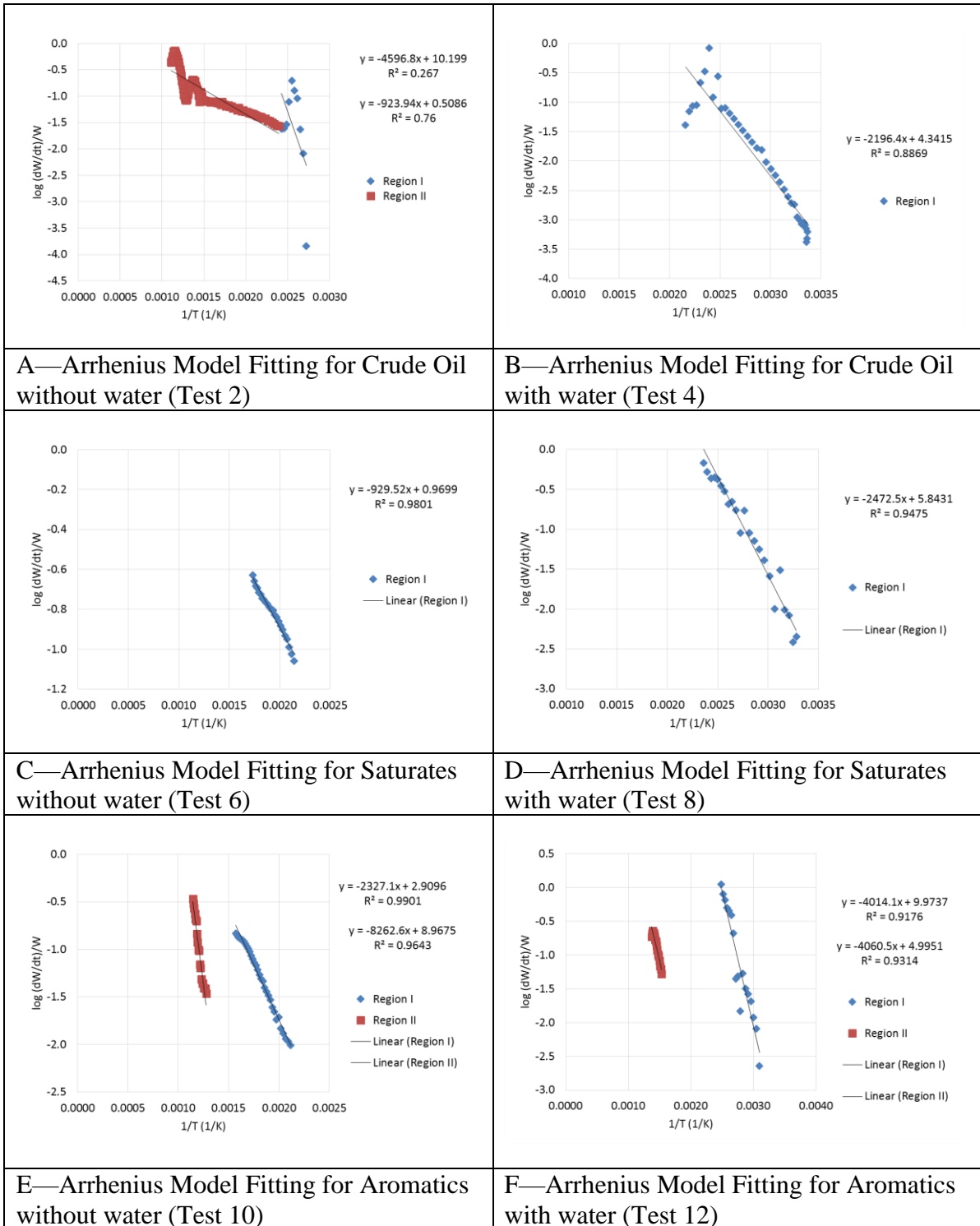
| A— Weight loss behavior of C10 functional group without water at low heating rate (5 °C/min) | B—Weight loss behavior of C10 functional group with water at low heating rate (5 °C/min) |
| C—Weight loss behavior of C10 functional group without water at high heating rate (20 °C/min) | D— Weight loss behavior of C10 functional group with water at high heating rate (20 °C/min) |

Figure 4 C13—Weight Loss Behavior Of C10 Hydrocarbon Functional Groups: Decane (Dark Blue), Decanal (Light Green), Decanol (Dark Green), and Decanone (Dark Blue) during Combustion under Air Injection

161

| A— Heat Flow behavior of C10 functional group without water at low heating rate (5 °C/min) | B— Heat Flow behavior of C10 functional group with water at low heating rate (5 °C/min) |
| C—Heat Flow behavior of C10 functional group without water at high heating rate (20 °C/min) | D— Heat Flow behavior of C10 functional group with water at high heating rate (20 °C/min) |

Figure 4 C14—Heat Flow Behavior Of C10 Hydrocarbon Functional Groups: Decane (Dark Blue), Decanal (Light Green), Decanol (Dark Green), and Decanone (Dark Blue) during Combustion under Air Injection

A—TG and DTG graphs for Alkanes without water (Test 41)	B—TG and DTG graphs for Alkanes with water (Test 43)
C—TG and DTG graphs for Aldehydes without water (Test 45)	D—TG and DTG graphs for Aldehydes with water (Test 47)
E—TG and DTG graphs for Alcohols without water (Test 49)	F—TG and DTG graphs for Alcohols with water (Test 51)

Figure 4 C15—TG/DTG Graphs for Arrhenius Model Calculation of Chemicals Combustion at Low Heating Rate (Refer Table 4.4 for Experiment Name Coding)
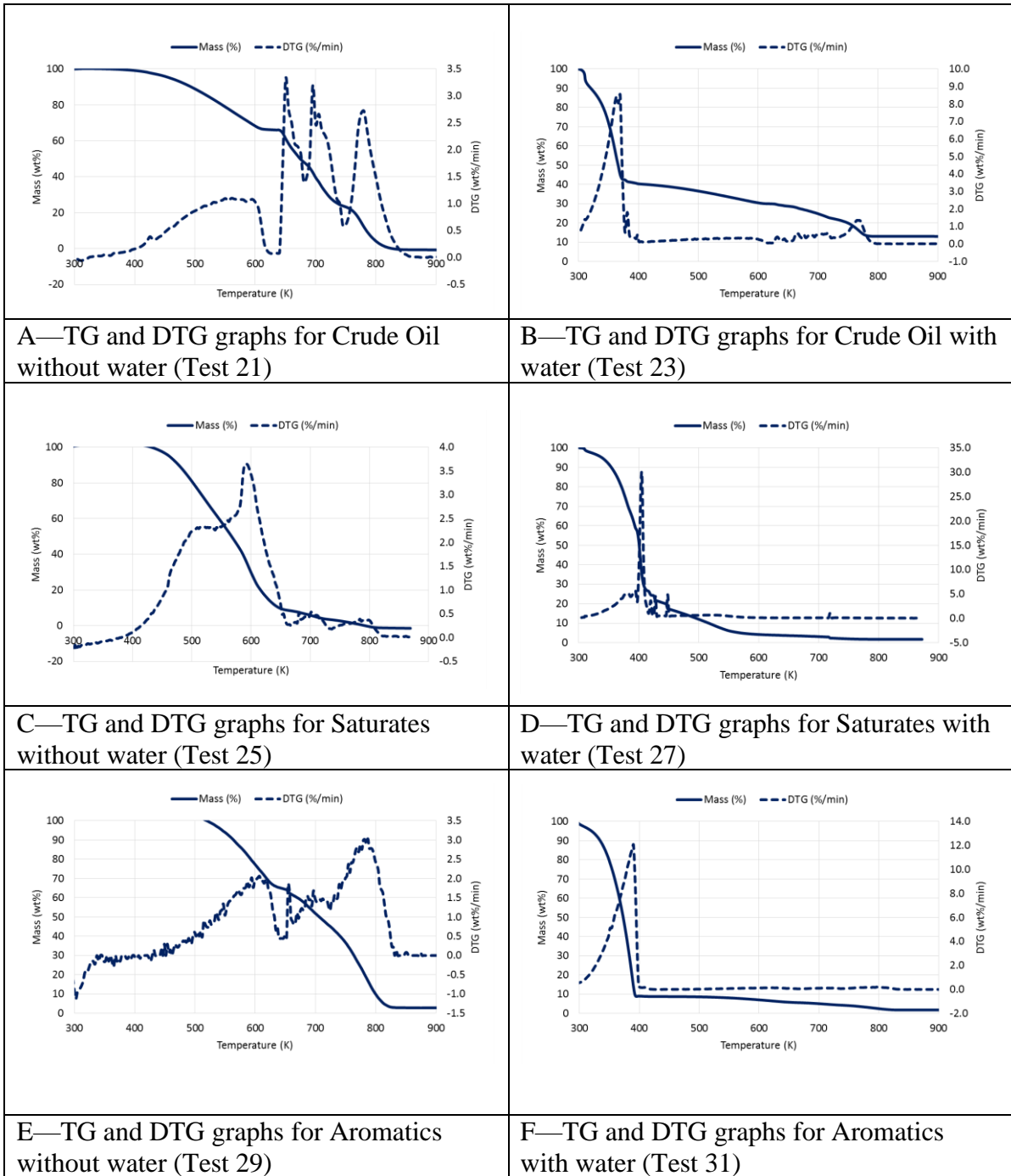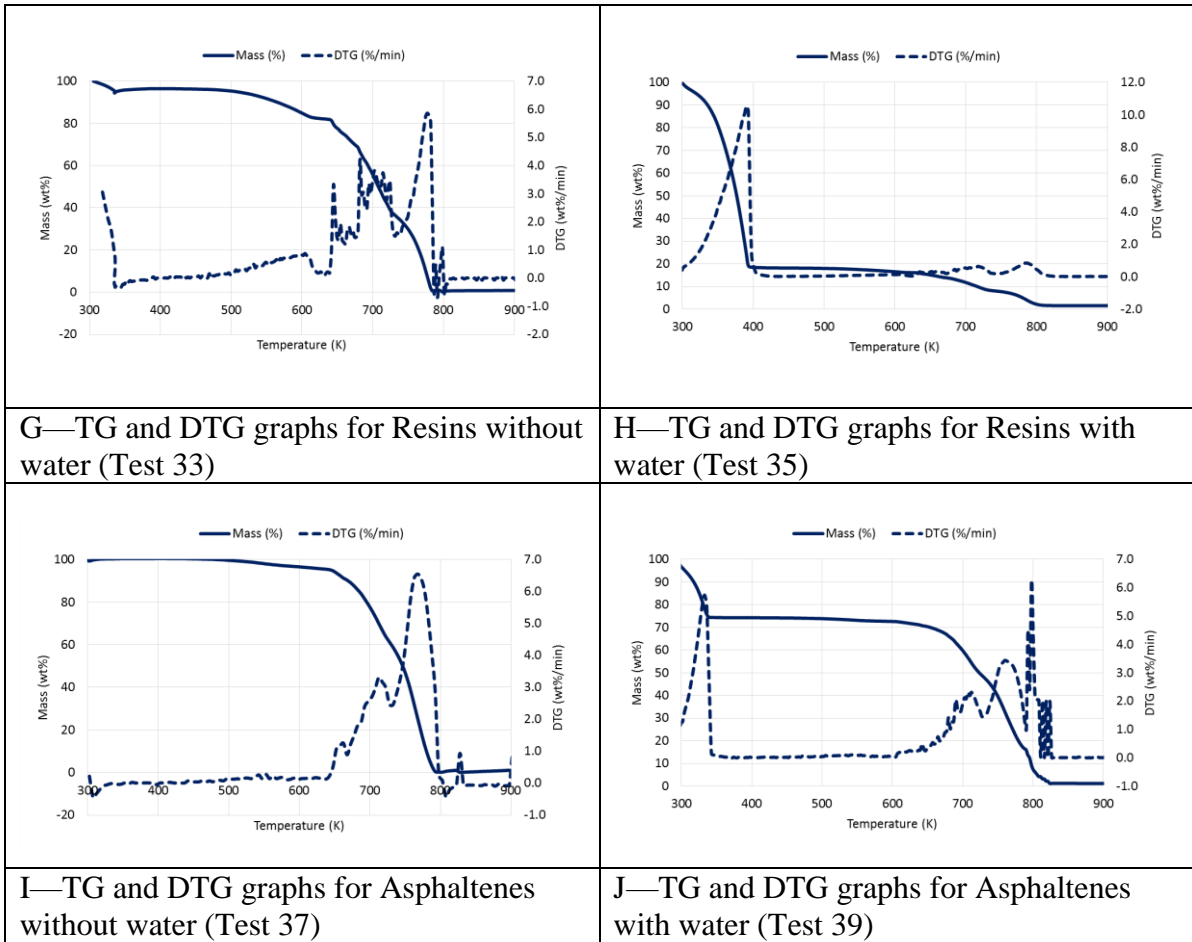
| G—TG and DTG graphs for Ketones without water (Test 53) | H—TG and DTG graphs for Ketones with water (Test 55) |

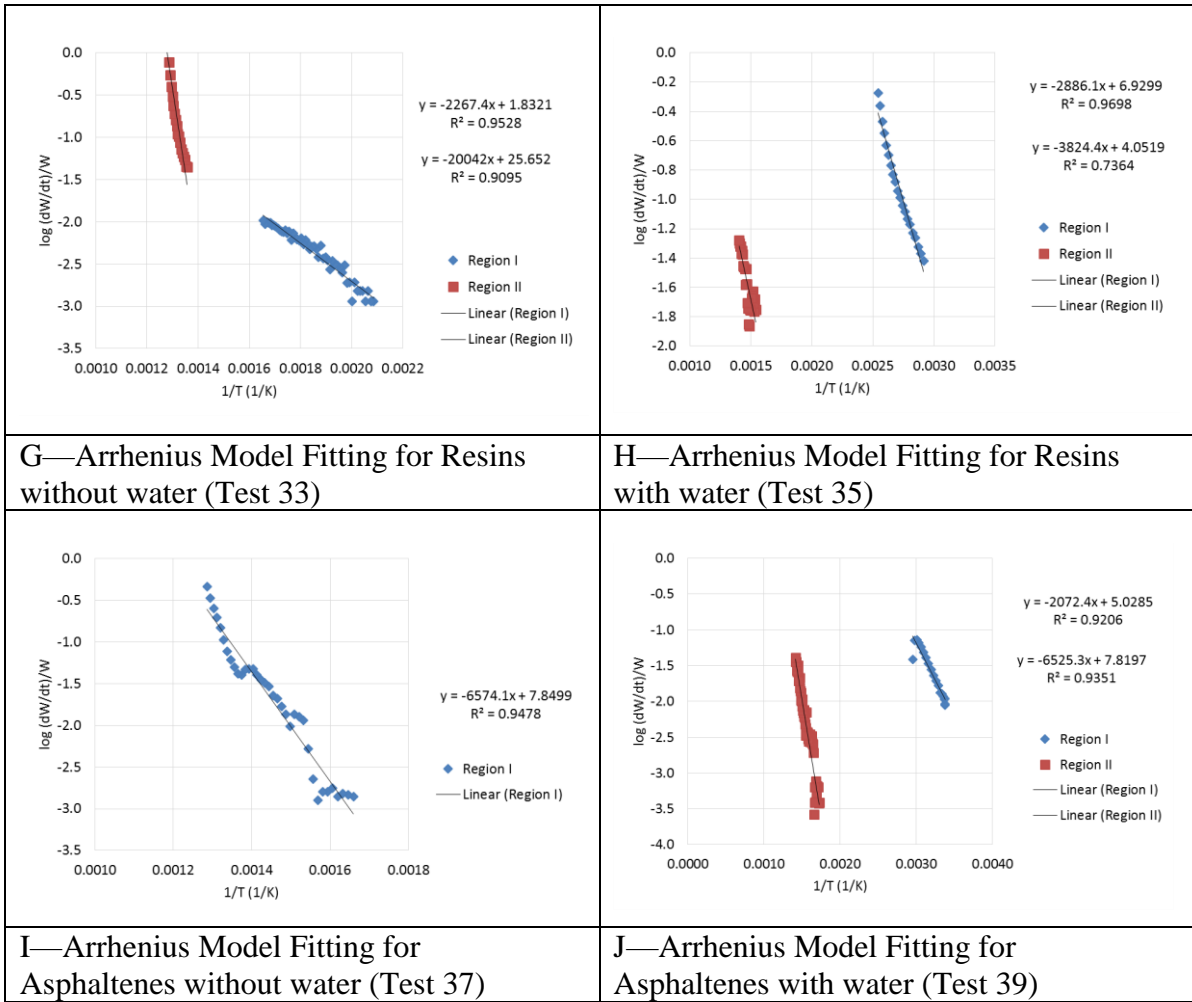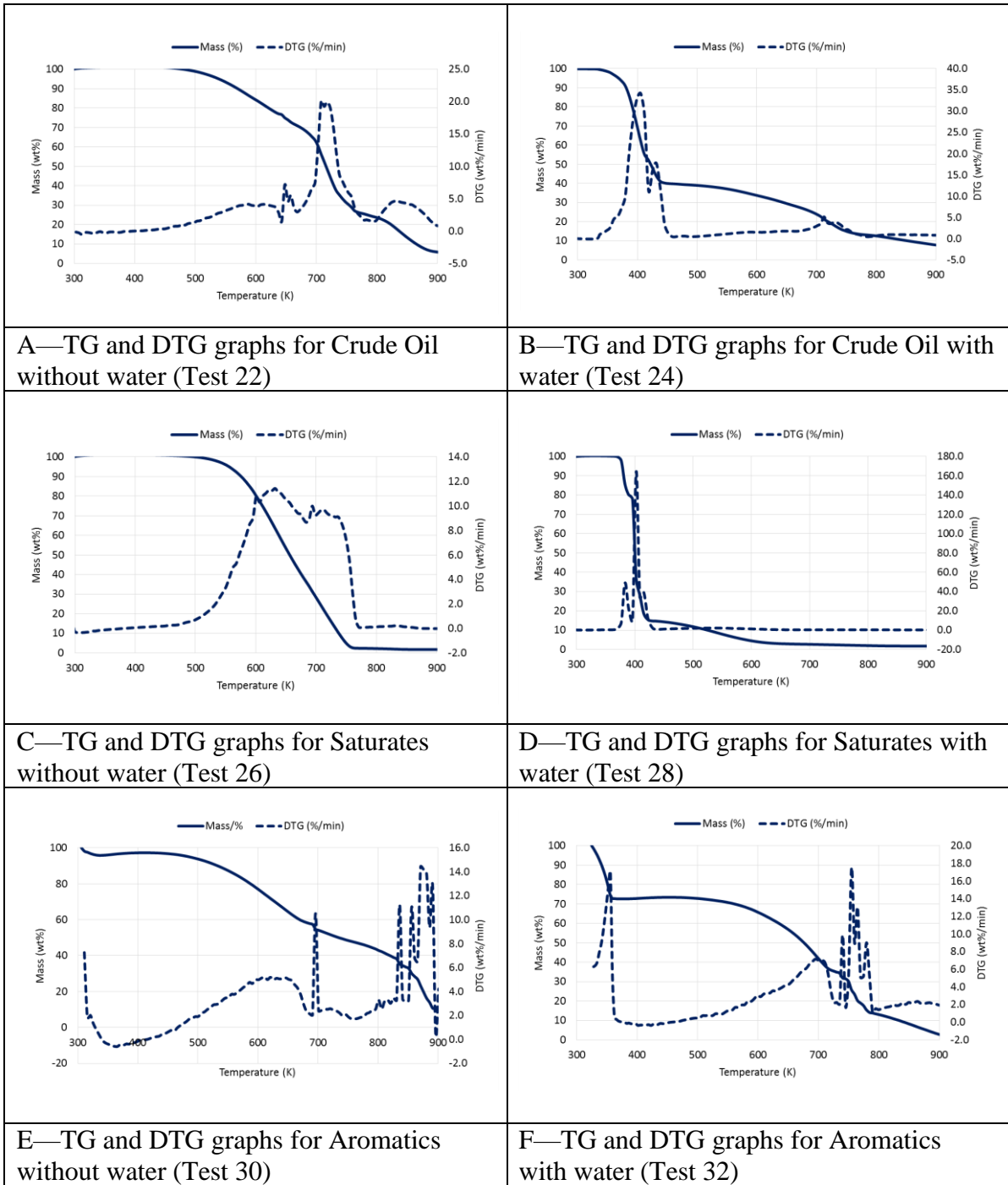**Figure 4 C15 (cont.)—TG/DTG Graphs for Arrhenius Model Calculation of Chemicals Combustion at Low Heating Rate (Refer Table 4.4 for Experiment Name Coding)**

A—Arrhenius Model Fitting for Alkanes without water (Test 41)	B—Arrhenius Model Fitting for Alkanes with water (Test 43)
C—Arrhenius Model Fitting for Aldehydes without water (Test 45)	D—Arrhenius Model Fitting for Aldehydes with water (Test 47)
E—Arrhenius Model Fitting for Alcohols without water (Test 49)	F—Arrhenius Model Fitting for Alcohols with water (Test 51)
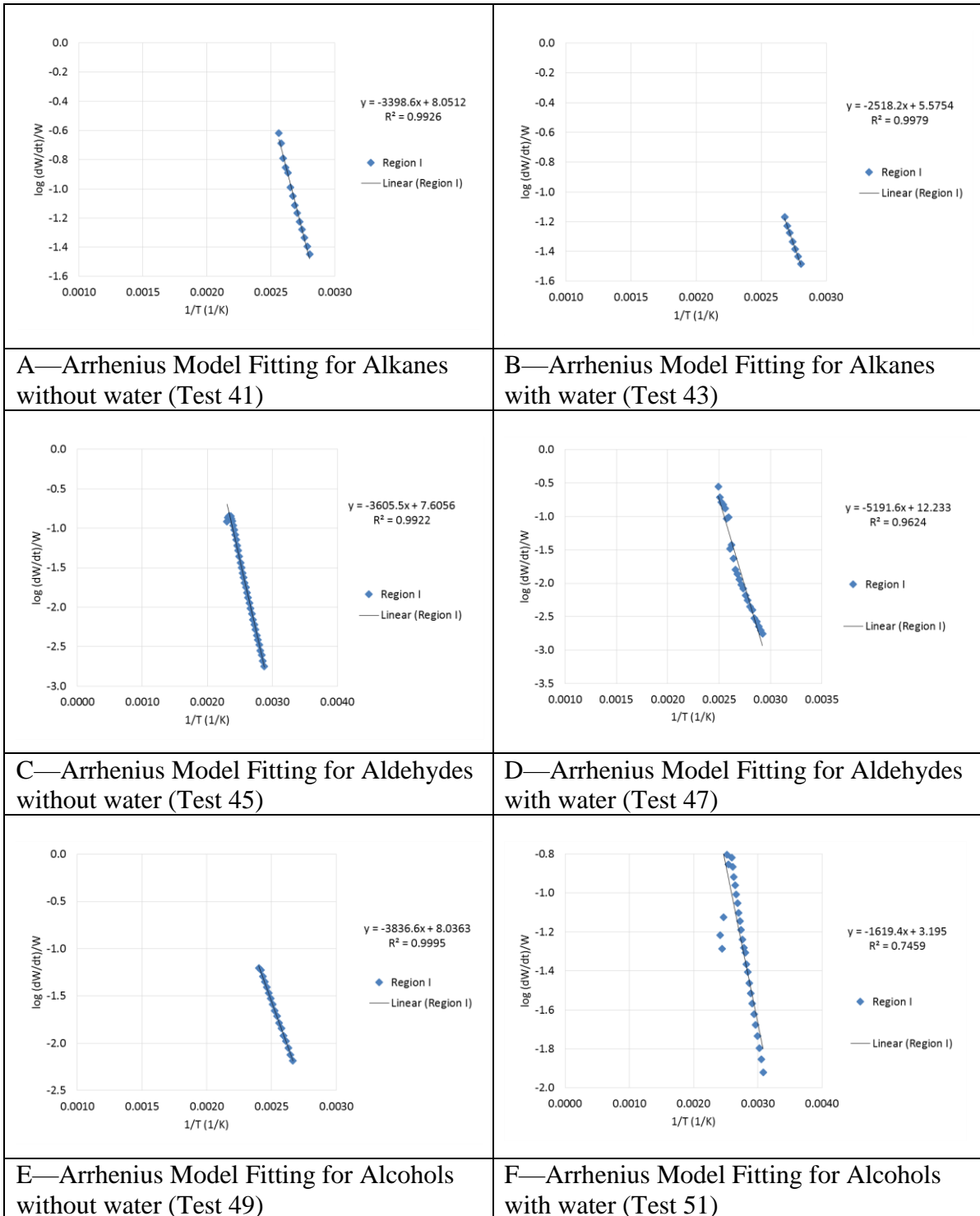
Figure 4 C16—Arrhenius Model Fitting Graphs for Chemicals Combustion at Low Heating Rate (Refer Table 4.4 for Experiment Name Coding)

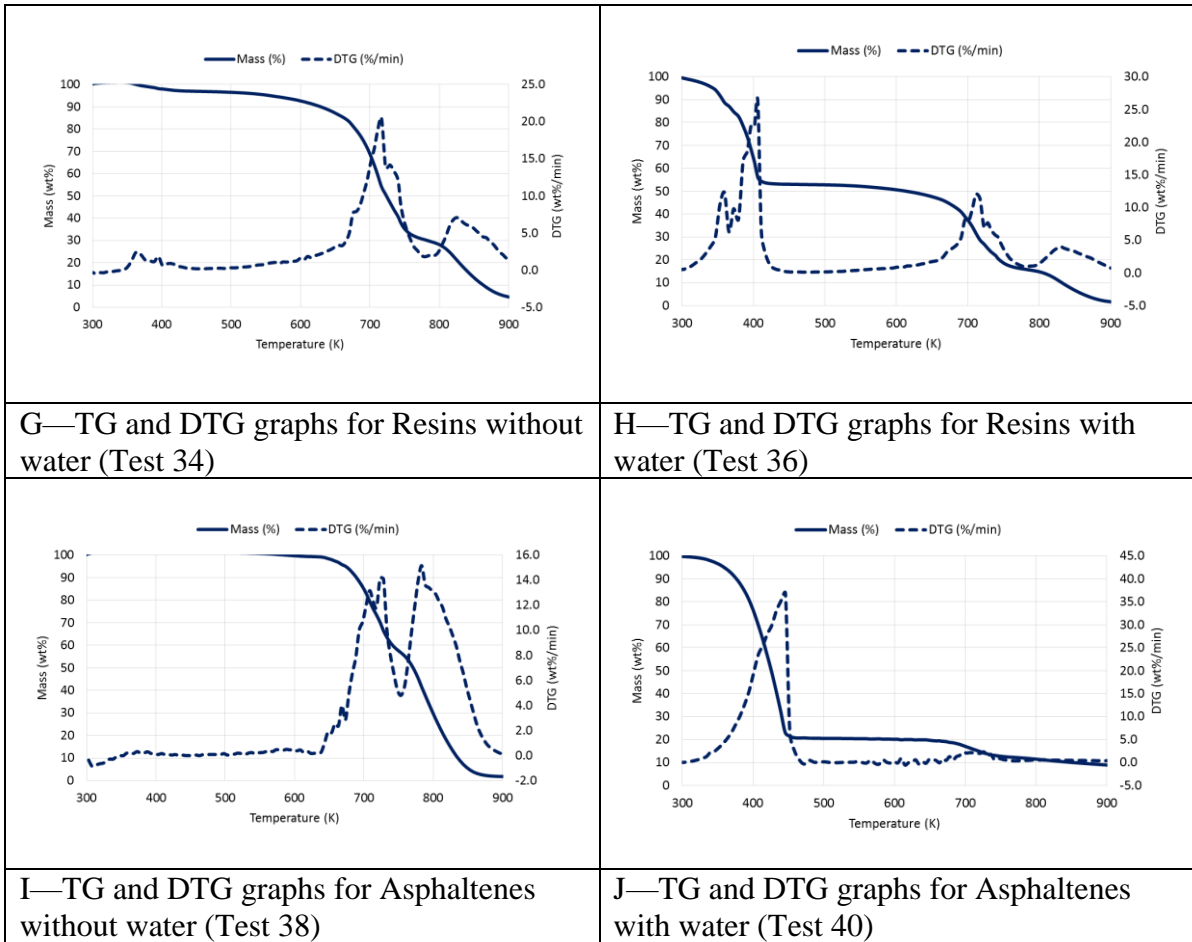| G— Arrhenius Model Fitting for Ketones without water (Test 53) | H—Arrhenius Model Fitting for Ketones with water (Test 55) |
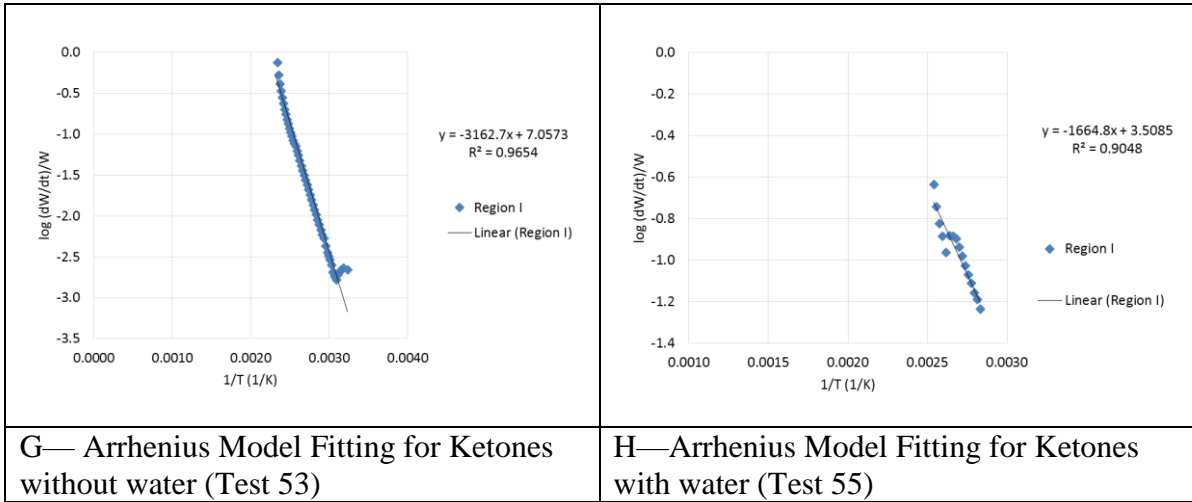
Figure 4 C16 (cont.)—Arrhenius Model Fitting Graphs for Chemicals Combustion at Low Heating Rate (Refer Table 4.4 for Experiment Name Coding)

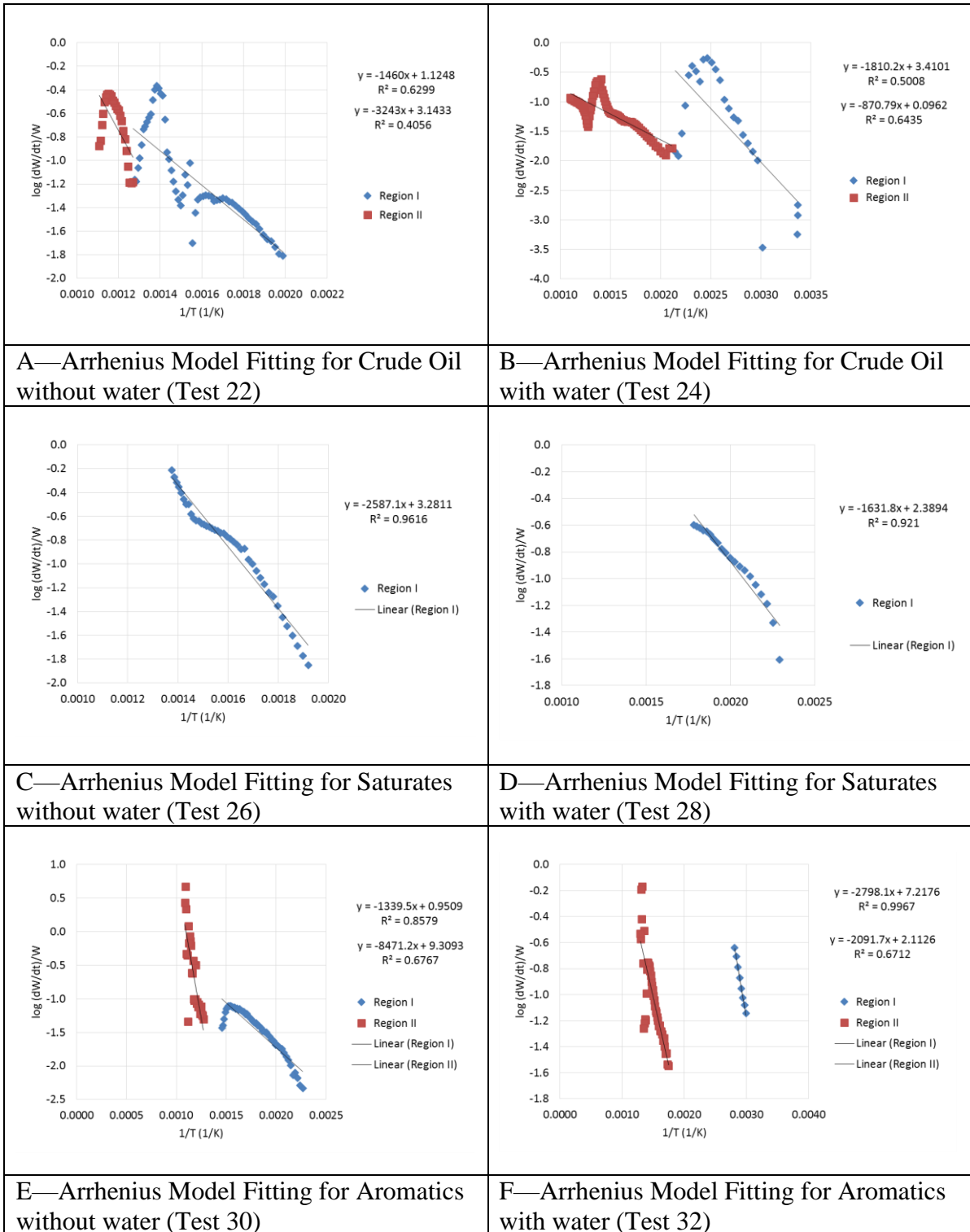|	
A—TG and DTG graphs for Alkanes without water (Test 42)	B—TG and DTG graphs for Alkanes with water (Test 44)
C—TG and DTG graphs for Aldehydes without water (Test 46)	D—TG and DTG graphs for Aldehydes with water (Test 48)
E—TG and DTG graphs for Alcohols without water (Test 50)	F—TG and DTG graphs for Alcohols with water (Test 52)
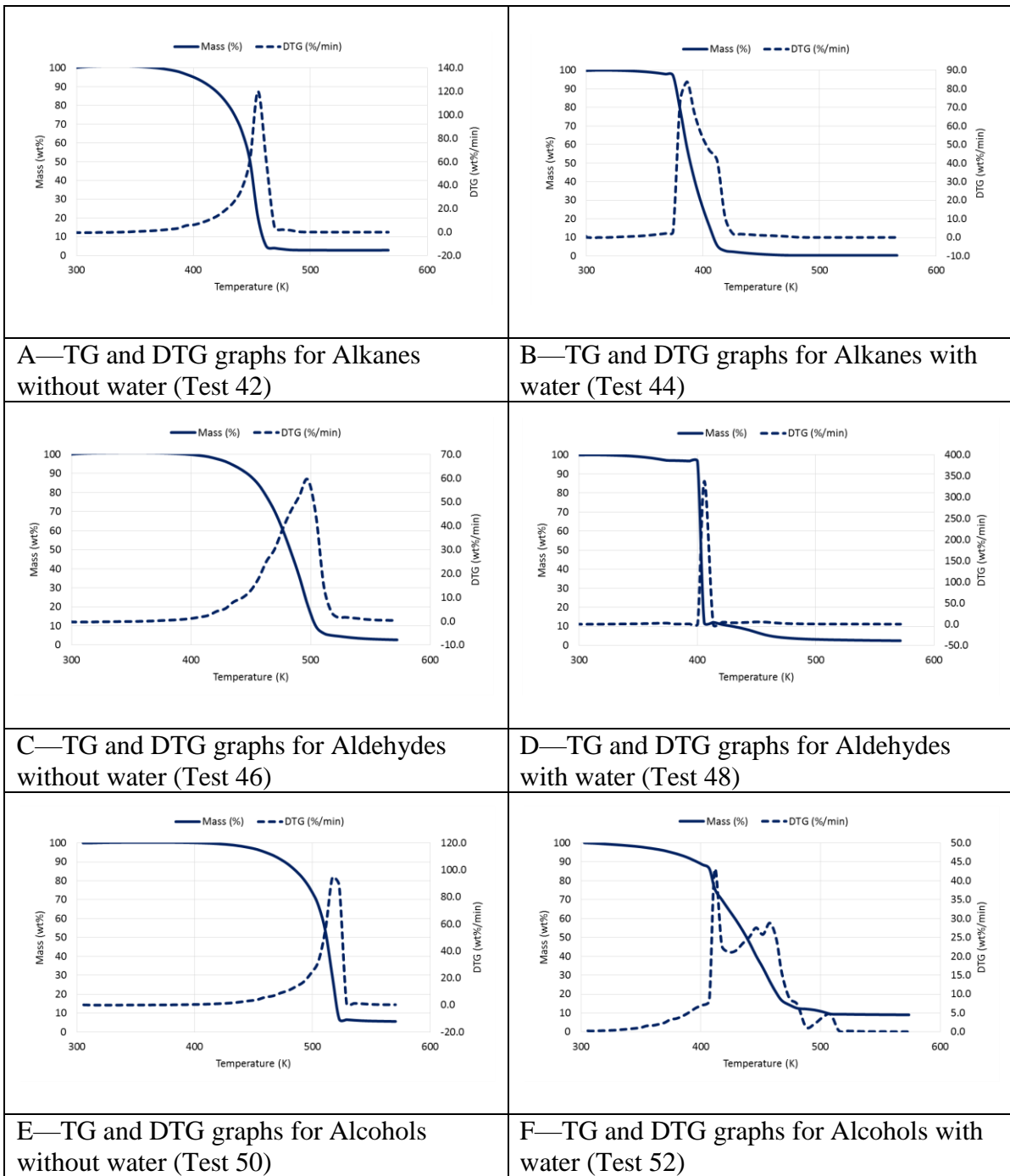
Figure 4 C17—TG/DTG graphs for Arrhenius Model Calculation of Chemicals Combustion at High Heating Rate (Refer Table 4.4 for Experiment Name Coding)

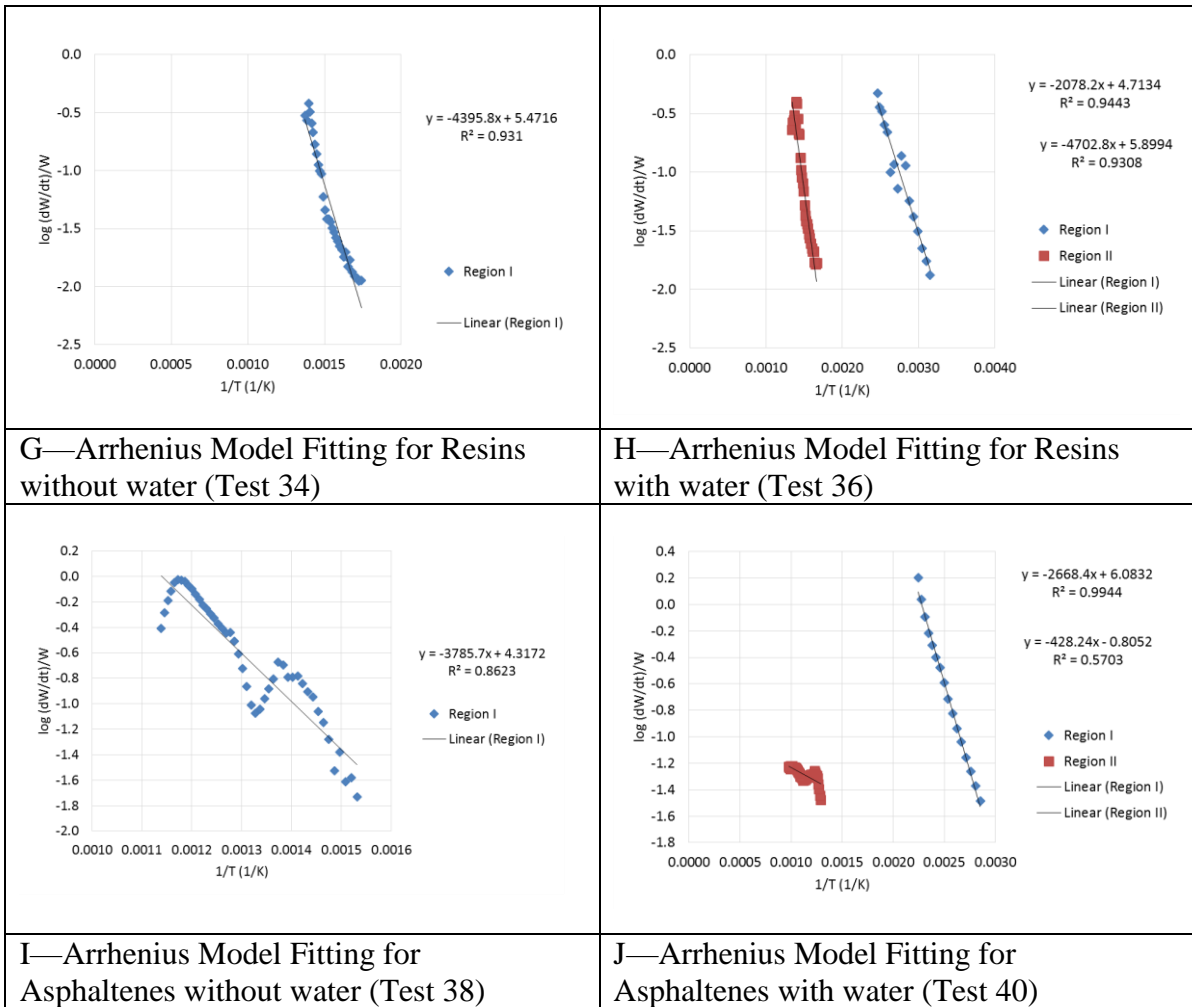| G—TG and DTG graphs for Ketones without water (Test 54) | H—TG and DTG graphs for Ketones with water (Test 56) |
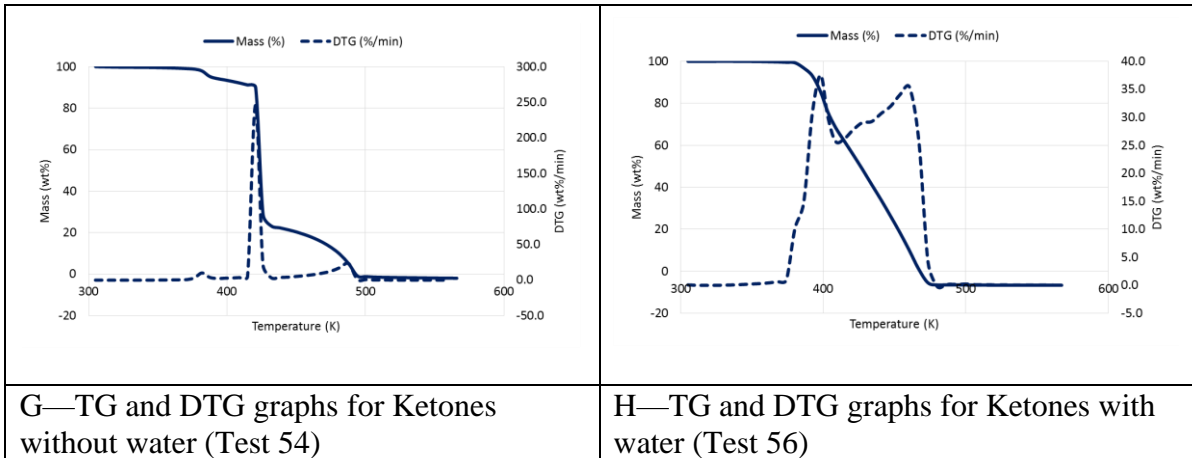
Figure 4 C17 (cont.)—TG/DTG graphs for Arrhenius Model Calculation of Chemicals Combustion at High Heating Rate (Refer Table 4.4 for Experiment Name Coding)
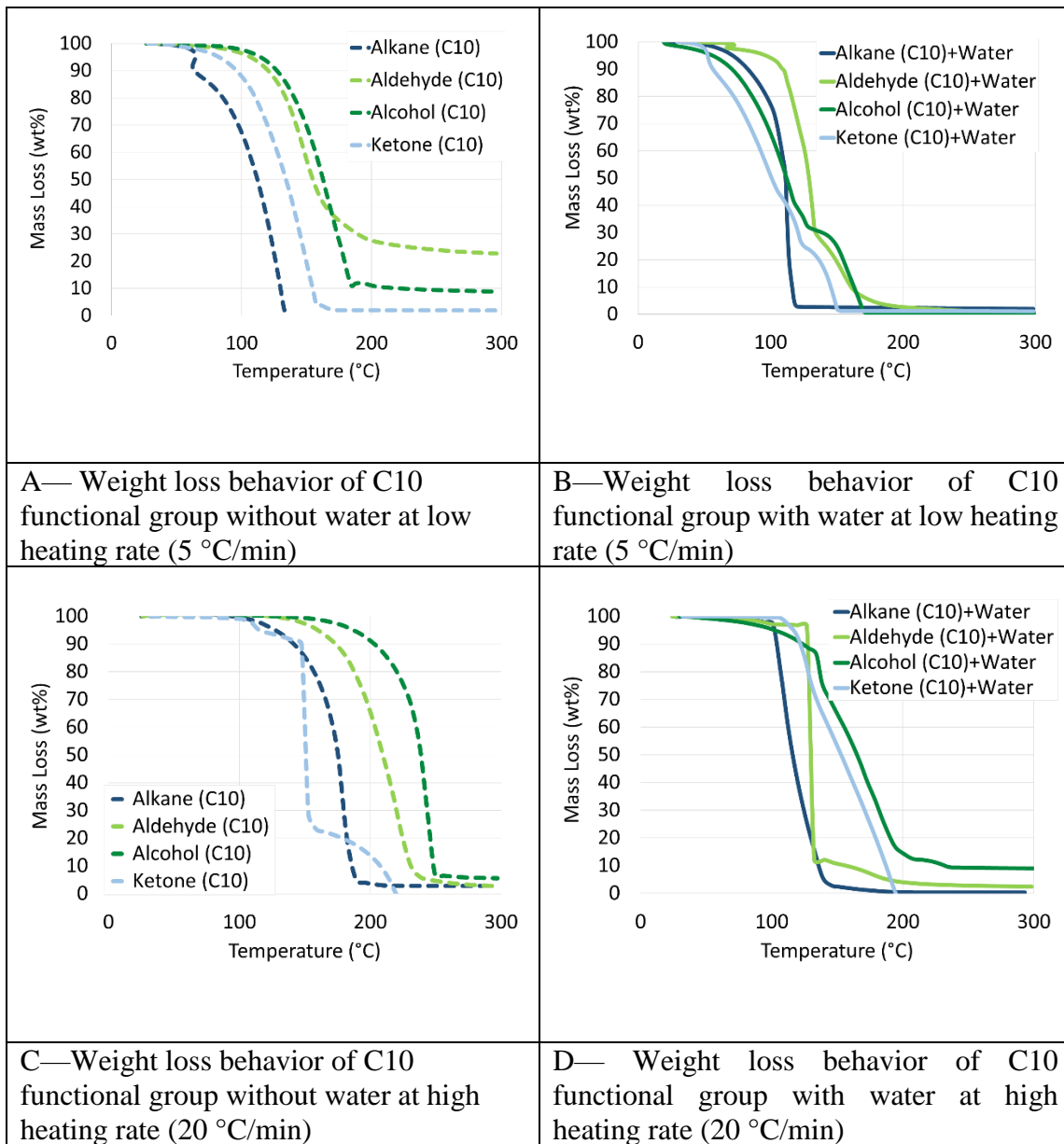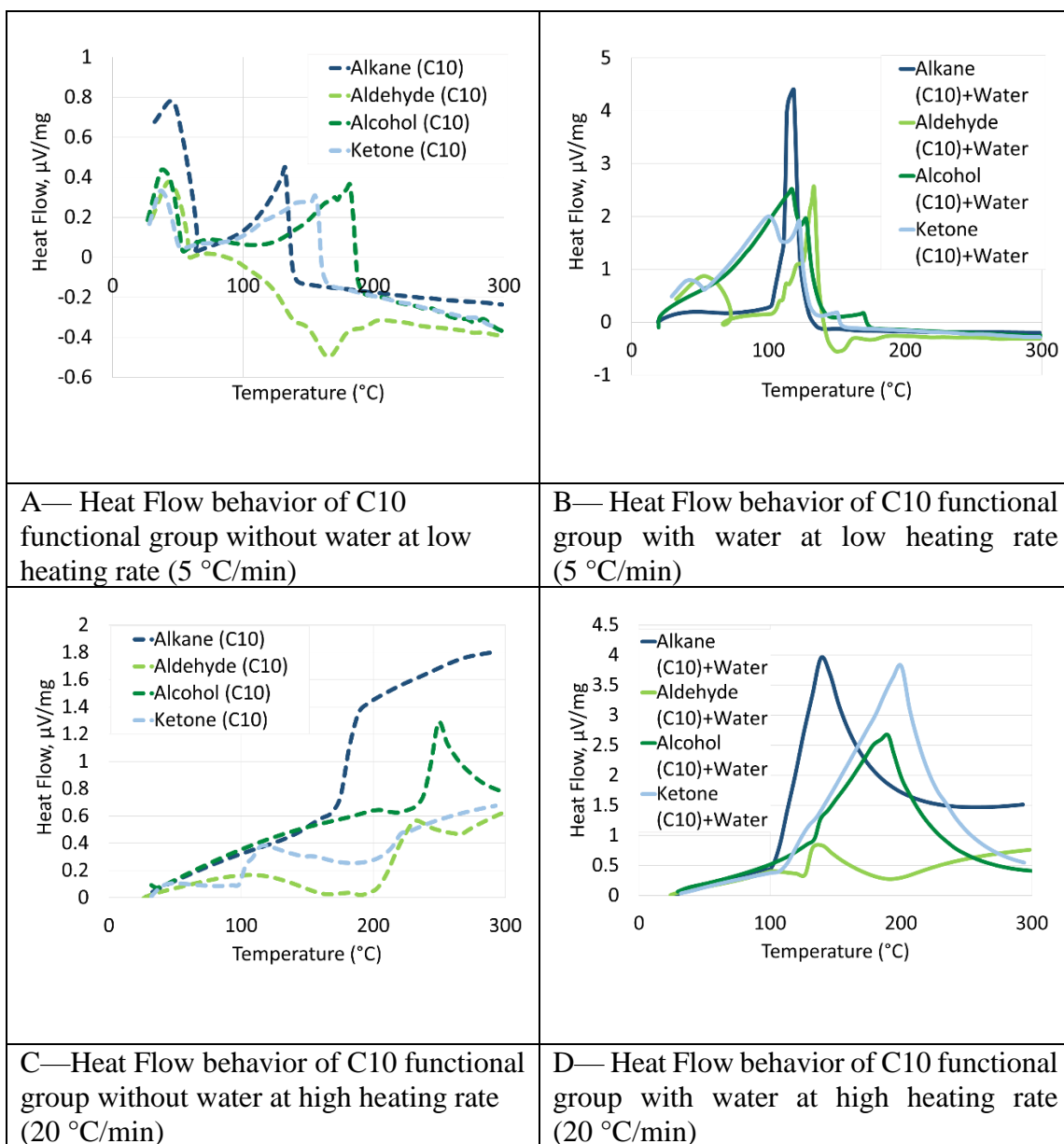
A—Arrhenius Model Fitting for Alkanes without water (Test 42)	B—Arrhenius Model Fitting for Alkanes with water (Test 44)
C—Arrhenius Model Fitting for Aldehydes without water (Test 46)	D—Arrhenius Model Fitting for Aldehydes with water (Test 48)
E—Arrhenius Model Fitting for Alcohols without water (Test 50)	F—Arrhenius Model Fitting for Alcohols with water (Test 52)
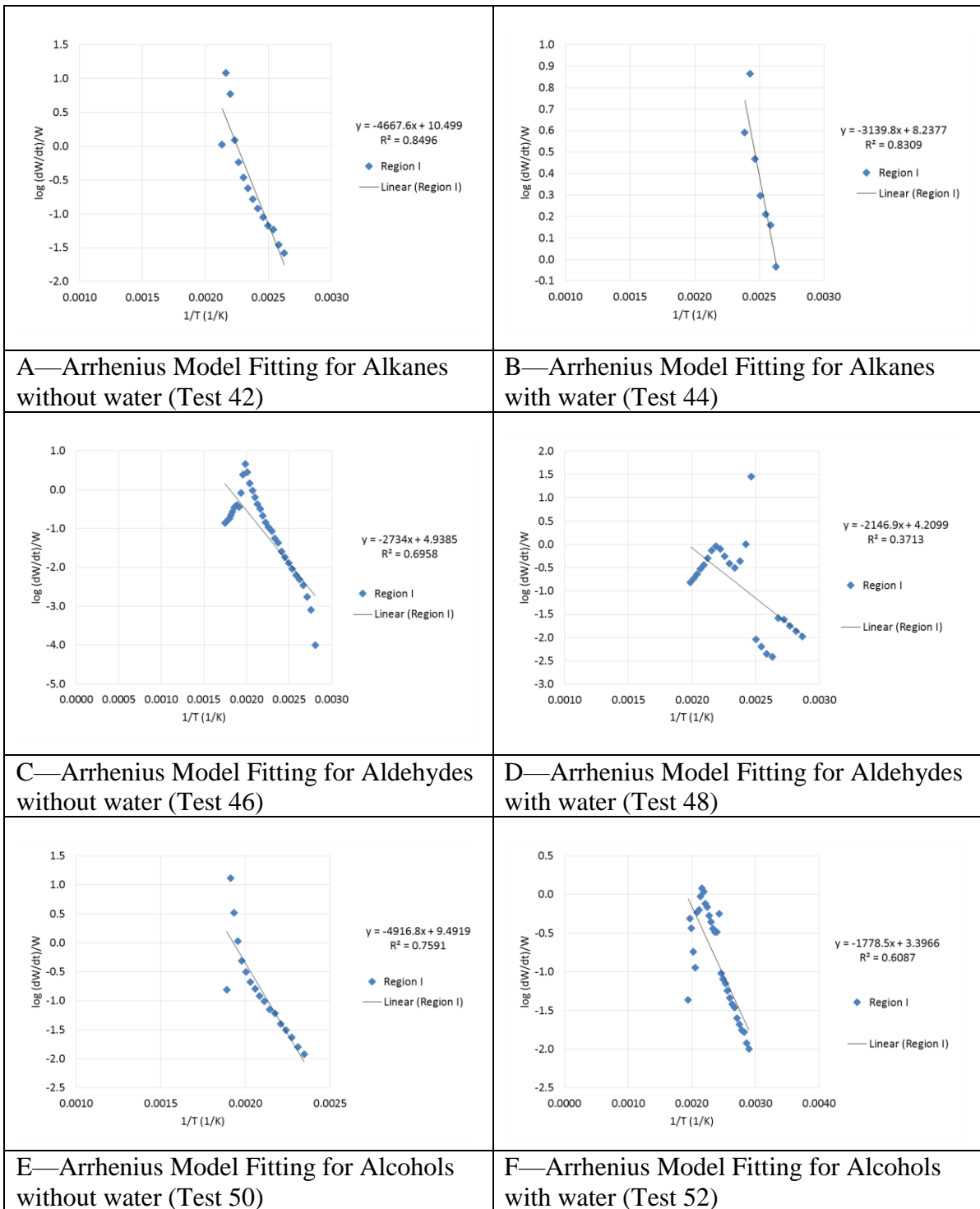
Figure 4 C18—Arrhenius Model Fitting Graphs for Chemicals Combustion at High Heating Rate (Refer Table 4.4 for Experiment Name Coding)

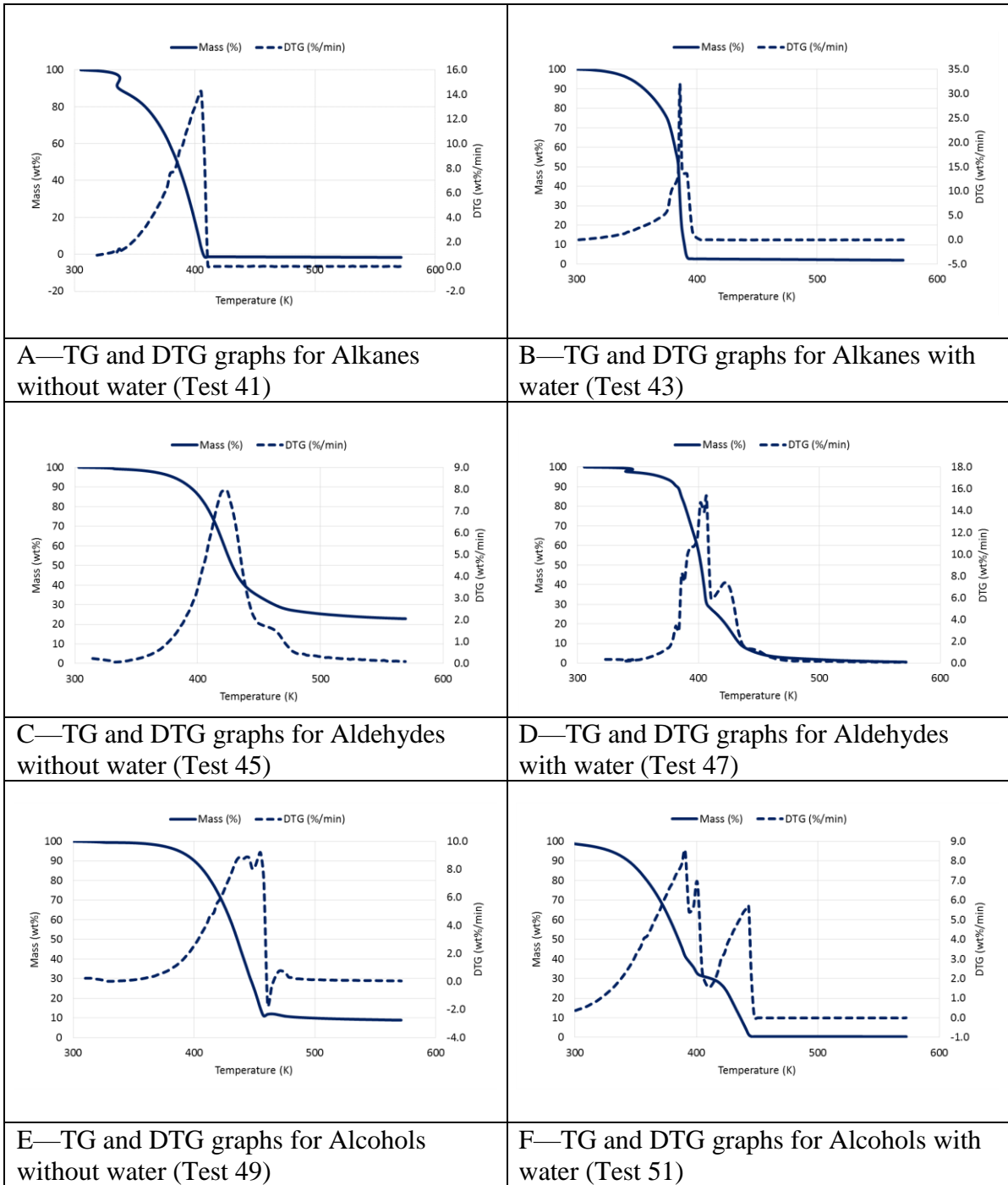| G—Arrhenius Model Fitting for Ketones without water (Test 54) | H—Arrhenius Model Fitting for Ketones with water (Test 56) |
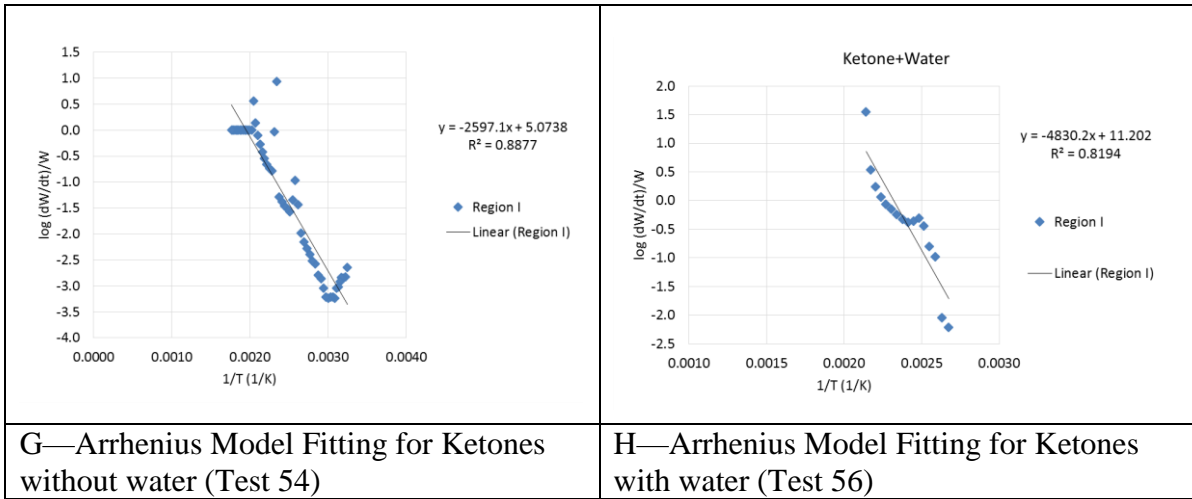
Figure 4 C18 (cont.)—Arrhenius Model Fitting Graphs for Chemicals Combustion at High Heating Rate (Refer Table 4.4 for Experiment Name Coding)
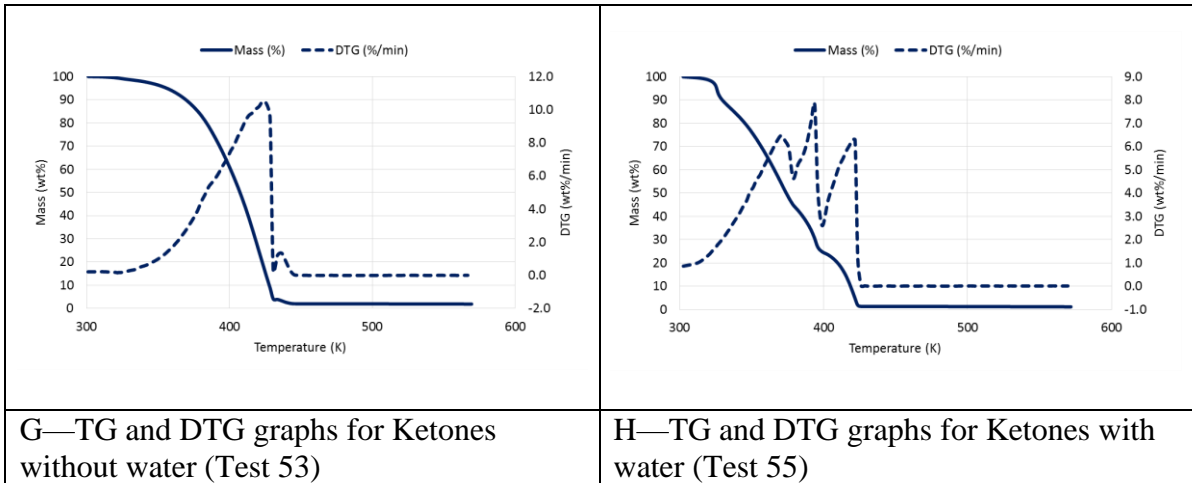
A—TGA of Oil A with different clay amount	B—DSC of Oil A with different clay amount
C—TGA of Initial Oil A and Reservoir Rock Component	D—DSC of Initial Oil A and Reservoir Rock Component
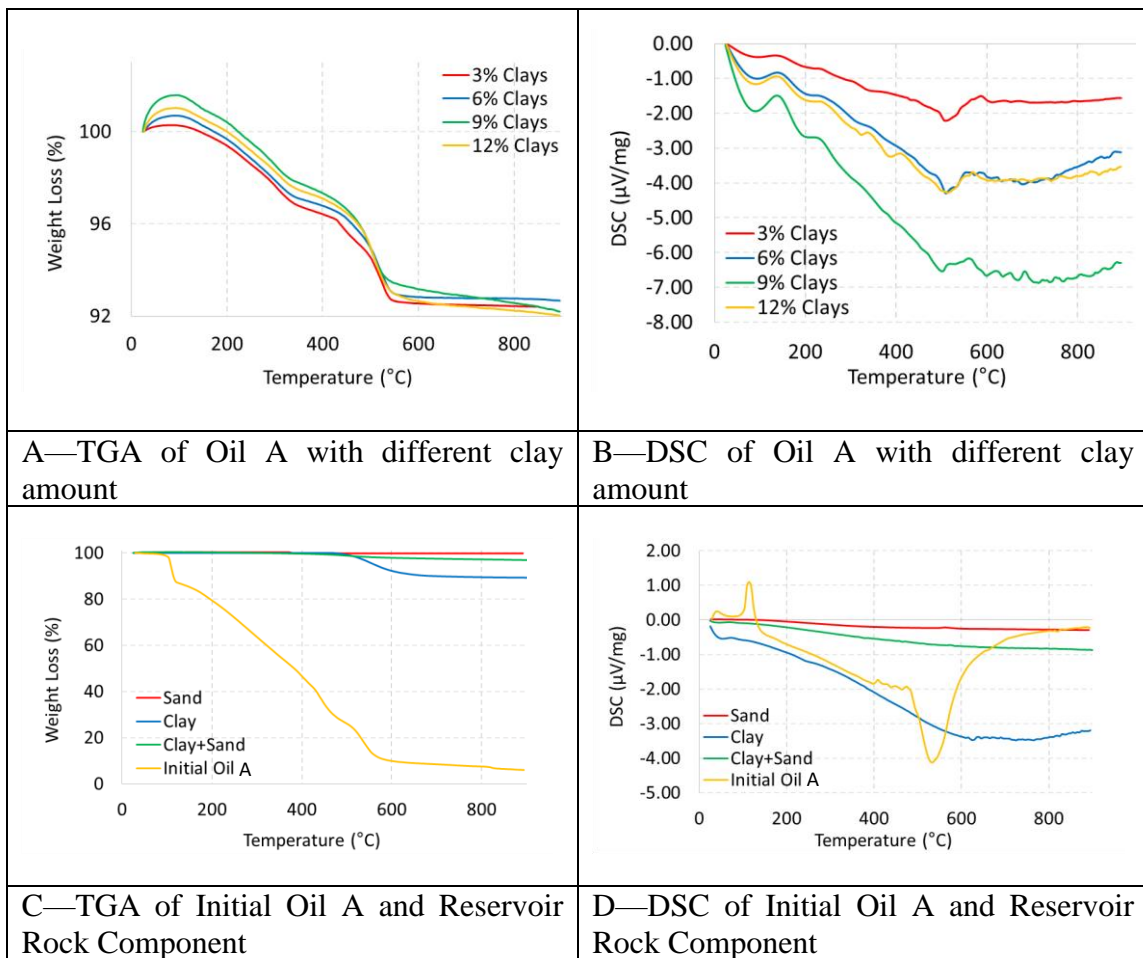
Figure 4 D1—TGA (On the Left) and DSC (On the Right) Analysis of Oil A Samples for Different Clay Amount, Initial Oil A and Reservoir Rock Components at 15 °C/Min during Combustion Under Air Injection

| A—TG and DTG graphs for 3% Clay (Test 7) | B—TG and DTG graphs for 6% Clay (Test 8) |
| C—TG and DTG graphs for 9% Clay (Test 9) | D—TG and DTG graphs for 12% Clay (Test 10) |
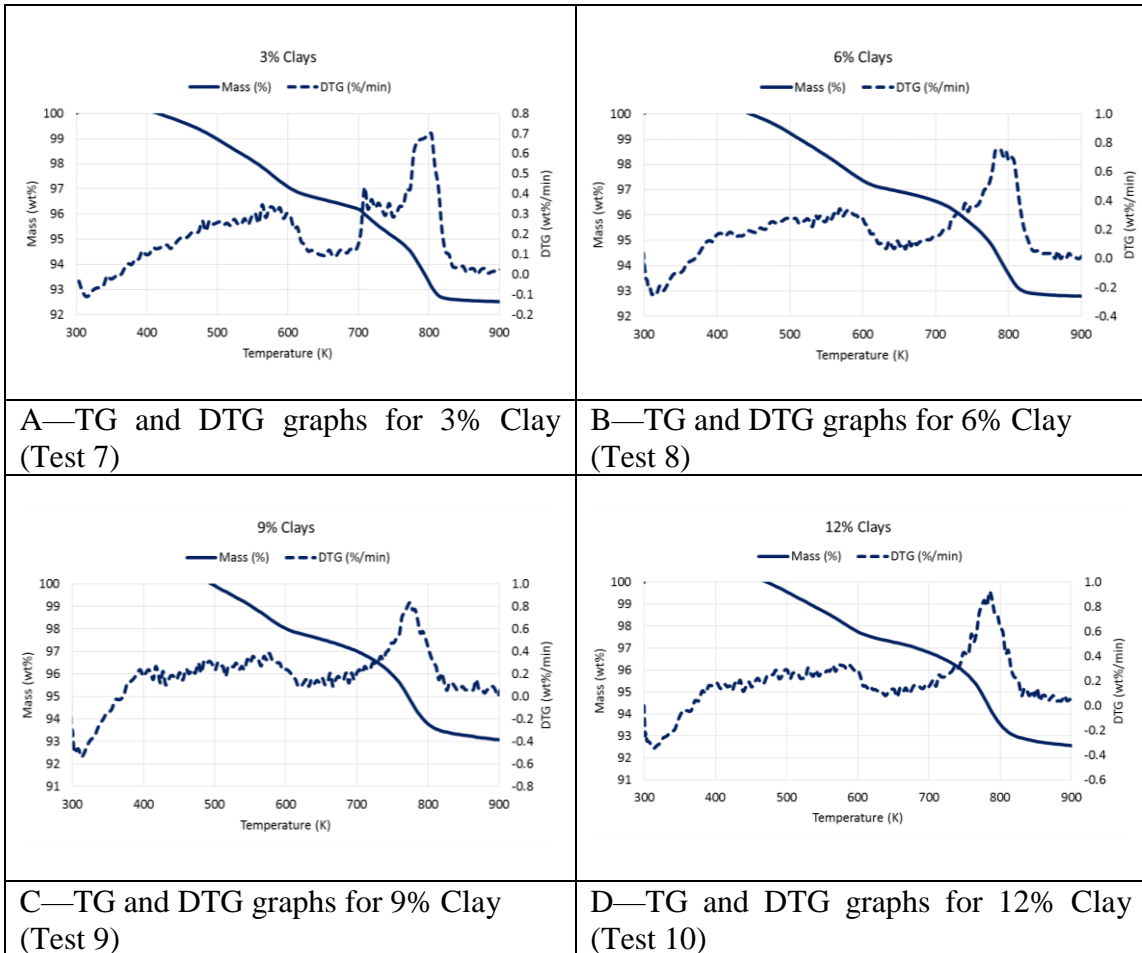
Figure 4 D2—TG/DTG graphs for Arrhenius Model Calculation (Refer Table 4.5 for Experiment Name Coding)

A—Arrhenius Model Fitting for 3% Clay (Test 7)	B—Arrhenius Model Fitting for 6% Clay (Test 8)
C—Arrhenius Model Fitting for 9% Clay (Test 9)	D—Arrhenius Model Fitting for 12% Clay (Test 10)
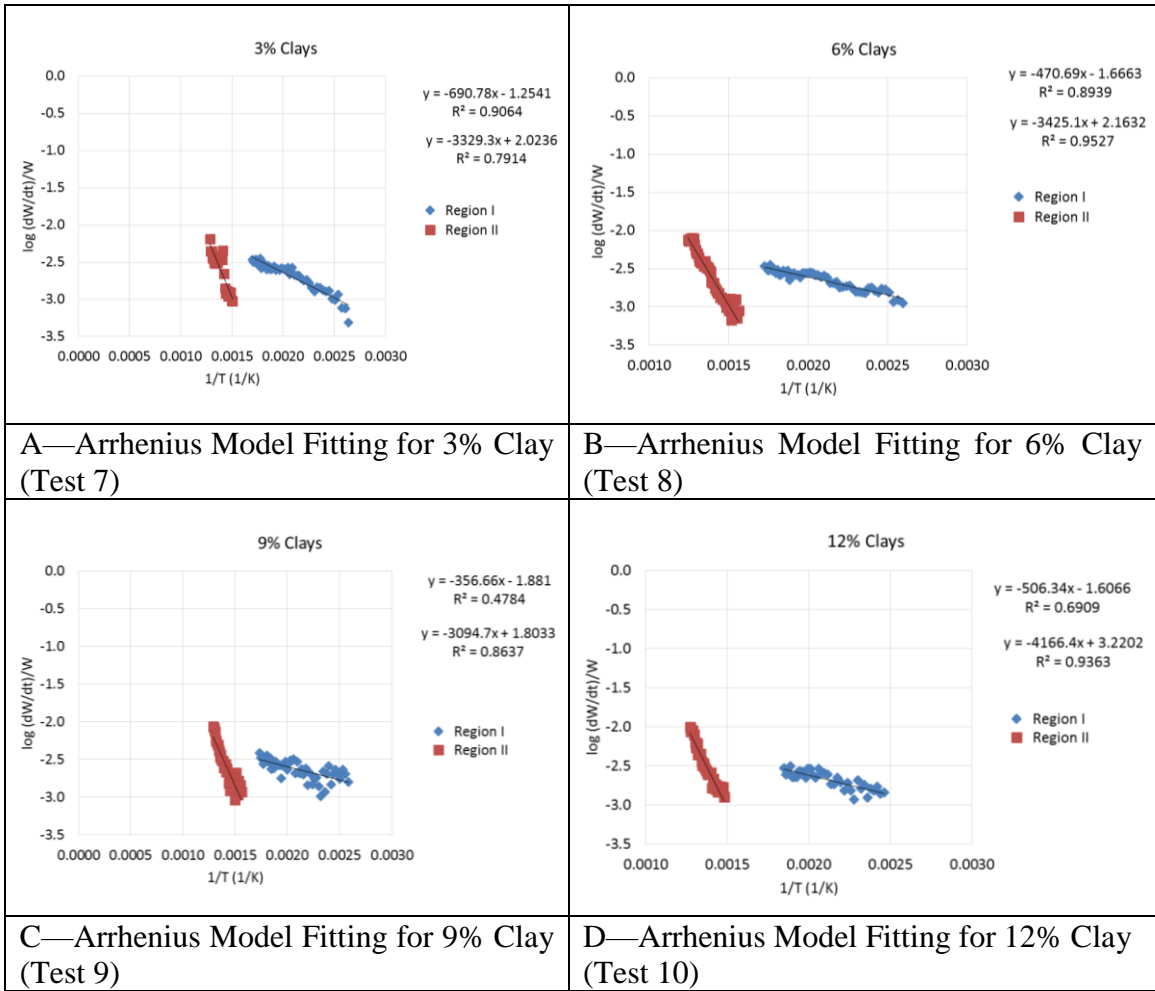
Figure 4 D3—Arrhenius Model Fitting Graphs for LTO (Region I) and HTO (Region II) (Refer Table 4.5 for Experiment Name Coding)

| A—TGA of Ottawa Sand, Dolomite, and Calcite | B—DSC of Ottawa Sand, Dolomite, and Calcite |
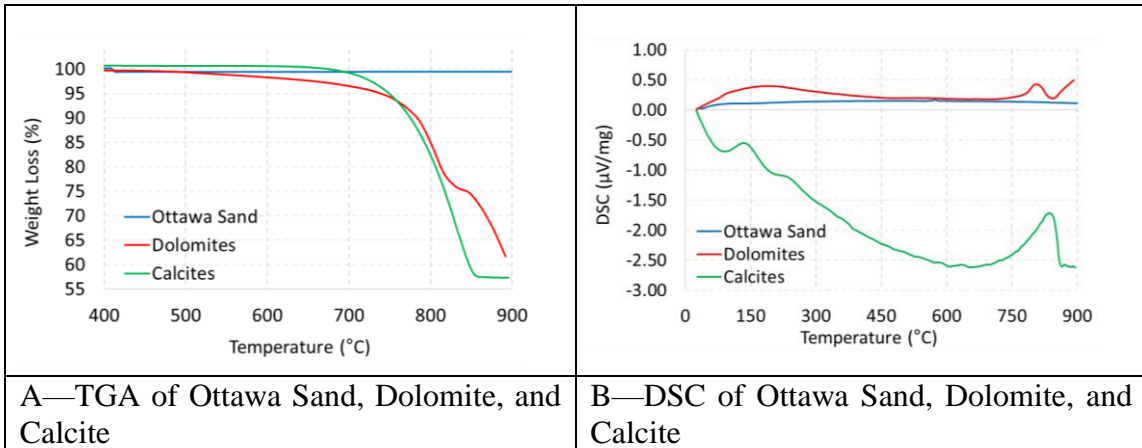
Figure 4 D4—TGA (On the Left) and DSC (On the Right) Analysis of Reservoir Rocks at 15 °C/Min during Combustion under Air Injection

| A—TGA of Oil A with and without carbonate | B—DSC of Oil A with and without carbonate |
| C—TGA of Oil A Saturates with and without carbonate | D—DSC of Oil A Saturates with and without carbonate |
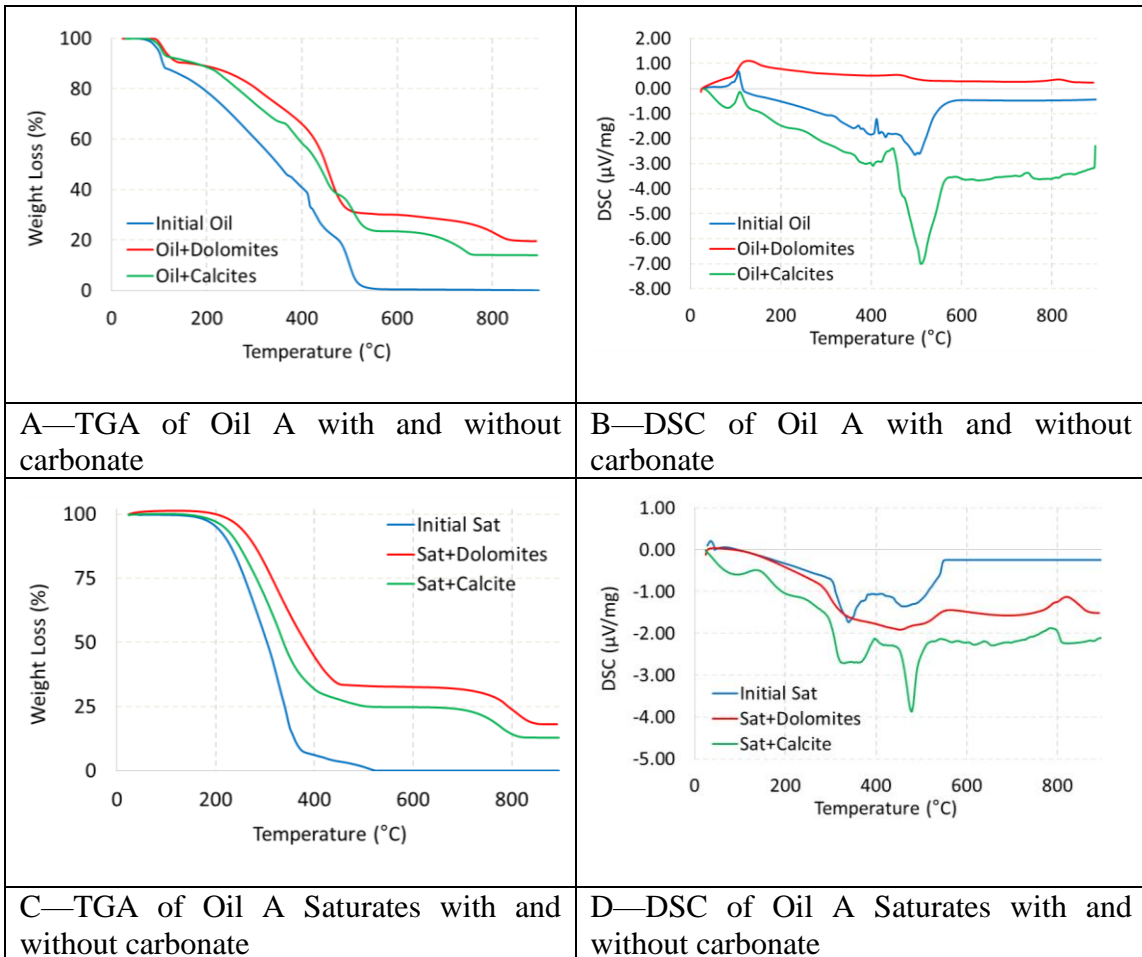
Figure 4 D5—TGA (on the Left) and DSC (on the Right) Analysis of Oil A and Its SARA Fractions With Carbonates at 15 °C/Min during Combustion under Air Injection

E—TGA of Oil A Aromatics with and without carbonate	F—DSC of Oil A Aromatics with and without carbonate
G—TGA of Oil A Resins with and without carbonate	H—DSC of Oil A Resins with and without carbonate
I—TGA of Oil A Asphaltenes with and without carbonate	J—DSC of Oil A Asphaltenes with and without carbonate

Figure 4 D5 (cont.)—TGA (on the Left) and DSC (on the Right) Analysis of Oil A and Its SARA Fractions With Carbonates at 15 °C/Min during Combustion under Air Injection

A—TG and DTG graphs for Initial Oil (Test 1)	B— TG and DTG graphs for Initial Oil-Calcite (Test 11)	C— TG and DTG graphs for Initial Oil-Dolomite (Test 12)
D—TG and DTG graphs for Initial Saturates (Test 13)	E— TG and DTG graphs for Initial Saturates-Calcite (Test 14)	F— TG and DTG graphs for Initial Saturates-Dolomite (Test 15)
G—TG and DTG graphs for Initial Aromatics (Test 16)	H— TG and DTG graphs for Initial Aromatics-Calcite (Test 17)	I— TG and DTG graphs for Initial Aromatics-Dolomite (Test 18)
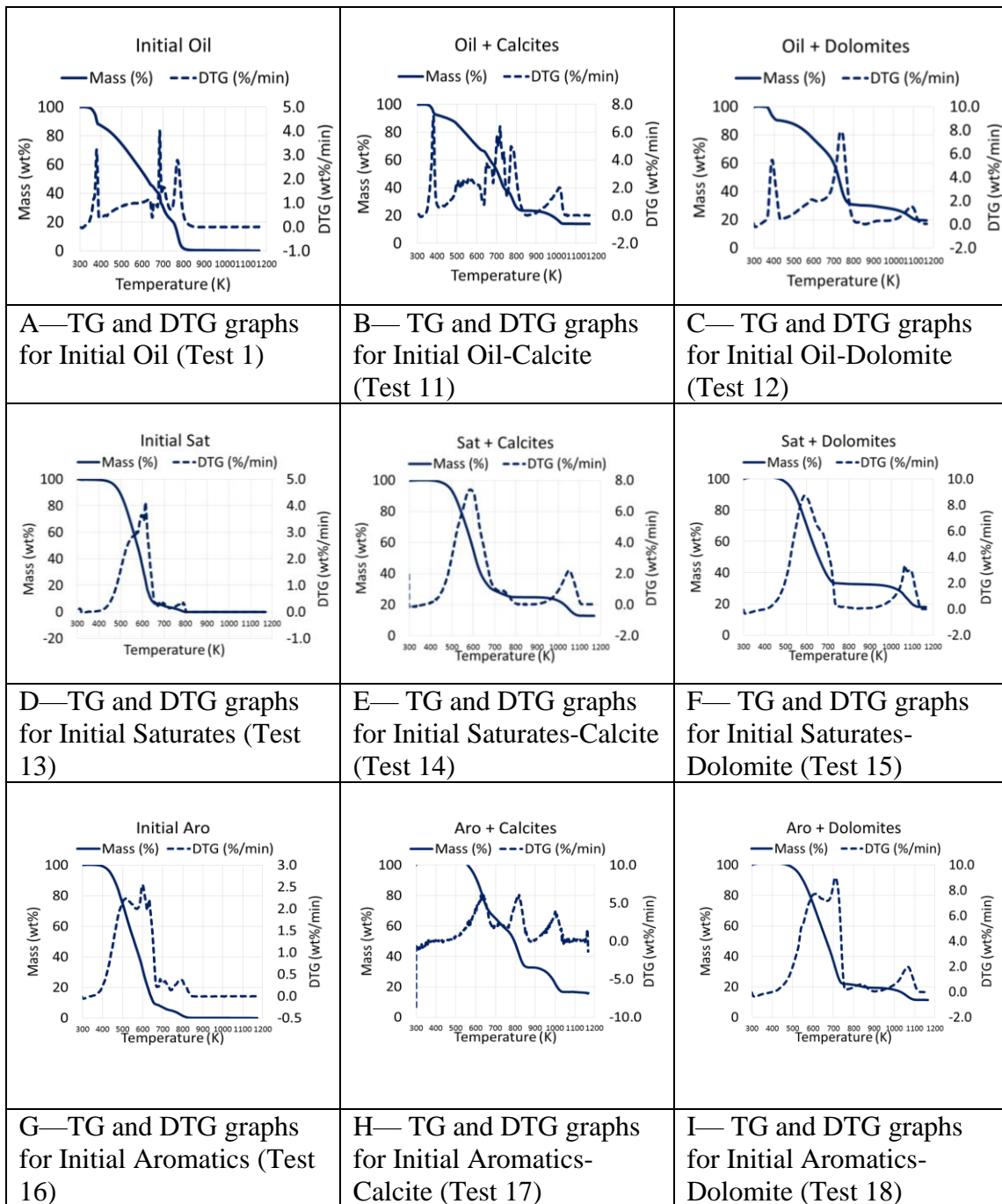
Figure 4 D6—TG/DTG Graphs for Arrhenius Model Calculation (Refer Table 4.5 for Experiment Name Coding)

176

| J—TG and DTG graphs for Initial Resins (Test 19) | K—TG and DTG graphs for Initial Resins-Calcite (Test 20) | L—TG and DTG graphs for Initial Resins-Dolomite (Test 21) |
| M—TG and DTG graphs for Initial Asphaltenes (Test 22) | N— TG and DTG graphs for Initial Asphaltenes - Calcite (Test 23) | O— TG and DTG graphs for Initial Asphaltenes – Dolomite (Test 24) |
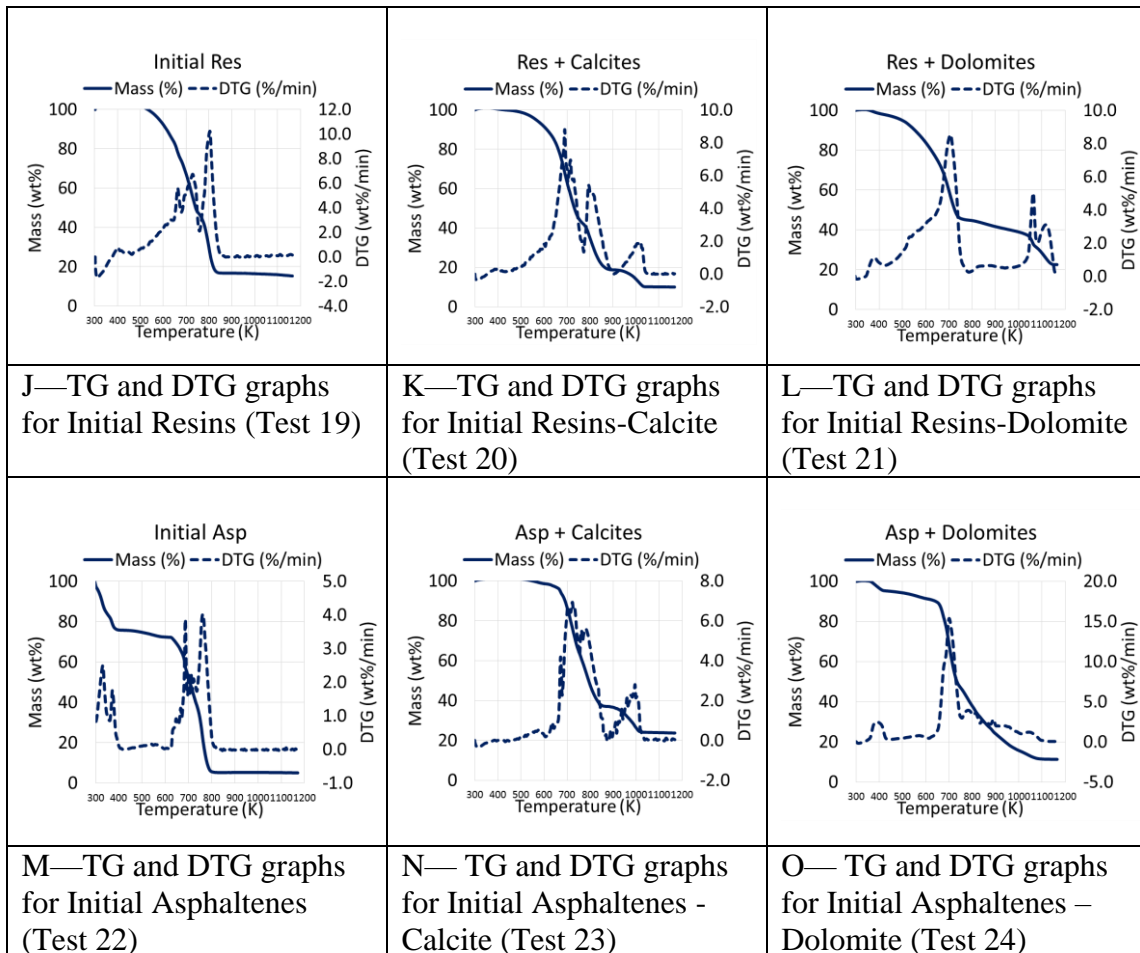
Figure 4 D6 (cont.)—TG/DTG Graphs for Arrhenius Model Calculation (Refer Table 4.5 for Experiment Name Coding)

A—Arrhenius Model Fitting for Initial Oil (Test 1)	B— Arrhenius Model Fitting for Initial Oil-Calcite (Test 11)	C— Arrhenius Model Fitting for Initial Oil-Dolomite (Test 12)
D—Arrhenius Model Fitting for Initial Saturates (Test 13)	E— Arrhenius Model Fitting for Initial Saturates-Calcite (Test 14)	F— Arrhenius Model Fitting for Initial Saturates-Dolomite (Test 15)
G—Arrhenius Model Fitting for Initial Aromatics (Test 16)	H— Arrhenius Model Fitting for Initial Aromatics-Calcite (Test 17)	I— Arrhenius Model Fitting for Initial Aromatics-Dolomite (Test 18)

Figure 4 D7—Arrhenius Model Fitting Graphs for LTO (Region I) and HTO (Region II) (Refer Table 4.5 for Experiment Name Coding)
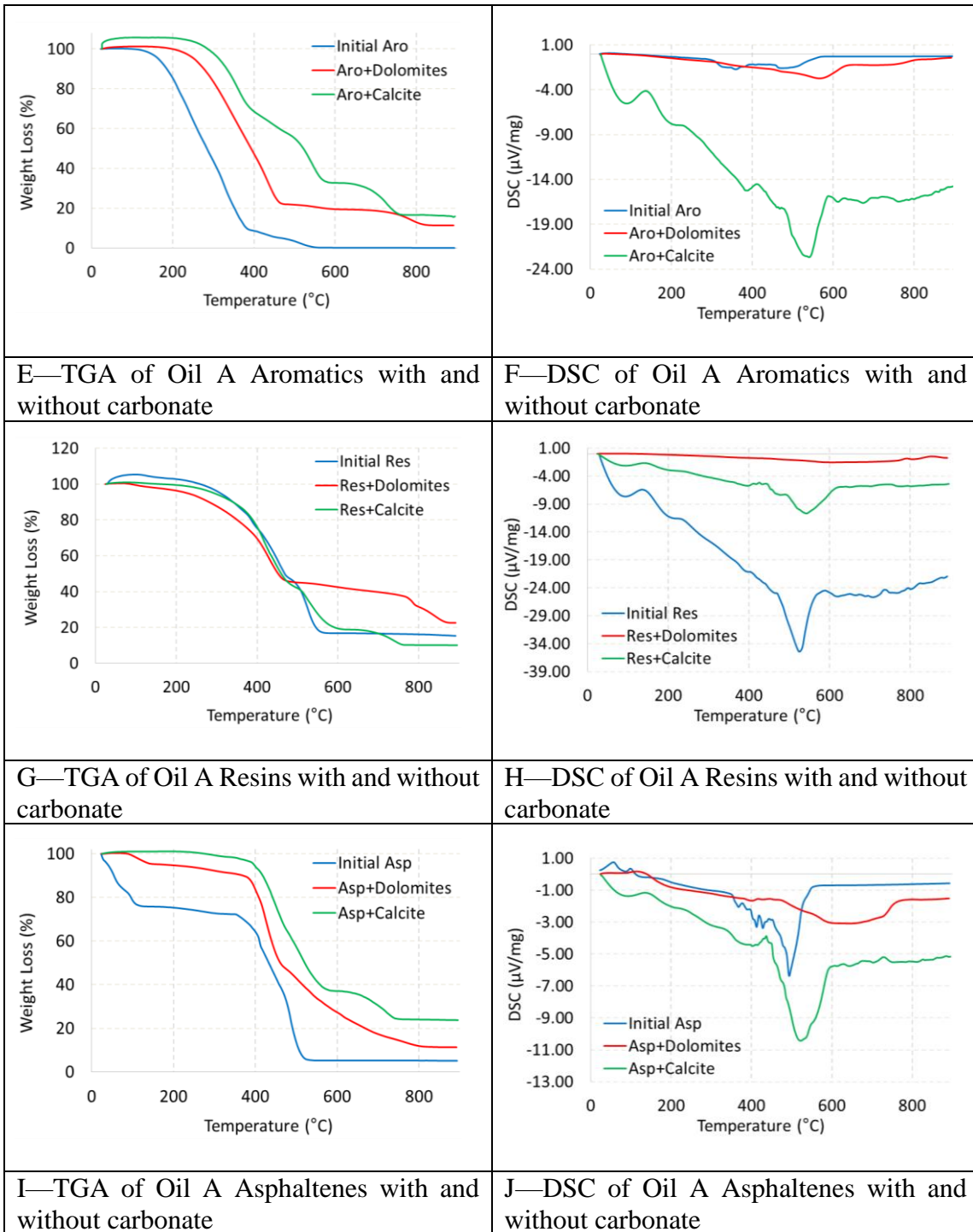
178

J—Arrhenius Model Fitting for Initial Resins (Test 19)	K— Arrhenius Model Fitting for Initial Resins-Calcite (Test 20)	L— Arrhenius Model Fitting for Initial Resins-Dolomite (Test 21)
M—Arrhenius Model Fitting for Initial Asphaltenes (Test 22)	N— Arrhenius Model Fitting for Initial Asphaltenes –Calcite (Test 23)	O— Arrhenius Model Fitting for Initial Asphaltenes -Dolomite (Test 24)
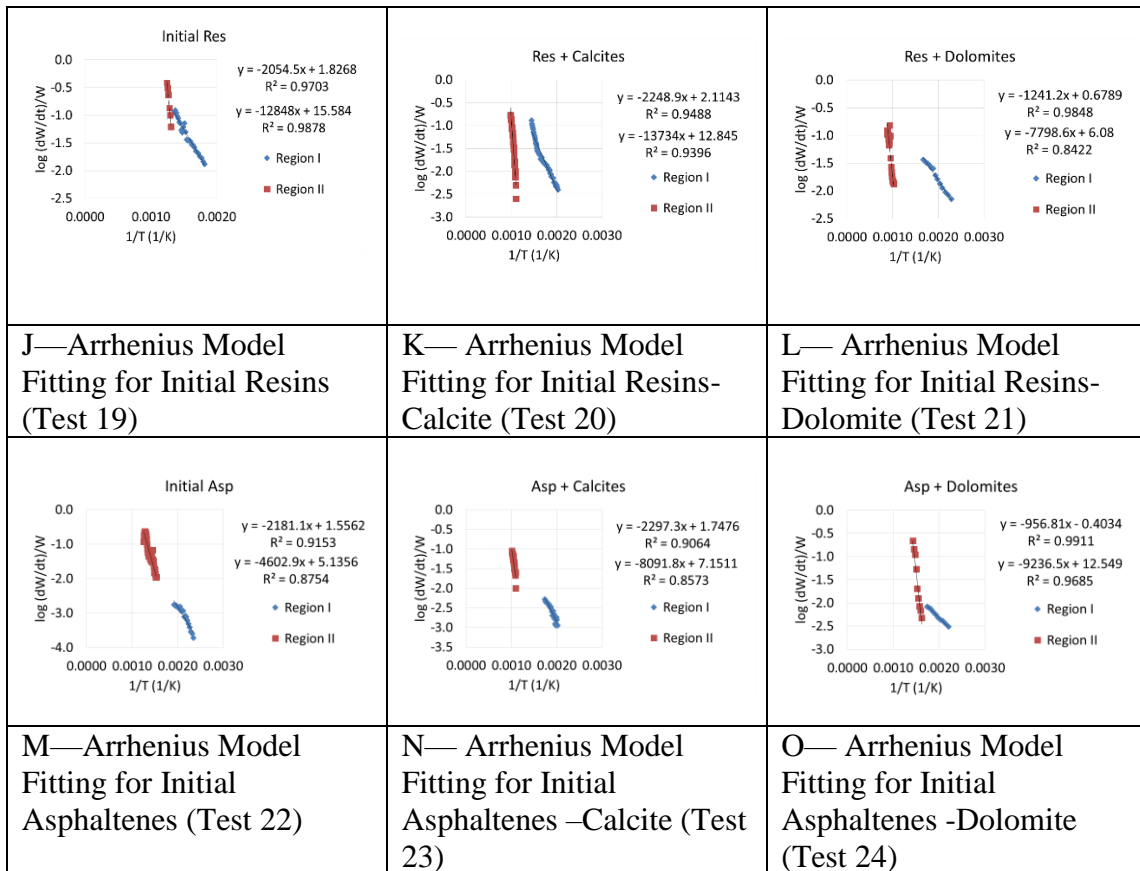
Figure 4 D8—Arrhenius Model Fitting Graphs for LTO (Region I) and HTO (Region II) (Refer Table 4.5 for Experiment Name Coding)

5. CONCLUSIONS AND FUTURE STUDIES

Conclusions

The main objective of this dissertation is to extend further the understanding of chemical reactions that happen during the in-situ combustion of bitumen and heavy oils in different reservoirs. The obtained results of this investigation will be used to enhance existing reservoir models to better estimate the ISC performance for field tests.

This study has shown that crude oil combustion performance varies depending on oil compositions. Initial oil with low viscosity, high API gravity, and low asphaltenes content resulted in the highest oil recovery because of the high C-H stretch content in saturates fraction that leads saturates to ignite faster. High viscosity, high API gravity, and high asphaltenes content crude oil combustion with clay produce a less oxygenated compound in their resins fraction. On the other hand, medium viscosity, low API gravity, and medium asphaltenes content crude oil combustion with clay produce more oxygenated compound in the resins.

It has been found that clay expedites the combustion front by increasing the oxygen utilization rate and the oxygenated group amount in asphaltenes only for high API gravity initial crude oil. For all oil compositions, the double bond and oxygenated functional groups in aromatics fraction reduced after combustion; however, clay presence increased the amount of these functional groups. It has been observed that clay does not act as a catalyst for all oil compositions.

180

Combustion with clay completely removes the emulsified water (O-H bond) in the asphaltenes fraction. Resins fraction displayed higher absorbance values in the fingerprint region (oxygenated functional group and C-H bond) as compared to aromatics, suggesting that resins contain more significant amounts of heteroatoms and longer hydrocarbon chains, which is why it is a heavier fraction.

Sulfur in the produced asphaltenes increased for all types of crude oils after the combustion experiment. Hence, less sulfur was deposited on the spent rock and spent rock produced coke surface. The spent rock analysis indicates that clay leads to higher oxygen uptake as compared to the case without clay. The presence of clay decreases the deposition of carbon on the spent rock, but increases the deposition of oxygen on the spent rock for the oil with high V, Si, Ca, Fe, Cl, and Ni content. Clay aids combustion by increasing the surface area of asphaltenes (from produced asphaltenes) which results in more coke formation (EDS spent rock).

The combustion tube experiment results were then integrated with analytical modeling, kinetic modeling, and SARA fractions of produced oil. The finding shows that aromatics fraction behaves like buffer and an increase in aromatics fraction content in oil makes the activation energy lesser. Asphaltenes dispersion is encouraged by resins and aromatics fractions. On the other hand, asphaltenes coagulation is induced more by saturates fraction. Stable asphaltenes (dispersed in crude oil) require less heat to be cracked to form fuel. The formed fuel is defined with H/C ratio, as the H increases in the fuel, it becomes more saturated.

This dissertation also covered the effects of reservoir fluids (oil composition and initial water presence) and reservoir rocks mineralogy (clay amount and carbonate presence) on combustion kinetics of ISC through TGA/DSC experiments. The results of this research show that the burning behavior of oil during ISC is affected by several factors. First, the crude oil composition and initial water content have a significant impact on ISC performance. The initial water content in Oil A increased the activation energy required, but when water was removed, it resulted in lower activation energy for both LTO and HTO regions. Water presence increased the activation energy for saturates combustion which requires higher ignition heat. This heat is then consumed through the combustion of heavier components that require less heat in the presence of water. Hence, water presence aids the combustion process. Heavier fractions (resins and asphaltenes) dominate the reaction pathways, thus decreasing the energy requirement and generate a large heat making the combustion effective.

The burning behavior of the aromatics depends on the oxygenated functional group existing in aromatics fractions. As ketones showed the only significant change in the presence of water, ketones in deasphalted oil may be responsible for the natural burning behavior of crude oils. The reaction kinetics study provided an insight on the impact of water addition on the kinetic energy needed for the combustion to occur. The results suggest that the chemical structure of aromatics fraction and aromatic hydrocarbons in resins fraction is critical for the success of ISC. Water and aromatics fraction interaction at elevated temperatures favors ISC reactions.

Lastly, reservoir rocks also affect ISC performance. An increased amount of clay decreased the activation energies and the Arrhenius constants of the reactions (LTO and HTO) and increased the heat of combustion which was indicative of the catalytic properties of clay. However, the results might indicate that the clay-oil pair used in this study may have an optimum reaction at 9% clay content. In the experiment with carbonate, calcite seemed to generate the highest heat generation for Oil A and its SARA fractions at the HTO region except resins. Meanwhile, dolomite was reducing the heat generation of Initial Oil A due to the high activation energy needed to overcome the energy barrier for asphaltenes. Aromatics-calcite and resins- dolomite interaction favor combustion in carbonate.

The approach used in this dissertation is a fresh take on determining the reaction kinetics of the ISC process by coupling the combustion tube experimental results with the kinetic experiments. This study will help reduce the complexity of the process by trying to develop a simplified approach towards a better understanding of ISC chemical reactions for different types of crude oil and reservoir. The results from this dissertation can help operators to decide if ISC is applicable to their reservoir by looking at the reservoir fluids and rock mineralogy analytical modeling and reaction kinetics parameters.

Future Studies

For the purpose of future research, there are some recommendations to be considered. First of all, this dissertation is introducing a new approach to predict ISC performance from analytical modeling of combustion tube results and analytical modeling of reactions kinetics. Besides the effect of crude oil composition, clay (kaolinite and illite), initial water saturation, initial oil saturation, emulsified water, and carbonates (dolomite and calcite) there are other factors that can be studied by using the method introduced by this research. Studies for different porosity, permeability, salinity, and other rock lithology and mineralogy can be done in the future.

Other than that, the combustion tube experiment conducted for this study was done on a one-dimensional (1-D) setup. Hence, future combustion tube study can be done on two-dimensional (2-D) and three-dimensional (3-D) setup to investigate the effect of combustion front movement and reaction pathways at different dimensions. This can also be a better representation of reservoir and can be extended to field scale.

REFERENCES

Abuhesa, M. B. and Hughes, R. 2008. Comparison of Conventional and Catalytic In Situ Combustion Processes for Oil Recovery. *Energy & Fuels* **23** (1): 186-192. http://dx.doi.org/10.1021/ef800804a

Adegbesan, K. O., Donnelly, J. K., Moore, R. G., and Bennion, D. W. 1986. Liquid Phase Oxidation Kinetics of Oil Sands Bitumen: Models for In Situ Combustion Numerical Simulators. *AIChE Journal* **32** (8): 1242-1252. https://doi.org/10.1002/aic.690320803

Akih-Kumgeh, B. and Bergthorson, J. M. 2011. Ignition of C3 Oxygenated Hydrocarbons and Chemical Kinetic Modeling of Propanal Oxidation. *Combustion and Flame* **158** (10): 1877-1889. https://doi.org/10.1016/j.combustflame.2011.02.015

Akin, S., Kok, M. V., Bagci, S., and Karacan, O. 2000. Oxidation of Heavy Oil and Their SARA Fractions: Its Role in Modeling In-Situ Combustion. Paper presented at the SPE Annual Technical Conference and Exhibition, Dallas, Texas, 1-4 October 2000. SPE-63230-MS. http://dx.doi.org/doi.org/10.2118/63230-MS.

Aleksandrov, D. and Hascakir, B. 2015. Laboratory Screening Tests on the Effect of Initial Oil Saturation for the Dynamic Control of In-situ Combustion. *Fuel Processing Technology* **130**: 224-234. http://dx.doi.org/10.1016/j.fuproc.2014.10.027

Aleksandrov, D., Kudryavtsev, P., and Hascakir, B. 2015. Impact of Frature Orientation on In-Situ Combustion Performance. Paper presented at the SPE Latin American and Caribbean Petroleum Engineering Conference, Quito, Ecuador, 18-20 November 2015. SPE-177063-MS. http://dx.doi.org/10.2118/177063-MS.

Ambalae, A., Mahinpey, N., and Freitag, N. 2006. Thermogravimetric Studies on Pyrolysis and Combustion Behavior of a Heavy Oil and Its Asphaltenes. *Energy & Fuels* **20** (2): 560-565. https://doi.org/10.1021/ef0502812

Arrhenius, S. 1889. On the Rate of Reaction of the Inversion of Sucrose by Acids. *Zeitschrift fuer physikalische Chemie* **4**: 226-248.

Asomaning, S. 2003. Test Methods for Determining Asphaltene Stability in Crude Oils. *Petroleum Science and Technology* **21** (3-4): 581-590. https://doi.org/10.1081/LFT-120018540

ASTM. 2007. Standard Test Method for Characteristic Groups in Rubber Extender and Processing Oils and Other Petroleum-Derived Oils by the Clay-Gel Absorption Chromatographic Method. *West Conshohocken, PA*. https://doi.org/10.1520/D2007-11R16

ASTM. 2014. Standard Test Method for Compositional Analysis by Thermogravimetry. *West Conshohocken, PA*. https://doi.org/10.1520/E1131-08R14

Bagci, S. 1998. Estimation of Combustion Zone Thickness During In-Situ Combustion Processes. *Energy & Fuels* **12** (6): 1153-1160. https://doi.org/10.1021/ef980013m

Bai, B. 2012. Technology Focus: EOR Performance and Modeling. *J Pet Technol* **64** (01): 60-60. SPE-0118-0038-JPT. https://doi.org/10.2118/0118-0038-JPT

Bailey, H. and Larkin, B. 1959. Heat conduction in underground combustion. *Transactions of The American Institute of Mining and Metallurgical Engineers* **216**: 123-129.

Bailey, H. and Larkin, B. 1960. Conduction-Convection in Underground Combustion. SPE-1482-G.

Barnard, J. A. 1960. The Pyrolysis of Isopropanol. *Transactions of the Faraday Society* **56**: 72-79. http://dx.doi.org/10.1039/TF9605600072

Barnard, J. A. and Hughes, H. W. D. 1960. The Pyrolysis of N-propanol. *Transactions of the Faraday Society* **56**: 64-71. https://doi.org/10.1039/TF9605600064

Belgrave, J., Moore, R., Ursenbach, M., and Bennion, D. 1993. A Comprehensive Approach to In-situ Combustion Modeling. *SPE Advanced Technology Series* **1** (01): 98-107.

Belgrave, J. D. M., Moore, R. G., and Ursenbach, M. G. 1994. Gas Evolution from the Aquathermolysis of Heavy Oils. *The Canadian Journal of Chemical Engineering* **72** (3): 511-516. https://doi.org/10.1002/cjce.5450720317

Belgrave, J. D. M., Moore, R. G., and Ursenbach, M. G. 1997. Comprehensive Kinetic Models for the Aquathermolysis of Heavy Oils. *J Can Pet Technol* **36** (04). PETSOC-97-04-03. https://doi.org/10.2118/97-04-03

Benkhedda, Z., Landais, P., Kister, J., Dereppe, J. M., and Monthioux, M. 1992. Spectroscopic Analyses of Aromatic Hydrocarbons Extracted from Naturally and Artificially Matured Coals. *Energy & Fuels* **6** (2): 166-172. http://doi.org/10.1021/ef00032a008

Bousaid, I. 1989. Multiple-quenched Fireflood Process Boosts Efficiency. *Journal of petroleum technology* **41** (11): 1,202-201,209. SPE-16739-PA. https://doi.org/10.2118/16739-PA

Bousaid, I. and Ramey Jr, H. 1968. Oxidation of Crude Oil in Porous Media. *SPE J.* **8** (02): 137-148. SPE-1937-PA. https://doi.org/10.2118/1937-PA

Boylan, D. B. and Tripp, B. W. 1971. Determination of Hydrocarbons in Seawater Extracts of Crude Oil and Crude Oil Fractions. *Nature* **230**: 44-47. https://doi.org/10.1038/230044a0

Briggs, P. J., Baron, P. R., Fulleylove, R. J., and Wright, M. S. 1988. Development of Heavy-oil Reservoirs. *Journal of Petroleum Technology* **40** (02): 206-214. https://doi.org/10.2118/15748-PA

Brons, G. and Siskin, M. 1994. Bitumen Chemical Changes during Aquathermolytic Treatments of Cold Lake Tar Sands. *Fuel* **73** (2): 183-191. https://doi.org/10.1016/0016-2361(94)90112-0

Burger, J. G. 1972. Chemical Aspects of In-situ Combustion-Heat of Combustion and Kinetics. *SPE J.* **12** (05): 410-422. https://doi.org/10.2118/3599-PA

Burger, J. G., Sourieau, P., Combarnous, M., and Ramey Jr, H. 1985. *Thermal Methods of Oil Recovery*. p.63-87. United States: Gulf Publishing Company, Book Division.

Butler, R. M. 1991. *Thermal Recovery of Oil and Bitumen*. p.285–358. New Jersey: Prentice Hall.

Calemma, V., Iwanski, P., Nali, M., Scotti, R., and Montanari, L. 1995. Structural Characterization of Asphaltenes of Different Origins. *Energy & Fuels* **9** (2): 225-230. http://doi.org/10.1021/ef00050a004

Castanier, L. M. and Brigham, W. E. 2003. Upgrading of Crude Oil via In-situ Combustion. *Journal of Petroleum Science and Engineering* **39** (1): 125-136. https://doi.org/10.1016/S0920-4105(03)00044-5

Chen, Z., Zhu, H., Yan, Z., Zhao, L., Shen, Y., and Misra, A. 2016. Experimental Study on Physical Properties of Soft Soil after High Temperature Exposure. *Engineering Geology* **204**: 14-22. https://doi.org/10.1016/j.enggeo.2016.01.014

Cho, Y., Na, J.-G., Nho, N.-S., Kim, S., and Kim, S. 2012. Application of Saturates, Aromatics, Resins, and Asphaltenes Crude Oil Fractionation for Detailed Chemical Characterization of Heavy Crude Oils by Fourier Transform Ion Cyclotron Resonance Mass Spectrometry Equipped with Atmospheric Pressure Photoionization. *Energy & Fuels* **26** (5): 2558-2565. https://10.1021/ef201312m

Chu, C. 1963. Two-Dimensional Analysis of a Radial Heat Wave. Paper presented at the SPE Production Research Symposium, U. of Oklahoma, Norman, Oklahoma, April 29-30. SPE-560-PA. https://10.2118/560-pa.

Chu, C. 1981. State-of-the-art Review of Fireflood Field Projects. *J Pet Technol* **34** (01). SPE-9772-PA. https://doi.org/10.2118/9772-PA

Cinar, M., Castanier, L. M., and Kovscek, A. R. 2011a. Combustion Kinetics of Heavy Oils in Porous Media. *Energy & Fuels* **25** (10): 4438-4451. https://doi.org/10.1021/ef200680t

Cinar, M., Hascakir, B., Castanier, L. M., and Kovscek, A. R. 2011b. Predictability of crude oil in-situ combustion by the isoconversional kinetic approach. *SPE J.* **16** (03): 537-547. SPE-148088-PA. https://doi.org/10.2118/148088-PA

Coats, A. and Redfern, J. 1964. Kinetic Parameters from Thermogravimetric Data. *Nature* **201** (4914): 68-69.

Company, B. 2017. *BP Statistical Review of World Energy*. p.6-39.London.

Crocker, M. E., Donaldson, E. C., and Marchin, L. M. 1983. Comparison and Analysis of Reservoir Rocks and Related Clays. Paper presented at the SPE Annual Technical Conference and Exhibition, San Francisco, California, 5-8 October. SPE-11973-MS. https://10.2118/11973-MS.

Crookston, R. B., Culham, W. E., and Chen, W. H. 1979. A Numerical Simulation Model for Thermal Recovery Processes. *SPE J.* **19** (01): 37-58. SPE-6724-PA. https://doi.org/10.2118/6724-PA

Curran, H. J., Gaffuri, P., Pitz, W. J., and Westbrook, C. K. 2002. A Comprehensive Modeling Study of Iso-octane Oxidation. *Combustion and Flame* **129** (3): 253-280. https://doi.org/10.1016/S0010-2180(01)00373-X

da Silva Ramos, A. C., Haraguchi, L., Notrispe, F. R., Loh, W., and Mohamed, R. S. 2001. Interfacial and Colloidal Behavior of Asphaltenes Obtained from Brazilian Crude Oils. *Journal of Petroleum Science and Engineering* **32** (2): 201-216. https://doi.org/10.1016/S0920-4105(01)00162-0

Dechelette, B., Heugas, O., Quenault, G., Bothua, J., and Christensen, J. 2006. Air Injection-improved Determination of the Reaction Scheme with Ramped

Temperature Experiment and Numerical Simulation. *J Can Pet Technol* **45** (01). PETSOC-06-01-03. https://doi.org/10.2118/06-01-03

Douté, C., Delfau, J.-L., and Vovelle, C. 1997. Modeling of the Structure of a Premixed n-Decane Flame. *Combustion science and technology* **130** (1-6): 269-313. https://doi.org/10.1080/00102209708935746

Escobar, G. P., Beroy, A. Q., Iritia, M. P., and Huerta, J. H. 2004. Kinetic Study of the Combustion of Methyl-ethyl Ketone Over α-hematite Catalyst. *Chemical Engineering Journal* **102** (2): 107-117. https://doi.org/10.1016/j.cej.2003.09.006

Fassihi, M. R., Brigham, W. E., and Ramey Jr, H. J. 1984a. Reaction Kinetics of In-situ Combustion: Part 1-Observations. *SPE J.* **24** (04): 399-407. SPE-8907-PA. https://doi.org/10.2118/8907-PA

Fassihi, M. R., Brigham, W. E., and Ramey Jr, H. J. 1984b. Reaction Kinetics of In-Situ Combustion: Part 2-Modeling. *SPE J.* **24** (04): 408-416. SPE-9454-PA. https://doi.org/10.2118/9454-PA

Fassihi, M. R., Gillham, T. H., Yannimaras, D. V., and Hassan, D. 1996. Field Tests Assess Novel Air-injection EOR Processes. *Oil and Gas Journal* **94** (21).

Fatemi, S. M., Ghotbi, C., Kharrat, R., and Badakhshan, A. 2011. Application of Toe-to-Heel Air Injection (THAI) Process in Fractured Carbonate Systems: 3D Simulation of the Effect of Fractures Geometrical Properties, Reservoir and Operational Parameters. Paper presented at the SPE EUROPEC/EAGE Annual Conference and Exhibition, Vienna, Austria, 23-26 May 2011. http://doi.org/10.2118/143434-MS.

Friedman, H. L. 1964. Kinetics of Thermal Degradation of Char-Forming Plastics from Thermogravimetry. Application to a Phenolic Plastic. In *Journal of Polymer Science: Polymer Symposia*, 6:183-195: Wiley Online Library.ISBN 1935-3065.

Glatz, G. 2011. In-Situ Combustion Kinetics of a Central European Crude for Thermal EOR. Paper presented at the SPE Annual Technical Conference and Exhibition, Denver, Colorado, USA, 30 October - 2 November. SPE-152363-STU. https://doi.org/10.2118/152363-STU.

Green, J. B., Yu, S. K. T., Pearson, C. D., and Reynolds, J. W. 1993. Analysis of sulfur compound types in asphalt. *Energy & Fuels* **7** (1): 119-126. https://doi.org/10.1021/ef00037a019

Gutierrez, D., Skoreyko, F., Moore, R., Mehta, S., and Ursenbach, M. 2009. The Challenge of Predicting Field Performance of Air Injection Projects based on Laboratory and Numerical Modelling. *J Can Pet Technol* **48** (04): 23-33. PETSOC-09-04-23-DA. https://doi.org/10.2118/09-04-23-DA

Hammershaimb, E., Kuuskraa, V., and Stosur, G. 1983. Recovery Efficiency of Enhanced Oil Recovery Methods: A Review of Significant Field Tests. Paper presented at the SPE Annual Technical Conference and Exhibition, San Francisco, California, 5-8 October 1983. SPE-12114-MS. https://doi.org/10.2118/12114-MS.

Han, X.-W., Zhou, C.-R., and Shi, X.-H. 2012. Determination of Specific Heat Capacity and Standard Molar Combustion Enthalpy of Taurine by DSC. *Journal of thermal analysis and calorimetry* **109** (1): 441-446. https://doi.org/10.1007/s10973-011-1670-y

Hascakir, B. 2015. Description of In-situ Oil Upgrading Mechanism for In-situ Combustion Based on a Reductionist Chemical Model. Paper presented at the SPE Annual Technical Conference and Exhibition, Houston, Texas, USA, 28-30 September 2015. SPE-175086-MS. http://doi.org/10.2118/175086-MS.

Hascakir, B., Glatz, G., Castanier, L. M., and Kovscek, A. 2011. In-situ Combustion Dynamics Visualized with X-ray Computed Tomography. *SPE J.* **16** (03): 524-536. http://doi.org/10.2118/135186-PA

Hascakir, B. and Kovscek, A. R. 2014. Analysis of In-Situ Combustion Performance in Heterogeneous Media. Paper presented at the SPE Heavy Oil Conference Calgary, Alberta, Canada, 10-12 June 2014. http://10.2118/170008-MS.

Hascakir, B., Ross, C., Castanier, L., and Kovscek, A. 2013. Fuel Formation and Conversion During In-Situ Combustion of Crude Oil. *SPE J.* **18** (06): 1,217-211,228. SPE-146867-PA. http://doi.org/10.2118/146867-PA

Hayashitani, M., Bennion, D. W., Donnelly, J. K., and Moore, R. G. 1978. Thermal Cracking Models for Athabasca Oil Sands Oil. Paper presented at the SPE Annual Fall Technical Conference and Exhibition, Houston, Texas, 1-3 October 1978. SPE-7549-MS. https://doi.org/10.2118/7549-MS.

Hein, F. J. 2006. Heavy Oil and Oil (Tar) Sands in North America: An Overview & Summary of Contributions. *Natural Resources Research* **15** (2): 67-84. https://doi.org/10.1007/s11053-006-9016-3

Heufer, K., Fernandes, R., Olivier, H., Beeckmann, J., Röhl, O., and Peters, N. 2011. Shock Tube Investigations of Ignition Delays of N-butanol at Elevated Pressures between 770 and 1250K. *Proceedings of the Combustion Institute* **33** (1): 359-366. https://doi.org/10.1016/j.proci.2010.06.052

Horowitz, H. and Metzger, G. 1963. A New Analysis of Thermogravimetric Traces. *Analytical Chemistry* **35** (10): 1464-1468. https://doi.org/10.1021/ac60203a013

Howie, R. and Broadhurst, F. 1958. X-ray Data for Dolomite and Ankerite. *American Mineralogist* **43** (11-12): 1210-1216.

Ingraham, T. and Marrier, P. 1964. Activation Energy Calculation from a Linearly-increasing-temperature Experiment. *The Canadian Journal of Chemical Engineering* **42** (4): 161-163. https://doi.org/10.1002/cjce.5450420406

Ismail, N. and Hascakir, B. 2017. Increased Asphaltenes Surface Aids Fuel Formation with the Presence of Clays during In-Situ Combustion. Paper presented at the SPE Annual Technical Conference and Exhibition, San Antonio, Texas, USA, 9-11 October 2017. SPE-187362-MS. https://10.2118/187362-MS.

Ismail, N., Klock, K., and Hascakir, B. 2016. In-Situ Combustion Experience in Heavy Oil Carbonate. Paper presented at the SPE Canada Heavy Oil Technical Conference Calgary, Alberta, Canada, 7-9 June 2016. SPE-180724-MS. https://doi.org/10.2118/180724-MS.

Ismail, N., Seber, E., and Hascakir, B. 2018. Role of Aromatics Fraction of Crude Oils on In-Situ Combustion Performance. Paper presented at the SPE Improved Oil Recovery Conference, Tulsa, OK, 14-18 April 2018. SPE-190307-MS. https://doi.org/10.2118/190307-MS.

Jewell, D. M., Albaugh, E. W., Davis, B. E., and Ruberto, R. G. 1974. Integration of Chromatographic and Spectroscopic Techniques for the Characterization of Residual Oils. *Industrial & Engineering Chemistry Fundamentals* **13** (3): 278-282. https://doi.org/10.1021/i160051a022

Jia, H., Zhao, J.-Z., Pu, W.-F., Liao, R., and Wang, L.-L. 2012. The Influence of Clay Minerals Types on the Oxidation Thermokinetics of Crude Oil. *Energy Sources, Part A: Recovery, Utilization, and Environmental Effects* **34** (10): 877-886. https://doi.org/10.1080/15567036.2012.656219

Johnson Jr, L. and Romanowski Jr, L. 1987. *Evaluation of Steam-to-Oxygen Ratios for Forward Combustion in Asphalt Ridge Tar Sand*. p.5-9. Western Research Inst., Laramie, WY (USA).

Kar, T., Mukhametshina, A., Unal, Y., and Hascakir, B. 2015. The Effect of Clay Type on Steam-Assisted-Gravity-Drainage Performance. *J Can Pet Technol* **54** (06). SPE-173795-PA. https://doi.org/10.2118/173795-PA

Kar, T., Williamson, M., and Hascakir, B. 2014. The Role of Asphaltenes in Emulsions Formation for Steam Assisted Gravity Drainage (SAGD) and Expanding Solvent-SAGD (ES-SAGD). Paper presented at the SPE Heavy and Extra Heavy Oil Conference - Latin America, Medellin, Colombia, 24-26 September. SPE-171076-MS. http://dx.doi.org/10.2118/171076-MS.

Kasper, T., Struckmeier, U., Oßwald, P., and Kohse-Höinghaus, K. 2009. Structure of a Stoichiometric Propanal Flame at Low Pressure. *Proceedings of the Combustion Institute* **32** (1): 1285-1292. https://doi.org/10.1016/j.proci.2008.06.040

Khvostichenko, D. S. and Andersen, S. I. 2008. Interactions Between Asphaltenes and Water in Solutions in Toluene. *Energy & Fuels* **22** (5): 3096-3103. https://doi.org/10.1021/ef700757h

Kisler, J. and Shallcross, D. 1997. An Improved Model for the Oxidation Processes of Light Crude Oil. *Chemical Engineering Research and Design* **75** (4): 392-400. https://doi.org/10.1205/026387697523859

Klein, J. C. and Hercules, D. M. 1983. Surface Characterization of Model Urushibara Catalysts. *Journal of catalysis* **82** (2): 424-441. https://doi.org/10.1016/0021-9517(83)90209-9

Klock, K. and Hascakir, B. 2015. Simplified Reaction Kinetics Model for In-Situ Combustion. Paper presented at the SPE Latin American and Caribbean Petroleum Engineering Conference, Quito, Ecuador, 18-20 November 2015. SPE-177134-MS. https://doi.org/10.2118/177134-MS.

Kok, M. 1993. Use of Thermal Equipment to Evaluate Crude Oils. *Thermochimica Acta* **214** (2): 315-324. http://doi.org/10.1016/0040-6031(93)80068-L

Kok, M. 2002. Combustion Kinetics of Crude Oils. *Energy Sources* **24** (1): 1-7. https://doi.org/10.1080/00908310252712253

Kok, M. 2006. Effect of Clay on Crude Oil Combustion by Thermal Analysis Techniques. *Journal of Thermal Analysis and Calorimetry* **84** (2): 361-366. http://10.1007/s10973-005-7153-2

Kok, M. and Acar, C. 2005. Kinetics of Crude Oil Combustion. *Journal of thermal analysis and calorimetry* **83** (2): 445-449. http://10.1007/s10973-005-7152-3

Kok, M. and Karacan, C. 2000. Behavior and Effect of SARA Fractions of Oil During Combustion. *SPE Reservoir Evaluation & Engineering* **3** (05). https://doi.org/10.2118/66021-PA

Koottungal, L. 2014. 2014 Worldwide EOR Survey. *Oil & Gas Journal* **112** (4): 78-91.

Kozlowski, M., Punase, A., Nasr-El-Din, H., and Hascakir, B. 2015. The Catalytic Effect of Clay on In-Situ Combustion Performance. Paper presented at the SPE Latin American and Caribbean Petroleum Engineering Conference, Quito, Ecuador, 18-20 November 2015. SPE-177166-MS. https://doi.org/10.2118/177166-MS.

Krump, H., Alexy, P., and Luyt, A. S. 2005. Preparation of a Maleated Fischer-Tropsch Paraffin Wax and FTIR Analysis of Grafted Maleic Anhydride. *Polymer Testing* **24** (2): 129-135. https://doi.org/10.1016/j.polymertesting.2004.09.011

Kudryavtsev, P. and Hascakir, B. 2014. Towards Dynamic Control of In-situ Combustion: Effect of Initial Oil and Water Saturations. Paper presented at the SPE Western North American and Rocky Mountain Joint Meeting, Denver, Colorado, 17-18 April 2014 SPE-169542-MS. https://doi.org/10.2118/169542-MS.

Leaute, R. and Collyer, C. 1984. Laboratory Studies of In Situ Combustion with Cold Lake Crude. Paper presented at the Annual Conference on Upgrading Technology and Petroleum Recovery, Calgary.

Lee, C.-H., Mong, H.-Y., and Lin, W.-C. 2002. Noninterferometric Wide-field Optical Profilometry with Nanometer Depth Resolution. *Optics letters* **27** (20): 1773-1775. https://doi.org/10.1364/OL.27.001773

Lee, W. J. and Li, C.-Z. 2007. Coke Formation and Reaction Pathways of Catalyst-Surface-Generated Radicals during the Pyrolysis of Ethane using Ni Mesh Catalyst. *Applied Catalysis A: General* **316** (1): 90-99. https://doi.org/10.1016/j.apcata.2006.09.018

Mamora, D. D., Ramey Jr, H. J., Brigham, W. E., and Castanier, L. M. 1984. Kinetics of In Situ Combustion. **24** (04). https://doi.org/10.2118/8907-PA

Manrique, E. J., Muci, V. E., and Gurfinkel, M. E. 2006. EOR Field Experiences in Carbonate Reservoirs in the United States. *SPE Res Eval & Eng* **10** (06). SPE-100063-PA. https://doi.org/10.2118/100063-PA

Marjerrison, D. and Fassihi, M. 1994. Performance of Morgan Pressure Cycling In-situ Combustion Project. Paper presented at the SPE/DOE Improved Oil Recovery Symposium, Tulsa, Oklahoma, 17-20 April 1994. SPE-27793-MS. https://doi.org/10.2118/27793-MS.

Martin, J. C. 1959. The Effects of Clay on the Displacement of Heavy Oil by Water. Paper presented at the Venezuelan Annual Meeting, Caracas, Venezuela, 14-16 October 1959. SPE-1411-G. https://doi.org/10.2118/1411-G.

Martin, W., Alexander, J., and Dew, J. 1958. Process Variables of In-situ Combustion. *Petroleum Transactions, AIME* **213**: 28-35. SPE-914-G.

McCain Jr, W. D. 1999. *Properties of Petroleum Fluids*. p.39-108. Oklahoma, USA: PennWell Corporation.

Meyer, R. F., Attanasi, E. D., and Freeman, P. A. 2007. *Heavy Oil and Natural Bitumen Resources in Geological Basins of the World*. p.3.

Milliken, T., Oblad, A., and Mills, G. 1955. Clays and Clay Technology. *Calif. Div. Mines, Bull* **169**: 314.

Mitra, S., Bhushan, B. V., Pilli, V. R., Kumar, S., Sur, S., Mehta, S. A., and Moore, R. G. 2010. Feasibility of Air Injection in a Light Oil Field of Western India. Paper presented at the SPE Oil and Gas India Conference and Exhibition, Mumbai, India, 20-22 January 2010. SPE-126234-MS. https://doi.org/10.2118/126234-MS.

Moore, R., Ursenbach, M., Laureshen, C., Belgrave, J., and Mehta, S. 1999. Ramped Temperature Oxidation Analysis of Athabasca Oil Sands Bitumen. *J Can Pet Technol* **38** (13). PETSOC-99-13-40. http://doi.org/10.2118/99-13-40

Moore, R. G., Laureshen, C. J., Mehta, S. A., and Ursenbach, M. G. 1997. Observations and Design Considerations for In-Situ Combustion Projects. Paper presented at the Annual Technical Meeting, Calgary, Canada, 8-11 June. PETSOC-97-100. https://doi.org/10.2118/97-100.

Morrow, A. W., Mukhametshina, A., Aleksandrov, D., and Hascakir, B. 2014. Environmental Impact of Bitumen Extraction with Thermal Recovery. Paper presented at the SPE Heavy Oil Conference-Canada, Calgary, Alberta, Canada, 10-12 June. SPE-170066-MS. https://doi.org/10.2118/170066-MS.

Mostafavi, V., Razzaghi, S., and Kharrat, R. 2007. Feasibility study of Insitu Combustion in Carbonate Reservoirs. Paper presented at the SPE Middle East Oil and Gas Show and Conference, Manama, Bahrain, 11-14 March 2007. SPE-105576-MS. http://doi.org/10.2118/105576-MS.

Mullins, O. C., Seifert, D. J., Zuo, J. Y., and Zeybek, M. 2012. Clusters of Asphaltene Nanoaggregates Observed in Oilfield Reservoirs. *Energy & Fuels* **27** (4): 1752-1761. http://10.1021/ef301338q

Musser, B. J. and Kilpatrick, P. K. 1998. Molecular Characterization of Wax Isolated from a Variety of Crude Oils. *Energy & Fuels* **12** (4): 715-725. https://doi.org/10.1021/ef970206u

Neasham, J. W. 1977. The Morphology of Dispersed Clay in Sandstone Reservoirs and its Effect on Sandstone Shaliness, Pore Space and Fluid Flow Properties. Paper presented at the SPE Annual Fall Technical Conference and Exhibition, Denver, Colorado, 9-12 October. SPE-6858-MS. https://doi.org/10.2118/6858-MS.

Nelson, T. W. and McNeil, J. S. 1961. How to Engineer an In-Situ Combustion Project. *Oil & Gas Journal* **59** (23): 58-65.

Ozawa, T. 1965. A New Method of Analyzing Thermogravimetric Data. *Bulletin of the chemical society of Japan* **38** (11): 1881-1886.

Ozawa, T. 1970. Kinetic Analysis of Derivative Curves in Thermal Analysis. *Journal of Thermal Analysis and Calorimetry* **2** (3): 301-324.

Penberthy, W. L., Berry, H. J., and Ramey, H. J. 1968. Some Fundamentals of Steam-Plateau Behavior in Combustion Oil Recovery. Paper presented at the 43d Annual Fall Meeting of the Society of Petroleum Engineers of AIME, Houston, Texas, September 29. SPE-2213-MS. http://10.2118/2213-ms.

Pepiot-Desjardins, P., Pitsch, H., Malhotra, R., Kirby, S., and Boehman, A. 2008. Structural Group Analysis for Soot Reduction Tendency of Oxygenated Fuels.

Combustion and Flame **154** (1): 191-205. https://doi.org/10.1016/j.combustflame.2008.03.017

Pfeiffer, J. P. and Saal, R. 1940. Asphaltic Bitumen as Colloid System. *The Journal of Physical Chemistry* **44** (2): 139-149. https://doi.org/10.1021/j150398a001

Prakoso, A., Punase, A., and Hascakir, B. 2015. A Mechanistic Understanding of Asphaltene Precipitation from Varying Saturate Concentration Perspective. Paper presented at the SPE Latin American and Caribbean Petroleum Engineering Conference, Quito, Ecuador, 18-20 November 2015. http://doi.org/10.2118/177280-PA.

Prakoso, A., Punase, A., Rogel, E., Ovalles, C., and Hascakir, B.-. 2018. Effect of Asphaltenes Characteristics on its Solubility and Overall Stability. *Energy & Fuels* **6** (32): 6482-6487. https://doi.org/10.1021/acs.energyfuels.8b00324

Prakoso, A. A., Punase, A. D., and Hascakir, B. 2016. A Mechanistic Understanding of Asphaltenes Precipitation from Varying Saturate Concentration Perspectives. *SPE Prod & Oper* **32** (01). SPE-177280-PA. http://doi.org/10.2118/177280-PA

Prats, M. 1982. *Thermal Recovery*. p.88-112. Dallas: Society of Petroleum Engineers of AIME.

Pu, W., Chen, Y., Li, Y., Zou, P., and Li, D. 2017. Comparison of Different Kinetic Models for Heavy Oil Oxidation Characteristic Evaluation. *Energy & Fuels* **31** (11): 12665-12676. http://doi.org/10.1021/acs.energyfuels.7b02256

Radler, M. 1996. Worldwide Refining Survey. *Oil and Gas Journal* **94** (52): 49-94.

Raicar, J. and Procter, R. 1984. *Economic Considerations and Potential of Heavy Oil Supply from Lloydminster–Alberta, Canada*. p.212-219

New York: McGraw-Hill.

Raju, P., Khurana, R., Munimani, B., Mehta, B., and Kumar, S. 2010. Reservoir Rock Influence on Air Injection Process: A Laboratory Investigation. Paper presented at the Petrotech, New Delhi, India, 31 October-3 November 2010.

Ramey, H. 1971. In Situ Combustion. Paper presented at the 8th World Petroleum Congress, Moscow, USSR, 13-18 June 1971. WPC-14229.

Ramey, H. J. 1958. Transient Heat Conduction During Radial Movement of a Cylindrical Heat Source - Applications to the Thermal Recovery Process. Paper presented at the 33rd Annual Fall Meeting of Society of Petroleum Engineers, Houston, Texas, October 5-8. SPE-1133-G.

Ranjbar, M. 1993. Influence of Reservoir Rock Composition on Crude Oil Pyrolysis and Combustion. *Journal of analytical and applied pyrolysis* **27** (1): 87-95. https://doi.org/10.1016/0165-2370(93)80024-T

Ranzi, E. 2006. A Wide-Range Kinetic Modeling Study of Oxidation and Combustion of Transportation Fuels and Surrogate Mixtures. *Energy & Fuels* **20** (3): 1024-1032. https://doi.org/10.1021/ef060028h

Ranzi, E., Frassoldati, A., Granata, S., and Faravelli, T. 2005. Wide-Range Kinetic Modeling Study of the Pyrolysis, Partial Oxidation, and Combustion of Heavy N-Alkanes. *Industrial & Engineering Chemistry Research* **44** (14): 5170-5183. https://doi.org/10.1021/ie049318g

Rodriguez, N., Marsh, H., Heintz, E., Sherwood, R., and Baker, R. 1987. Oxidation Studies of Various Petroleum Cokes. *Carbon* **25** (5): 629-635. https://doi.org/10.1016/0008-6223(87)90215-6

Rohman, A. and Man, Y. C. 2010. Fourier Transform Infrared (FTIR) Spectroscopy for Analysis of Extra Virgin Olive Oil Adulterated with Palm Oil. *Food research international* **43** (3): 886-892. https://doi.org/10.1016/j.foodres.2009.12.006

Saal, R. N. J. and Labout, J. W. A. 1940. The Rheological Properties of Asphaltic Bitumens. *The Journal of Physical Chemistry* **44** (2): 149-165. https://10.1021/j150398a002

Salooja, K. 1965. The Role of Aldehydes in Combustion: Studies of the Combustion Characteristics of Aldehydes and of their Influence on Hydrocarbon Combustion Processes. *Combustion and Flame* **9** (4): 373-382. https://doi.org/10.1016/0010-2180(65)90026-X

Sarathi, P. 1998. *In-Situ Combustion Handbook Principles and Practices.* . p.1-146.Tulsa, OK: Report DOE/PC/91008-0374, OSTI ID 3174.

Serinyel, Z., Black, G., Curran, H., and Simmie, J. 2010a. A Shock Tube and Chemical Kinetic Modeling Study of Methy Ethyl Ketone Oxidation. *Combustion Science and Technology* **182** (4-6): 574-587. https://doi.org/10.1080/00102200903466129

Serinyel, Z., Chaumeix, N., Black, G., Simmie, J., and Curran, H. 2010b. Experimental and Chemical Kinetic Modeling Study of 3-pentanone Oxidation. *The Journal of Physical Chemistry A* **114** (46): 12176-12186. https://doi.org/10.1021/jp107167f

Shah, A. A., Fishwick, R. P., Leeke, G. A., Wood, J., Rigby, S. P., and Greaves, M. 2011. Experimental Optimization of Catalytic Process in Situ for Heavy-Oil and Bitumen Upgrading. *J Can Pet Technol* **50** (11-12): 33-47. SPE-136870-PA. http://doi.org/10.2118/136870-PA

Socrates, G. 2004. *Infrared and Raman Characteristic Group Frequencies: Tables and Charts*, 3. p.50-165. Middlesex, UK: John Wiley & Sons.

Speight, J. G. 1991. *The Chemistry and Technology of Petroleum*. p.187-208. New York: CRC press.

Stamplecoskie, K. G., Scaiano, J. C., Tiwari, V. S., and Anis, H. 2011. Optimal Size of Silver Nanoparticles for Surface-Enhanced Raman Spectroscopy. *The Journal of Physical Chemistry C* **115** (5): 1403-1409. http://10.1021/jp106666t

Stuart, B. H. 2004. *Infrared Spectroscopy: Fundamentals and Applications*. p.71-94. Sussex, England: John Wiley & Sons.

Sufi, A. H. 1989. Injectivity Enhancement in Tar Sands a Physical Model Study. *J Can Pet Technol* **28** (01). PETSOC-89-01-06. https://doi.org/10.2118/89-01-06

Sulzer, P. T. 1955. The Prevention of Oil Ash Deposition by Means of Fuel Additive. Paper presented at the 4th World Petroleum Congress, Rome, Italy, 6-15 June.

Svrcek, W. and Mehrotra, A. 1989. Properties of Peace River Bitumen Saturated with Field Gas Mixtures. *Journal of Canadian Petroleum Technology* **28** (02).

Tadema, H. 1959. Mechanism of Oil Production by Underground Combustion. Paper presented at the 5th World Petroleum Congress, New York, USA, 30 May-5 June. WPC-8121.

Tang, G.-Q. and Morrow, N. R. 1999. Influence of Brine Composition and Fines Migration on Crude Oil/Brine/Rock Interactions and Oil Recovery. *Journal of Petroleum Science and Engineering* **24** (2-4): 99-111. https://doi.org/10.1016/S0920-4105(99)00034-0

Thomas, G. W. 1963. A Study of Forward Combustion in a Radial System Bounded by Permeable Media. Paper presented at the SPE Annual Fall Meeting, New Orleans, Texas, October 6-9. SPE-681-PA. http://10.2118/681-pa.

Turta, A., Chattopadhyay, S., Bhattacharya, R., Condrachi, A., and Hanson, W. 2007. Current Status of Commercial In Situ Combustion Projects Worldwide. *J Can Pet Technol* **46** (11). PETSOC-07-11-GE. https://doi.org/10.2118/07-11-GE

Unal, Y., Kar, T., Mukhametshina, A., and Hascakir, B. 2015. The Impact of Clay Type on the Asphaltene Deposition during Bitumen Extraction with Steam Assisted Gravity Drainage. Paper presented at the SPE International Symposium on Oilfield Chemistry, The Woodlands, Texas, USA, 13-15 April 2015. SPE-173795-MS. http://doi.org/10.2118/173795-MS.

Unur, E. 2013. Functional Nanoporous Carbons from Hydrothermally Treated Biomass for Environmental Purification. *Microporous and Mesoporous Materials* **168**: 92-101. http://dx.doi.org/10.1016/j.micromeso.2012.09.027

Van Wylen, G. J., Sonntag, R. E., and Borgnakke, C. 1994. *Fundamentals of Classical Thermodynamics*. p.130-141. Michigan, USA: Wiley.

Verkoczy, B. 1993. Factors Affecting Coking in Heavy Oil Cores, Oils and SARA Fractions under Thermal Stress. *J Can Pet Technol* **32** (07): 25-33. PETSOC-93-07-02. http://doi.org/10.2118/93-07-02

Verkoczy, B. and Jha, K. 1986. TGA/DSC Investigations of Saskatchewan Heavy Oils and Cores

J Can Pet Technol **25** (03). PETSOC-86-03-05. https://doi.org/10.2118/86-03-05

Vogel, L. C. and Krueger, R. F. 1955. An Analog Computer for Studying Heat Transfer During a Thermal Recovery Process. Paper presented at the Petroleum Branch Fall Meeting, New Orleans, Texas, October 2-5. SPE-534-G.

Vossoughi, S., Bartlett, G. W., and Willhite, G. P. 1982a. Development of a Kinetic Model for In-situ Combustion and Prediction of the Process Variables using TGA/DSC Techniques. Paper presented at the SPE Annual Technical Conference and Exhibition.

Vossoughi, S. and El-Shoubary, Y. 1987. Kinetics of Crude Oil Coke Combustion. Paper presented at the SPE International Symposium on Oilfield Chemistry, San Antonio, Texas, 4-6 February 1987. SPE-16268-MS. https://doi.org/10.2118/16268-MS.

Vossoughi, S., Willhite, G., El-Shoubary, Y., and Bartlett, G. W. 1983. Study of Clay Effect on Crude Oil Combustion by Thermogravimetry and Differential Scanning Calorimetry. *Journal of Thermal Analysis and Calorimetry* **27** (17): 17-36. https://doi.org/10.1007/BF01907318

Vossoughi, S., Willhite, G. P., Kritikos, W. P., Guvenir, I. M., and El Shoubary, Y. 1982b. Automation of an In-Situ Combustion Tube and Study of the Effect of Clay on the In-Situ Combustion Process. *Society of Petroleum Engineers Journal* **22** (04): 493-502. SPE-10320-PA. http://doi.org/10.2118/10320-PA

Wang, Y., Hill, A. D., and Schechter, R. S. 1993. The Optimum Injection Rate for Matrix Acidizing of Carbonate Formations. Paper presented at the SPE Annual Technical Conference and Exhibition, Houston, Texas, 3-6 October 1993. SPE-26578-MS. https://10.2118/26578-MS.

Wang, Z., Fingas, M., and Li, K. 1994. Fractionation of a Light Crude Oil and Identification and Quantitation of Aliphatic, Aromatic, and Biomarker Compounds by GC-FID and GC-MS, Part II. *Journal of Chromatographic Science* **32** (9): 367-382. https://doi.org/10.1093/chromsci/32.9.367

Westbrook, C. K., Pitz, W. J., Herbinet, O., Curran, H. J., and Silke, E. J. 2009. A Comprehensive Detailed Chemical Kinetic Reaction Mechanism for Combustion of N-Alkane Hydrocarbons from N-Octane to N-Hexadecane. *Combustion and flame* **156** (1): 181-199. https://doi.org/10.1016/j.combustflame.2008.07.014

Wilt, B. K., Welch, W. T., and Rankin, J. G. 1998. Determination of Asphaltenes in Petroleum Crude Oils by Fourier Transform Infrared Spectroscopy. *Energy & Fuels* **12** (5): 1008-1012. http://doi.org/10.1021/ef980078p

Wu, C. and Fulton, P. 1971. Experimental Simulation of the Zones Preceding the Combustion Front of an In-situ Combustion Process. *SPE J.* **11** (01): 38-46. SPE-2816-PA. http://doi.org/10.2118/2816-PA